Dissertation

zur Erlangung des Doktorgrades
der Fakultät für Chemie und Pharmazie der
Ludwig-Maximilians-Universität München

Gelatin Nanoparticles as a Modern Platform for Drug Delivery

-

Formulation Development and Immunotherapeutic Strategies

vorgelegt von

Sebastian Fuchs
aus Heinsberg

2010

ERKLÄRUNG

Diese Dissertation wurde im Sinne von § 13 Abs. 3 bzw. 4 der Promotionsordnung vom 29. Januar 1998 von Herrn Prof. Dr. Gerhard Winter und Herrn Dr. Conrad Coester als Tutor betreut. Mit Erteilung der Lehrbefugnis wurde die Betreuung ab Februar 2009 von Herrn PD Dr. Conrad Coester übernommen.

EHRENWÖRTLICHE VERSICHERUNG

Diese Dissertation wurde selbständig, ohne unerlaubte Hilfe erarbeitet.

München, den 02. Juli 2010

(Sebastian Fuchs)

Dissertation eingereicht am: 02. Juli 2010

Erstgutachter: PD Dr. Conrad Coester

Zweitgutachter: Prof. Dr. Gerhard Winter

Tag der mündlichen Prüfung: 29. Juli 2010

Fortiter in re, suaviter in modo.

Claudio Aquaviva (1543 – 1615)

Meinen Eltern

In Liebe und Dankbarkeit

ACKNOWLEDGEMENTS

The thesis on hand was prepared between July 2006 and April 2010 at the Department of Pharmaceutical Technology and Biopharmaceutics at the Ludwig Maximilians University Munich. First and foremost, I would like to thank **Prof. Dr. Gerhard Winter** for making me a member of his group and to supervise my thesis. As doctoral father he provided guidance with industrial experience spiced with a potion of humor.

The actual filed of research was due to **PD Dr. Conrad Coester**. Only by the intense and lively direct discussions with and directions by him could this work mature to its accomplishment. Furthermore, he established most of all the collaborations that formed the strong interdisciplinary character of this thesis.

The art of GNP manufacturing involving all labeling and freeze drying techniques do I owe to **Dr. Klaus Zwiorek** and **Dr. Jan Zillies**, my direct predecessors.

A big thanks goes over the big pound to **Prof. Thomas Anchordoquy** who inspired me with an alternative perspective on academic approaches, scientific discussion culture and of course for hosting me for a research stay in Denver, Colorado. Along, I thank his team members **Dr. Michelle Zeles-Hahn** and **Dr. Long Xu** for sharing unique experiences both in Munich and Denver and for help in literature organization.

Without the many engaged cooperation partners this thesis would not have been possible. The last and most progressive project was with equine clinic's **Prof. Dr. Heidrun Gehlen** and **Dr. Anna May**. Her grad student **John Klier** was the major factor of success in the trial and we perfectly worked together till the very last day of his and my dissertation. Thank you, Johnny! Within the same veterinarian department, a fruitful collaboration was conducted with **Prof. Dr. Ralf Müller** on the immunotherapy in dogs. His postdoc, **Dr. Ana Rostaher**, and I explored the *in vitro* abilities of CpG loaded GNPs together. **Dr. Karin Weber** gave decisive technical and intellectual support and contributed rich experience.

The all-longest standing cooperation was with **PD Dr. Carole Bourquin** of the clinical pharmacology in **Prof. Dr. Stefan Endres'** department. She established the CpG-GNP adjuvant strategy in anti-cancer immunotherapy together with my predecessor Dr. Klaus Zwiorek. Important immunologic input and laboratory

execution came from **Dr. David Anz**, steady lab overview from **Nadja Sandholzer** and finally and decisively **Dr. Cornelia Wurzenberger**. Special thanks go to her for the outstanding support prior my oral presentation on isRNA delivery. A short side project within the same department was initiated by **PD Dr. Max Schnurr**. I thank him and his team for their work and for confidence in my GNPs.

Studies on the biodistribution of radio-labeled GNPs were performed in the Technical University's clinic department of nuclear medicine under the supervision of **Prof. Hans-Jürgen Wester**. I would like to thank him for his steady and very intense discussions familiarizing me with the various crucial demands of chemistry in nuclear medicine. The initial strategy on radio-labeling was co-devised by **Dr. Jörg Auernheimer**, consuming animal work was performed by **Katharina McGuire** and co-workers.

The most analytical part of the thesis was the URT cooperation with TF instruments, represented by **Dr. Daniel Gau**. For two years, **Richard Parlitz** accompanied and tutored me from the first project plans till revising the publication. Thank you for all the efforts!

First engagement in formulation development in an immunotherapeutic setting against hypersensitivity resulted in a patent with Cytos Biotechnology AG, Zurich, Switzerland. Here, my grateful thanks go to responsible **Dr. Alain Tissot** and **Dr. Vania Manolova** for their strong support in this project and for sharing their vast experience with me resulting in a joint patent applicaton.

Prof. Dr. Markus Pietzsch and his group at the department of Pharmaceutical Technology and Biopharmacy, University of Halle-Wittenberg is acknowleged for the fruitful cooperation project on transglutaminase-based nanoparticle crosslinking.

Within our department I have to thank **PD Dr. Stefan Zahler** for introducing me into the art of confocal microscopy and **Sebastian Hertel** into the techniques of vibrating mesh devices. **Christian Minke** of the central analytics facility kindly operated the MAS-NMR and the REM.

Furthermore, I thank my three master students **Martina Sprengholz**, **Isabel Schönle** and **Marika Kutscher**, who co-worked on my projects providing significant results, for their excellent input and friendly discussions.

Finally, as it is all about people, who create the working atmosphere that enable

productivity, I thank **Prof. Dr. Wolfgang Frieβ**, help- and heartful technician **Alice Hirschmann** and my fellow PhD student colleagues **Miriam Prinz, Dr. Kathrin Schersch, Dr. Tim Serno** (oboe)**, Eva-Maria Ruberg, Dr. Martin Schwab** (who I joint in quite metaphysical students' oral examinations)**, Raimund Geidobler, Elsa Kis, Gerhard Sax, Dr. Sylvia 'Schnabbi' Kiese, Lars Schiebelbein, Katja Schmid, Sarah Claus** (clarinet), **Winfried Schlögel, Markus Hofer, Thomas Bosch, Philipp Matthias, Sebastian Hertel, Dr. Ahmed Youssef, Dr. Weiwei Tian, Dr. Virginie leBrun, Dr. Stefan Gottschalk, Dr. Rainer Lang, Dr. Frank Schaubhut, Dr. Johannes Mathes (**trumpet**), Dr. Kathrin Mathis, Dr. Florian Matl, Dr. Cornelius Pompe, Dr. Eva Rosenberg** as well as **Dr. Julia Myschik** and **Dr. Ahmed Besheer** of the last years in- and outside the institute. Most do I have in mind the "bubble lab" crew with **Dr. Steliyan Tinkov** who broadened my freedom of mind, **Dr. Stephan Schultes** who broadened my idea of the history of humor and finally **Dr. Klaus Freitag**, who broadened my horizon by sharing the Denver experience by joining the group of Prof. Tom Anchordoquy. Their successors, **Elisabeth Härtl** and **Matthaeus Noga**, shared my final time in the lab and were so much more than just labmates. Finally, I am very thankful for concluding proof reading and formatting help kindly provided by **Regina Mayer** and **Jakob Pumberger**, respectively.

Anselma Murswiek is acknowledged for designing the front cover picture as an allegory on nanoparticle-mediated DNA immunotherapy.

Summary of the thesis

Nanoparticles are under comprehensive investigation as a promising platform for drug delivery since three decades. However, the transition from encouraging pre-clinical research to clinical studies and finally regulatory approval has not yet occurred for solid colloidal nanoparticles. This work shall contribute to bridging that gap. Convinced that therapeutic nanoparticulate formulations should be as extensively characterized and be kept as simple as possible, this thesis exemplarily describes analytical methods and production improvements for gelatin nanoparticles (GNPs) and proposes their employment in a variety of immunotherapeutic applications.

Up-scaling of the original manufacturing setup was technically enabled and resulted in ten-fold increased batch sizes. Systematic correlation studies facilitated the establishment of a set of equations to predict necessary GNP preparation parameters for each relevant batch size. This shall contribute to future higher GNP demand in clinical manufacturing.

Moreover, the feasibility of replacing well-established but initially toxic starting material glutaraldehyde as a cross-linking agent by the enzymatic alternative transglutaminase was demonstrated. Transglutaminase-crosslinked GNPs featured narrow particle size distributions and high storage stability.

Ultrasonic resonator technology was demonstrated as a capable tool in relative GNP size analysis and DNA surface binding detection which could serve in future as a non-destructive tool for online in-process control in continuous GNP production. Within this study, a discriminative response of cationized and non-cationized GNPs towards distinctive buffers was observed. The swelling and size reduction was found to be in accordance with the sequence of salts of the Hofmeister series.

Of special importance was the successful radio-labeling of GNPs by radionuclides $^{111}In^{+}$ or $^{68}Ga^{3+}$, respectively, to monitor their biodistribution after s.c. or i.v. administration both by conservative sectioning and Positron Emission Tomography. PEGylation was conducted and proofed for several molecular weights. However, no enhanced circulation properties could be obtained due the prevalent hydrophilic properties of the starting molecule gelatin. Nevertheless, the

radio-labeling technique could be beneficial in new applications such as the monitoring of inhaled GNPs and in the quantification of the resulting lung deposition.

In continuation of promising *in vitro* and *in vivo* studies on the employment of GNP-bound CpG-DNA as an adjuvant in ovalbumin (OVA)-targeted cancer immunotherapy, initial trials on the immunostimulatory (is) RNA-mediated immunostimulation clearly demonstrated the potential of GNPs to assist addressing also the Toll-Like receptor 7. Here, isRNA superiorly entered the target lysosome when transport was GNP-mediated e.g. in contrast to DOTAP-mediated transport. GNPs effectively protected the isRNA from degradation upon RNAse challenge. Immunostimulation was successful as revealed by activation of relevant cell markers such as CD69 and most important, survival of pre-immunized and OVA-expressing tumor challenged mice was significantly prolonged. Ongoing studies indicate that this promising strategy is working in a therapeutic model setting, too. Thus, GNP-based isRNA formulations could be capable to cure existing tumors.

Immunomodulating effectiveness of GNP-bound CpG-DNA was demonstrated in a preclinical canine study. The impressive benefit of CpG A-class delivery by GNPs to peripheral blood mononuclear cells in terms of antiallergic IL-10 release was revealed in a canine *in vitro* study. This laid the foundation for further, now starting, in vivo studies to elucidate the possibility of a therapeutic option against common canine atopic dermatitis by modulating CpG-based immunotherapy.

Finally, a novel approach in therapy of common equine allergic condition of recurrent airway obstruction (RAO) was established, constituting the first-time ever immunotherapeutic clinical study associated with a colloidal carrier system. First, an appropriate combination of nebulizer and spacer to nebulize CpG-GNP formulations was developed for witch a patent was field. Then, a suitable CpG sequence to stimulate equine BAL cells was identified.

On cytokine detection level, it was remarkably possible to distinguish RAO-affected from healthy horses *in vitro*. Most notably, regulatory cytokine IL-10 expression was significantly triggered *in vivo* by five consecutive inhalations in RAO-affected horses. The entirety of clinical parameters assessed after nanoparticle treatment indicated a partial remission of the allergic condition. In particular, breathing rates were lowered to physiologic level, blood oxygen partial

pressure was significantly elevated, the pathogenic TBS score values were moderately reduced and the RAO-determinant content of neutrophile granulocytes within the TBS was more than halved on average. Therefore, this preliminary clinical study showed for the first time safety and curative effectiveness of colloidal nanocarrier-mediated immunotherapy in food-producing animals.

CONTENTS

ACKNOWLEDGEMENTS VII

SUMMARY OF THE THESIS..... XI

CONTENTS XV

LIST OF ABBREVIATONS XXIII

I GENERAL INTRODUCTION.....1

1. ON THE ART OF DRUG DELIVERY BY NANOTECHNOLOGY.....1

1.1 The aim of this thesis.....1

1.2 Why nanotechnology for drug delivery?.....2

2. OVERVIEW ON STARTING MATERIALS AND PRODUCTION METHODS.....6

2.1 Established non-proteineous starting materials.....6

2.2 Proteins as constitutive material for nanoparticles.....6

2.2.1 Albumine.....7

2.2.2 Legumine, gliadine, elastinlike polypeptide, β-galactoglobulin, silk 8

2.2.3 Gelatin.....9

2.3 Preparation methods of protein nanoparticles.....11

2.3.1 Coacervation process.....11

2.3.2 Solvent extraction or emulsion process.....12

2.3.3 Salt precipitation.....12

3. THE ADMINISTRATION ROUTE 13

3.1 Intravenous application.....13

3.2 Subcutaneous application.....16

3.3 Pulmonal application.....17

3.4 Oral application 18

II FORMULATION DEVELOPMENT OF PLAIN GELATIN NANOPARTICLES.....21

1. UPSCALING THE ESTABLISHED GNP PRODUCTION METHOD 21

1.1 Rationale of the upscaling process 21

1.2 Materials and methods.....22

1.2.1 Standard preparation of gelatin nanoparticles via two step desolvation technique 22

1.2.2 Scale-up of the gelatin nanoparticle standard preparation method.....23

1.2.3 Modifications of the upscaled gelatin nanoparticle preparation method: Equipment changes. 23

1.2.4 Characterization of gelatin nanoparticles 24

1.2.4.1 Determination of concentration.....24

1.2.4.2 Determination of particle size 24

1.2.4.3 Determination of zeta potential 24

1.2.5 Cationization of upscaled GNPs 25

1.3 Results and discussion 25

1.3.1 Effects of equipment changes 25
1.3.1.1 Effects on particle size and polydispersity index 25
1.3.1.2 Effects on particle yield 27
1.3.2 Stability of gelatin nanoparticles of upscaled batch sizes 29
1.3.3 Introduction of an evaporation step 30
1.3.4 Correlation studies 32
1.3.4.1 General correlation studies 32
1.3.4.2 Correlation studies within batches of the same size 35
1.3.5 Preliminary constitution of an interdependency network of production parameters 38
1.3.6 Reducing the amount of glutaraldehyde 41
1.3.7 Cationization of upscaled GNPs. 43
1.4 Conclusion 45
2. HYDRATION OF GNPS 47
2.1 Scope of the hydration project 47
2.2 Materials and Methods 48
2.2.1 Hydrogenation by sodium cyanoborohydride 48
2.2.2 Hydrogenation by hydrogen/carbon-bound palladium 48
2.2.3 Assessment of particle stability by PCS after hydrogenation 49
2.2.4 Scanning electron microscopy of GNPs 49
2.2.5 Liquid 13C-NMR for hydrogenation proof 49
2.2.6 Solid state magic angle spinning NMR for hydrogenation proof 50
2.2.7 Lyophilization of GNPs 50
2.3 Results and Discussion 51
3. ENZYMATIC CROSS-LINKING OF GNPS 61
3.1 Introduction 61
3.2 Materials and methods 63
3.2.1 Materials 63
3.2.2 Enzyme preparation 63
3.2.3 Production of gelatin nanoparticles 64
3.2.4 Cross-linking methods 65
3.2.5 Particle analysis by PCS and turbidity measurement 65
3.2.6 Stability tests 66
3.2.7 Statistical analysis 66
3.3 Results and discussion 66
3.3.1 Effect of purification method on particle integrity 66
3.3.2 Effect of cross-linking parameters during incubation 67
3.3.3 Turbidity monitoring during enzymatic cross-linking time 67
3.4 Particle size analysis during the enzymatic cross-linking time 71
3.4.1 Effect of storage temperature on particle stability 72
3.5 Conclusions 73

III ENLARGING THE ANALYTICAL TOOLBOX FOR GELATIN NANOPARTICLES 75

1. BASIC SETPOINTS IN PCS-BASED NANOPARTICLE SIZE MEASUREMENT 75
2. ULTRASONIC RESONATOR TECHNOLOGY AS A NEW QUALITY CONTROL METHOD EVALUATING GNPS AND NUCLEIC ACID LOADING 78
2.1 Introduction 78
2.2 Materials and Methods 82
2.2.1 Preparation and characterization of gelatin nanoparticles. 82
2.2.2 DNA loading onto gelatin nanoparticles. 83
2.2.3 Turbidity, URT and density measurements. 84
2.3 Results and Discussion 85
2.3.1 Particle size and concentration evaluation. 85
2.3.2 Determination and evaluation of ODN loading onto GNPs. 91
2.4 Conclusions 97
3. EVALUATING SALTS OF THE HOFMEISTER SERIES REGARDING THEIR IMPACT ON GNP PARTICLE SIZE ALTERATION AND INITIAL IMMUNOSTIMULATORY TRIALS 99
3.1 Introduction and objectives 99
3.2 Materials and Methods: 100
3.2.1 Deviations in GNP preparation from the standard protocol 101
3.2.2 Methods regarding Hofmeister series 101
3.3 Results and Discussion 102
3.4 Conclusion 109
4. IMAGING TECHNIQUES FOR NANOCARRIERS 110
4.1 Survey on options to track nanoparticle biodistribution 110
4.2 Materials and Methods 113
4.2.1 Preparation and characterization of PEGylated gelatin nanoparticles 113
4.2.1.1 Preparation of PEGylated gelatin nanoparticles 113
4.2.1.2 Characterization of PEGylated gelatin nanoparticles via PEG assay 113
4.2.2 Preparation and characterization of PEGylated and glycine-linked GNPs 114
4.2.2.1 Preparation of PEGylated and glycine-linked GNPs 114
4.2.2.2 Characterization of PEGylated and glycine-linked gelatin nanoparticles via TNBS assay 115
4.2.3 Preparation of DOTA- and RGD-linked radio labeled gelatin nanoparticles 116
4.2.4 Preparation of Alexa 633 and ^{111}In-labeled gelatin in solution 117
4.2.5 Biodistribution study via non-invasive positron emission tomography (PET) 118
4.2.6 Conventional biodistribution study via γ counter 118
4.2.7 Confocal laser scanning microscopy (CLSM) of tumor tissue 119
4.3 Result and Discussion 119
4.3.1 The impact of particle size and concentration on biodistribution 119
4.3.2 Quantification of PEGylated gelatin nanoparticles via PEG assay 120
4.3.3 Quantification of PEGylated and glycine-linked gelatin nanoparticles via TNBS assay 123
4.3.4 In vivo and ex vivo studies of s.c.-administered modified GNPs 124

4.3.4.1 Biodistribution study via non-invasive positron emission tomography (PET) 125
4.3.4.2 Conventional biodistribution study via γ counter 126
4.3.4.3 Confocal laser scanning microscopy (CLSM) of tumor tissue 128
4.3.5 In vivo and ex vivo studies of i.v.-administrated plain and PEGylated GNPs 129
4.3.6 Differentiation of biodistribution profiles of soluble gelatin in from GNPs: particles matter. 132

IV GELATIN NANOPARTICLES AS A VALUABLE TOOL IN IMMUNOTHERAPY 135

1. IMMUNOTHERAPY BY NUCLEIC ACIDS – WHY? 135
1.1 Historical perspective 135
1.2 The principle of CpG-mediated immunostimmulation 135
1.3 Other nucleic acid-derived therapeutic strategies 137
1.4 Nucleic acid-based immunotherapeutic strategies against cancer 138
2. ANTITUMORAL RESPONSE TRIGGERED BY GNP-BOUND RNA TO AGONIST TLR7 138
Introduction 139
Materials and Methods 141
Mice 141
Reagents and cell lines 141
Preparation of cationized gelatin nanoparticles 141
Bone marrow cell culture 142
Fluorescence microscopy 142
Quantification of cytokines and flow cytometric analyses 143
Induction of OVA-specific CD8 T cell proliferation 143
Immunization with OVA 144
Tumor monitoring 144
Statistics 144
Results 144
Nanoparticle-delivered RNA oligonucleotides efficiently trigger an innate immune response 144
Nanoparticle formulation of immunostimulatory RNA oligonucleotides promotes their uptake into intracellular compartments 146
Nanoparticle formulation protects immunostimulatory RNA oligonucleotides from degradation by RNases 148
Nanoparticle-bound RNA oligonucleotides trigger antigen-specific CD8 T cell and antibody responses 149
Nanoparticle-bound RNA oligonucleotides induce an efficient antitumoral response .. 149
Discussion and outlook 151
3. IN VITRO EFFECTS OF CPG OLIGODEOXYNUCLEOTIDES DELIVERED BY GELATIN NANOPARTICLES ON CANINE PERIPHERAL BLOOD MONONUCLEAR CELLS OF ATOPIC AND HEALTHY DOGS 154
3.1 Introduction 154
3.2 Material and methods 156

3.2.1 Animals 156
3.2.2 CpG sequence 157
3.2.3 Preparation of GNPs 157
3.2.4 ODN loading of Cationized GNP 157
3.2.5 Blood sampling and PBMC isolation 158
3.2.6 Monitoring CpG-GNP uptake by cultured PBMCs of healthy dogs 158
3.2.7 PBMC cultivation and immunostimulation 159
3.2.8 Quantification of cytokines 160
3.2.9 Statistical Analysis 162
3.3 Results 162
3.3.1 Formulation quality control 162
3.3.2 CpG-GNP uptake by cultured PBMCs of healthy dogs 163
3.3.3 Cytokine quantification 163
3.4 Discussion 169
4. NUCLEIC ACID-BASED IMMUNOTHERAPY AGAINST HYPERSENSITIVITY – PREFORMULATION STUDIES FOR AN INHALATIVE CPG-GNP FORMULATION FOR RAO THERAPY IN HORSES 173
4.1 Recent developments in nanoparticle administration by inhalation 173
4.2 Materials and Methods 176
4.2.1 Materials 176
4.2.2 Preparation of the CpG-GNPs 176
4.2.3 Determination of nanoparticle properties and dispersion viscosity 177
4.2.4 GNP aerosolization 177
4.2.5 Droplet size analysis 179
4.2.6 Deposition study 179
4.2.7 Cell culture and immunostimulation 180
4.3 Results 182
4.3.1 Particle characterization upon nebulization by pMDI and VM-devices 182
4.3.2 Nebulization efficiency of VM-devices 184
4.3.3 Output rates of VM-devices 185
4.3.4 Consistency of concentration after nebulization 185
4.3.5 Aerosol particle size characterization 185
4.3.6 Deposition study 186
4.3.7 Stimulation of IL-10 release in vitro 187
4.4 Discussion 188
4.5 Conclusion 191
5. IMMUNOSTIMULATION OF BRONCHOALVEOLAR LAVAGE CELLS FROM RECURRENT AIRWAY OBSTRUCTION-AFFECTED HORSES BY DIFFERENT CPG-CLASSES BOUND TO GELATIN NANOPARTICLES 193
5.1 The significance of RAO and the potential of CpG immunotherapy in horses 193
5.2 Materials and methods 195
5.2.1 Horses and physical lung examination 195
5.2.2 Oligodeoxynucleotides 195

5.2.3 Preparation of ODN loaded GNP ... 196
5.2.4 Preparation of cells and cell culture ... 196
5.2.5 Immunostimulation by ODN and cytokine quantification (ELISA) ... 197
5.2.6 Cell viability by MTT-assay ... 197
5.2.7 Statistical analysis ... 198
5.3 Results ... 198
5.3.1 Quality control and formulation study of CpG-GNP ... 198
5.3.2 Cytokine release in cell culture upon stimulation by CpG/CpG-GNP ... 198
5.3.2.1 IL-10 release ... 198
5.3.2.2 IL-4 release ... 200
5.3.2.3 IFN-γ release ... 202
5.3.3 MTT assay ... 203
5.4 Discussion ... 205
6. A NEBULIZED GELATIN NANOPARTICLE-BASED CPG FORMULATION IS EFFECTIVE IN IMMUNOTHERAPY OF ALLERGIC HORSES. ... 210
6.1 Introduction ... 210
6.2 Materials and methods ... 211
6.2.1 Nanoparticle production and loading. ... 211
6.2.2 Oligodeoxynucleotides. ... 211
6.2.3 CpG-GNP formulation. ... 212
6.2.4 Nebulization. ... 212
6.2.5 Clinical examination and lung scoring. ... 213
6.2.6 Cell culture and in vitro cytokine quantification. ... 214
6.2.7 Statistical analysis. ... 215
6.3 Results and Discussion ... 215
6.3.1 Tracking the regimen's therapeutic effect in vitro ... 215
6.3.2 Therapeutic effect on cytokine level in vivo ... 216
6.3.3 Curative effectiveness of the GNP-based formulation ... 218
6.4 Conclusion ... 221

V FINAL CONCLUSION AND OUTLOOK ... 223

1. ENHANCED PRODUCTION OPPORTUNITIES ... 223
2. ANALYTICS ... 223
3. IMMUNOTHERAPY ... 224
3.1 Adjuvant cancer immunotherapy ... 224
3.2 Immunomodulative effectiveness of GNP-bound CpG-ODN in a preclinical canine study ... 224
3.3 Immunomodulative therapy of RAO horses – preliminary clinical trial ... 224
3.4 Outlook on further planned clinical studies on RAO ... 225
4. OUTLOOK ON THE PERSPECTIVE OF NANOPARTICLES IN NANOMEDICINE ... 226

VI REFERENCES……229

VII APPENDIX……251

LIST OF ABBREVIATONS

A	
ACS	American Cancer Society
AmV	automated mircoviscosimeter
API	active pharmaceutical ingredient
B	
BAL	bronchoalveolar lavage
BALF	bronchoalveolar lavage fluid
C	
°C	degree(s) Celsius
CAS	chemical abstracts service
CD	cluster of differentiation
CD8+	cytotoxic T cell
CFC	chlorofluorocarbon
CLSM	confocal laser scanning microscopy
cm	centimeter(s)
COB	chronic obstructive bronchitis
CpG	cytosine phosphate guanine
D	
Da	dalton(s)
DLS	dynamic light scattering
DMSO	dimethyl sulfoxide
DNA	deoxyribonucleic acid
DOTA	1,4,7,10-tetraazacyclododecane-1,4,7,10-tetraacetic acid
DPI	dry powder inhaler
E	
EDC	1-ethyl-3-(3-dimethylaminopropyl) carbodiimide hydrochloride
ELISA	enzyme-linked immunosorbent assay
EMEA	European Medicines Agency
EPR	enhanced permeability and retention
F	
FDA	Food and Drug Administration
Fig.	Figure
FPF	fine particle fraction
G	
g	acceleration of gravity
g	gram(s)
GNP	gelatin nanoparticle(s)
H	
HEPES	4-(2-hydroxyethyl)-1-piperazineethanesulfonic acid
HPW	high purified water

HFA	hydrofluoroalkane
I	
IEP	isoelectric point
IFN	interferon
IL	interleukin
i.v.	intravenous
K	
kDa	kilodalton(s)
M	
M	molar
min	minute(s)
mg	milligram(s)
ml	milliliter(s)
µl	microliter(s)
µm	micrometer(s)
MMAD	mass median aerodynamic diameter
MPS	mononuclear phagocytotic system
mS	millisiemens
MTT	3-(4,5-Dimethylthiazol-2-yl)-2,5-diphenyltetrazolium bromide
mV	millivolt(s)
N	
NCS	isothiocyanate
NE	nebulization efficiency
nm	nanometer(s)
NP	nanoparticle
P	
PAMP	pathogen-associated molecular patters
PBS	phosphate buffered saline
PdI/PDI	polydispersity index
PEG	poly(ethylene glycol)
PET	positron emission tomography
pg	pictogram(s)
PLA	poly(lactic acid)
PLGA	poly(lactic co-glycolic acid)
pMDI	pressured metered dose inhaler
pmol	picomole(s)
PRR	pattern recognition receptor
R	
RAO	recurrent airway obstruction
PdI	polydispersity index
RF	respirable fraction
RGD	arginine-glycine-aspartic acid
rhTG	recombinant human transglutaminase
rpm	revolutions per minute

S

s.c.	subcutaneous

T

Tab.	Table
TG	transglutaminase
TLR	Toll-like receptor
TNBS	2,4,6-trinitrobenzene sulfonic acid
T-reg	CD4+ CD25+ T regulatory cell

V

VM	vibrating mes

I General Introduction

1. On the art of drug delivery by nanotechnology

1.1 The aim of this thesis

"*Fortiter in re, suaviter in modo*": What Jesuit general Claudio Aquaviva[1] coined over 400 years ago with a metaphysic vision in mind can be directly transferred to the prime goal of drug delivery nowadays: going ambitiously for the target, but doing it in a smart and balanced way. Within this thesis, the "modo", the kind of "magic bullets" (Paul Ehrlich) to target only the illness without harming the host, is carried out by gelatin nanoparticles (GNPs). Key applications of the delivery system GNPs as a whole were addressed and extensively and comprehensively assessed. Already established uses could be further strengthened leading to recommendations for future employments of this promising tool. Some applications were found to be less beneficial than other obtainable means being of current interest in nanotechnology research and development. Therefore, a contribution to a more success-orientated use by avoiding future less promising GNP applications was performed. Finally, completely new insights were gained in some basic research aspects of formulation and in new fields of administration as well as a considerable broadening in the recipient species from mice up to dogs and horses was a mayor success.

The main mechanistic amendment to the scientific field of GNP application was performed by the introduction of an antiallergic immunomodulatory therapy through so called Cytosine phosphodiester guanidine (CpG) oligonucleotides. Contrasting the original pursuit to boost immune response by CpG or more recently by RNA analogs towards undesired structures such as tumors –or in other groups infectious specimens- it was possible to introduce GNPs as a crucial device in CpG delivery in down regulating immune responses. This was shown to be beneficial in events of hypersensitivity such as canine atopic dermatitis *in vitro* and equine recurrent airway obstruction (RAO) *in vitro* and *in vivo*.

---

[1] Raffaele Aurini, *Acquaviva d'Aragona Claudio*, in *Dizionario bibliografico della Gente d'Abruzzo*, vol. III, Teramo, Ars et Labor, 1958, e in nuova edizione ampliata, a cura di Fausto Eugeni, Luigi Ponziani, Marcello Sgattoni, Colledara, Andromeda editrice, 2002, vol. III, pp.55-62

1.2 Why nanotechnology for drug delivery?

The development of delivery devices featuring high accuracy, safety and efficiency remains a main challenge towards directed drug delivery. Nanotechnology has been a key driving factor in the past decades' publication activity started by Speiser and coworkers (Marty et al. 1978). Altogether, nanoparticles – generally defined as a colloidal system featuring solid particles sized 1- 1000 nm (Kreuter 1983) – emerged as a frequent key term in publications to include patents (Fig. 1a).

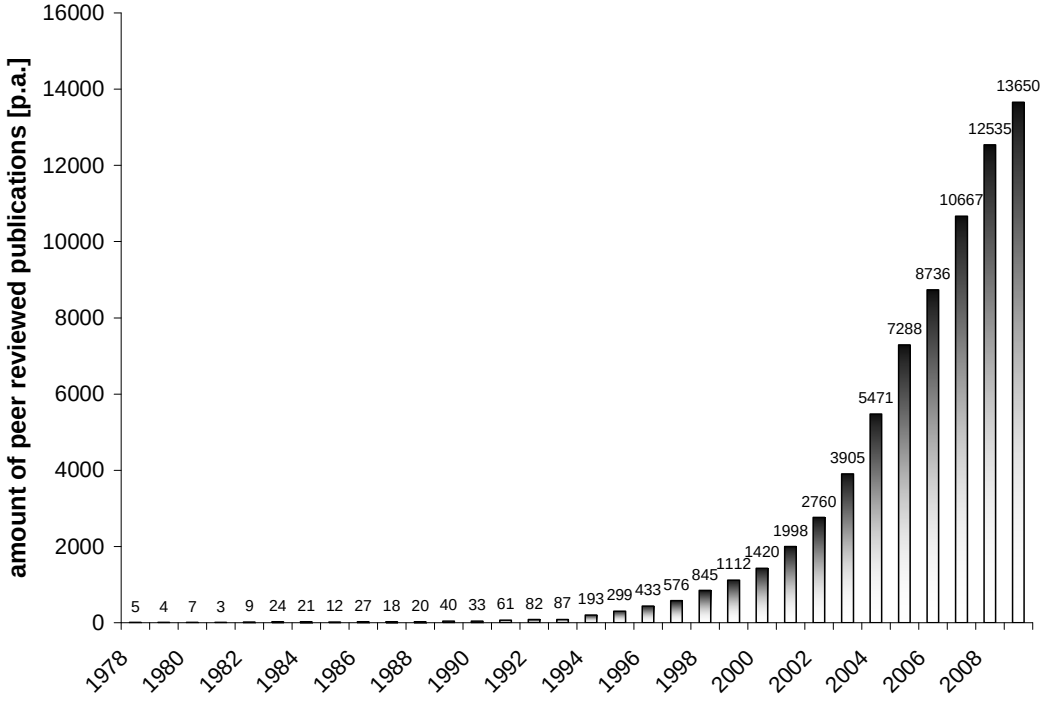

Fig. 1a: *Amount of peer-reviewed publications on nanoparticles in general per indicated year.*

They cover all fields of material science related to engineering, physics and medicine. Within the term "nanoparticles", the topic drug delivery accounted for up to 1.5% of the combined search hits "nanoparticle" and "drug delivery" in 2008 as per CAS's SciFinder database of bibliographic information (Fig. 1b). The still strengthening scientific output can be followed by these numbers of publications. In parallel, the number of published articles on the term nanomedicine increased clearly resulting from the considerable drug-delivery

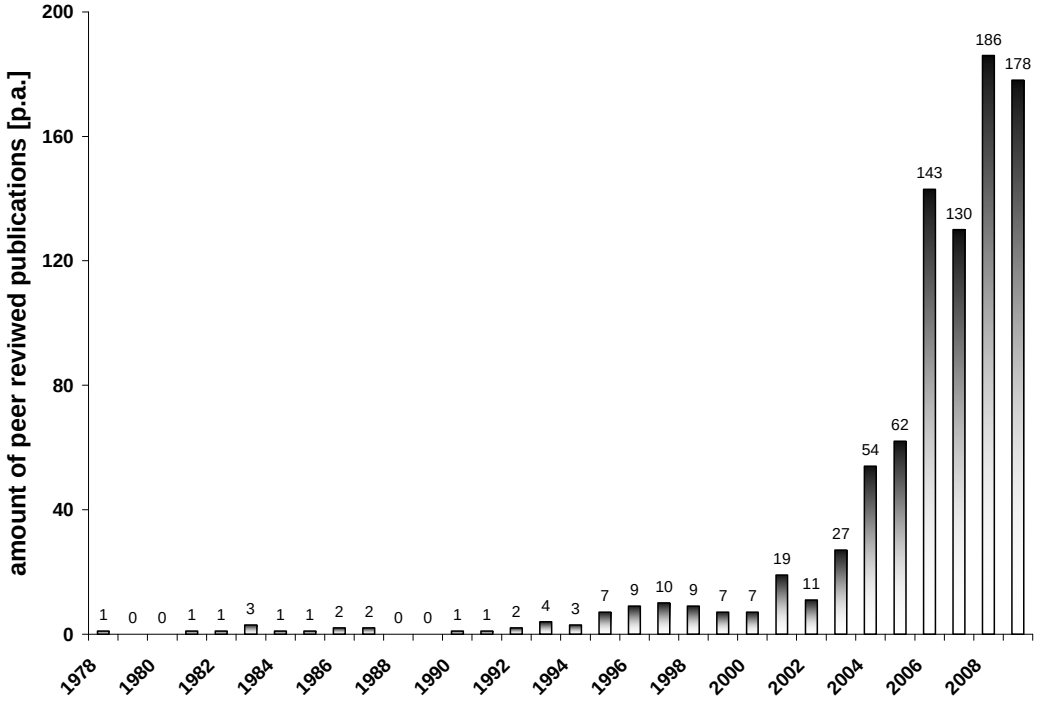

Fig. 1b: *Amount of peer-reviewed publications on nanoparticles in drug delivery per indicated year.*

aspect of nanotechnology (Fig. 1c). As a sub discipline, nanomedicine emerged combining fields of medicine, pharmaceutical technology, chemical analytics and material science. This shall enable the creation of a potent market for nanotechnology-enabled drug delivery which is projected to reach $26 billion by 2012 with high two-digit annual growth rates[2].

According to the European Science Foundation's "Forward Look on Nanomedicine", Nanomedicine is characterized as depending on complex systems in nanometer scale consisting of at least two components. One component is the active pharmaceutical part and the other is related to support or boost the special function in diagnosing, treating or preventing a disease, injury or pain (Duncan 2000; Duncan et al. 2006; Duncan 2006; Lehr 2007).

Within nanomedicine, the drug delivery sector dominates with 70% of total sales, 76% of issued scientific publications and 59% of granted patents (Gurusamy 2007).

[2] http://www.marketresearch.com/product/display.asp?productid=1692509&SID=30048100-474535314-495102710&kw=Nanoparticle%09Drug%09Delivery%09Markets, 20-Apr-10

So why is nanotechnology in drug delivery a worthwhile option? Traditional small molecule drugs (SMD) are frequently formulated as a solid dosage form and administered orally. However, the new driving forces e.g. in cancer and anti-autoimmune diseases therapies belong to the biologicals' field which is in most cases subjected to non-oral administration. Biologicals are mostly protein therapeutics like antibodies, vaccines or cell growth factors which as a group constitute the most rapidly increasing categories of drugs accounting for 10.9% of

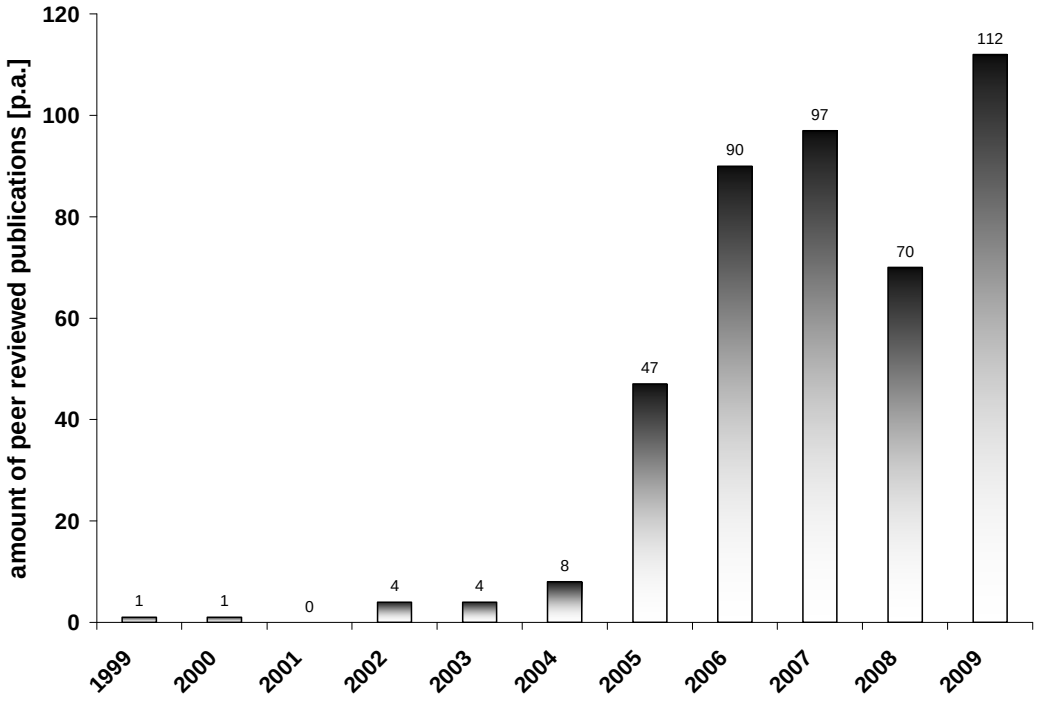

Fig. 1c: *Amount of peer-reviewed publications on nanomedicine per indicated year.*

global therapeutics' growth in the past five years (Yang et al. 2009). Moreover, according to the "Autoimmune Market Forecast to 2014"[3] all over biological sales are projected to hit $55 billion by 2014. Further developments look at the introduction of more therapeutic proteins, peptides, plasmids or oligonucleotides as drug substances that require a multitude of special formulations (Allen and Cullis 2004; Solaro et al. 2010). This demand for suitable carrier systems will significantly increase to eventually enable drugs to be reasonably employed clinically. Additionally, packing existent SMDs into nanocarriers was investigated as an attractive method to improve their biocompatibility, bioavailability and

[3] http://biotechconnection.com/p=3, 20-Apr-10

safety (Debbage 2009) and therefore improve the therapeutic index of already introduced drugs (Allen and Cullis 2004). This is due to the fact that increasing SMD dosage translates into higher possible toxic effects once the drug encounters normal cells in contrast to the target. Especially for potent anticancer agents, this issue gets more and more addressed. These ideal carriers should prevent the eventually sensitive drug from early enzymatic or pH-associated degradation, prolong half life, reduce dosing and consequently lead to less side effects (Torchilin 2007). Moreover, such devices are intended to deliver the drug payload exclusively to the site of disease which is referred here to as “targeting” coming close to Paul Ehrlich’s magic bullets (Debbage 2009). Especially in the field of DNA-based and small interference RNA (siRNA)-based therapeutic attempts such as gene therapy, viral vectors were considered the ideal targeting shell (Reischl and Zimmer 2009). However, fundamental problems related to toxicity, immunogenicity and large-scale production justified the development of non-viral vectors in the nanometer range with individual passive or active targeting abilities (Mintzer and Simanek 2009).

To enable these tasks, multifunctional nanoparticles that carry the therapeutic or imaging payload and possess biological surface modifiers such as targeting moieties or simply polyethyleneglycole (PEG) for unspecific targeting have been proposed. The latter is attributed to the concept that hydrophilization of particle surfaces (Storm 1995, (Brannon-Peppas et al. 2007) results in longer circulation times after i.v. administration hence increasing the chance to find the target. This is decisive as a failure of the drug in reaching the target constitutes a failure of the whole therapy (Debbage 2009).

2. Overview on starting materials and production methods

2.1 Established non-proteineous starting materials

Nanoparticulate systems such as solid spheres, micellar emulsions and liposomes relied on a variety of starting materials. For the former, several biocompatible and partly biodegradable macromolecules obtained attention. Conventional synthetic macromolecules were among the first used and comprised as prototypes poly(lactid acid) (PLA), poly(lactic-coglycolic acid) (PLGA) (Park et al. 2009) and poly(cyano acrylate) (Diepold et al. 1989). Particularly the latter was early investigated for drug loading and intracellular endosomal localization (Couvreur et al. 1979). Furthermore, polyelectrolytes such as poly(ethylenimine) PEI-based polyplexes demonstrated their non-viral gene delivery potential (Gharwan et al. 2003) while related toxicological issues were addressed (Zintchenko et al. 2008). Other coated nanoparticles based on cationic polyplexes exhibited tunable tissue targeting for specific gene delivery (Harris et al. 2010). Among the polysaccharides, chitosan was investigated as a suitable nanoparticle basic material to carry proteins (Amidi et al. 2006), cytotoxic agents (Janes et al. 2001) or DNA-based drugs (Bernkop-Schnuerch et al. 2006). Metal nanoparticles constitute another class as inert but not biodegradable carriers e.g. for anti-cancer drug delivery (Brown et al. 2010) or magnetic targeting or imaging (Smith et al. 2010). Lipids are mostly employed for gene delivery as lipoplexes (Koh et al. 2010) but also as solid-lipid nanoparticles for diverse parenteral applications (Joshi and Mueller 2009).

2.2 Proteins as constitutive material for nanoparticles

A main advantage of proteins compared to synthetic polymer-based systems is their frequent compatibility with biologic systems and their general biodegradability (Wang and Uludag 2008). Furthermore, by their nature they offer a multitude of moieties accessible to modifications to tailor drug-binding, imaging or targeting entities. Safety concerns may arise from folding pattern-derived immunogenicity or from contamination with transmissible diseases. The latter can be ruled out by a careful choice of source such as natural material that went through intensive processing under aseptic conditions or the use of recombinant material.

2.2.1 **Albumin**

The blood transporter protein human serum albumin (HSA) probably is one of the most recognized and intensively investigated proteineous starting materials, today from recombinant offspring. Beyond research and development, two HSA-based products successfully entered the market, Abraxane™ and Albunex™ (Wang and Uludag 2008). However, they both do not constitute a nanoparticulate formulation which is defined as a colloidal system of solid discrete and continuously shaped integrative particles in the lower nanometer range. Albunex provides clinical benefits and was on the market already since 15 years without implications of immunogenicity (Christiansen et al. 1994).

It is an ultrasound contrast agent consisting of a slowly diffusing gas C3F6 encapsulated by an elastic HSA shell (Postema and Schmitz 2007). Therefore, it constitutes a well studied microbubble formulation (MacDonald et al. 2004) with an average "particle" size of 3 – 5 µm (Barnhart et al. 1990). Recent promising development strategies of mircobubbles comprised drug targeting such as for doxorubicin for antitumor therapy (Tinkov et al. 2010) or the prospect of local gene therapy (Frenkel and Li 2006).

Abranxane is a self-assembling nanoagglomerate (Xiao et al. 2009) of HSA and paclitaxel produced by high-pressure homogenization (Moreno-Aspitia and Perez 2005). Resulting sizes account for about 130 nm. Originally designed as a biocompatible formulation without irritating polyethylated castor oil and polysorbate against metastatic breast cancer (Gradishar et al. 2005; Harries et al. 2005), it was meanwhile preclinically evaluated for other anti-cancer employments (Xiao et al. 2009).

As starting material for colloidal nanoparticles, HSA served in several *in vitro* (Kissel and Roser 1991) and *in vivo* studies such as to antibody-mediated target leukemic cells and primary T-lymphocytes (Dinauer et al. 2005) or to be delivered to neurons by Apo E mediated transcytosis (Zensi et al. 2009), respectively. Although albumin is not immunogenic per se, cross-linked particles can enhance the immunogenicity of antigens loaded onto these hapten-acting particles. For instance, anti-ibuprofen antibodies are gained by albumin particle-bound ibuprofen to develop ELISAs (Grafe and Hoffmann 2000).

2.2.2 **Legumine, gliadine, elastinlike polypeptide, β-galactoglobulin, silk**

Other proteins used for nanoparticle production were plant-derived such as legumin and gliadin (Wang and Uludag 2008). The latter is a lipophilic protein with a low aqueous solubility. When preparing nanoparticles from this starting material, loading capacities do largely depend on the hydrophobicity of the agent such as vitamin E (Duclairoir et al. 2003). More studies were conducted on protamine which -as a cationic protein- exhibited capabilities for promising immunostimulatory DNA or basic fibroblast growth factor (FGF2) transport (Mori et al. 2010). Moreover, it exhibited size-tuning properties when employed in the form of different salts in HSA nanoparticle production (Mayer et al. 2005). Particles of tunable size were also produced from denatured whey protein by pH-cycling treatment (Giroux et al. 2010). As an environment-responsive basic proteineous material, elastinlike polypeptide (ELP) was examined (Fujita et al. 2009). Its special feature is the reversible response to thermal change which exhibits a soluble state below and a solid state above the transition temperature (Maham et al. 2009). In the latter state, sticking to target tissues is possible. The substance is biodegradable and proofed tumor accumulation in an *in vivo* model (Liu et al. 2006). It holds promises to carry lipophilic drugs but attention must be paid to the critical temperature at which the particles start to form aggregates *in vivo* (Fujita et al. 2009).

Globular proteins were used to associate with anionic polysaccharides to form particulate structures in the nanometer scale as potential delivery devices (Jones et al. 2010). Therefore, β-galactoglobulin was thermally treated for conformation changes, pH-adjusted and mixed with a pectin solution to form particles of discrete size properties.

A rather new starting material of natural origin is silk protein (Zhang et al. 2007). Delivery of DNA was successfully reported for gene transfer *in vitro* (Numata et al. 2009). Furthermore, formulation studies revealed interesting results such as a sustained release and enhanced insulin stability when the covalently silk protein-bound insulin was challenged with gastric trypsin (Kundu et al. 2010). Others reported successful sustained release of VEGF (Yan et al. 2009). However, advanced employment of this subtype of protein nanoparticles is not at hand at present although successful robust salting-out production method was reported recently (Lammel et al. 2010).

2.2.3 **Gelatin**

Ongoing research interest was conceded to gelatin over the last years (Young et al. 2005b) for several reasons. Gelatin is a natural polymer derived from collagen recognized as a biodegradable and biocompatible starting material being in use as plasma expander for decades (Ward et al. 1977b). The natural source of gelatin is from animals. It is obtained mainly by acidic or alkaline, but also thermal or enzymatic degradation of the collagen. Collagen forms 30% of all vertebrate body protein with a majority in bone and skin. More than 90% of the extra cellular protein in the tendon and bone and more than 50% protein in the skin consist of collagen (Friess 1998). The high stability bases on the unique triple-helix structure consisting of three polypeptide α-chains. So far 27 collagen types have been isolated so far (Brinckmann et al. 2005), however, collagen type I (skin, tendon, bone), type II (hyaline vessels) and type III are used for the production of gelatin only (Babel 1996).

Gelatin type A (**a**cid), which is obtained from porcine skin with acidic pre-treatment prior to the extraction process, can be distinguished from type B (**b**asic), that is extracted from ossein and cut hide split from bovine origin. Here an alkaline process, also known as “liming” is applied. Amide groups of asparagine and glutamine are hydrolyzed into carboxyl groups during this process, therefore many of the residues are converted to aspartate and glutamate (Young et al. 2005; Tabata and Ikada 1998). As a result, the isoelectric point (IEP) of type B gelatin is not at pH 9.0 like type A and collagen itself, but the higher number of carboxyl groups per molecule reduces the IEP to pH 5.0.

While gelatin and the delivery systems based on this polymer are biocompatible and biodegradable without toxic degradation products (Tabata and Ikada 1998; Kawai et al. 2000; Yamamoto et al. 2001; Ward et al. 1977), they are since a long time known for high physiological tolerance and low immunogenicity. The overall beneficial properties of gelatin contributed to its proven record of safety as food supplement which is also documented by the classification as “Generally Recognized as Safe” (GRAS) by the US Food and Drug Administration (FDA). Moreover, intravenously administered applications like plasma expanders (e.g. Gelafundin™, Gelafusal™) consist of gelatin derivatives. Other uses of gelatin include sealants for vascular prostheses (Kuijpers et al. 2000). Furthermore, due to its biodegradeability molecular weight is not restricted to 40 kDa for renal

elimination. Hence, the larger particles build a suitable platform for numerous structural potential modifications on the surface coupled to the many accessible functional groups. Lysine provides accessible prime amino groups e.g. for crosslinking and marker coupling as described in due course.

Nanoparticles prepared by a two step desolvation technique and subsequent chemical cross-linking (Coester et al. 2000) maintained their non-toxic properties while featuring a higher storage stability than liposomal liquid formulations and good *in vivo* stability upon administration (Coester et al. 2006). Although no undesired effects which could be attributed to GNPs were observed *in vitro* or *in vivo*, two issues are worth being discussed: safety of the starting material gelatin and secondly safety of the chemical particle cross-linking by glutaraldehyde. The unlikelihood of transmittable diseases to endure the collagen processing steps was evaluated in the peak-time of the mad cow disease. To rule out this matter completely, gelatin of porcine origin was used in many studies throughout. Although not reported for this gelatin offspring, immunogenicity is a possible point to consider with all protein formulations. Replacing animal-derived gelatin by recombinant human gelatin did not result in different serum chemistry parameters in humans (Won and Kim 2009). Furthermore, no overall significant benefit related to *in vitro* cell viability is gained when animal-derived gelatin is replaced by rHG and glutaraldehyde by genipin (Won and Kim 2009). Other concerns included the potential reactivity of imines resulting from the glutaraldehyde cross-linking. However, a chemical reduction of the imines to imides did not result in a higher stability of GNPs (see III.2). Furthermore, a complete removal of GA by repeated purifications steps in the production of GA-cross-linked GNPs was the most probable reason for non-toxicity. Due to many years of safe experience with glutaraldehyde both *in vitro* and *in vivo*, at present additional costs are not justified by the potential advances. Nevertheless, promising alternatives to glutaraldehyde to facilitate possible human applications in future are at hand. Recently, we reported suitable process conditions in which recombinant transglutaminase effectively cross-linked GNPs (Fuchs et al. 2010). Optimum size and size distributions comparable to those cross-linked by glutaraldehyde were received and suitable storage stability was proven. While the possible therapeutic applications are discussed later in detail, it is worth to be mentioned that the gelatin matrix with diverse moieties facilitates the surface

decoration with targeting functions such as antibodies (Balthasar et al. 2005). Furthermore, GNPs allowed a matrix loading even with proteins like insulin which was evaluated recently (Ofokansi et al. 2010).

2.3 Preparation methods of protein nanoparticles

2.3.1 Coacervation process

Due to relatively mild conditions the coacervation or equally coined desolvation process turned out to be the most appropriate and frequent method to prepare protein-based nanoparticles. In brief, a colloidal system is created when the solvent in which the protein was initially dissolved is gradually extracted into an anti-solvent phase. Thereby a phase separation occures which results in a phase of solid colloid dispersed in a second phase consisting of the anti-solvent and the initial solvent (Weber et al. 2000). Consequently, solvent and anti-solvent must be miscible such as water as solvent and ethanol or acetone as anti-solvent whereof the latter was often used to produce GNPs by a two step desolvation technique (Coester et al. 2000; Langer et al. 2003). While a stable size is reached after an initial process period the further addition of anti-solvent leads to increased particles yield in the course of desolvation (Weber et al. 2000). Furthermore, the pH value of the protein solution prior to desolvation has an impact on the resulting particle size and yield due to higher probability of protein coacervation at net-zero surface charge at the isoelectric point. This was observed for particles derived from gelatin, HSA, BSA and β-lactoglobulin (Coester et al. 2000; Ko and Gunasekaran 2006; Langer et al. 2003) To stabilize colloidal nanoparticles by establishing covalent bonds between prime NH_2-groups by chemical cross-linkers such as glutaraldehyde or glyoxal were widely employed without negative side effects (Weber et al. 2000). As the carcinogenic properties of free glutaraldehyde is a known issue, methods like high-temperature cross-linking (Chen et al. 1994) or macromolecular cross-linking (Lin et al. 1994) were discussed but imply the risk of harming possible drug load. Therefore, we currently investigate the possibility of enzymatic cross-linking of protein nanoparticles.

2.3.2 **Solvent extraction or emulsion process**

Adopting the emulsification and solvent extraction methods from synthetic polymer-based nanoparticle production to proteins as a starting material, the latter needs to be present in solution in an aqueous buffer. By adding an anti-solvent, a W/O emulsion is prepared from which nanoparticles are received after solvent and anti-solvent removal. A double emulsion technique involving W/O/W emulsions allows encapsulation of proteins and hydrophilic drugs (Sussman et al. 2007). In general, the method lacks from relatively large particle sizes which were reported between 100 - 800 nm for BSA nanoparticles depending on protein concentration and solvent to non-solvent ratio (Mishra et al. 2006). On the other hand, high encapsulation rates were achieved (Chawla and Amiji 2002).

2.3.3 **Salt precipitation**

The salting out method proteins was described e.g. for HAS as a simple method to gain protein aggregates and eventually nanoparticles (Coester 2000). Proteins with therapeutic properties can be transferred into nanoparticles without the need of further particulate auxiliary particles. Therefore, the protein gets cross-linked with multivalent ions (Yang et al. 2009).

However, this method retains the risk of changed bioactivity and lost conformation which is more an issue when therapeutic proteins are involved like insulin (Fan et al. 2006) compared to proteins with solely carrier functions (Coester et al. 2000). Reported higher heterogeneity in particle sizes makes this method inferior to above described (Wang and Uludag 2008).

3. The administration route

3.1 Intravenous application

Intravenous injection is the standard form of application for all delicate formulations that are intended to be bioavailable immediately and distribute to an otherwise difficult to reach pathologic part of the body.

Several obstacles exist that nanoparticles encounter once administered into the blood stream that a soluble SMD in comparison experiences to a lower degree.

The tasks can be abbreviated to four steps: the unspoiled navigation through the blood stream, the evasion of biological barriers, the site- or cell specific localization and finally the exclusive targeting of the biological pathway to treat the pathological condition the whole system was made for (Ferrari 2008). Intravascular application is immediately followed by quick dissemination as one pass in human circulation accounts for about 15 seconds. The chance that a drug reaches the target “en bloc” is thereby almost ruled out. SMDs can easier diffuse through membranes or around barriers while nanoparticles more easily get trapped. Furthermore, they have to escape the engulfment of the reticuloendothelian system (RES) also more recently known as the mononuclear phagocyte system (MPS) (Vonarbourg et al. 2006). This installation lowers blood concentrations even of anticipatory engineered nanoparticles to 5-10% after 8 hours compared to the initial dose (Gaur et al. 2000) and consequently lead to liver, spleen and lung accumulation (Ferrari 2005). PEGylation still is one of the major techniques said to counter fight early phagocytosis and prolong free circulation of nanoparticles (Gref et al. 2000; Vonarbourg et al. 2006). PEG was identified to lower opsonization by shielding effects. PEGylation mechanisms have been studied in detail to include the deshielding process once the carrier reached the pathological site (Romberg et al. 2008). In 1994, the first PEGylated protein therapeutic entered the market to be administrated systemically in contrast to SMANCS’s local application. Oncaspar® (PEGylated l-asparaginase) was used to treat acute lymphoblastic leukaemia (ALL). (Fuertges and Abuchowski 1990) It appeared to cause significantly less hypersensitivity reactions and showed more than fifteen fold higher blood residence times. The concept of nanoparticle PEGylation is later discussed in detail in chapter III.4.

Once the nanocarriers survived the MPS infringements, they have to evade the vessel via the endothelial cell barrier to include the subepithelial basement membrane, transverse the extra-cellular matrix and enter the target cell. The details of nanoaparticles' opportunities to enter cells is discussed comprehensively elsewhere (Hillaireau and Couvreur 2009). As mostly receptor mediated endocytosis occurs here, the nanoparticles get trapped in the endosomal-lysosomal intracellular compartment and are separated from the cytosol. As long as the target is not within the endosome, which is discussed later for toll-like-receptor targeting, endosomal escape is needed without any damage to the carried drug payload. Strategies included pH associated endosomal burst or the introduction of specific molecules like melittin (Meyer et al. 2007). The accessibility varies largely between single organs or just tissues. While the hepatocytes in the post-vascular space are immediately accessible, strong barriers towards the testis and the central nerve system are effectively protective (Debbage 2009). The permeation of the latter, the blood brain barrier (BBB) is a promising but challenging chapter of nanoparticulate targeting on its own (Zensi et al. 2009). Especially here, newly developed large molecule drugs like recombinant proteins depend on a carrier to get selective access to the brain. Gelatin and albumin-based nanocarriers demonstrated their capabilities when being modified by polysorbate-80 or apolipoprotein E (apoE) (Barbu et al. 2009). Polysorbate-80 increased the apoE concentration adsorbed to the nanoparticle surface which could subsequently make use of the LDL-receptor mediated endocytotic pathway to enter brain endothelial cells (Wong 2010). Direct coupling of apoE onto protein nanoparticle surface omitted the polysorbate-80 link and resulted in at least comparable therapeutic effects when a drug was delivered in a murine *in vivo* model (Michaelis et al. 2006). Others used surface-bound transferring to facilitate PEGylated albumin nanoparticles to target a drug substance to the brain (Mishra et al. 2006).

On the other hand, pathologic conditions can ease the accessibility for nanoparticles. For example, inflammation increases vascular permeability and thus endothelial barrier functions are reduced. The most prominent example was observed in tumors, where non-proliferating and non-fenestrated blood vessels with intact barrier properties get transformed into proliferating vessels featuring

fenestrated endothelium and thus reduced barrier properties (Roberts and Palade 1997). As fenestration can reach 200 – 600 nm gaps, transition of nanoparticles is facilitated. Additionally, reduced lymphatic drainage allows accumulation of entered material (Sharma and Sharma 2008) which together led to coining the phenomenon enhanced permeability and retention effect (EPR) (Matsumura and Maeda 1986). Yet, this effect is in concurrence with the still in place obstacles mentioned above.

Examples that successfully included this mechanism were long-circulating PEGylated liposomes (Torchilin 2005; Torchilin 2007).

However, if the target is within the MPS, an i.v. application is indicated. Recently, GNPs were shown to selectively deliver NF-κB inhibiting decoy oligonucleotides to liver resident macrophages (Kuppfer cells) after administration via the portal vain in male Sprangue-Dawley rats (Hoffmann 2006; Hoffmann et al. 2009). Within the Kupffer cells the intracellular targeting of the GNPs to the endosome could be proven by selective fluorescent staining of the carrier, the payload and the cellular compartment and subsequent CLSM analysis (Zillies 2007). Consequently, NF-kappaB activation was inhibited which resulted in an reduced liver injury in experimental fulminant hepatitis but conversely increased in an ischemia-reperfusion model (Hoffmann et al. 2009).

Besides the currently all absorbing delivery role as a passive drug carrier, nanoparticles might act as nanomedicine themselves (Ferrari 2008). Therefore, shape and size depending distribution and self-toxicity are detrimental (Decuzzi and Ferrari 2007). Consequently, nanoparticles which are toxic due to their basic material and which specifically address target cells could be used as chemotherapeutic. Size is a major determinant for circulation and specific cellular uptake properties but also shape is influential. Disk-like or hemispherical particles evade phagocytosis better than spherical ones and are more likely to adhere to endothelium (Geng et al. 2007). These properties might contribute to future cancer therapeutics acting by the virtue of outer form after i.v. administration.

3.2 Subcutaneous application

In contrast to the i.v. route, subcutaneous administration offers the feature of no rapid dissemination of the injected nanocarriers (Debbage 2009). Therefore, a depot effect can be achieved and the MPS is not an immediate threat. On the contrary, this route is just of advantage, if the system is known to be capable to the target this way. For example, targeting draining lymph nodes is by far easier than i.v. because a slow interstitial flow of 0.1-1 µm s^{-1} sweeps s.c. injected material towards the lymphatic capillaries in most tissues (Swartz 2001). Furthermore, the route of injection can have a crucial influence on the release of immunogenic and inflammatory cytokines. An illustrative example constitutes the use of CpG-oligonucleotides (CpG-ODNS) which serve as immunostimulatory adjuvants by addressing endosome-based Toll-Like Receptors 9 (TLR9) in antigen presenting cells with promising applications in cancer and allergy therapy (Krieg 2006). Intravenous injection of CpG-ODN could result in general immune stimulation with side effects such as spleen cirrhosis. On the contrary, s.c. administered GNP-bound CpG-ODN was not distributed systemically due to the locally restricted distribution and remained at the site of injection where phagocytosis by APCs occurred. As the latter migrated to the nearest lymph nod, a local yet potent immunization against an employed model antigen could be achieved by the CpG-ODN adjuvant there without the risk of systemic side effects such as a septic shock or immune responses against the carrier material gelatin. (Bourquin et al. 2008; Zwiorek 2006).

A heavily investigated field of new drugs that required advanced drug delivery systems is nucleotide-based therapeutics (Patil et al. 2005). A thought significant advantage of this class of therapeutics is their determined specific way of action once the target is related to a certain disease. Strategies include gene transfer, gene silencing or antisense therapy and selective immunostimulation. Gene silencing by siRNA for cancer therapy initiated a research cascade on suitable delivery strategies mostly administered locally (Ozpolat et al. 2009). The latter was boosted by the understanding of CPG-ODNs (Krieg 2006) witch are mostly administered subcutaneously. The same route is applicable to plasmid-based TLR agonists delivered by cationic liposomes (Dow 2008). However, due to some clinical drawbacks, promising trials on Dynavax (DeFrancesco 2008) and other anti-cancer ODN-based drugs (Schmidt 2007) lowered the speed towards market

approval by the regulatory bodies significantly. Nevertheless, encouraging information still comes from ongoing clinical trials on allergy to involve CpG-ODNs formulated with VLP drug delivery nanosystems (Senti et al. 2009).

The related importance of the immunomodulation by ODNs by impacting cytokine release profiles is stressed by the fact that this year's Paul Ehrlich prize was awarded to Charles Dinarello for his pioneering work on cytokines which holds great potential to further improve treatments[4]. Other groups focused on ODN and isRNA-based nucleosides as adjuvants delivery by GNPs to trigger controlled immune responses to model antigens such as Ovalbumine *in vivo*. Thereby, pre-immunized mice received model-antigen expressing tumors which were significantly reduced in size the course of the GNP-bound CpG therapy which led to longer survival rates, too (Bourquin et al. 2008; Zwiorek et al. 2008). The challenge of curing existent tumors in mice without any pretreatment is currently met which should reflect clinical therapeutic conditions in a more real manner.

3.3 Pulmonal application

The inhalative route constitutes a very attractive alternative to deliver API by nanoparticles both locally and systemically. Direct targeting of the therapeutic area of interest enables a reduction in administered drug amount compared to e.g. the oral or i.v. route (Vaughn et al. 2006) leading to reduced systemic side effects (Keller 1999). Investigated non-pressurized application systems cover dry powder inhalers (DPIs), pneumatic jet inhalers, ultrasound nebulizers and most recently vibrating mesh (VM) devices (Waldrep and Dhand 2008). Employed examples were polyacrylate nanoparticle-bound Salbutamol sulfate (Hadinoto *et al.* 2007), PLGA (Beck-Broichsitter et al. 2010) and Chitosan-NP-bound Insulin (Grenha *et al.* 2005). However, pure nanoparticle formulations cannot be delivered that way due to too small particle size (< 1µm) and resulting low lung deposition and likely exhalation (Sung *et al.* 2007). Therefore, excipients like micronized lactose are needed (Finlay *et al.* 2005). Hence, GNP aerosols were successfully formulated as DPI after spray drying loaded with a placebo drug (Sham *et al.* 2004).

[4]http://www.ucdenver.edu/about/newsroom/newsreleases/Pages/Dinarello%E2%80%99s%E2%80%9Cfevermolecule%E2%80%9DbreakthroughsearnEhrlichPrize.aspx

However, initial interest in the nanoparticle-pulmonal research focused on nanotoxicology as concerns arose on carcinogen properties of industrial combustive dusts. Furthermore, toxic properties of carbon nanotubes were intensively investigated in this context (Warheit 2009). Nevertheless, protein nanoparticles have to be considered less a toxicological issue due to biocompatibility and -especially- biodegradability. Besides branched polymers, GNPs were of considerable interest (Tseng et al. 2007). Tseng et al introduced jet-nebulized cisplatin loaded nanoparticles *in vivo* (Tseng et al. 2009). Chapter VI.4 of this thesis further examined the possibilities to nebulize GNPs either via pressurized metered dose inhalers or vibrating mesh (VM) devices. It could be clarified that VM devices are more suitable in creating GNP vapor to reach the deep airways and to deliver intact ODNs in order to perform local immunotherapy (Fuchs 2010). Based on these results, we moved to introduce the system *in vivo* for the first time in a veterinarian clinical study.

3.4 Oral application

The oral administration of protein-based nanoparticles remains challenging due to the proteolytic and acidic environment the formulation has to pass. Nevertheless, the route constitutes a worthy access due to the ease of application and the non-requirement of specific application devices. Delivering delicate drugs by protective nanoparticles is an obvious aim. Insulin as the presently most frequently parentally used drug substance consequently is a promising candidate. Ofokansi et al succeeded in developing a gelatin-based slow release formulation capable of surviving the harsh stomach conditions and received for this work the “CRS consumer and diversified products paper award” 2008, New York City, USA.

Also attempts to explore the possibilities of mucosal immunization via the oral route were conducted (Chadwick et al. 2010; Chadwick et al. 2010). Ovalbumine as a carrier protein for CpG-ODNs induced a Th1 polarized immune response with resulted in typical IFN-γ release and elevated IgG2a titers (Alignani et al. 2005).

To eliminate the risk of proteolytic degradation of protein-based carriers, they can further encapsulated in a protective resistant shell. These nanoparticle-in-microsphere oral systems (NiMOS) consisted of outer poly(epsilon-caprolactone)

microspheres of 8 – 30 µm which included 80 – 300 nm GNPs that were eligible for plasmid delivery (Chadwick et al. 2010; Bhavsar and Amiji 2007). Local transfection therapy was for instance proofed against inflammatory bowl disease in a murine *in vivo* model (Bhavsar and Amiji 2008).

II Formulation development of plain Gelatin Nanoparticles

1. Upscaling the established GNP production method

1.1 Rationale of the upscaling process

Upscaling is a common challenge in the biopharmaceutical development and production (Cacciuttolo and Arunakumari 2006). Motivations to engage this challenge include an effective decrease in unit costs as well as to satisfy a higher product demand e.g. if a product promotes from clinical to commercial manufacturing. Moreover, the prospect of fewer variations if the demand for one project is satisfied out of a large batch instead of several small ones often appears convincing. However, frequent challenges to overcome are the possible alteration of the product by changes in employed materials (surfaces), instruments (sheer forces), excipients (buffers, organic solvents) and cleaning strategies (Cacciuttolo and Arunakumari 2006). These considerations should be more and more applied on the still emerging field of targeted drug delivery devices.

The first GNP preparation methods lacked robustness in reproducibility and homogeneity of the produced particles (Oppenheim 1981). Gelatin as a biopolymer featured not only appealing properties like biocompatibility and low price but also a very high heterogeneity in terms of molecular weight distribution. Therefore, manufacturing of gelatin drug carrier systems of sufficient quality were not at hand until the two step desolvation technique was developed by Coester *et al*. Therein, a higher molecular weight fraction with a cut-off of roughly 65 kDa (Zwiorek 2006) was separated from a lower one during a first step, before the particles were formed in a second desolvation step. This protocol offered the possibility to produce homogeneous colloidal gelatin spheres which can easily be surface modified due to their variety of functional groups according to the different amino acids (Coester et al. 2000). Furthermore, this method allowed the employment of commercially available gelatin instead of special batches with a narrow MW distribution (Zwiorek 2006).

This advanced preparation method was established for a relatively small laboratory scale employing an initial mass of 1.25 g of gelatin per batch. In order to enlarge this process and the resulting particle yield, a series of upscaling

experiments up to ten-fold batch size was initiated. Based on the standard process parameters, the influence of various laboratory equipments was investigated and preliminary GNP stability tests were run. Furthermore, an evaporation step was introduced to cope with the large organic solvent volumes resulting from the upscaled desolvation process. Moreover, the amount of toxic glutaraldehyde that is finally used to crosslink the nanoparticles was halfed and the impact on particle integrity was examined. Finally, it was evaluated whether statistical correlations between the most important production parameters existed and a reciprocal interdependent network was established to make projections for further upscaling plans. As delivering nucleic acid-based therapeutics emerged as the driving factor for GNP employment, the related cationization as the prime particle surface modification deserved special attention. Therefore, the feasibility to cationize GNPs from upscaled batches was tracked likewise.

1.2 Materials and methods

1.2.1 Standard preparation of gelatin nanoparticles via two step desolvation technique

GNPs were prepared according to the original preparation method by dissolving 1.25 g of gelatin type A (Bloom 175, Sigma, Taufkirchen, Germany) in 23.75 g of 0.2 µm filtered (Acrodisc, Pall, Dreieich, Germany) high purified water (HPW) under gentle heating to 50 °C. Constant stirring (500 rpm) was maintained during the whole preparation procedure. A first desolvation step was initiated by the addition of 25 ml of acetone. After sedimentation of the precipitated gelatin fractions for about 20 s, the supernatant consisting of dispersed as well as dissolved gelatin was discarded. Then, the sediment was weighed and redissolved by the addition of 0.2 µm filtered HPW up to 25.0 g under heating to 50 °C. The pH (pH Meter MP 220, Mettler Toledo, Greifensee, Switzerland) was further adjusted to 2.5 with 2 M HCl. GNPs were formed *in situ* during a second desolvation step by drop wise addition of about 90 ml of acetone (3-5 ml/min) by a burette. After ten minutes, 175 µl of glutaraldehyde (25 %) were added to the reaction vessel, an Erlenmeyer flask, to crosslink the nanoparticles. Finally, after overnight stirring in an extractor hood, the particles were purified by two-fold centrifugation (19000 g for 18 min; Sigma Laborzentrifugen, Osterode,

Germany), redispersion in 0.2 µm filtered HPW and filtration through a 5 µm 0.2 µm filtered HPW rinsed filter (VWR, Fontenay sous Bois, France). The purified nanoparticles were stored as dispersion in HPW at 8 °C[1].

1.2.2 Scale-up of the gelatin nanoparticle standard preparation method

In order to scale up the GNP standard preparation method, the batch size was first doubled. Consequently, 2.50 g of gelatin type A (Bloom 175) were dissolved in 47.50 g of 0.2 µm filtered HPW. Accordingly, the volume of acetone added for the first desolvation step, the mass of HPW added to redissolve the sediment and the amount of glutaraldehyde finally added to crosslink the nanoparticles were duplicated whereas temperature, stirring speed, pH, speed of acetone addition, centrifugation speed and centrifugation time were adopted from the standard preparation protocol. The sedimentation time and the volume of acetone added for the second desolvation step were each adapted to the batch size by visual judging of sediment formation and grade of turbidity, respectively. Turbidity was additionally measured by a nephelometer (Nephla, Dr. Lange, Berlin, Germany). In further experiments the batch size was increased three-, five- and ten-fold.

1.2.3 Modifications of the upscaled gelatin nanoparticle preparation method: Equipment changes.

The glass burette (Brand, Wertheim, Germany) used for the addition of acetone during the second desolvation step (see 1.2.1.) was first replaced by a peristaltic pump (4.9 ml/min; Sotax, Basel, Switzerland) employing acetone-proofed flexible tubes (Ismatec, Wertheim, Germany). Further, the previously used Erlenmeyer flask was replaced by a round bottom flask of an adequate volume.

For batch sizes greater or equal than three-fold an evaporation step was introduced to exclude residual acetone. Therefore, the non-purified GNP dispersion was transferred into a round bottom flask (1 l) and acetone was removed by a rotary evaporator (Heidolph Instruments, Schwabach, Germany) at a temperature of

40°C under low vacuum. The particles were then purified as described in the standard preparation protocol.

Moreover, the amount of glutaraldehyde (25 % V/V), added after the second desolvation step to crosslink the nanoparticles, was halved and the stability of the resulting particles was monitored.

1.2.4 Characterization of gelatin nanoparticles

1.2.4.1 Determination of concentration

About 20 µl of the aqueous GNP dispersion were dropped in a little aluminum vessel. That way, three samples were prepared. They were then dried in a drying chamber heated to 60 °C until their masses reached a constant level. In order to calculate the concentration of the dispersion (m/m), the aluminum vessels had to be weighed in empty, full and completely dried status (microbalance, Mettler Toledo, Greifensee, Switzerland).

1.2.4.2 Determination of particle size

An expendable cuvette was twice rinsed with 0.2 µm filtered HPW, before it was filled up to a height of about 1 cm with 0.2 µm filtered HPW again. Then, 15 µl of the aqueous GNP dispersion were added and mixed. Particle size and polydispersity index (PDI) were finally measured with a Zetasizer Nano ZS employing photon correlation spectroscopy (PCS; Malvern Instruments, Worcestershire, United Kingdom). Each indicated value was the mean of at least 15 subruns.

1.2.4.3 Determination of zeta potential

A zeta cuvette comprising two electrodes was once rinsed with 0.2 µm filtered HPW, before 65 µl of the aqueous GNP dispersion (see 2.2.) were filled in. Then, 650 µl of phosphate buffered saline (PBS) or 10 mM NaCl were added. Zeta potential was finally measured with a Zetasizer Nano ZS at a measuring voltage of 40 mV employing the standard Smoluchowski model. Each indicated value was the mean of 50 subruns.

1.2.5 Cationization of upscaled GNPs

First, standard conditions as established for single size batches (Zwiorek et al. 2008) were applied on a threefold up-scaled batch to include a reaction volume of 20 ml at room temperature with an incubation time of 30 minutes and an effective concentration of 0.50 mg of each cationization reagent (Cholamin and EDC) In parallel, the pH value was adjusted to values of 3.5, 4.0, 4.25, 4.5, 4.75, 5.0 and 5.5 for samples subjected to the above mentioned conditions. Furthermore, reaction volume was adjusted to adjust the starting GNP concentration (1.0 and 2.0 mg/ml) and cationization reagent concentrations (1.0, 2.0 and 3.0 mg/ml for cholamin and 1.1, 2.2 and 3.3 mg/ml for EDC). Monitored quality parameters included visible particles, GNP size and size distribution as well as the zeta potential.

1.3 Results and discussion

1.3.1 Effects of equipment changes

First, the influence of equipment changes on GNP properties were determined. Therefore, GNPs in one- to three-fold batch sizes were prepared employing an Erlenmeyer flask and burette, Erlenmeyer flask and peristaltic pump and finally round bottom flask and peristaltic pump as combinations of laboratory equipment. GNPs that were manufactured that way were examined by PCS to determine particle size and PDI. Further, drying loss experiments were run to determine the concentration of the GNP dispersion and the particle yield, respectively.

1.3.1.1 Effects on particle size and polydispersity index

In general, particle size is an important parameter for the characterization of nanoparticles, especially when they are intended for clinical use e.g. in cancer applications. In this case, particle size should preferably not exceed a target value of 200 nm when administrated i.v. to benefit from the enhanced permeability and retention effect (EPR) which is characteristic for tumor vasculature (Torchilin 2007). Larger particles also increase the risk for thrombosis and should consequently be avoided. However, for s.c. delivery, particles up to 350 nm can be suitable when a local presentation of drugload is indended (Zwiorek 2006).

Fig. 1 displays the particle size resulting from the different employed preparation methods that were each used for one-, two- and three-fold batch size. Fortunately, all the manufactured particles do not exceed a size of 200 nm.

The columns on the left side (Erlenmeyer flask, burette) indicate that an upscaling of the standard preparation method is generally possible. Although the particle size increases with the batch size, the GNPs seem to be of high quality. So, the PDI values of two- and three-fold batch size average 0.030 and 0.027, respectively whereas the one of the standard batch size averages 0.096. Values below 0.1-0.15 can be regarded as strong indication for monomodal particle distribution (Pishvaei et al. 2006).

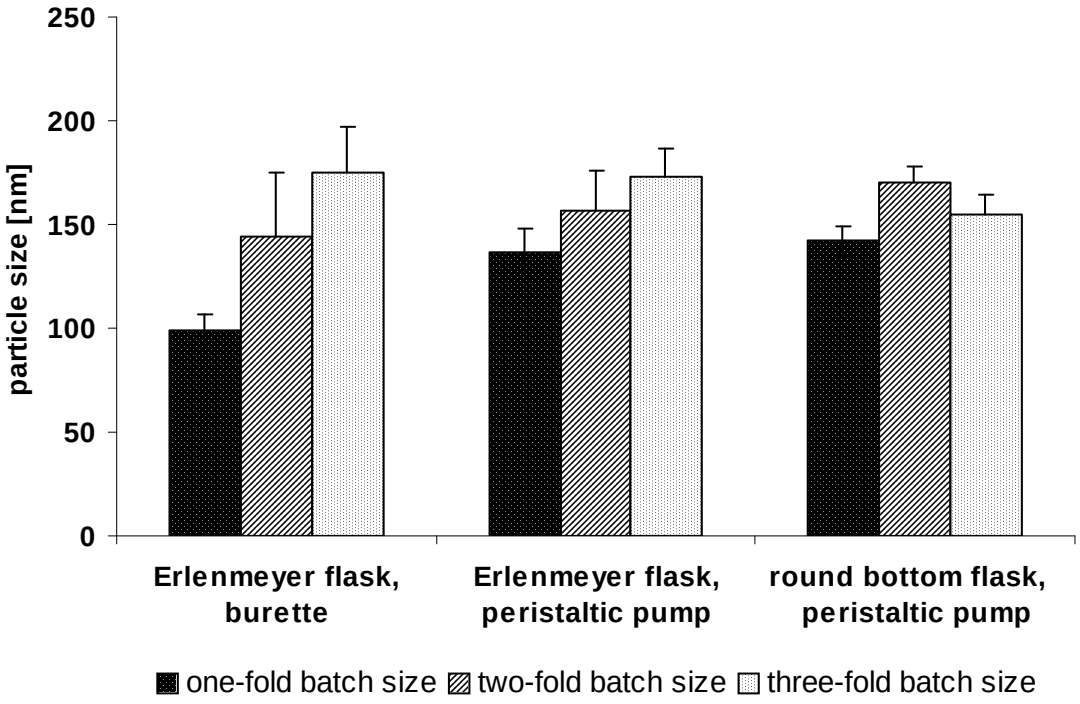

Fig. 1. *Particle size resulting from three different GNP preparation methods, each employed for one-, two- and three-fold batch size. Each data point displays the mean of three single batches (n=3, ± S.D., altogether nine individual measurements).*

In order to semi automate the GNP production process, the burette was replaced by a peristaltic pump. That way, the speed of acetone addition was exactly adjusted to 4.9 ml/min and maintained during the whole second desolvation step. As a consequence, slightly smaller particle size standard deviations of the upscaled batches than by using the burette were observed as it can be see columns in the middle). Furthermore, the related mean PdI values are still in a range

indicating high GNP quality. Once again, the particle size increases with the batch size. Although this seems to be characteristic for the scale-up in Erlenmeyer flasks, we could confute this hypothesis in further experiments including five- and ten-fold batch sizes.

Finally, the Erlenmeyer flask was replaced by a round bottom flask of an adequate volume. So, we could further improve the particle size standard deviations (see columns on the right side) while the mean PdI values remained nearly constant. Nevertheless, the production of nanoparticles in round bottom flasks is not as easy to handle as in Erlenmeyer flasks during the desolvation process as they need additional fixation for safe positioning. On the other hand, employment of round bottom flasks allows the removal of organic solvents without the need of intermediate vessel change.

Summarizing, each investigated method is appropriate for an upscaling of the GNP standard preparation method and leads to particles of high quality.

1.3.1.2 **Effects on particle yield**

One of the main objectives of an upscaling process is to increase the yield of the manufactured product while its high quality is maintained. For the scale-up of the GNP production process the latter was already demonstrated so that the GNP yield can exclusively be focused in the following.

Fig. 2 shows the GNP yield resulting from the different preparation methods described in 3.1. that were each employed for one-, two- and three-fold batch size. Referring to the initially employed gelatin mass, the yield was invariably specified in %. Thus, the resulting normalized values of the different batches couldn be checked against each other. They generally varied between 1.5 % and 13.0 %.

The black columns which display the GNP yield of the standard-sized batches indicate that the preparation process could be optimized, first by replacing the burette by a peristaltic pump, then by replacing the Erlenmeyer flask by a round bottom flask. That way, the GNP yield almost decupled. Unfortunately, this trend did not proceed in two- and three-fold batch sizes.

The columns on the left side (Fig. 2) show that the applied method employing Erlenmeyer flask and burette led to mean GNP yields smaller than 5 % and

relatively high standard deviations, which were both inapplicable for further scale-up experiments.

Regrettably, the GNP yields of the upscaled batch sizes were not optimized by replacing the burette by a peristaltic pump (see columns in the middle). Quite the opposite, the particle yields further declined. However, the standard deviations could clearly be reduced.

When the Erlenmeyer flask was finally replaced by a round bottom flask (see columns on the right side), the GNP yield of the two-fold batch size markedly increased by 5.4% up to 9.4%. Nevertheless, it did not measure up to the mean yield of the standard batch size (13.0%). Its standard deviation also worsened again.

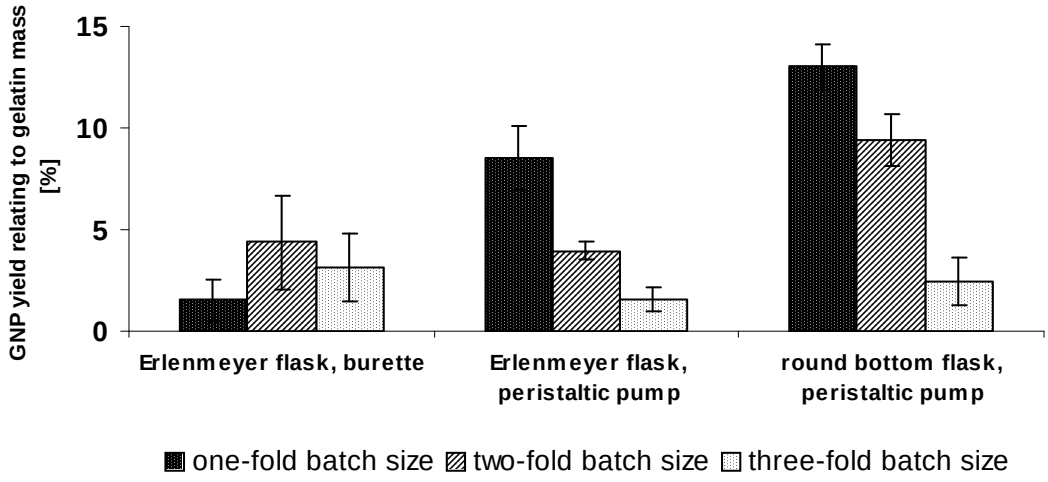

Fig. 2. *GNP yield relating to the initially employed gelatin mass, which resulted from three different GNP preparation methods, each employed for one-, two- and three-fold batch size. Each data point displays the mean of three single batches (n=3, ± S.D., altogether nine individual measurements).*

With the exception of the first dark column, the particle yield decreased with an increasing batch size meaning that the efficiency of the GNP production process declines. This was probably due to the sedimentation time starting after the first desolvation step, which was adapted to the batch size by visual judging of the sediment formation. Presumably, with respect to larger total volumes and therefore longer particle sedimentation distances this time needed to be prolonged in future upscaling experiments. Additionally, both the centrifugation speed and time greatly influenced the GNP yield. Consequently, they should not be handled

as constant process parameters but dynamically be adapted to the requirements of each batch. However, a “one fits all” procedure would be more desirable to avoid time consuming pre-studies to optimize each single batch.

Summarizing, each investigated upscaled GNP preparation method employing a peristaltic pump provided heretofore non-satisfactory yields in comparison to those of the standard-sized preparation methods. Although the GNP preparation in round bottom flasks seemed to be more effective than the preparation in Erlenmeyer flasks, we continued our experiments using Erlenmeyer flasks because of an easier and hence time-saving handling. However, a future use of round bottom flaks should not be excluded due to the ease of subsequent organic solvent evaporation whithout the need of in between vessel change.

1.3.2 **Stability of gelatin nanoparticles of upscaled batch sizes**

In the development of new dosage forms stability plays a decisive role as it acts as an indicator for storability. Former studies that were carried out by Coester *et al.* evinced GNP stability over a time period of at least three months (Coester et al. 2000). As those particles resulted from standard-sized batches, here the upscaled batch sizes, particularly at two- and three-fold batch sizes, were aimed at, involving Erlenmeyer flask and burette.

Fig. 3 depicts such a stability study over a time period of 35 and 37 days, respectively. The nanoparticles were stored as dispersion in HPW at a temperature of 4 °C and periodically measured with a Zetasizer Nano ZS. Both, particle size and zeta potential are parameters providing stability information. If for example an agglomeration took place, the particle size and also the appropriate PdI values would increase. Moreover, the zeta potential would presumably rise to zero indicating a loss of electrostatic repulsion between the single GNPs.

It was fortunately possible to demonstrate particle stability over the whole period investigated. Thus, GNPs of both upscaled batch sizes showed constant size values. The corresponding PdI values of 0.041 ± 0.014 for two-fold batch size and 0.015 ± 0.017 for three-fold batch size also provided satisfactory results as they indicate high GNP quality and remained relatively unaltered over the course of

time. When the zeta potential was regarded in the same context, slight variations

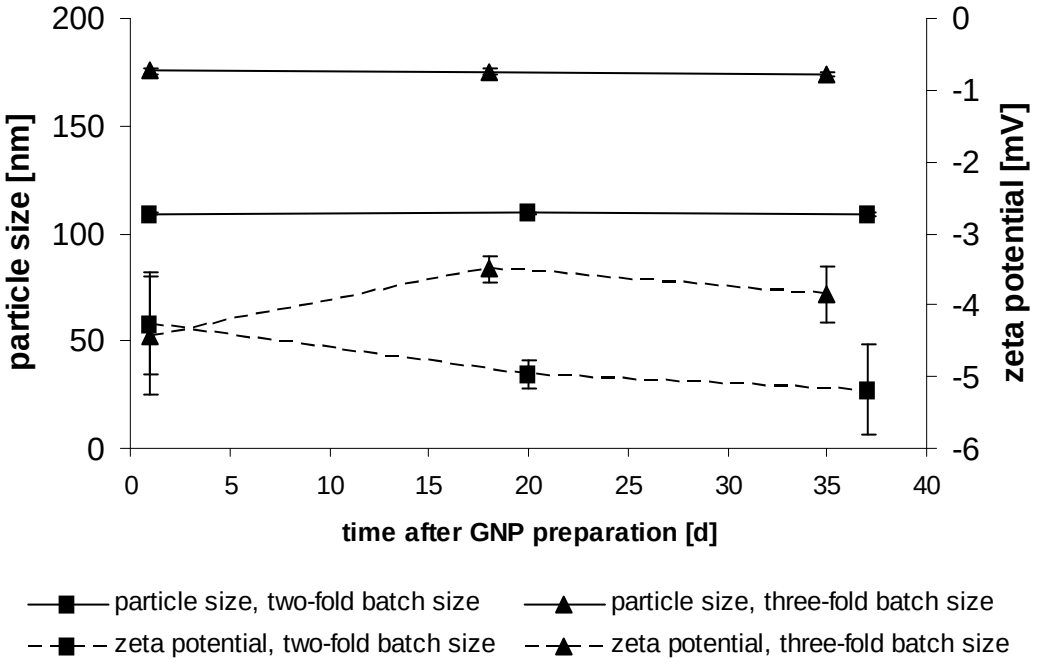

Fig. 3. *Stability study over a time period of at least 35 d of GNPs (Erlenmeyer flask, burette) resulting from an upscaled batch size (two- and three-fold, respectively). Particle size and zeta potential were considered. Each data point represents a single batch with three individual measurements (n=3, ± S.D.).*

were detected, which were probably due to the interference-prone zeta cuvettes. Nevertheless, all the detected values stayed in an acceptable range.

As this study provides very promising results concerning short-term stability, it should be continued to get some results for long-term stability. Furthermore, the storage conditions of the GNP dispersion could be modified in future experiments to find out whether the temperature or the pH values do have some influence on stability.

1.3.3 **Introduction of an evaporation step**

The standard preparation protocol demanded the purification of GNPs by two-fold centrifugation. As each centrifugation step claims a time of 18 min, the purification procedure is relatively time-consuming. The total capacity of the used centrifuge is further limited to an overall maximum of about 70 ml so that only GNP dispersions of standard-sized batches can be treated at once. In the case of

upscaled batch sizes, the common overnight loss of acetone is not sufficient to reach total volumes less or equal than 70 ml. Therefore, a time-saving evaporation step removing acetone under vacuum at a temperature of 40 °C was introduced. The particles could afterwards be purified as described in the standard protocol and size and zeta potential could finally be measured by a Zetasizer Nano ZS.

Fig. 4 displays particle size and zeta potential of GNPs of 5.6-fold batch size, which were either purified according to the standard protocol or to the advanced method including an evaporation step. Therefore, the GNP dispersion of one single batch (Erlenmeyer flask, burette) was divided into two parts.
Whereas the zeta potential remains absolutely constant when a rotary evaporator is additionally used, the particle size slightly increases. Nevertheless, the appropriate PdI value (0.031) indicates high GNP quality.

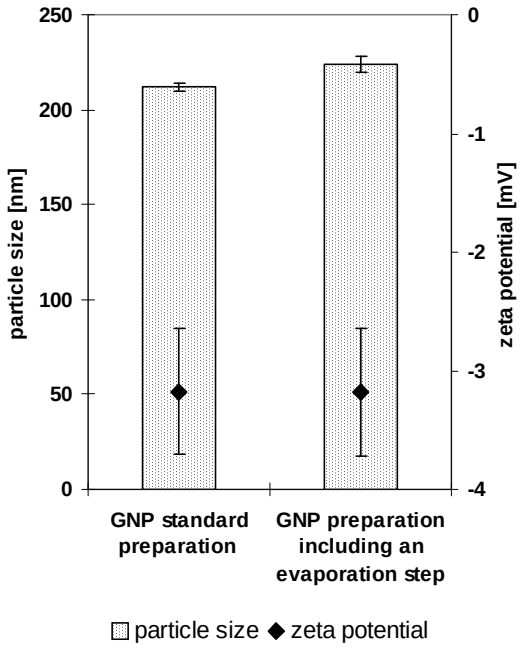

Fig. 4. *Comparison of particle size and zeta potential of GNPs of an upscaled batch size (5.6-fold) that were either prepared by the standard protocol or by an advanced method including an evaporation step. Each data point represents a single batch (n=1, altogether three individual measurements ± S.D.; Erlenmeyer flask, burette).*

Summarizing, the introduction of an evaporation step does not diminish GNP quality and can hence be recommended for the preparation of upscaled batch sizes. The increase of particle size is small and considered irrelevant.

1.3.4 **Correlation studies**

With the objective to figure out whether connectednesses between the single process parameters such as batch size or sediment mass do exist, we run further upscaling experiments employing Erlenmeyer flask and peristaltic pump again. Therein, five- and ten-fold batch sizes were included. The particle size as well as the concentration of the GNP dispersion, both necessary for the evaluation of the following correlation studies, was determined as described.

1.3.4.1 **General correlation studies**

The correlation studies below generally refer to one-, two-, five- and ten-fold batch sizes. Each data point therein displays the mean of altogether three single batches.

The sediment mass and volume of acetone added for the second desolvation step in correspondence to the batch size

Fig. 5 demonstrates strong linear correlations in both cases, emphasized by coefficients of determination of 0.9953 (sediment mass) and 0.991 (volume of acetone), respectively. Hence, the appropriate linear equations can be used to predict either the sediment mass or the volume of acetone that has to be added for the second desolvation step of heretofore non-investigated batch sizes (n-fold):

- sediment mass [g] = $1.1671 \cdot n + 0.4988$ [1]
- volume of acetone [ml] = $68.844 \cdot n + 25.204$ [2]

According to this, we are now also able to predict the volume of acetone when the sediment mass is already known:

- volume of acetone [ml] = $58.987 \cdot$ sediment mass [g] - 4.2186 [3]

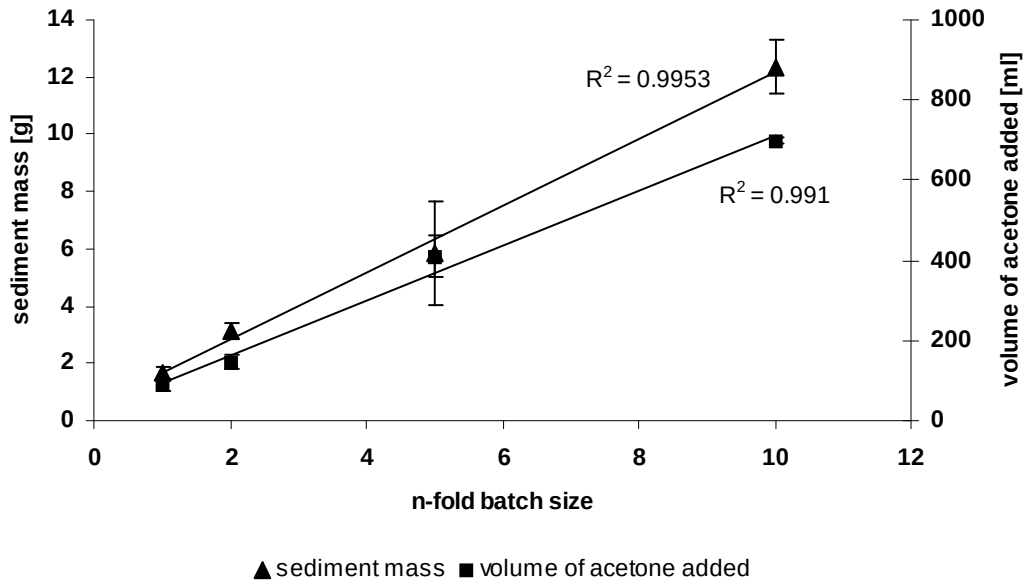

Fig. 5. *Correlation between sediment mass and n-fold batch size and correlation between volumes of acetone added for the second desolvation step and n-fold batch size, respectively. Each data point displays the mean of three single batches (n=3, ± S.D.; Erlenmeyer flask, peristaltic pump).*

Summarizing, this mathematical analysis facilitates the planning of further upscaling experiments as the sediment mass and the consumption of acetone can easily be prognosticated. Especially the latter leads to an advantage: the addition of acetone during the second desolvation step can now completely be automated because a visual judgement of turbidity or a nephleometric measurement is not necessary any more. Future upscaling studies may eventually require a validation of this production step referring the the particle size.

The particle size and yield in correspondence to the batch size

Fig. 6 shows a linear correlation for the first case, which is characterized by a coefficient of determination of 0.9357. This permits the prediction of the particle yield of heretofore non-investigated batch sizes (n-fold):

- particle yield [mg] = 27.68 · n + 51.146 [4]

Allowing for the mathematical formulas developed in 3.4.1.1. (see [1] and [2]), it is possible to calculate the absolute particle yield when either the sediment mass or the volume of acetone added for the second desolvation step is known:

- particle yield [mg] = 23.72 · sediment mass [g] + 39.316 [5]
- particle yield [mg] = 0.402 · volume of acetone [ml] + 41.012 [6]

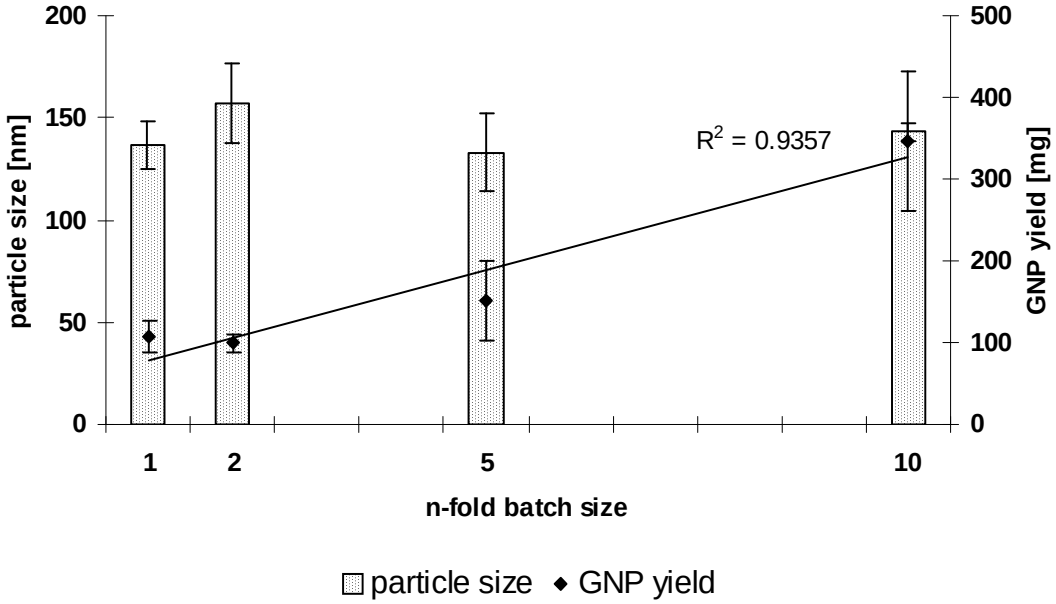

Fig. 6. *Correlation between particle size and n-fold batch size and correlation between absolute GNP yield and n-fold batch size, respectively. Each data point displays the mean of three single batches (n=3, ± S.D., altogether nine individual measurements; Erlenmeyer flask, peristaltic pump).*

In contrast, the particle size seems not to depend on the batch size and is therefore also independent of the sediment mass, the volume of acetone added for the second desolvation step and the particle yield. It generally varies between 133 nm and 157 nm.

Summarizing, the absolute particle yield depends on the batch size whereas the particle size does not show a comparable relationship. Future experiments should clarify the role of the sedimentation time as well as the centrifugation speed and time which may have an influence on both, absolute particle yield and size. Relative particle yield would be of interest from a commercial point of view but would require MW analysis before and after the first desolvation step and before and after the purification process. However, preliminary estimation indicate a

percental loss of particle yield during the purification process by centrifugation of 20 – 30%.

1.3.4.2 **Correlation studies within batches of the same size**

The following correlation studies refer to one-, two- and five-fold batch sizes. Each data point therein represents a single batch within a series of three batches of the same size.

The volume of acetone added for the second desolvation step in correspondence to the sediment mass

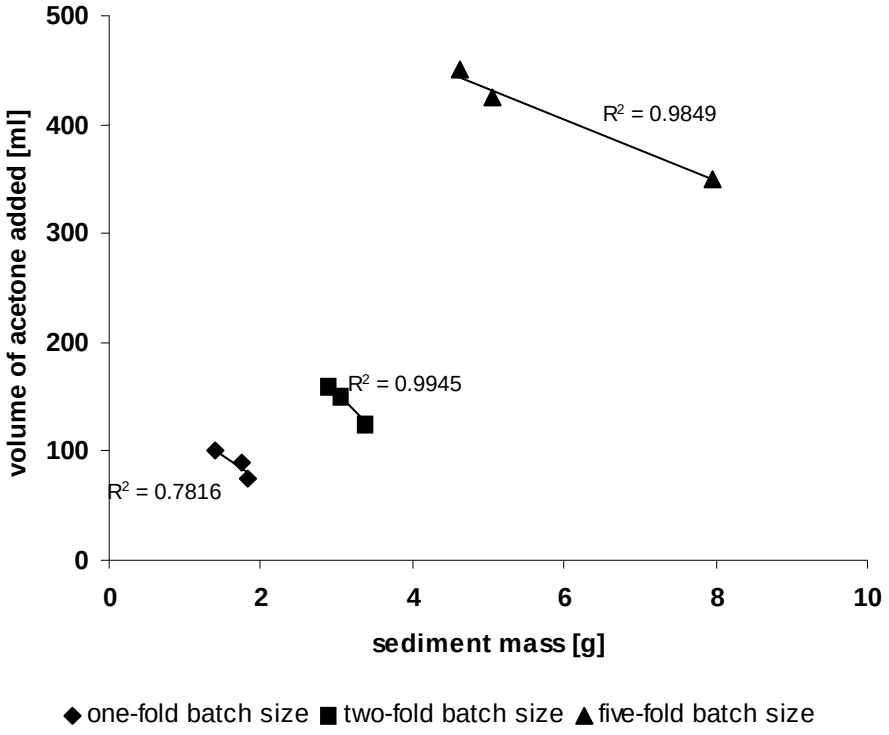

Fig. 7. *Correlation between volumes of acetone added for the second desolvation step and sediment mass. Each data point represents a single batch within a series of three batches of the same size (n=3, ± S.D.; Erlenmeyer flask, peristaltic pump).*

Fig. 7 confirms a linear correlation between the volume of acetone that was added for the second desolvation step and the sediment mass within a series of batches of the same size. Hence, the volume of acetone decreased with increasing sediment mass which in turn has a crucial impact on the achieved particle size (Zwiorek 2006). Although the corresponding coefficients of determination were

increasingly satisfactory (one-fold batch size: 0.7816, two-fold: 0.9945, three-fold: 0.9849), it was hitherto not possible to exactly predict the behaviour of non-investigated batch sizes because of differing slopes of the already existing trend lines.

The particle size in correspondence to the sediment mass

In contrast to the general correlation study above where a connectedness between particle size and any other considered factor such as volume of acetone had to be excluded for simplification, we are now able to relate particle size to the sediment mass. Fig. 8 shows a linear correlation between the two, which is characterized by coefficients of determination between 0.6406 (two-fold batch size) and 0.9653 (five-fold). Once again, the exact prediction of the GNP size of heretofore non-prepared batch sizes remained unfortunately impossible as each already investigated batch size brought along a different trend line slope. Nevertheless, it was evidenced that the particle size within batches of the same size increases with an increasing sediment mass confirming earlier findings based on a lower number of non-validated batches (Zwiorek 2006).

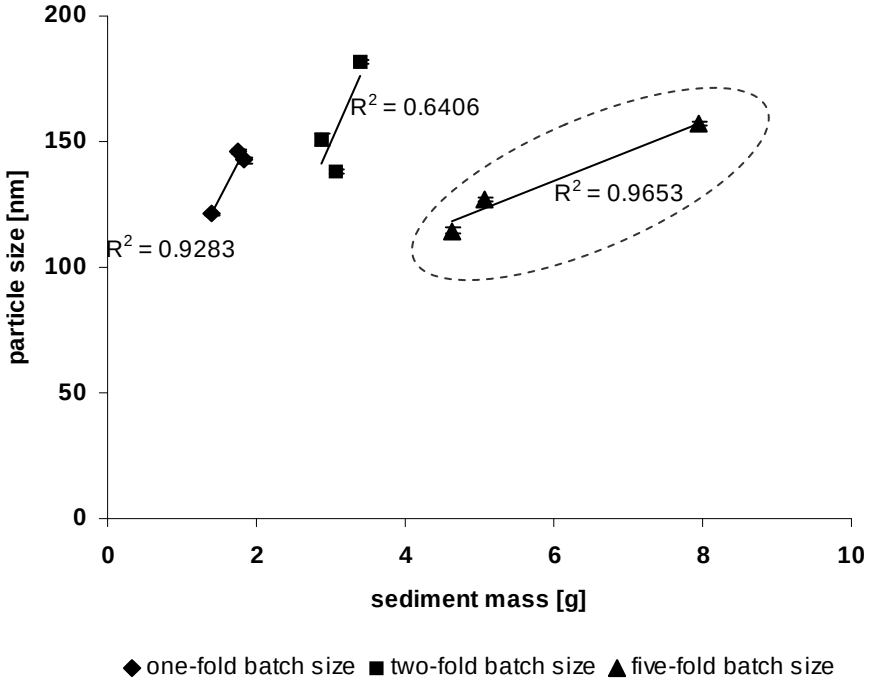

Fig. 8. *Correlation between particle size and sediment mass. Each data point represents a single batch within a series of three batches of the same size (n=1,*

altogether three individual measurements ± S.D.; Erlenmeyer flask, peristaltic pump).

The particle yield in correspondence to the sediment mass

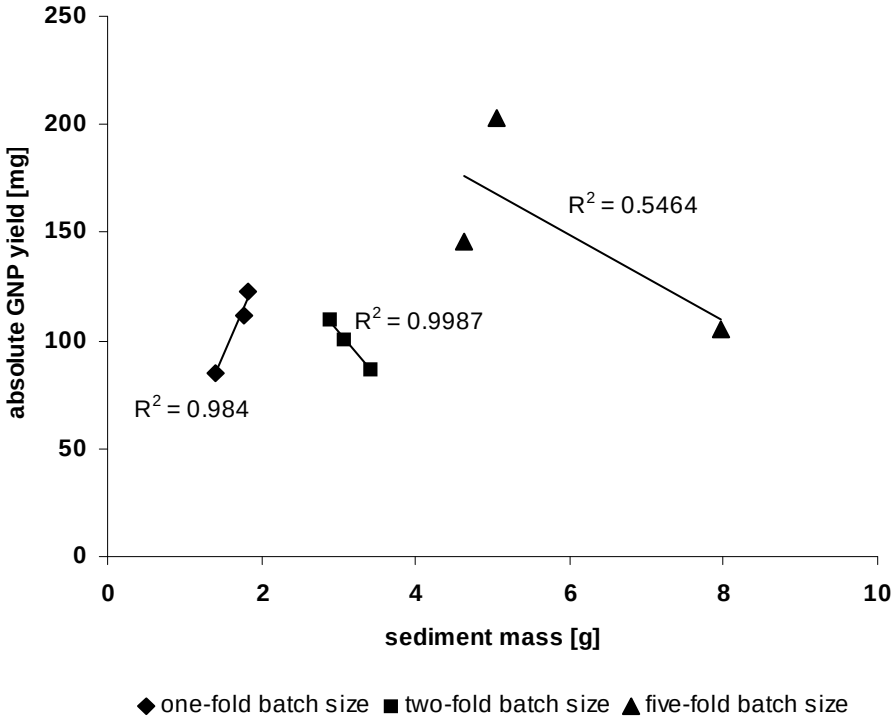

Fig. 9. *Correlation between GNP yield and sediment mass. Each data point represents a single batch within a series of three batches of the same size (n=3, ± S.D.; Erlenmeyer flask, peristaltic pump).*

The final step aimed at clarifying whether there was also a relationship between the sediment mass and the particle yield within batches of the same size. Regarding the standard and two-fold batch sizes (Fig. 9) strong linear correlations were obtained emphasized by coefficients of determination of 0.984 and 0.9987, respectively. Surprisingly, the GNP yield of one-fold batch sizes increased with an increasing sediment mass whereas the yield of two-fold batch sizes decreased. Five-fold batch sizes further behave similarly to two-fold batch sizes, but have to be considered critically as their coefficient of variation accounts for only 0.5464. Nevertheless, despite this difficulty to predict yield from five-fold upscaling the higher alsolute yield justifies future employment of this approach due to the

avoidance of particle size variances between multitudes of regular small-sized batches.

1.3.5 Preliminary constitution of an interdependency network of production parameters

The finding of above discussed single interdependeces between each paired individual parameters already facilitated simple related projections. However, obtaining a full overview of relations between all involved parameters accessible for quantification would be highly desirable. In case a statistical context existed between the various decisive steps in the manufacturing process, a predictable scale up from threefold to tenfold or even higher could become possible. Therefore, a preliminary set of 8 threefold up-scaled batches was produced parallely and 8 key production parameters were recorded. These did not include the initial mass of starting material gelatin A which was kept constant at about 3.75 g. Furthermore, the sediment mass resulting from the first desolvation step, the volume of added acetone in the second desolvation step, the dispersions' turbidity after accomplishment of the second desolvation step, the size of the obtained particles, the percental loss of particle mass during purification, the applied gravitation forces (speed) by centrifugation during particle purification, the time that was allowed for the addition of acetone until occurrence of turbidity in the second desolvation step and finally the yield given as absolute mass of nanoparticles as the final outcome (Tab. 1).

Mass [mg]	Sediment [mg]	Volume of acetone [ml]	Turbidity /ml [FNUs/ml]	Size [nm]	Percent loss [%]	Speed [g]	Time [min]	Yield [mg]
3.75	7.97	300	2.390	179.0	15.06	20100	50	783.619
3.79	6.60	275	2.255	197.7	19.07	19530	52	528.031
3.75	5.97	325	1.800	169.2	10.56	20100	50	562.754
3.88	5.27	250	2.864	157.1	8.32	20500	24	715.414
3.77	4.38	252	2.377	160.1	14.59	20333	24	486.911
3.82	3.70	265	2.389	163.4	4.31	21475	22	424.547
3.75	2.05	260	0.301	147.6	38.29	20904	73	122.980
3.77	3.23	260	0.469	143.2	35.91	20904	73	262.020

Tab. 1: *Survey of the investigated process parameters from threefold upscaled batches (n=8).*

The 8 chosen parameters offer altogether 28 pairwise senseful interrelationships. Values were plotted against each other and linear coefficients of determination were obtained (Tab. 3). Coefficients of determination $R^2 > 0.8$ were considered as indicators of strong correlation while $0.8 > R^2 > 0.5$ were such of weak correlation (Schnell et al. 2007). Values below 0.5 were not regared as indicators of any correlation and were not reflected in the following equations.

Number	x/y	Best fit equation	Coefficient of determination
3	Percental loss/turbidity	lnY=-0.064x+1.558	0.862
4	Percental loss/yield	lnY=-0.039x+6.777	0.661
5	Time/ percental loss	Y=1.48x+18.97	0.777
9	Turbidity/ time	Y=-19.11x+81.46	0.756
10	Turbidity/ yield	lnY=-0.516(1/x)+6.577	0.895
11	Sediment/ percental loss	lnY=30.34(1/x)-3.966	0.512
13	Sediment/ turbidity	lnY=-2.520(1/lnx)+2.234	0.741
15	Sediment/ yield	lnY=-4.982(1/x)+7.259	0.930
17	Turbidity/ size	lnY=0.069(1/lnx)+5.054	0.535
24	Speed/size	Y=9E+06(1/x)-291.1	0.588
26	Speed/ sediment	Y=1E+06(1/x)-45.00	0.578
27	size/sediment	Y=-2568(1/x)+20.64	0.681

Tab. 2: *Equations with corresponding coefficients of determination obtained from linear plotting (n=8) of relevant production parameter results. Numbers in the first column represent the attributed experiment number in the consecutive trial equivalent to those shown in Fig. 3. Equations missing featured R^2-values < 0.5.*

Consequently, all coefficients of determination as the prime reference to proof correlation –but not necessarily causality- could be visualized in a network between the 8 major process parameters (Fig. 10). Strong correlations were e.g. found for the pairs turbidity and yield (R^2 =0.895) or sediment and yield (R^2 =0.930). The former is of particular importance because turbidity is an easily and quickly accessible measurand. Therefore, in process controls would be possible and the production could be stopped at a point of time when a sufficient yield is conceivable long before the consuming purification process with subsequent gravimetrical concentration determination and yield calculation is performed.

A less strong but still significant correlation (R^2=0.681) was found between the resulting particle size and the sediment. This result confirmed earlier reports in our group (Zwiorek 2006) which led to the conclusion that a higher yield is potentially at the expense of a small particle size. Moreover, the higher the applied gravitation force during the purification centrifugation was, the larger became the particles most likely to occasionally forced aggregation (R^2=0.588). Interestingly, no significant correlation was found between the volume of added acetone and the resulting yield. This indicated that once the process is running, at a later stage (the second desolvation step) the yield could hardly be enlarged anymore. Moreover, the volume of acetone e.g. the addition of an excess of desolvant did not influence the particle size which led to the conclusion that the size was already predetermined and more influenced by the earlier applying parameters such as sediment mass.

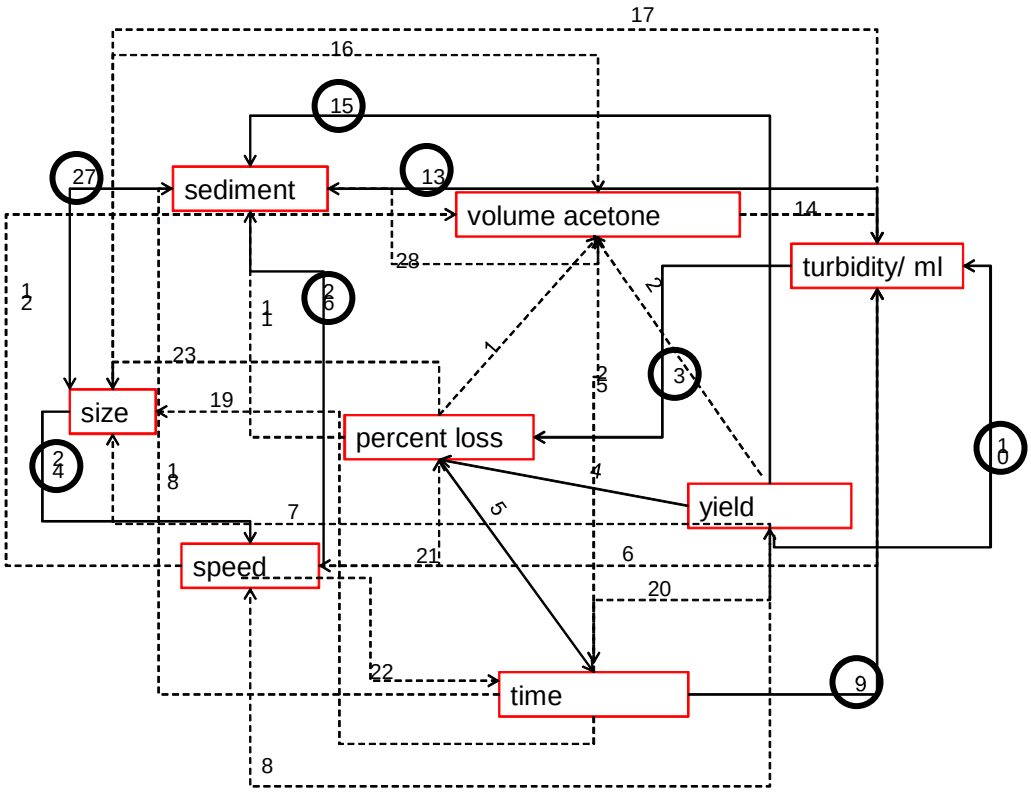

Fig. 10: *Network of interrelations of major process parameters. Solid arrows indicate linear coefficients of determination above R^2>0.5 while dashed arrows represent respective values below R^2<0.5 meaning a lack of linear correlation*

In summary, helpful projections could be made such as the correlation between turbidity and yield which had practical significance in the investigation in chapter II.3.

However, in this trial the statistical basis was still rather narrow and should be significantly enlarged before moving to a potential future clinical manufacturing to obtain data suitable for robust process validation. Moreover, more complex mathematical models of correlation could probably express relations better than this simple linear-only model applied herein. They would help to adequately meet pre-set GNP target properties such as upper size limits while optimal yields and the lowest possible amounts of organic desolvent are obtained at the same time.

1.3.6 **Reducing the amount of glutaraldehyde**

Besides glutaraldehyde, the reagents necessary for the production of GNPs are non- or minor toxic and relatively inexpensive, which displayed an advantageous precondition for upscaling experiments. However, glutaraldehyde which was finally employed to crosslink the nanoparticles counts among environmentally hazardous substances, as discussed comprehensively in chapter II.3. Although no toxicity was revealed both in own *in vitro* and *in vivo* studies so far, its use should be pared down to the minimum and therefore eventually be employed in lower quantities than in the so present standard protocoll.

Fig. 11 shows particle size and zeta potential of GNPs of three-fold batch size that were either prepared by the standard protocol or by an advanced method employing only half of the regularly used amount of glutaraldehyde.

Both preparation methods led to particles of high quality, emphasized by mean PdI values of 0.036 (standard method) and 0.028 (advanced method), respectively. However, the GNPs of the standard method were slightly smaller. As this difference amounted to less than 15 nm, it should be neglected and a GNP production with halved amount of glutaraldehyde should be recommended in order to save expenses and to reduce the risk of working with toxic substances. Of course, the stability of GNPs prepared by the advanced method is further crucial for a recommendation like this.

So, it was further examined whether nanoparticles prepared by the glutaraldehyde-saving method were as stable as commonly prepared GNPs within the first days

post-production. Therefore, particle size and zeta potential were measured again three days after the first measurement (see 2.4.) as we expected to collapse the dispersion, if at all, in an early post-preparation state. Fortunately, particle size as well as zeta potential did not markedly vary in comparison to the first measurement, which indicates GNP stability. According to these promising results, long-term stability could be presumed, but has certainly to be verified in future experiments.

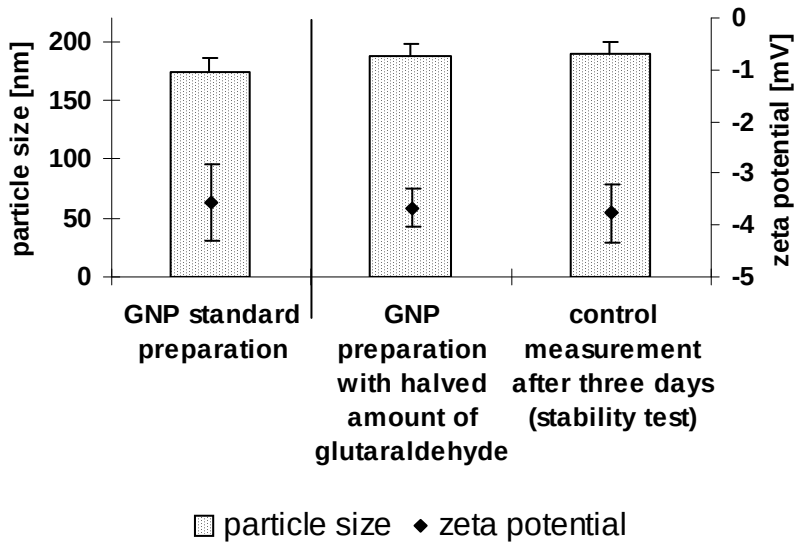

Fig. 11. *Comparison of particle size and zeta potential of GNPs of an upscaled batch size (three-fold) that were either prepared by the standard protocol or by an advanced method with halved amount of glutaraldehyde. Each data point displays the mean of three single batches (n=3, ± S.D., altogether nine individual measurements).*

With regard to particle quality and stability, on the present data the halving of the amount of glutaraldehyde seems to be unproblematic. Control experiments after three and six months confirmed the stability in particle size. Therefore, a further reduction of glutaraldehyde could be taken into be consideration from a toxicolic point of view. However, glutaraldehyde free residuals offer aldehyde free functional groups which turned out to be crucial in some post-manufacturing processing like surface PEGylation (Zillies et al. 2007). Consequently, each case requires a careful consideration of priorities.

1.3.7 **Cationization of upscaled GNPs.**

The delivery of nucleic acid-based active ingredients constituted one of the main driving factors to initiate the up-scaling of GNP production in order to provide sufficient amounts of the carrier for potential clinical studies. Therefore, the possibility to cationize also GNPs from up-scaled batches for subsequent nucleic acid surface loading needed to be elucidated. To obtain robust information if the conducted cationization resulted in GNPs of sufficient colloidal stability, crucial parameters such as particle size, size distribution (PDI) and visible particle impurities were assessed in dependence of variable process parameters such as starting particle concentration, pH value and concentration of cationization agents. First, the impact of altering the pH value was analyzed while the other production parameters were left as standard for the original batch size to include a GNP concentration of 3-5 mg/ml and reagent concentrations of 0.5 mg/ml.

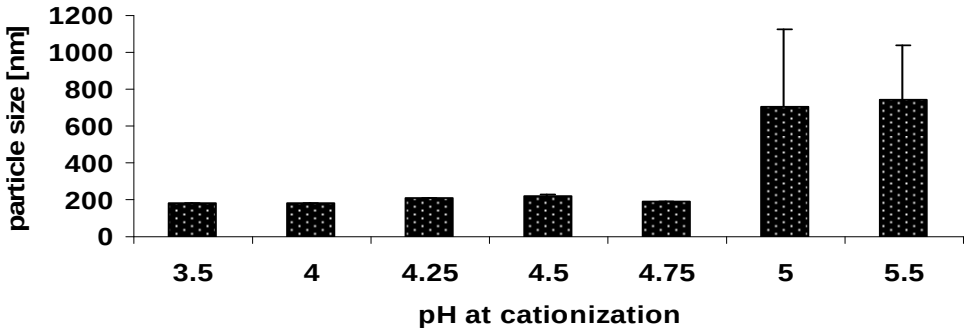

Fig. 12: *Impact of process pH value on resulting particle size during cationization of a threefold up-scaled batch (n=3 ± S.D.).*

As revealed by Fig. 12, the particle size remains constant for the observed range of pH 3.5 – 4.75 at 200 nm. When passing the threshold of pH 4.75, particle sizes rose to more than 600 nm indicating massive aggregation and dispersion instability which should be avoided. Moreover, visual inspection of the relevant dispersions was performed (Tab. 3).

pH	3.5	4.0	4.25	4.5	4.75	5.0	5.5
sedimentation tendency (48 h)	-	+	+	+	++	+++	++++
flocculation	-	-	-	-	++	++	++++

Tab. 3: *Impact of process pH value on GNP dispersion stability (visual inspection) during cationization of a threefold up-scaled batch with "-" for absence of relevant phenomenon up to "++++" for heavy occurrence.*

Although pH 4.75 emerged as a threshold value for colloidal stability based on instantly measured particle sizes, visual inspection revealed inconsistencies even below this point. Flocculation occurred down to pH 4.75 and (slight) sedimentation tendency down to pH 4.0 (Tab. 3). At this low value, sufficient cationization could no longer be granted. Therefore, further parameters but the pH value were varied to obtain stable cationized GNP batches.

c(GNP) [mg / ml]	c (Cholamin / EDC) [mg / ml]	size [nm]	PDI	Zetapot. [mV]	Visible particles
1	1.0 / 1.1	270.27	0.093	2.91	++
1	2.0 / 2.2	292.4	0.060	6.86	-
1	3.0 / 3.3	327.4	0.100	7.56	-
2	1.0 / 1.1	349.17	0.255	4.86	+++
2	2.0 / 2.2	289.6	0.081	7.07	+
2	3.0 / 3.3	296.5	0.041	7.87	-

Tab. 4: *Impact of starting GNP and reagents' concentration on particle and dispersion quality.*

While the prevalent pH value was constant at 4.5, starting GNP concentration was lowered to 1 and 2 mg/ml respectively. However, the influence of this parameter was marginal in comparison to the concentration of the applied cationization agents cholamin and EDC. When raising their concentration to 3 and 3.3 mg/ml,

respectively, aggregation (visible particles) was avoided (Tab. 4). This was due to a sufficient elevation of the zeta potential. The given values (Tab. 4) were measured in PBS and translate to about threefold higher values when measured in otherwise (chapter III.2) used 10 mM NaCl. The maintenance of particle size was demonstrated impressively for the 2 mg/ml GNP starting concentration which should be regarded as the maximum to avoid excessive interparticulate interaction as seen when employing the standard GNP concentration (3-5 mg/ml). Furthermore, keeping the pH at a maximum of 4.5 ensured EDC-mediated catalysis while a still secure distance from gelatin A IEP was sustained. Summarizing, cationization reagent's addition needed to be adapted to the volume of the reaction batch and the particle size. As a minimum, reagent:GNP ratio should account for 1:1 and 1.5:1 to ensure sufficient cationization in large volumes. Finally, effective cationization prevents aggregation electrostatically as revealed by sufficiently high zeta potential values.

1.4 Conclusion

In order to scale up the established GNP preparation method (Coester et al. 2000), we first run some basic experiments showing that an upscaling was generally possible without reducing particle quality. Then, we investigated the influence of different laboratory equipments, finally deciding in favor for the combination of Erlenmeyer flask and peristaltic pump. Further experiments confirmed the stability of GNPs of upscaled batch sizes for at least 35 days and revealed that the introduction of an evaporation step did not affect GNP quality.

Supported by these promising results, initial correlation studies up to ten-fold batch size were started, which enabled development of several mathematical formulas linking batch size, sediment mass, volume of acetone added for the second desolvation step and particle yield. These formulas contribute to facilitate future upscaling experiments as the outcome of the preparation of heretofore non-investigated batch sizes can be predicted by calculation. Moreover, the combination of all involved process parameters and their interdependence-expressing coefficients of determination allowed the visualization of a network making predictions in several cases reliable. Therefore, a precondition for further upscaling for clinical manufacturing was established although more work is needed to guarantee robustness over larger populations of batches. Furthermore,

the cationization of up-scaled GNP batches succeeded after small process modifications

With the objective to finally optimize the upscaled GNP production process, it was tried to reduce the amount of toxic glutaraldehyde. Fortunately, it could be demonstrated that both, particle quality and stability do not suffer from halving the amount of glutaraldehyde.

2. Hydration of GNPs

2.1 Scope of the hydration project

According to the original GNP manufacturing protocol (Coester et al. 2000), GNPs were stabilized in the final production step by glutaraldehyde-mediated cross-linking. Resulting permanent chemical bonds between ω-amine groups of lysines in adjoined gelatin molecules prevented freshly formed particles from early disintegration. Consequently, the involved elimination reaction classified as an alkylimino-de-oxo-bisubstitution of the ω-amines and the aldehydes led to the formation of imines. The acidic condition from the second desolvation step was beneficial to catalyze the nucleophilic addition-type reaction. The product was considered stable (March 1992) but could potentially be subjected to consecutive reactions such as hydrolysis, Diels-Alder reactions or reactions with amines to aminals. However, the occurrence of the related necessary reaction conditions *in vivo* is unlikely. Furthermore, since glutaraldelyde was first used to cross-link protein-based nanoparticles (Weber et al. 2000), no toxic side reactions or gelatin-associated immunity reactions were observed (Zwiorek 2006). Nevertheless, the abolishment of imines would constitute a worthwhile option to rule out a residual risk in the light of a later use in humans. Yet, the stability and integrity of the resulting imine-free particles needed to be ensured before any toxicological investigations appeared as reasonable. The most appealing method to transform an imine to a functionality of lower reactivity is a reduction from which secondary amines are obtained (March 1992). The appropriate way of hydrogenation must reflect the possible threat the reaction constitutes towards other functionalities and bindings within the molecule. The widely used reducing agent sodium borohydride reduces amides as well which would unselectively result in a breakdown of the primary structure of the gelatin protein matrix. Therefore, sodium cyanoborohydride with the formula $NaBH_3(CN)$ was chosen as a reducing agent with lower nucleophilic properties and consequently higher selectivity towards imines (Borch et al. 1971). Furthermore, hydration by hydrogen gas catalyzed by palladium fixed on large surface carbon beads in a 10% (w/w) ratio was considered due to its weak amide but potent imine reducing properties.

Therefore, the aim of this experiment was to confirm if a successful hydrogenation occurred and if the resulting particles maintained sufficient stability for *in vivo* settings later. Analytically, the first point was engaged by

nuclear magnetic resonance spectroscopy (NMR) as the state-of-the-art method to identify functional groups by tracking spins of atomic nuclei. The nanoparticle stability was assessed via PCS.

2.2 Materials and Methods

2.2.1 Hydrogenation by sodium cyanoborohydride

As the preferential reaction milieu for hydrogenation by sodium cyanoborohydride was pH 5.5 - 6, 100 ml of a 0.1 M potassium hydrogenphthalate buffer and 100 ml of a 0.1 M sodium acetate buffer were prepared. Therefore, 2.042 g potassium hydrogenphthalate (Sigma, Taufkirchen, Germany) and 1.36 g sodium acetate (Merck, Darmstadt, Germany) supplemented by 5.22 ml of 0.1 M acidic acid were diluted in 100 ml of HPW, respectively. For a quantitative selective catalytic reduction, a 1 : 1.6 molar ratio of glutaraledhyde and sodium cyanoborohydride was employed. Preparations were incubated in Eppendorf caps in aliquots of 300 µl at 22°C for 17 h at 300 rpms. After finished incubation, samples were purified by four subsequent centrifugation and washing steps, respectively. Purification in terms of reducing the amount of residual catalyst was monitored photometrically at 254 nm in each washing step.

2.2.2 Hydrogenation by hydrogen/carbon-bound palladium

As an example, an aliquot containing 10 mg GNP dispersion from the up-scaled batch was transferred to a reaction flask with gas inlet. 444 mg of carbon-bound palladium (Pd) catalyst were added and dispersed in 150 ml of methanol. Hydrogen gas was provided at a pressure of 2 bars. The incubation time was set to 24 h and the consumed hydrogen volume was 480 ml. The coarse carbon catalyst particles were separated from the GNPs by filtration through an established cellulose acetate filter featuring a 5 µm pore size which was previously validated to have low GNP retention properties in contrast to common organic solvent-proofed filter alternatives. However, due to the sensitivity of the filter material towards the dispersant, the methanolic particle dispersion was diluted 1 : 10 before filtration and concentrated afterwards by three subsequent centrifugation and washing steps. The concentration was raised hereby again to the original value.

2.2.3 **Assessment of particle stability by PCS after hydrogenation**

Hydrogenated and non-hydrogenated samples were first subjected to 4 particle size measurements (n=3, S.D.) over a time period of 72 h to obtain preliminary particle size data at room temperature to identify the better suited method related to particle stability. Particle size and size distribution alterations were assessed. Furthermore, samples were stored for 330 h at three distinctive temperatures (4°C, 25°C and 37°C) at physiologic pH value (pH 7.4) to obtain extended stability data. Per reading point, 10 µl of GNP formulation were sampled and added to 500 µl HPW in a PMMA halfmicro cuvette and susbsequently analyzed by a Zetasizer ZS Nano (Malvern Instruments, Malvern, UK). Results were intensity weighted.

2.2.4 **Scanning electron microscopy of GNPs**

Aqueous dispersions of GNPs were centrifuged, the supernatant was removed and redispersed in 96% (v/v) ethanol (VWR, Ismaning,Germany). 50 µl of ethanolic dispersion where applied on an adhesive carbon grid mounted onto a scanning electron microscopy (SEM) probe holder. Subsequently, the samples were carbon-sputtered and therefore ready for SEM analysis. To identify the composition of chemical elements within the hydrogenated samples, SEM with enhanced (semi)quantitative elementary analysis was conducted by a JSM 6500 F equipped with an energy dispersive x-ray (EDX) technology (JEOL, Tokyo, Japan). Related element calculation was performed via INCA software (Oxford Instruments, Oxford, UK)

2.2.5 **Liquid 13C-NMR for hydrogenation proof**

For each single 13C-NMR analysis, an aliquot of GNP stock solution containing 3 mg GNPs was centrifuged and subsequently redispersed in D2O (Merck, Damrstadt, Germany). NMR glass tubes were filled with respective samples up to a filling height of 5 cm and finally sealed with rubber stoppers. Samples were measured at 400 MHz over 20000 scans by an NMR spectrometer (Bruker, Karlsruhe, Germany).

2.2.6 **Solid state magic angle spinning NMR for hydrogenation proof**

To avoid any potentially disturbing dispersant- nanoparticle interaction before or during the measurement, ^{13}C magic angle spinning (MAS)-NMR was chosen as a feasible alternative. MAS-NMR is an established method to perform solid-sate NMR spectroscopy (Schaefer and Stejskal 1976). By employing the magic angle θ_m, dipole-dipole interactions, chemical shift anisotropy and partly quadrupolar interactions are averaged out. This leads to a far narrower signal (chemical shift) compared to other forms of NMR. The θ_m was set to 54.74° in all measurements. The chemical shift results were given in parts per million (ppm).

Here, initially 1 mg of the lyophilized samples was filled into the designated special rotor as a dry substance and subsequently measured by an Avance 500 NMR spectromter (Bruker, Karlsruhe, Germany).

2.2.7 **Lyophilization of GNPs**

In order to perform MAS-NMR, GNPs needed to be employed as a solid matter instead of the standard aqueous dispersion. Therefore, dispersions of GNPs were diluted down to a concentration of 1.5 mg/ml. To achieve a higher yield of finished product, 50% of samples of batches hydrogenated by one of the two described methods and of a 50% reference non-hydrogenated batch were supplemented with sucrose (Sigma, Taufkirchen, Germany) as a lyoprotector as previously introduced for GNPs (Zillies et al. 2008). The final sucrose concentration was 10% /w/w). The other 50% of samples were not supplemented with a lyoprotector and left as a pure GNP dispersion. Resulting formulations were filled as 1 ml aliquots into 2R lyophilisation vials (Schott, Germany). This was applied both for batches from the standard-sized manufacturing process as well as batches from upscaled processes. Subsequently, samples were freeze-dried over a 48 h period in an 2 Epsilon freeze dryer (Christ, Osterode, Germany) at - 50°C and 0.03 mbar in the primary drying step to ensure full water removal. The process was modified from the previously established protocol for GNPs (Zillies et al. 2008). Following the drying cycle, vials were re-pressurized by nitrogen gas up to atmospheric conditions (1000 mbar) to avoid an applied vacuum because otherwise the low-densitiy GNP powder employed without cryoprotectant sucrose would have aerozolized and vanished upon opening.

2.3 Results and Discussion

Due to its high toxicity, complete removal of the catalyt sodium cyanoborohydride was a crucial task after the accomplishment of hydrogenation. Therefore, each supernatant resulting from centrifugation of each washing step was analyzed photometrically.

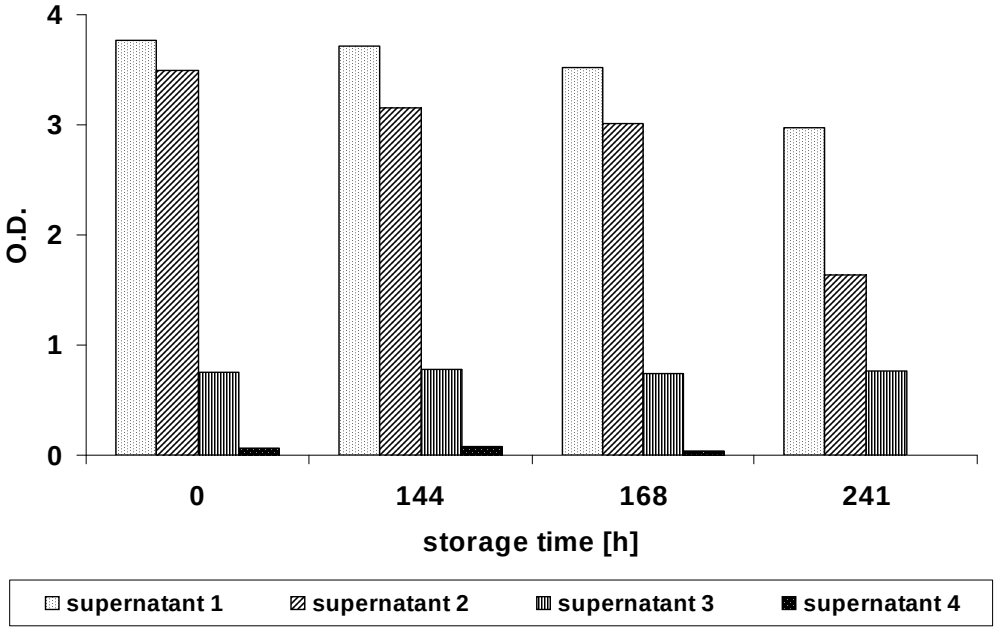

Fig. 1: *Optical density at 254 nm indicates a sharp decrease in $NaCN(BH)_3$ supernatant concentration between subsequent washing steps and a degradative reaction over time.*

As an example, Fig. 1 depicts the decrease in absorption and consequently in catalyst concentration found in the supernatants which were gained from washing step one down to step four. It was demonstrated that at least four subsequent washing steps were required to ensure absence of toxic catalyst residuals. Furthermore, a distinctive fall in absorption was observed within the two higher concentrated supernatants after 170 h. This reflects the reported slow degradation sodium cynoborohydride is subjected to (Borch et al. 1971). However, as the incubation period was set much shorter than 170 h, this degradation presumably had no disturbing impact on the catalytic process itself.

For hydrogenation by the heterogeneous catalyst hydrogen gas /carbon-bound palladium, no photometric determination of residues could be performed. Moreover, the visual inspection of the filters alone was not sufficient although

filters exhibited black carbon-associated colouring only on the educt but not on product side. Therefore, EDX elemental analysis data was taken into consideration.

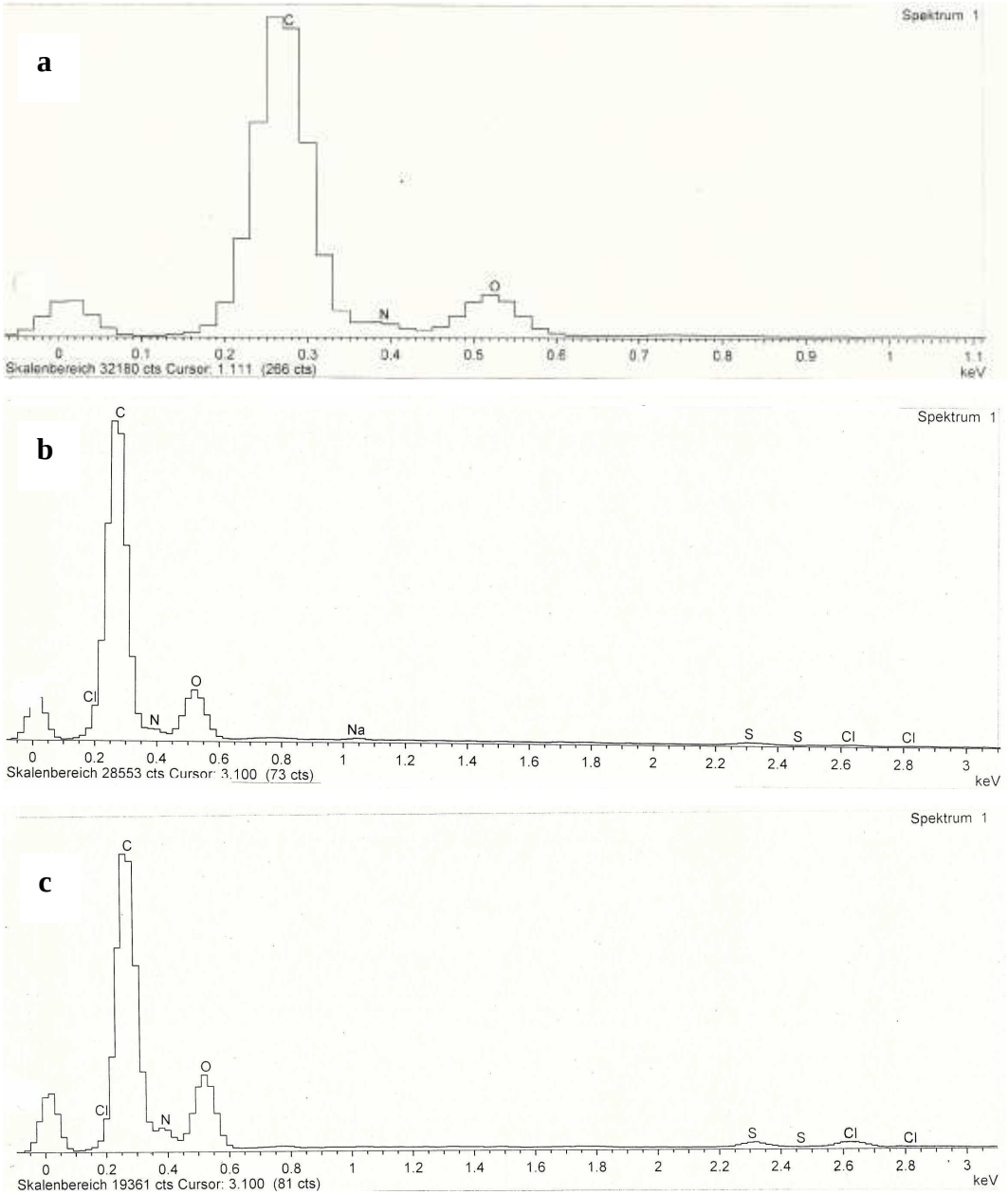

Fig. 2: *Elemental analysis by EDX.*

Here, the absence of palladium and of boron could be proven for hydrogen/carbon-bound palladium and for sodium cyanoborohydride-catalyzed samples, respectively (Fig. 2a, 2b). Furthermore, the elemental composition did not change considerably before and after hydrogenation (Fig. 2c).

However, a major change was observed when comparing the impact of the two chemical reduction methods' impacts on particle sizes (Fig. 3).

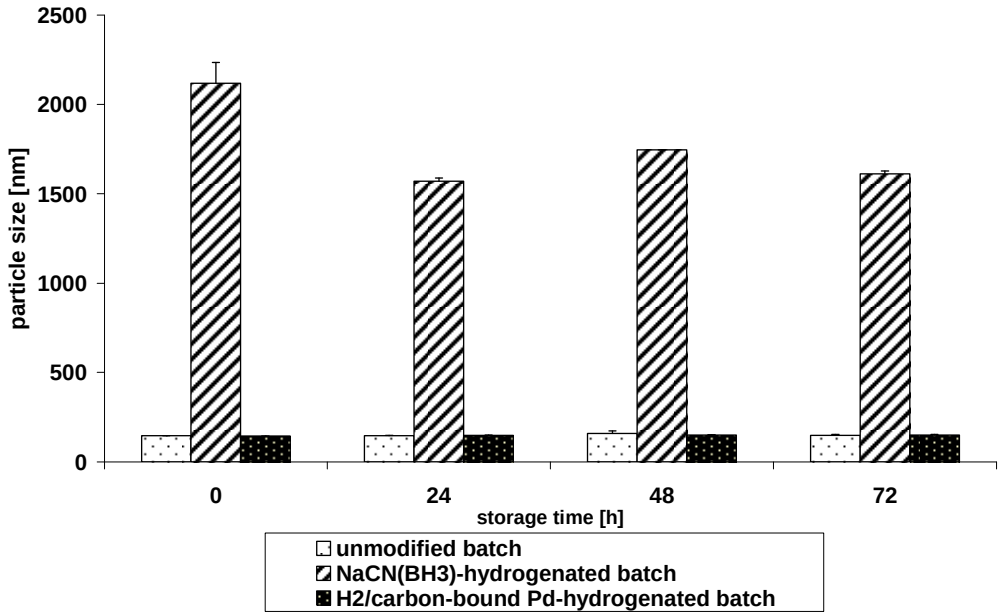

Fig. 3: *Comparison of particle sizes of non-hydrogenated and hydrogenated GNPs (n=3, ± S.D).*

While hydrogen/carbon-bound palladium hydrogenated GNPs maintain the size of non-hydrogenated GNPs (200 nm), sodium cyanoborohydride triggered a huge 10-fold increase in particle size (up to 2000 nm). Moreover, fluctuations between reading points were higher as well as the particle size distributions were broader (Fig. 3). Most likely the gelatin protein structure was chemically broken-up and consequently the particle integrity was affected. Therefore, hydrogenation by hydrogen/carbon-bound palladium was not followed anymore.

^{13}C NMR analysis was initially performed with liquid samples as no extensive sample preparation besides medium exchange (D_2O for HPW) was required. As GNPs were not exposed to D_2O previously, a brief GNP compatibility evaluation was introduced beforehand. However, Fig. 4 visualizes that particle stability and integrity was negatively affected by the pro-aggregation effect of D_2O onto GNP integrity. As soon as more than 50% of the dispersant were constituted by D_2O, particle sizes were dramatically rising. This trend even increased over the monitored time period (Fig. 4). Visible inspection revealed changes in the respective dispersions such as aggregate-forming and flocculation which supported PCS data which in turn indicated massive aggregation.

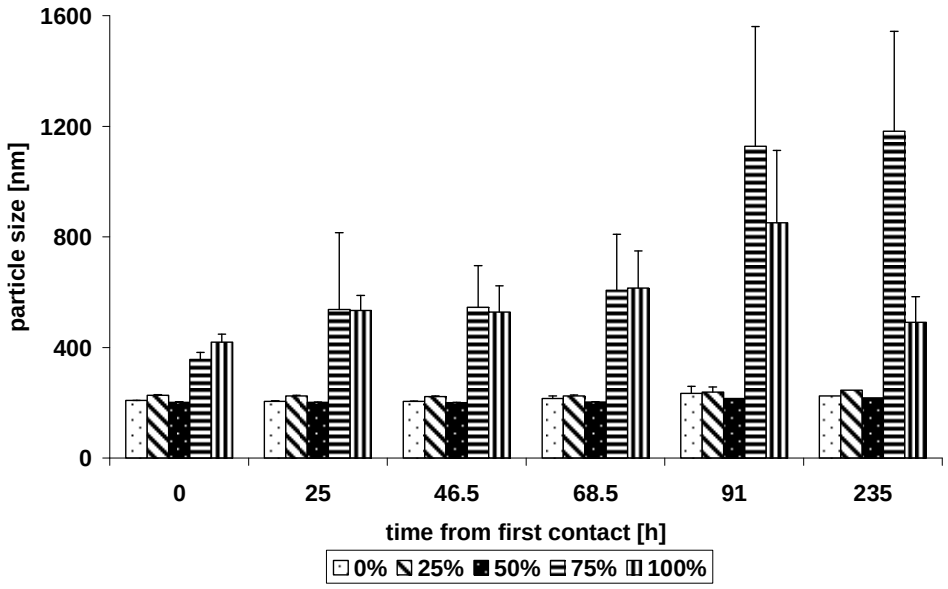

Fig. 4: *GNP particle sizes in dependence of the applied percentage of deuterium oxide (D_2O) within the aqueous dispersant to over time at 25°C (n=3 ± S.D.).*

Consequently, NMR measurements from liquid samples, although prolonged to 26 h and 20000 scans, did not result in meaningful data. Very broad amide bonds could only be supposed while possible imin bonds were superposed by the background noise (Fig. 5).

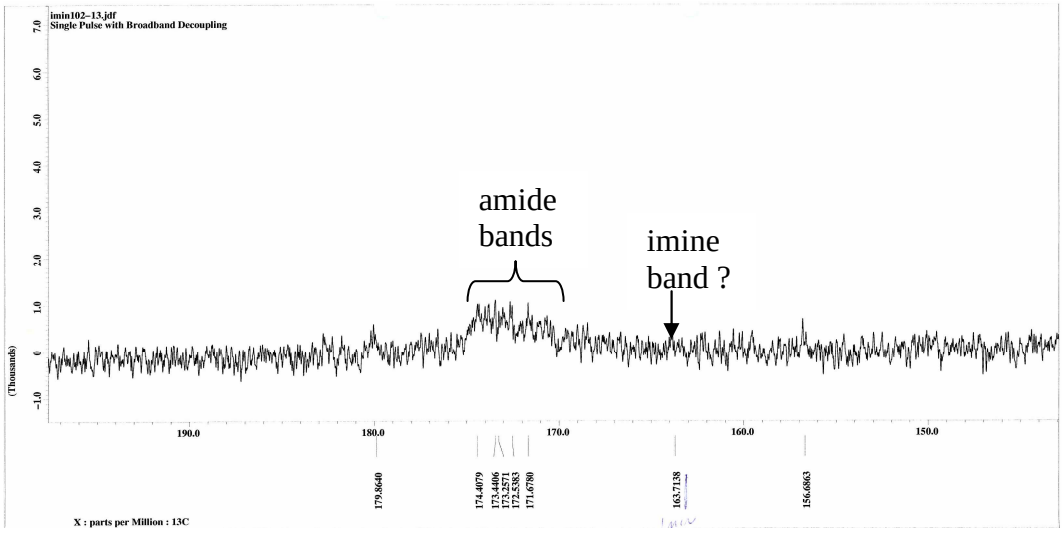

Fig. 5: *^{13}C NMR at 400 MHz over 20000 scans of $NaCN(BH)_3$-hydrogenated GNPs D_2O dispersion.*

Consequently, all further hydrogenation-proving NMR analysis was replaced by solid matter-considering MAS-NMR. This required the generation of dried GNPs.

Therefore, lyophilization as a validated method for GNP drying was conducted (Zillies et al. 2008).

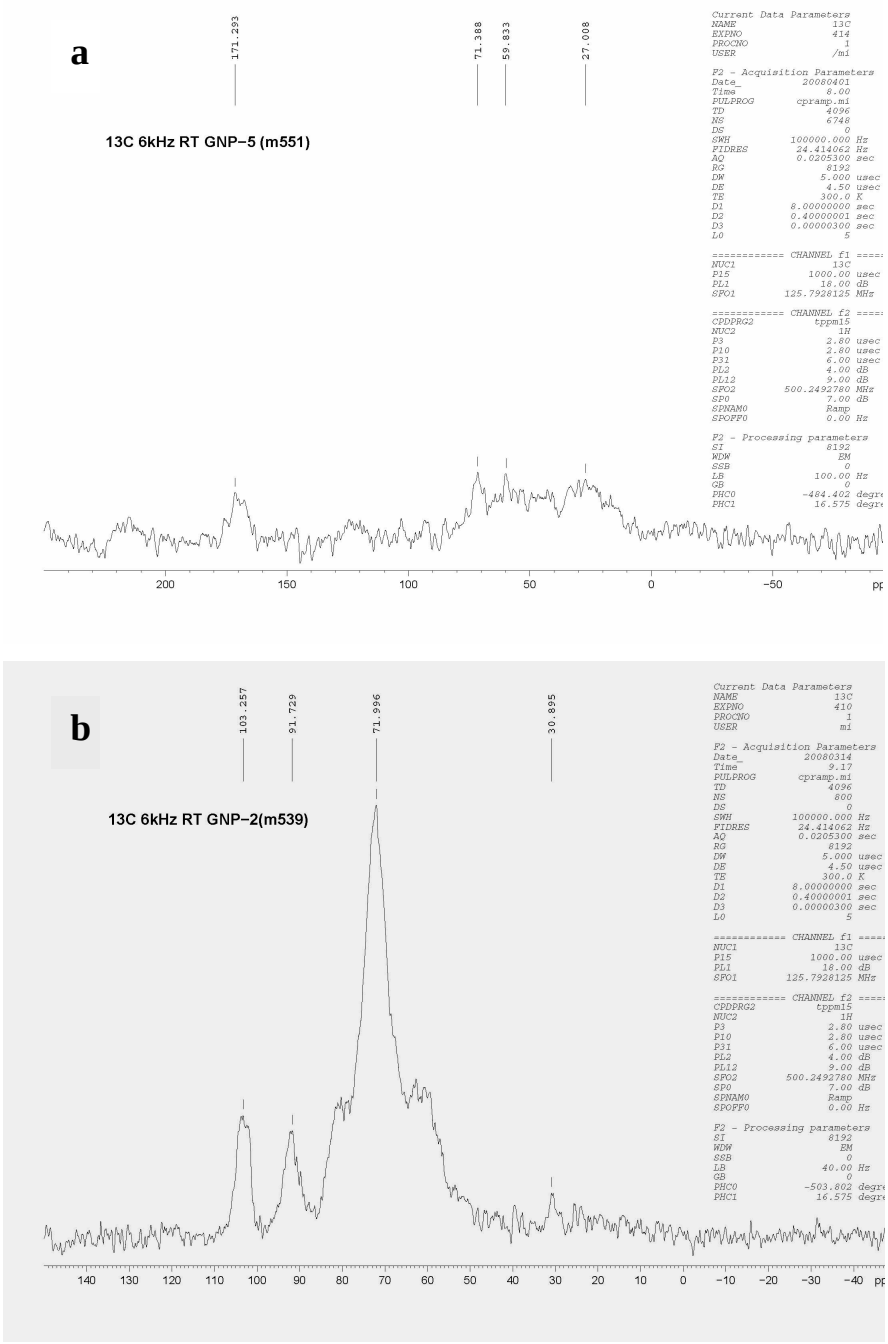

Fig. 6: *^{13}C MAS-NMR of non-hydrogenated GNPs without (a) and with cryoprotectant sucrose (10% w/w) (b).*

The NMR spectrum of a 500 mg GNP sample in Fig. 6a revealed too low band intensity and amplitude compared to background noise to conclude even the presence of the expected imine band at 163 ppm (Fig. 6a). The amide band at 171 ppm was broad but low in amplitude and hence could not be considered for any

subsequent comparisons. Moreover, addition of the sucrose as lyoprotector led the related signal to cover other bands (Fig 6b). Therefore, only sucrose-free lyophilisates were used afterwards.

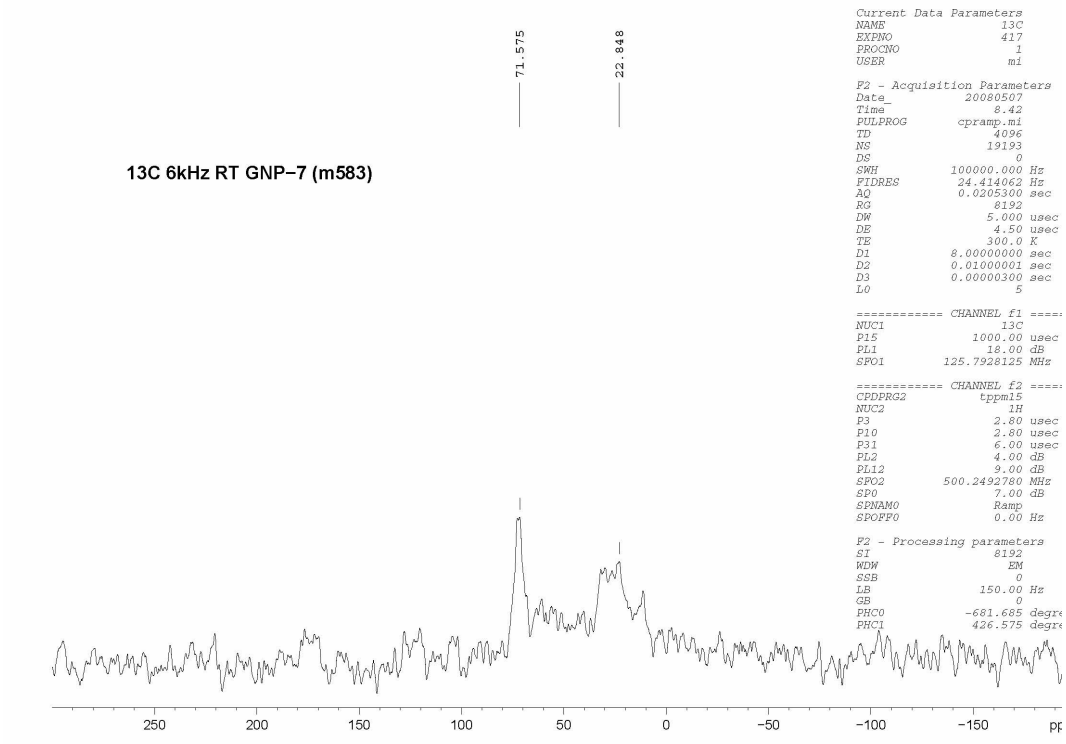

Fig. 7: *^{13}C MAS-NMR spretrum of $NaCN(BH)_3$-hydrogenated GNPs.*

Subsequently, the hydrogenated samples were subjected to MAS NMR. However, problems arose related to the limited mass of 0.3 mg GNP dry substance. The void volumes were filled with Teflon strip to ensure balanced rotation of the employed MAS rotors. Fig. 7 illustrates the impact of $NaCN(BH)_3$-mediated hydrogenation on the chemical structure of the gelatin. Amide bands were no longer detectable at 171- 175 ppm. Thus, a complete reduction of these groups was obvious leading to the conclusion that the protein structure was degraded at least in part due to excessive chemical reduction. This corresponds to the findings of heavy storage aggregation depicted in Fig. 8. Particle sizes increased 10-fold from initial 200 nm even when GNPs were stored at 4°C. Higher storage temperatures led to even higher mean sizes indicating a complete loss of nanoparticulate morphology.

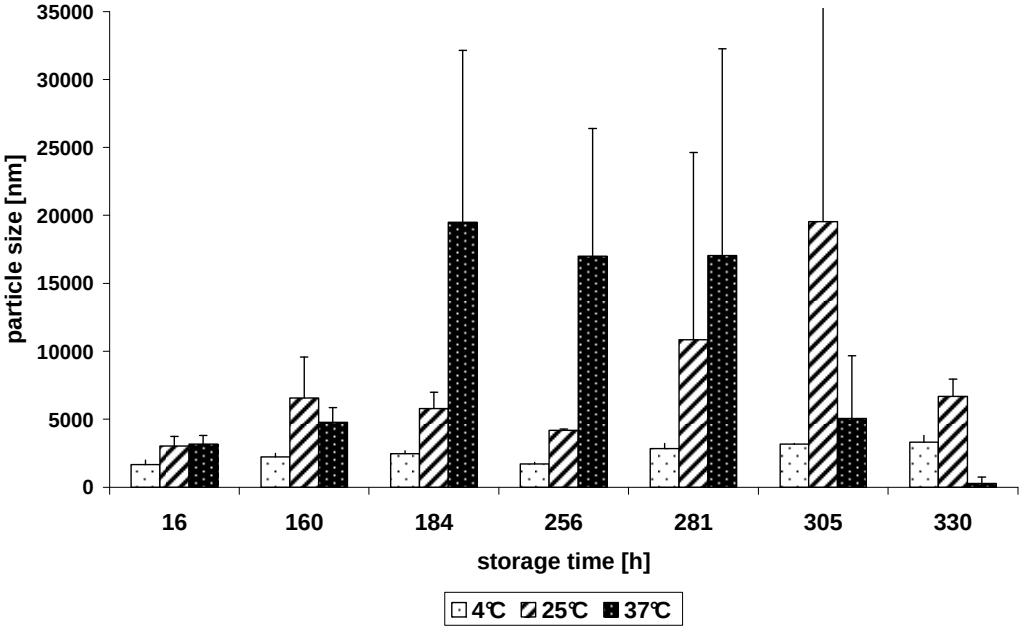

Fig. 8: *NaCN(BH)$_3$-hydrogenated GNP mean sizes (n=3, S.D.) over time at 4, 25 and 37°C storing temperature and pH 7.4 (n=3 ± S.D.).*

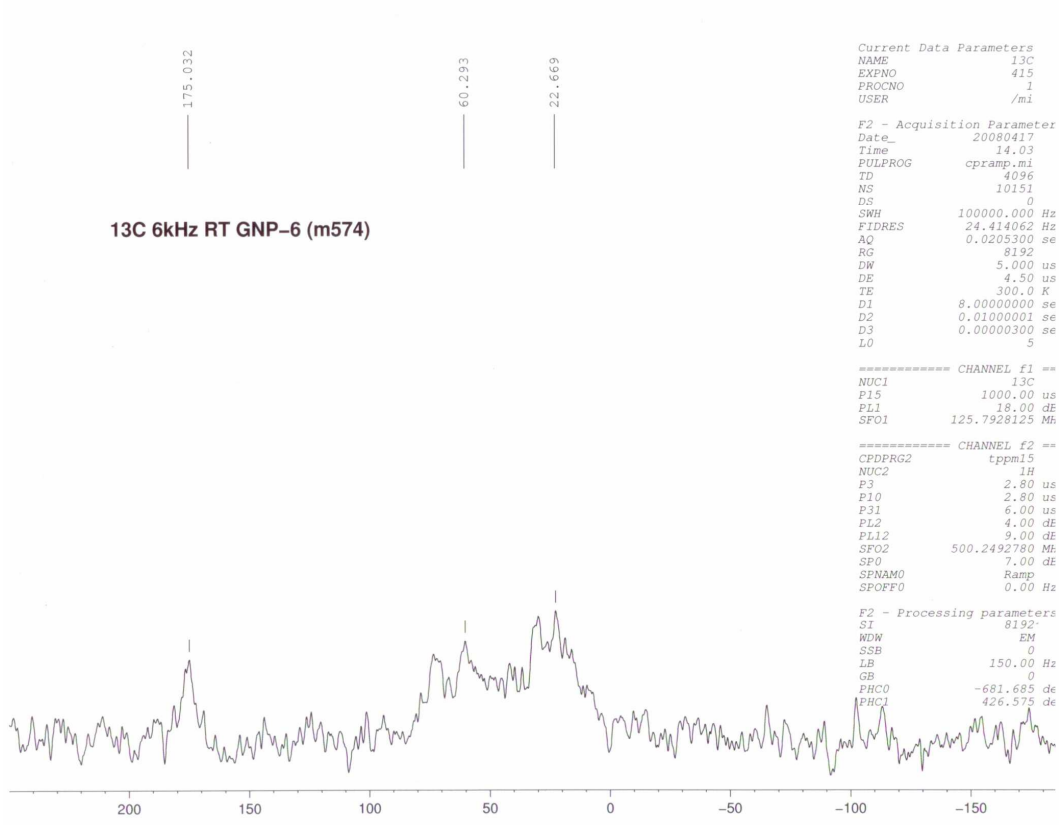

Fig. 9: *^{13}C MAS-NMR spretrum of H$_2$/carbon-bound Pd-hydrogenated GNPs.*

In contrast, H_2/carbon-bound Pd-hydrogenated GNPs featured a peak at 175 ppm indicating the presence of amide bands. Therefore, the primary protein structure

was not eliminated as with the former homogenoius catalyst. This was also reflected by the particle size monitoring over 330 h storage time (Fig 10).

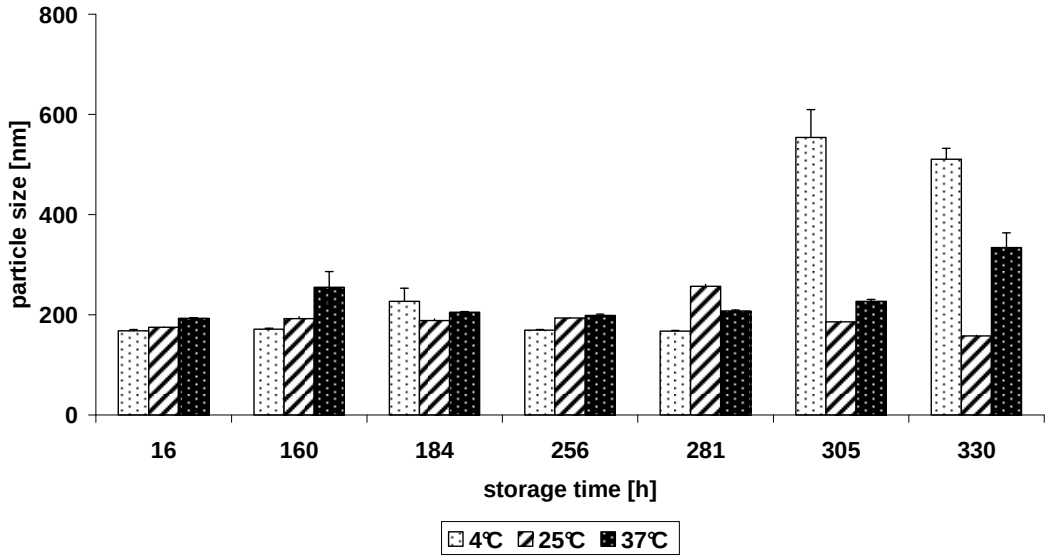

Fig. 10: *H_2/carbon-bound Pd-hydrogenated GNP mean sizes (n=3, S.D.) over time at 4, 25 and 37°C storing temperature and pH 7.4. Artefacts are present in 4°C samples at 305 and 330 min storage time (n=3, ± S.D.).*

GNPs featured size stability at least for 281 h when stored at 4°C. Storing at 25 and 37°C led to marginally significant higher particle sizes and size fluctuations between the reading points. No indication of complete loss of nanoparticulate morphology was found in contrast to the other catalyst-treated GNPs (Fig. 8). The reductive strength was thereby appropriate from a stability point of view. However, due to the overall poor signal-noise-ratio, no conclusion could be drawn neither to the existence of an imine band nor to its elimination in comparison to the non-hydrogenated GNPs (Fig. 6a). Therefore, a new series of experiments was required to obtain higher signal intensity by the employment of higher sample masses. Consequently, the previously introduced up-scaling process was used to employ higher amounts both of native and of H_2/carbon-bound Pd-hydrogenated GNPs. A 10-fold higher mass input led to the avisaged improved signal-noise ratio. Fig. 11a depicts the non-hydrogenated GNPs with regular amide bands at 171 ppm and the target structure of imines bands at 156 ppm.

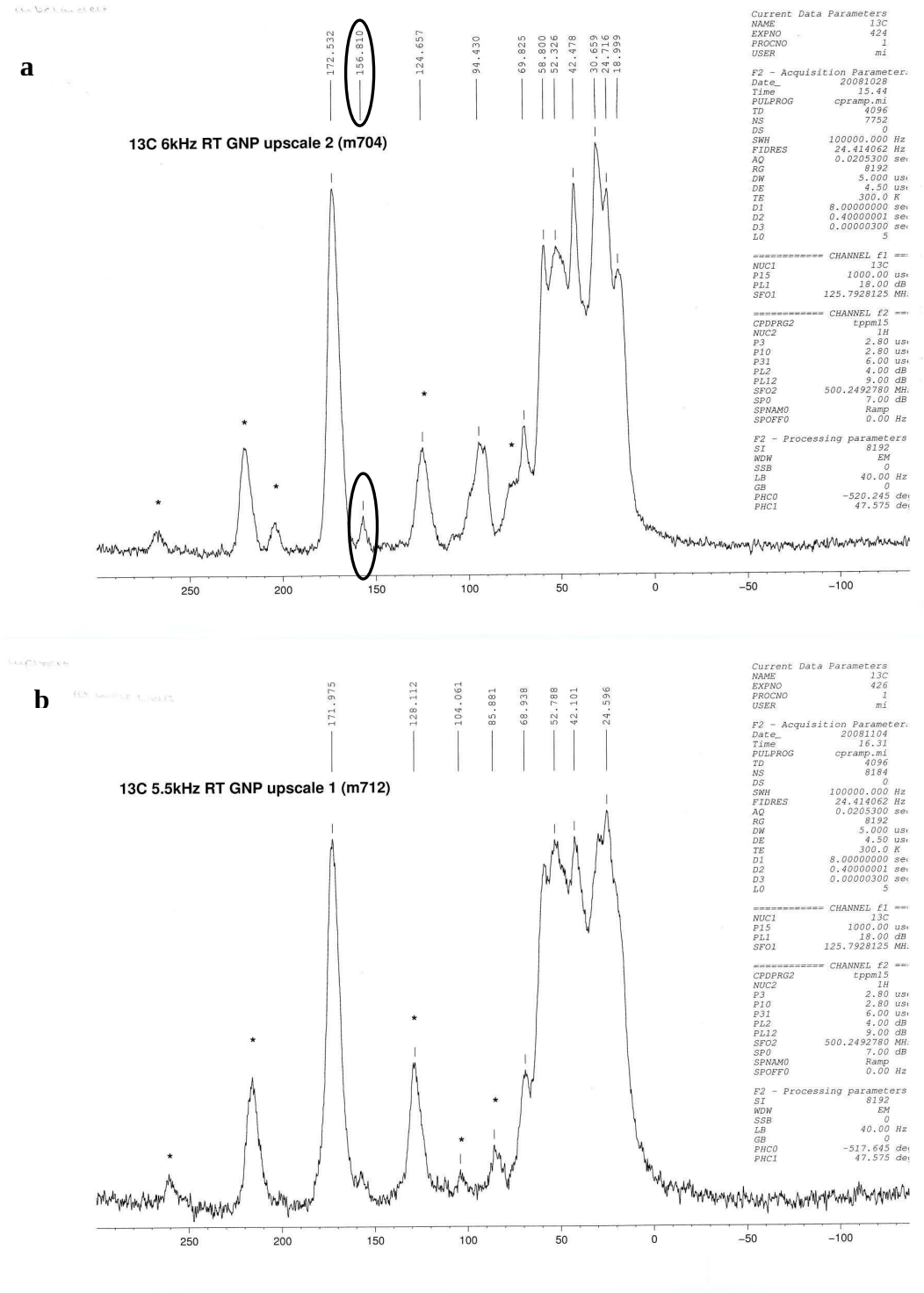

Fig. 11: *^{13}C MAS-NMR spretrum of native (a) and H_2/carbon-bound Pd-hydrogenated (b) GNPs.*

The imine band was successfully eliminated after the hydrogenation process confirming the effectiveness of the selected process (Fig. 11b). Moreover, all other bands remained unaffected supporting the identification of the method's selectivity. Again, this finding was in accordance with the observed short-term

stability of H_2/carbon-bound Pd-hydrogenated (b) GNPs (Fig. 10). However, stability was not increased compared the native non-hydrogenated GNPs.

In summary, the additional efforts were not justified by the resulting properties of hydrogenated GNPs. Although the hydrogenation process itself finally turned out to be successfully conducted, the particle mid-term stability was not superior. Furthermore, the hydrogenation itself and the subsequent –eventhough possible- purification at least double the GNP manufacturing time and costs per batch compared to the non.treated GNPs which already demonstrated their biocompatibility in several *in vivo* trials. Therefore, if a replacement of currently used glutaraledhyde-generated imins was required in future, other strategies should be followed. Nevertheless, this evidence would not have been possible without upcaling the GNP manufacturing process which was established by the present work.

3. Enzymatic cross-linking of GNPs

3.1 Introduction

Applying the two-step desolvation method for manufacturing gelatin nanoparticles, the tendency of aggregation of the GNPs could be reduced and particle production of reproducible size, size distribution and yield could be gained (Coester *et al.* 2000). The prepared GNPs showed a high stability and were up-scalable during manufacture.

While GNPs chemically cross-linked by glutaraldehyde did not trigger undesired immune or toxicological reactions, a reduction in biocompatibility of cross-linked gelatin-films was reported earlier (Van Luyn *et al.* 1995) and slight toxicity in peroral toxicology studies as well as contact dermatitis if applied on the skin were shown (Ballantyne and Jordan 2001). Otherwise, glutaraldehyde was widely employed for a range of industrial and biomedical applications to include cold sterilization and biocidal use in production sites (Ballantyne and Jordan 2001). As glutaraldehyde is consumed during the GNP cross-linking reaction and residuals are removed by particle purification, consequently no adverse effects could be observed.

Nevertheless, aiming at potential future applications of GNPs in humans (pharmaceuticals like food), substances like glutaraldehyde with a theoretical residual risk deserve attention in terms of “generally regarded as safe” replacements (Chau *et al.* 2005).

Hence, as a non-toxic alternative to the chemical cross-linker glutaraldehyde the enzyme transglutaminase (TG; E.C. 2.3.2.13), an enzyme whose subspecies microbial TG (MTG) is already used as a biocatalyst to covalently cross-link proteins in food chemistry (Boenisch *et al.* 2007), tissue engineering (Bertoni *et al.* 2006) and others (Zhu and Tramper 2008), is investigated here for GNP preparation.

The mammalian TGs are Ca^{2+}-depending enzymes which play various roles such as in blood clotting, HIV entering into target cells and the pathology of the celiac and Huntington diseases, but they are also generally stabilizing and protective in the cells (Griffin *et al.* 2002). In contrast, the microbial TGs isolated from Streptomyces are easier to produce, more feasible in biotechnologic applications due to their Ca^{2+} independence and have broader substrate specificity than mammalian tissue TGs (Cui *et al.* 2008; Lantto 2007).

These acyltransferases form intra- and intermolecular isopeptide bonds in and between many proteins by cross-linking the ε-amino groups of the amino acid lysine to the side chain amide group of glutamine thereby releasing one molecule of ammonia per crosslink (Figure 1) (Boenisch *et al.* 2007; Heidebach *et al.* 2008; Lantto 2007; Griffin *et al.* 2002).

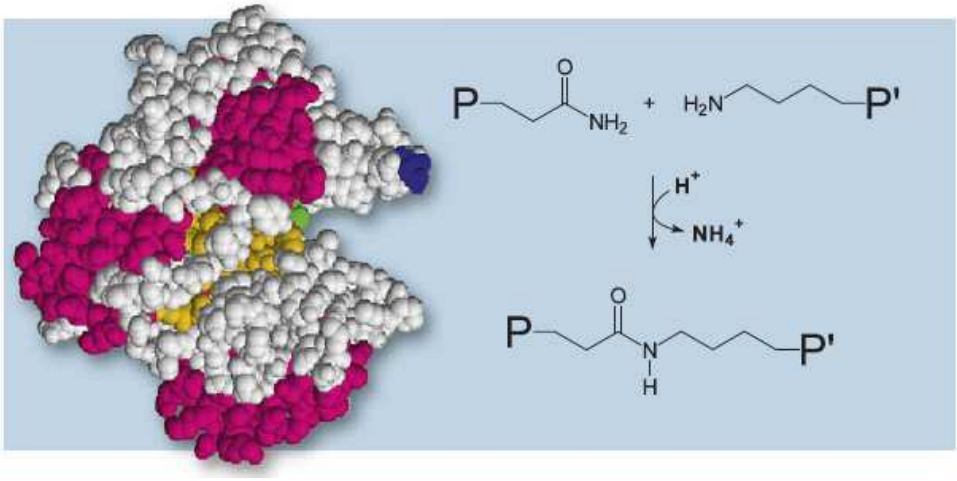

Fig. 1*: Protein cross-linking by transglutaminase between primary amino groups of the amino acids glutamine and lysine in course of which one molecule of ammonia is generated per crosslink (courtesy of Fuchsbauer, Darmstadt University of Appl. Sc., Germany)*

Enzymatic cross-linking is an attractive approach due to its high specificity of the enzyme catalysis controllable to a certain degree by changing pH and temperature. The pH activity curve for MTG for instance shows an optimum between pH 5 and 8 (Boenisch *et al.* 2007; Lantto 2007). Furthermore, it was reported that MTG showed no degradation but in contrast a slightly increased activity in the presence of low ethanol concentrations (Cui *et al.* 2008). This was in accordance with previous reports on the mammalian form of the enzyme being stimulated by organic solvents (Plishker *et al.* 1978).

To date, beyond food processing, MTGs demonstrated their ability to mechanically cross-link highly resistible gelatin-based scaffolds (Broderick *et al.* 2005), whereby cytoxicity was reduced compared to formation of gelatin-based scaffold by radical polymerization. (Barbetta *et al.* 2006) Further well documented examples for cross-linking with MTG are milk proteins like casein (Boenisch *et al.* 2007), hydroxyethyl starch conjugation (Besheer *et al.* 2009), gelatin barrier films (de Carvalho and Grosso 2004), fish gelatin-nanoclay (Bae *et al.* 2009) and matrix proteins in potential medical applications. (Collighan and

Griffin 2009) The use of transglutaminase was already considered in patents for nanoparticle crosslinking (Aimi *et al.* 2007; Aimi *et al.* 2007). However, no actual result data was ever published on this potential process attempt. Therefore, the stabilization of GNPs by MTG was investigated and discussed for the first time in this study.

3.2 Materials and methods

3.2.1 Materials

All used chemicals like gelatin type A from porcine skin (175 Bloom), glutaraldehyde and acetone were of analytical grade and purchased from sigma Aldrich GmbH (Taufkirchen, Germany). The recombinant microbial transglutaminase (rMTG) was produced by the group of Prof. Pietzsch, Department of Pharmaceutical Biotechnology Halle, Germany. The wild-type transglutaminase (Activa™ MTG) was manufactured by Ajinomoto Co. (Tokyo, Japan). Whereas the phosphate buffered saline (PBS) buffer was obtained ready to use from invitrogen GmbH (Karlsruhe, Germany), 12.11 g Tris(hydroxymethyl)-aminomethane (Sigma Aldrich GmbH) were dissolved in 1 l highly purified water (HPW) to prepare the 0.1 M Tris-buffer.

HPW was generated by a purelab® device (ELGA LabWater, Celle, Germany) and filtered with an acrodisc® 0.2 µm steril syringe filter (PALL lifescience, Dreieich, Germany). All employed media were sterilely filtered prior to use to prevent impurities.

3.2.2 Enzyme preparation

Cultivation of *E. coli* BL21(DE3) containing the plasmid pDJ1-3 (Marx *et al.* 2007) was carried out in the group of Prof. Pietzsch, Halle using a minimal medium according to Wilms et al. (Wilms *et al.* 2001). *E. coli* pDJ1-3 cells were adapted to the minimal medium by passaging cells grown on LB medium (Marx *et al.* 2007). In six consecutive cultivations, the portion of the complex medium was reduced to below 0.1 %. Cultivation was carried out at 37°C. For enzyme expression, the main culture was induced with 0.7 mM IPTG at a post-induction temperature of 29°C. Cells were harvested and rMTG was isolated using affinity chromatography as described elsewhere (Marx *et al.* 2008) with the following

modifications. 20% bio wet mass was suspended in disintegration buffer, Proteinase K was used for activation (12 U/g bio wet mass, incubation at 37°C for 2h). Eluted fractions were dialyzed against Tris-buffer and stored at -20°C after addition of glycerol and glutathione (GSH, final concentrations 50% glycerol, 2mM GSH).

3.2.3 **Production of gelatin nanoparticles**

Plain gelatin nanoparticles were prepared by a two step desolvation technique according to the established protocol (Coester *et al.* 2000; Zwiorek *et al.* 2004) without subsequent cross-linking by glutaraldehyde.

For controlled addition of acetone to the gelatin solution a Gilson peristaltic pump Miniplus 3 (ABIMED Analysentechnik GmbH, Langenfeld, Germany) was utilized.

In the process, feeding rates of acetone were 12 ml/min for the first and 5 ml/min for the second desolvation step. Sediment built after the first desolvation step was kept below 2.5 g while the pH-value after the second desolvation step was kept below 3.0.

As transglutaminase is sensitive to organic solvents, a purification of the acetone containing particle dispersion was considered crucial after the second desolvation step. To eliminate the acetone from the dispersion, five approaches were evaluated.

Firstly, vacuum evaporation was used as a commonly known and mild method. Therefore, 100 ml of dispersion were transferred to a round bottom flask 10 min after completion of the second desolvation step. Parameters were set either to 50°C, 200 rpm and vacuum for at least 30 min or to 25°C, 200 rpm and reduced vacuum for which a Laborrota 4001 (Heidolph Instruments GmbH & Co. KG, Schwabach, Germany) was used.

As the original protocol devises slow evaporation of acetone over night through constant stirring at room temperature, this was considered as the second alternative. Furthermore, evaporation at elevated temperature was performed as a third alternative to vacuum evaporation by transferring 30 ml of original dispersion to 1 l flat bottom flasks and stirred over night at 37°C.

Next, the option of direct centrifugation after the second desolvation step as a

rapid method was investigated.

Finally, the last approach comprised a significant dilution of acetone to allow sufficient enzymatic activity. Hence, 10 ml of the original post second desolvation particle dispersion were diluted with 65 ml of one of the three different media HPW, PBS or 0.1 M Tris-buffer. The 10 ml contained 0.2 g non-cross-linked GNPs, 5.7 g acetone and 2.8 g HPW on average.

3.2.4 **Cross-linking methods**

Subsequently, the nanoparticle dispersions from the above described methods were equally adjusted to pH-value 7.4 and temperated at 16°C, 25°C or 37°C. Thereupon, the cross-linking enzyme was added either as a solution or in powder. 100 µl solution of the recombinant enzyme (≙ 60 U in 50% glycerol, 1 mM GSH, 150 mM NaCl, 25 mM Tris-HCl, pH 8.0) or 600 mg commercial powder (1 % MTG stabilized with 99 % Maltodextrin), equally containing 60 U of enzyme, were added. Temperature of both enzyme preparations was either 4°C or -20°C at the moment of addition to the reaction dispersion and incubation time was set to 48 h.

3.2.5 **Particle analysis by PCS and turbidity measurement**

To determine the size of the prepared particles, standard Malvern Zetasizer® ZS nano device (Malvern, Worcestershire, United Kingdom) was used for analysis by PCS. Particle sizes were intensity weighted results (z-average) and size distributions were given as polydispersity indexes (PdI).

For evaluation of particle sizes during cross-linking incubation time, prior to all measurements 100 µl of the relevant dilution were transferred to halfmicro PMMA cuvettes and completed with HPW to a final volume of 600 µl. Correspondingly 10 µl of readily purified and concentrated dispersion for subsequent stability studies were added to 590 µl of HPW in the cuvettes. Mean sizes and size distributions (PdI) were defined as mean of three measurements, each consisting of at least 14 subruns.

Additionally, the turbidity of the samples was measured with a Nephla Dr. Lange turbidimeter (Hoch Lange GmbH, Düsseldorf, Germany) to compare the different rudiments during incubation. Results were given in formazine normalized units

(FNU). Therefore, 2 ml of each sample were filled into round glass cuvettes and inserted into the turbidimeter at defined intervals. The preceding method of turbidity measurement gave evidence of the particle formation. However, the designated product of discrete particles on the one hand and undesired aggregates on the other hand both contributed to turbidity and could not be distinguished by this method.

3.2.6 **Stability tests**

Purified and filtered nanoparticle dispersions were divided into equal volumes for stability testing at 4°C and 37°C, stored in a refrigerator and accordingly in a Certomat® IS (B. Braun Biotech International now Sartorius BBI Systems, Göttingen, Germany).

After certain time intervals, samples were taken and analyzed for stability by PCS.

3.2.7 **Statistical analysis**

Data was analysed for difference in turbidity between time points of incubation or between defined temperatures or medium composition using a paired t-test performed by Prism 5 (GraphPad Software Inc., La Jolla, USA).

3.3 Results and discussion

3.3.1 **Effect of purification method on particle integrity**

In standard purification of GNPs cross-linked by glutaraldehyde, vacuum evaporation was previously found to be beneficial as a method to shorten processing time. Therefore, it was assumed that this method could be used in purification of not yet cross-linked particles to remove large amounts of residual acetone of the second desolvation step, too. However, as soon as acetone started to evaporate at the chosen standard conditions (vacuum, 50°C and reduced vacuum at 25°C), dispersion turbidity started to fade. After clouding, the whole dispersion became a transparent viscous gelatin solution. The particle characteristic of the dispersion was completely lost. Preliminarily, it was assumed that phase transition and altered solubility led to the increasing particle

deformation. As this obviously was a consequence of the applied thermal and mechanical stress onto the not yet stabilized particles, further attempts aimed at less harsh conditions. Hence, vacuum was omitted and temperature was reduced. Still, no considerable amounts of particles were recovered after this process. The same effect was observed when directly centrifuging the particle dispersion without any prior thermal stress. Obviously, the resolvation was quicker than the acetone evaporation rate which finally led to gelatin dissolved in an acetone–water solution.

As purification after particle formation in the second desolvation step was impossible without loss of particle integrity, the last alternative was to reduce the percentile amount of contained acetone. Previously, Cui et al. demonstrated that low amounts of organic solvents such as ethanol do not influence the enzymatic activity of transglutaminase in a negative way. On the contrary, percentile concentrations of 10% Ethanol increased the activity, while amounts of up to 20% added volume of ethanol had no adverse effect (Cui *et al.* 2008). This was in accordance with earlier findings, that acetone known to be relatively aggressive in inducing protein precipitation (Yoon and Mckenzie 2005) was tolerated by human TG in low concentrations as well (Plishker *et al.* 1978). Consequently, as acetone is known to inactivate enzymes in lower concentrations than ethanol, the acetone concentration in all following trials was kept as low as at 10% (v/v) by applying a 1:7.5 (dispersion : water) dilution. Therefore, sufficient enzyme activity by diluting the dispersion with the different media was presumably ensured.

3.3.2 **Effect of cross-linking parameters during incubation**

The intention of analysing various cross-linking process parameters was to optimize yield of well characterized particles within a short period of time and to define simple and reproducible cross-linking conditions.

3.3.3 **Turbidity monitoring during enzymatic cross-linking time**

Nephelometry (turbidity measurement) was previously described as feasible to quantify low concentrated GNP dispersions below 1 mg/ml (Fuchs *et al*. 2009). Due to the requirement to keep the acetone percentage low, GNPs consequently were existent in concentrations of 0.25 mg/ml or less. Hence, nephelometry was

performed as a quick method to estimate particle quantity. In HPW, highly significant differences in turbidity were found between the three investigated temperatures over each incubation period. However, no significant differences in turbidity were found between samples incubated at 25°C and 37°C at the end of the incubation process after 48 h. Therefore, subsequent batches were treated at 25°C for good cross-linking yield in order to reduce thermal stress on the newly formed particles and consequently to preserve their structure and stability.

Comparing the turbidity over time in the three different media HPW, PBS and 0.1 M Tris-buffer it can be deducted that the enzymatic reaction led to the highest GNP yield as by turbidity in HPW (Figure 2). For PBS, turbidity stayed low after 21h of incubation and roughly triples until the final assessment time point at 48 h. However, turbidity remained at only a seventh of the turbidity achieved in HPW in the same time. The higher electrolyte concentration in PBS led to a significant decrease in enzyme-mediated particle stabilization. Results for Tris-buffer are significantly higher than those of PBS reaching more than 20% of the turbidity value achieved in HPW after 21 h (Figure 2). Tris-buffer is known as a good stabilizing medium as it does not have any oxidizing properties and maintains a pH value of 7.4 beneficial for TG activity. Furthermore, Tris-buffer is employed since 1966 to house reactions with TG and to assess enzymatic activity. However, even Tris-buffer cannot achieve the same turbidity as HPW. This effect might be related to the impact of ions on the particle size and matrix structure. It was shown earlier that GNPs start to decrease in size once confronted with ions (Fuchs et al. 2010). Consequently, the gelatin matrix allows less solubilised rMTG to penetrate the gelatin matrix and finally stabilize the particles over all by cross-linking. PBS featuring a higher ionic strength in comparison to 0.1 M Tris performed worst in the cross-linking process. HPW surprisingly appeared most suitable in this comparative study at 25°C with the maximum turbidity reached within 21 h. No significant reduction was subsequently detected from the second to the third sampling point. Therefore, the enzymatic reaction was regarded already completed after 21 h at the second sampling point (Figure 2). A quantitative gravimetrical concentration determination of post-centrifugation purificated particle dispersions (1.5 mg/ml ± 0.3 mg/ml) was only possible for the samples incubated in HPW. Concentrations of PBS or Tris-buffer derived particles were too low after purification by centrifugation to be quantified.

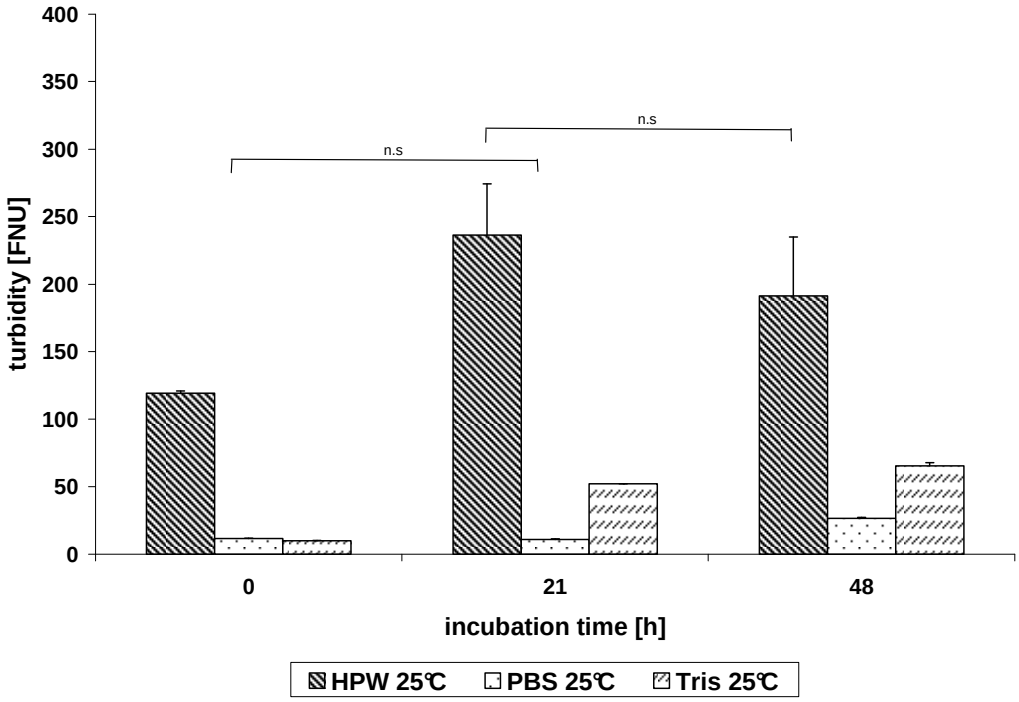

Fig. 2: *Turbidity is significantly depending on cross-linking incubation time with rMTGin the three different media equally temperated at 25 °C (n=3, ± S.D.). n.s. indicates no statistical significance.*

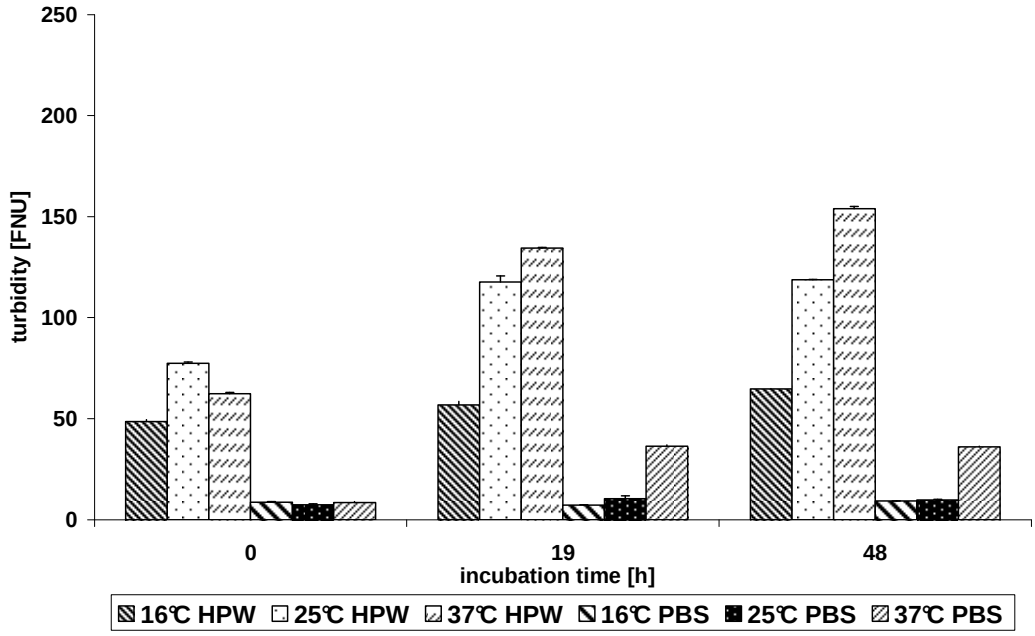

***Fig. 3**: Turbidity is significantly different in HPW and PBS depending on cross-linking incubation time and the applied reaction temperature (n=3, ± S.D.).*

Besides the appropriate medium, the most effective reaction time in terms of achieved particle yield was of interest. Therefore, a lower temperature (16°C) and

physiologic temperature (37°C) were tested. It can be stated that turbidity increased over time and with the applied reaction temperature (Figure 3). In HPW only at 37°C the turbidity increased further from the second to the third recorded sampling point. 37°C as incubation temperature is recommended to achieve high yields.

The turbidity of dispersions prepared with the commercial Activa™ enzyme fomulation could not be evaluated because remaining coarse powder particles disturbed the results. Furthermore, an additional purification step was required to eliminate remaining maltodextrin particles. Consequently, the approach to crosslink the particles with commercial powder Activa™ was not further followed.

Additionally, the temperature of the added enzyme solution was critical for the yield of resulting particles and the particle building process itself. In case of drop-wise addition of sub 0°C temperated enzyme solution, particle stability over time can not be held up which was also demonstrated by high PdI values in the relevant batches (data not shown). Nevertheless, the temperature of the dispersion has a modulating impact. Consequently, batches prepared at higher temperatures like 37°C are less impacted by the colloidal dispersing effect of sub-cooled drops of enzymatic solution. The chosen amount of MTG was based on the employment of glutaraldehyde in standard GNP production where 43.75 mg GT were used per batch (Zwiorek et al. 2008). This equals 0.438 mol and consequently can crosslink a maximum of 0.876 mol residual amino groups within the gelatin. Due to the above described necessary 1:7.5 dilution of the acetone-containing GNP dispersion after the second desolvation step, the resulting amount of amino groups is 0.1168 mol per batch based on above calculation. The added 100 µl of recombinant enzyme solution with a given stock enzymatic activity of 600 µmol/min/ml should theoretically transform this amount in 31.5 h. However, enzymatic activity was not expected to entirely last that long. Accordingly, as it could be derived from Figures 2 and 3, a longer incubation time than the interval till the first control sampling point is not indicated due to the lack of a relevant yield increase thereafter.

3.4 Particle size analysis during the enzymatic cross-linking time

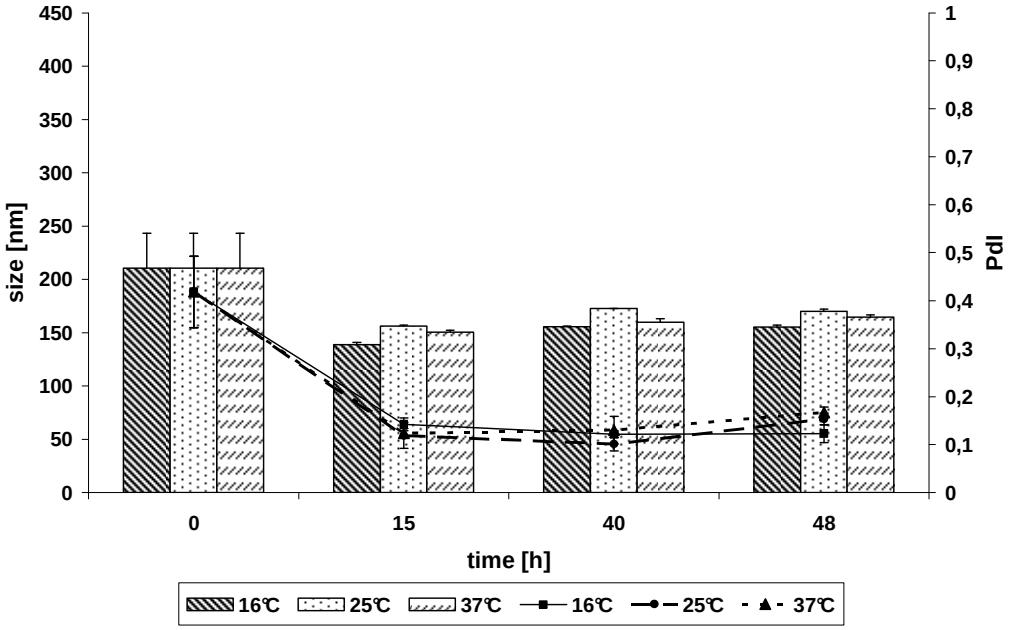

***Fig. 4**: Size (bars) and size distribution (curves) during initial particle formation time with pH-value adjusted to 7.4 and temperature of added enzyme of 4°C. (n=3, ± S.D.).*

GNPs quality attributes were monitored over an incubation period of 48 h. The chosen time frame was longer than the enzymatic reaction presuming took place in order to provide a safety margin for the detection of possible reverse reactions and resulting dissolution of the nanoparticles. Initially, formed particles featured a PdI of about 0.4 indicating an unfavourably broad particle size distribution (Figure 4). However, this is significantly diminished to monomodality indicating values close to 0.1 at all three following control sampling points while temperatures and stirring at about 300 rpm were kept constant (Figure 4). In addition to the decreasing particle size, this demonstrates sufficiently increasing particle stability within the enzymatic cross-linking period. Particle quality attributes remained constant after contact with the enzyme over 15 h. Within this period, the reaction was presumably completed as enzyme catalyzed reactions are accomplished quicker than the standard non-catalyzed glutaraldehyde-mediated cross-linking process.

Combined size and yield results suggest an incubation time of at least 12 h but do not point to additional effectiveness of the here employed maximum 48 h incubation period.

3.4.1 **Effect of storage temperature on particle stability**

Consistency in size and size distribution is an important indicator for particle integrity. A resolvation of insufficiently cross-linked particles' gelatin impacts these key parameters obtained by PCS analysis. Despite two measurement artefacts at 4°C (Figure 5a), high storage stability of rMTG-cross-linked particles was found (Figure 5a and 5b). In detail, standard deviations remained low, particle sizes constant and PdIs mostly under 0.2. Towards the end of the monitoring period, PdIs even fell below 0.1 in all cases indicating particle monodispersity. Consequently, obtained particles are suitable for standard storage conditions at 4°C as well as at 37°C being the physiologic temperature and therefore enabling the particles to be used *in vivo* and *in vitro*.

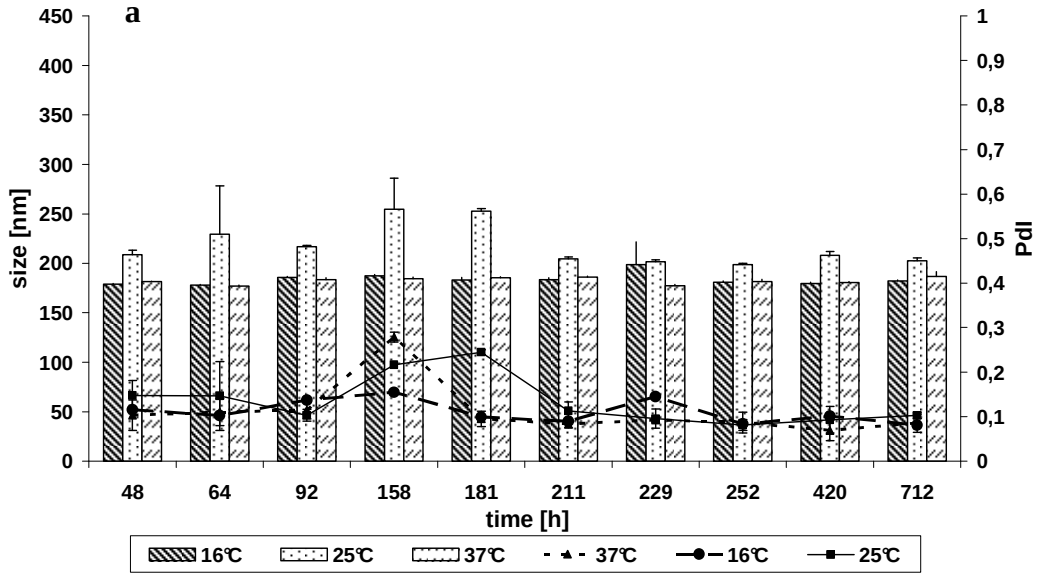

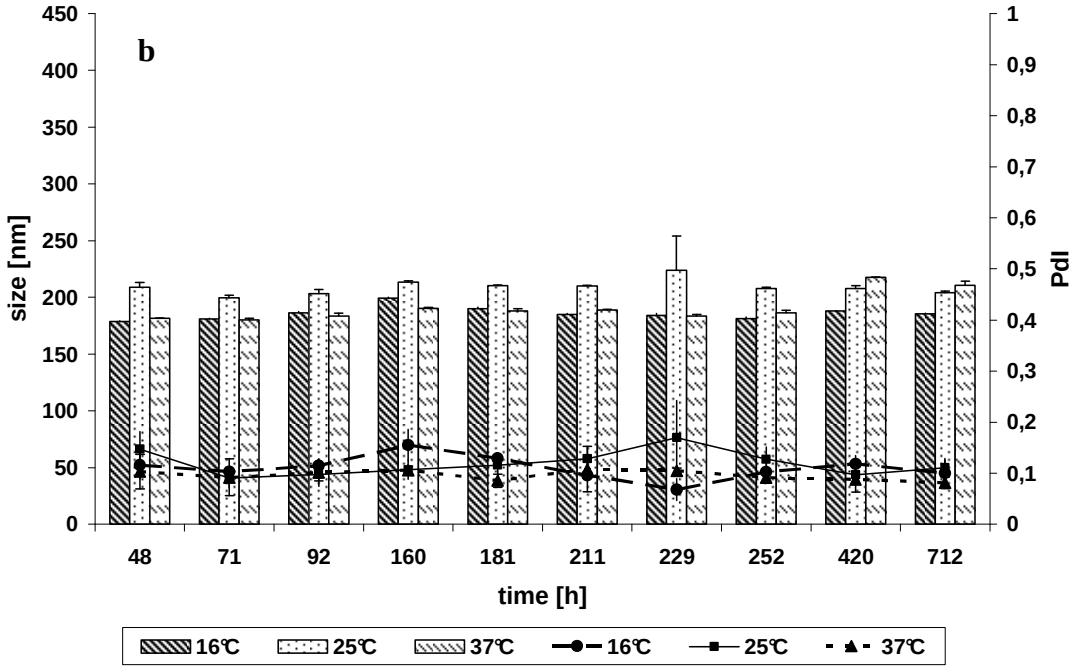

***Fig. 5**: Particle properties size (bars) and size distribution (curves) upon on storage stability testing over 4 weeks at 4°C (a) and 37°C (b) (n=3, ± S.D.).*

3.5 Conclusions

Feasibility of transglutaminase as a cross-linking agent in gelatin nanoparticle production was demonstrated in principle. The initial obstacle, to cope with the residual acetone, was overcome. Particles of defined size below 250 nm and narrow size distribution stable in a short range stability set up were produced successfully. The preferable medium for cross-linking was identified as water while preferable incubation time and temperature were 48 h and 25°C - 37°C respectively. Further improvements in product yield and various process parameters such as a reduction in incubation time are subject of later formulation development and upscaling. Summarising, transglutaminase widely used in food chemistry and biomaterial research is also a promising alternative in pharmaceutical GNP production to glutaraldehyde and other chemical cross-linkers' use in clinical studies. Concerning the potential immunogenicity, for drug formulation the application of a human transglutaminase is favourable. Therefore, further experiments are promising using this biocatalyst.

III Enlarging the analytical toolbox for gelatin nanoparticles

1. Basic setpoints in PCS-based nanoparticle size measurement

A crucial precondition for the entire set of following experiments that involve PCS-based size measurements, was the knowledge of a possible concentration influence onto received results. Due to the intrument's 173° backscattering design (Zetaziser ZS Nano, Malvern, UK), the manufacturer's specification promised a wide concentration and turbidity range of applicable dispersions accessible for substantial data collection. However, detailed information to confirm relevant concentration independence in nanoparticle size determination was not obtained and discussed previously. Especially, the circumstance if the frequently conducted cationization had an interfering impact should be ruled out as a precondition for all further investigations such as standard QC by PCS.

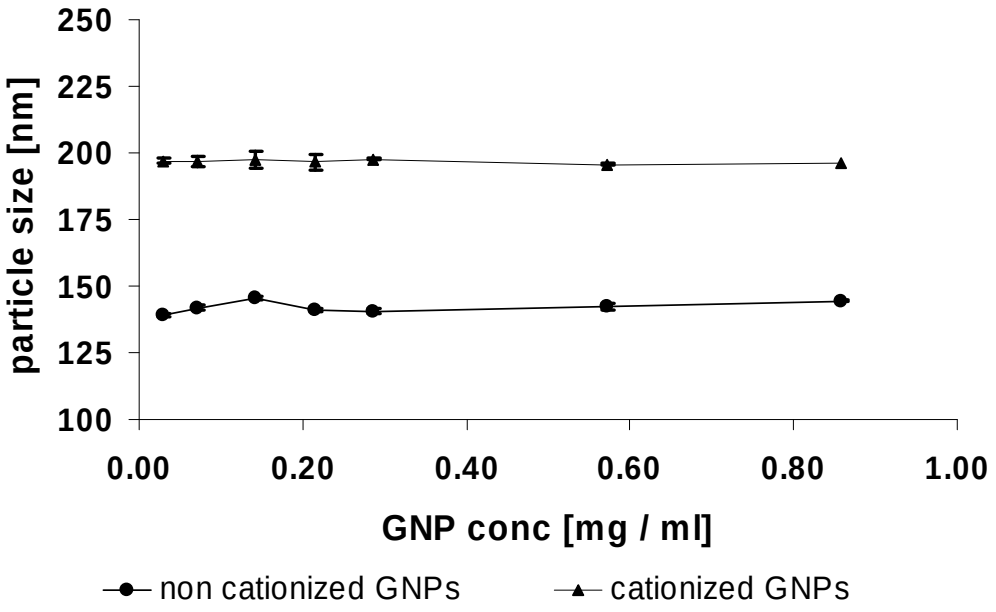

***Fig. 1**: Correlation between the GNP concentration and the PCS-determined sizes of non-cationized (closed circles) and cationized (closed triangles) GNPs (n=3, ± S.D.).*

Obviously, the particles size did not change along within the applied range of GNP concentration but stayed constant (Fig. 1). The same was found for the particle size distribution, characterized for Taking the PCS' measurement fault

tolerance (2%) and the very small error bars into account, no changes are detectable for the cationized GNPs and almost no changes for the non cationized GNPs. Alterations in viscosity were too small at concentrations below 0.1% (m/v) to influence the particles' Brownian molecular movement and consequently their determined hydrodynamic diameter. The cationization imposed a heavy influence on the particle size though. A 30 – 40% increase in particle size was found for this batch but even larger increases were found in other trials (Fuchs et al. 2010). The direct comparison was appropriate due to the fact that the examined cationized GNPs were derived from the batch of non cationized GNPs and thus, were of the same origin. The found influence of cationization on the particle size is furthermore discussed in detail with the insights gained from the ultrasound study (see chapter III.2).

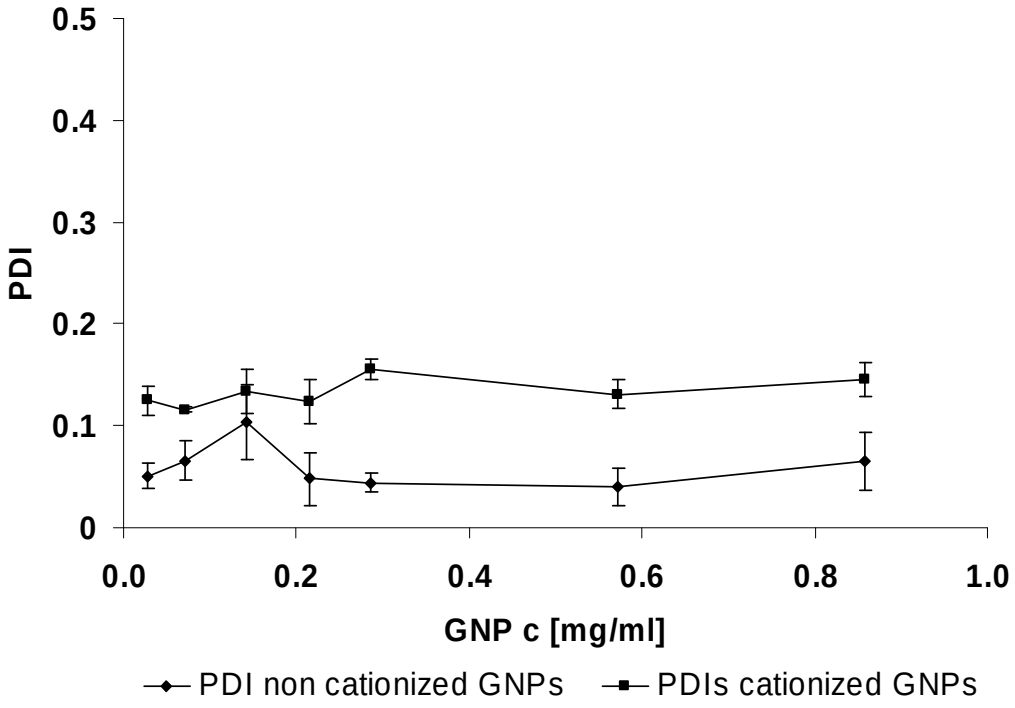

***Fig. 2**: Correlation between the GNP concentration and the PCS-determined PDI of non-cationized (closed circles) and cationized (closed triangles) GNPs. (n=3, ± S.D.)*

Along with the size and PDI of GNPs, the conductivity of the applied GNP dispersion was followed as a side result from Zeta potential measurements. (Fig. 3)

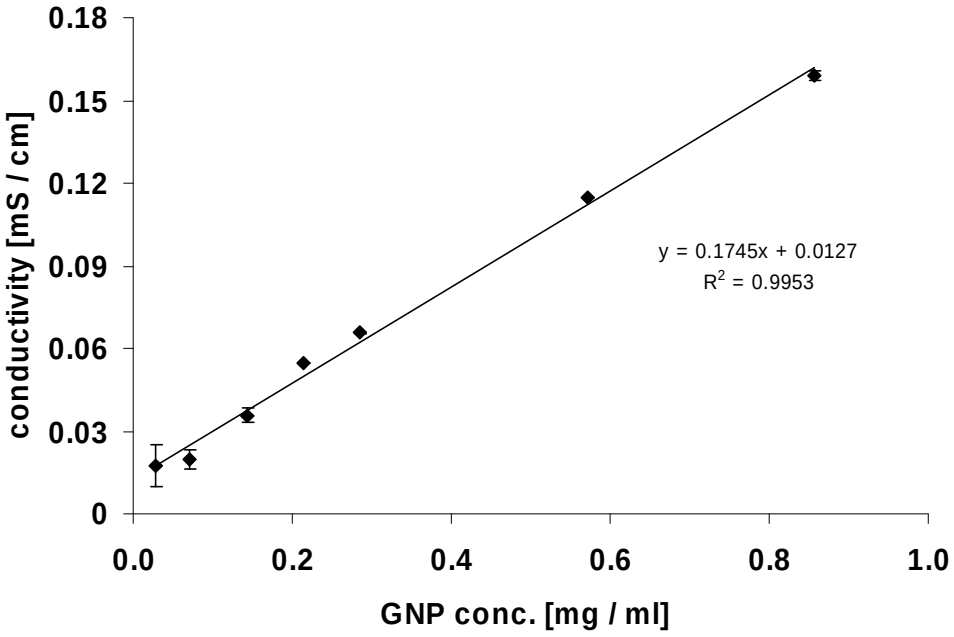

***Fig. 3**: Linear Correlation between the GNP concentration and the PCS-determined conductivity of cationized GNPs in HPW (n=3, ± S.D.).*

However, even though the increae in conductivity is linear and significant, the obtained values are still very low in comparison to electrolyte solutions like PBS. For comparison, water featuring conductivity below 0.055 µS / cm was employed as highly purified water throughout all herein reported studies. On the contrary, PBS exhibited values for conductivity and consequently covered all GNP-derived increases in particle concentration-dependent conductivity.

2. Ultrasonic resonator technology as a new quality control method evaluating GNPs and nucleic acid loading

2.1 Introduction

Analytical methods to determine the all decisive nanoparticle value, the size, consist of scanning electron microscopy (SEM), photon correlation spectroscopy (PCS), often also referred to as dynamic light scattering (DLS) and asymmetrical field flow field fractionation (AF4) coupled with multi angle light scattering (MALS) (Fraunhofer et al. 2004). Concentrations of nanoparticles are determined by turbidity, gravimetry or, in some limited cases, by absorption spectroscopy (Hurst et al. 2007). However, some of these methods suffer from time consuming protocols or a limited detection ranges. These deficiencies could pave the way for an alternative method like Ultrasonic Resonator Technology (URT).

In this study, size of cationized GNPs and their loading by ODNs was evaluated. The feasibility of GNPs as ODN carriers has been demonstrated previously (Zillies and Coester 2004).

More precisely, a double-stranded NF kappa B decoy DNA was predominantly used in the present study which was proven therapeutic efficiency in ischemia/reperfusion injury animal models. Assessment of quantitative ODN loading is a precondition for ratable *in vitro* or *in vivo* effects of the employed formulation, although in some cases loading was judged from the transfection efficiency only (Sokolova et al. 2007). However, to meet quality standards employable in further up scaling or approval by regulatory authorities, detailed knowledge of the loading status is essential. Therefore, various attempts have been made so far to quantify the effective payload on nanoparticles (Table 1).

method	advantageous	disadvantageous
centrifugation and spectrometric analysis of supernatant	well established; depending on supernatant analysis:cheap	low in precision, time consuming indirect measurement
size - loading correlation	quick	low in precision
surface charge - loading correlation	quick	low in precision
AF4	universal, precise	time consuming, expensive

Table 1. *Advantages and disadvantages of present nanoparticle surface loading analytics.*

Separating ODN loaded nanoparticles from the unbound, soluble ODN by ultracentrifugation (with or without size cut off membranes) has assumed a prominent role in assessing the loading yield.

The subsequent quantitative analysis of the supernatant for the soluble portion is performed by absorption measurement of unmodified ODN (Zwiorek et al. 2004). This can be done by quantitative fluorescence analysis of previously labeled DNA (Hurst et al. 2007) or post separation labeling and spectroscopic quantification by PicoGreen® quantification kit (Bivas-Benita et al. 2003; Gu et al. 2006; Huang et al. 2006; Kaul and Amiji 2005; Perez et al. 2001) or other fluorescent setups including Hoechst dyeing (Sun et al. 2005). Radioactive ^{32}P ODN labeling is another reported means (Chavany et al. 1992). In case of encapsulation, the carrier has to be disintegrated first to set free the total quantifiable ODN (Kaul and Amiji 2005) or the DNA can be chemically displaced by cutting the bonds from the nanoparticle surface with consecutive quantification after centrifugation purification (Hurst et al. 2007).

Other studies conducted were based upon a correlation between particle size change and varying loading efficiency (Jang et al. 2006), a decrease of surface charge (Giljohann et al. 2007) or on the optical FRET technique (Roy et al. 2005).

The same technical approach by centrifugation is widely common for determination of protein with follow up ELISA testing (Cetin et al. 2007) or small molecule drug loading onto nanocarriers (Petri et al. 2007).

A totally different approach to identify and quantify DNA, in its early stage of development, is the employment of nanopore devices (Archakov and Ivanov 2007). By pulling DNA through the nanopores, its electrical structure changes and emerges a ratable electrical resistance signal specific for the relevant nucleotide. Nevertheless a detachment of the DNA from the carrier is mandatory.

To summarize, the available methods for quantifying DNA loading of nanoparticles are partly time consuming and batch wise separation prior to determination method could suffer from a lack in accuracy (Table 1). The error in accuracy is likely due to contamination of the supernatant with non-sedimented particles that cannot be ruled out completely by cut off filtration. Furthermore, there is a potential risk that the preparation is no longer usable afterwards because of high sheer forces that impact on particle aggregation during complete

centrifugation, depending on the employed carrier system.

Alternatively, AF4 is a proven valuable method to separate and determine fractions of a formulation (Fraunhofer et al. 2004b; Zillies et al. 2007). Pursuant to its universal use the surface polyethylenglycol modification (PEGylation) of nanoparticles is quantitatively assessable even in the presence of ODN loading. Nevertheless, AF4 analysis of polymers and polymer particles is challenging and time consuming and not suitable for continuous production surveillance. Therefore, an additional new analytical method in combination with the established techniques for quality assessment of nanoparticulate loading shall be hereby proposed.

The spectroscopic methods described beforehand (UV, VIS, fluorescence and absorption) as well as commonly employed infrared spectroscopy (IR) and nuclear magnetic resonance (NMR) makes use of electromagnetic waves in analysis. However, ultrasonic spectroscopy used as a further spectroscopic method reveals relationships between acoustical patterns and sample's properties. It was used for a long time in medical diagnostics and entered into material science later (Chalikian et al. 1994; Funck et al. 1993; Sarvazyan 1991). Due to data resolution, specimen handling and design hold-ups to it has taken time for the ultrasonic spectroscopy to find its way into biomedical application (Negredo et al. 2007). In general, a high-frequency acoustical wave is passed through the sample leading to material properties related oscillating compression or decompression in the wave which causes again oscillations of the sample's molecular structure (Buckin et al. 2003). The total energy of sound employed for this study is extremely low and is classified as non-destructive. Furthermore, as sound waves (unlike optical waves) permeate turbid fluid formulations and they are applicable to practically all pharmaceutical relevant liquid preparations.

Ultrasonic spectroscopy calculates the absorption of the sound wave and speed of sound through a given sample (Buckin et al. 1989; Eggers 1992). Both properties are sensitive to changes in intermolecular interaction and molecular organization within the sample (Negredo et al. 2007). While the sound attenuation depends on chemical relaxation phenomena and bulk modulus of the sample, in this study resonating ultrasound is used to determine the sound velocity. The speed of sound (U) is directly linked to the thermodynamic property density (ρ) and mechanical property adiabatic compressibility β_S via the Newton Laplace equation:

$$U = \sqrt{\frac{1}{\beta_s \rho}}$$

The thermodynamic considerations used to determine the equation of state from the Laplace equation and the thermodynamic properties of the solution have been conducted previously in detail (Tikhonov et al. 1995). For dilute solutions, as investigated in this study, it is sufficient to use the linear term of the La Place equation only.

Using differential measurements (Sound velocity of sample minus sound velocity of reference, e.g. the corresponding buffer) the relationship between specific components of the sample and the propagation of the sound can be determined. In aqueous solutions water bound in hydration shells increase the overall speed of sound. This is due to the fact that hydration contributes negatively to the adiabatic compressibility while cavities do so positively (Gekko and Noguchi 1979; Gekko 2002). As the adiabatic compressibility β_S is reciprocally proportional to the speed of sound, an increase in hydration leads to an increase in the speed of sound. This is a simplified model since the contributions of all components are measured simultaneously. In this study, the surface loading of GNPs was examined and changes in ultrasonic velocity in the context of changes in surfaces exposed to the aqueous media were discussed. Hydration shells were also characterized by an increase in density. This effect was minor compared to the decrease in compressibility. Hence, an augmentation in the ultrasonic velocity signal stood for an increase in agents enlarging the hydration shells in the sample, which consisted of GNPs, ODN or ODN loaded GNPs in this study (Gekko 2002). Besides loading strategies, stability issues of the colloidal system as well as soluble ODN deserved attention. As an alteration in structure –due to aggregation or decomposition- will likely lead to hydration shell changes. Hence, monitoring the velocity of sound might provide valuable information on formulation stability.

Different ultrasonic velocimetry methods for biomolecules have been developed in the past. Sarvazyan distinguished the sing around method and the fixed-path interferometer (resonator) method (Sarvazyan 1991). While the first method was precise, the required high sample volume made it inefficient. By contrast, the resonator method combined high precision measurements with low required sample volumes below one milliliter. The resonator method or URT used in the

present study was incorporated in the ResoScan® System (Shah et al. 2007). It was equipped with a temperature-controlled twin sample cell of about 200 µl volume. A standing ultrasonic wave was created between two lithium niobate piezo electric transducers (Figure 1).

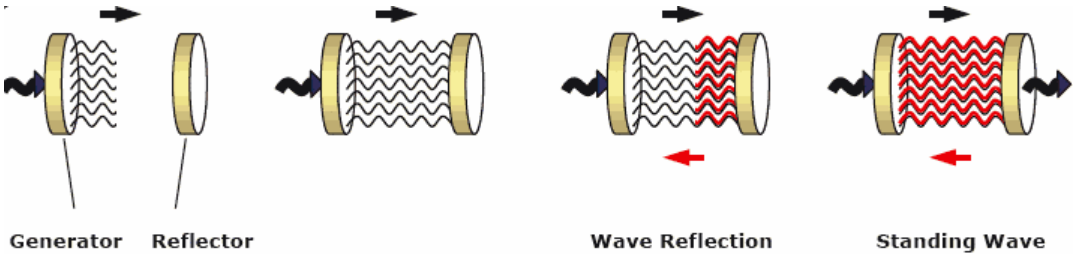

Fig. 1: *Creating and maintaining the standing ultrasound wave by continuous supply of electrically generated energy between the two gold coated transducers in the two instrument's chambers.*

One cell was used as the reference cell, the other one as the sample cell. The instrument measured the ultrasonic velocity in both cells and the software calculated the difference (dU). Positive values indicated a faster sound velocity in the sample than in the reference.

This study should demonstrate that the URT is generally suited to assess GNP – medium interactions as well as ODN loading by monitoring the interaction between the particle surface and the ODN. Encapsulations were not addressed by this method, as hydration shells were presumably just affected by surface phenomena. Furthermore, it was investigated if URT met the need for a sensitive analytical method for routine analysis of such nanoparticle dispersions without sample pretreatment.

2.2 Materials and Methods

2.2.1 Preparation and characterization of gelatin nanoparticles

Plain non-cationized and cationized GNPs were prepared according to the established protocol (Zwiorek et al 2004; Coester et al 2000) as described in chapter II, 1.2.1. Gelatin, cholamine and 1-Ethyl-3-(3-dimethylaminopropyl) carbodiimide, (EDC) were obtained from Sigma Aldrich (Taufkirchen, Germany) and Glutaraldehyde from Fluka (Switzerland). The cationization (modified from Zwiorek et al. 2008) was carried out by attaching permanent positive charges by quaternary cholamine (1 mg / mg GNPs) to the surface of readily prepared

spherical plain and processing at a pH of 4.5 and ambient temperature for 30 min. The cholamine binds via amid bonds to EDC activated residual carboxyl groups of the gelatin constituting the particles. Thereby the zeta potential of the GNPs changes from negative to positive values.

GNP concentration was determined gravimetrically. Therefore, a GNP dispersion aliquot of 25 µl was weighed with a Mettler Toledo UMX2® microbalance (Mettler, Greifensee, Switzerland). After evaporation of the solvent at 60°C the dry residue equaling the particle content was determined and the concentration calculated in mg / ml.

Intensity weighted particle sizes were gained by PCS using a Zetasizer Nano ZS® (Malvern Instruments, Worcestershire, England). To exclude the viscosity impact on PCS particle size results, the viscosity of particle dispersions of all applied media was determined individually with an Anton Paar AMVn® viscometer (Anton Paar, Graz, Austria). The viscosity values were entered in the Malvern software prior to each PCS measurement. Nanoparticles were diluted in sterile filtered, highly purified water (HPW) (purelab, ELGA LabWater, UK) or in isotonic phosphate buffered saline pH 7.4 (Dulbecco's® PBS, Invitrogen, Paisley, UK), in isotonic aqueous 2.5% glycerol or 5% glucose solution and measured in concentrations below 100 µg/ml at 25°C. As a reference and viscosity independent method, laser diffraction analysis of 1 mg / ml GNP dispersions was performed using a LA-950® laser diffraction particle size distribution analyzer (Horiba, Kyoto, Japan). For Zeta potential measurement before and after loading, GNP stock dispersions were diluted in PBS in a 1:10 ratio (V/V), filled in folded capillary cells (Malvern Instruments, Worcestershire, England).and measured in monomodal mode for high concentrated salts. Alternatively, measurements were conducted in HPW or 10 mM NaCl employing the general purpose mode for data processing of samples in low conductivity media.

2.2.2 **DNA loading onto gelatin nanoparticles**

22 base pairs double stranded (MW 7143 g / mol strand 1 and 7023 g / mol strand 2) nuclear factor (NF) kappa B decoy DNA or 30 bases single stranded 9418 g/mol DNA (Biomers GmbH, Ulm, Germany) were loaded onto GNPs in HPW in various concentrations (w/w). In case of cationized GNPs this process should be

predominantly electrostatically and self-assembling, while concerning non cationized GNPs only weak surface interactions as van der Waals bonds can be taken into consideration. The aseptically prepared samples of cationized or non-cationized GNPs were subsequently incubated for 2 h at 22°C and 750 rpm using a Thermomixer® (Eppendorf, Hamburg, Germany) device. As the cationization only addresses the surface of the GNPs, there is no significant incorporation into the GNPs bulk expected. Loading efficiency was checked photometrically at 260 nm wavelength (UV1, Thermo Fisher Scientific Inc., Waltham, USA) of samples' supernatant after ultracentrifugation and accepted, if loading was at least 97% (w/w).

2.2.3 **Turbidity, URT and density measurements**

Turbidity measurement was conducted with a Nephla® turbidimeter type CPG 239.52 operating at 860 nm and detecting scattered light at 90° angle. (Hach Lange GmbH, Düsseldorf, Germany). Results are given in formazine nephlometric units (FNU) as equivalents of turbidity.

The ultrasonic measurements were made with an acoustic interferometer (TF Instruments GmbH, Heidelberg, Germany) featuring a twin interferometer with two identical parallel resonance cavities holding sample volumes of 200 µl each. (Khan 2007) The wavelength of the ground wave is 14 mm ($\lambda 0$). This corresponds to a fundamental frequency of approximately 107 kHz. For the determination of the sound velocity overtones of the order 73 to 75 were used. The reproducibility of the measurement is ΔU = 0.020 m/s, while the temperature of the cell is adjusted to 25 ± 0.015 K with a temperature stability of ± 1 mK. GNP concentration was varied in size-concentration relation experiments while kept constant at 2 mg/ml in all loading settings.

Density measurements of GNPs dispersion and with ODN solution were conducted with a DMA-4500® device (Anton Paar GmbH, Graz, Austria).

If not stated otherwise, all measurements were performed from low to high concentrations in triplicate. If error bars are not indicated in figures, they are below resolution.

2.3 Results and Discussion

2.3.1 Particle size and concentration evaluation

The first aim of this study was to assess the capability of URT to distinguish different known particle sizes and correlate ultrasonic velocity with rising particle concentrations.

GNPs of 245 nm and 442 nm diameter as determined by PCS were diluted to several concentrations ranging from 0.1 to 10 mg / ml and characterized by turbidity measurement as a reference for the concentration evaluation by URT.

A linear relation between turbidity and concentration was found for concentrations below 1.25 mg/ml (R^2 = 0.9948). Above that, saturation was observed (Figure 2). This finding limits turbidity measurement because even rather low concentrated GNP dispersions are too opaque to be analyzed by light spectrometric based devices. Furthermore, this method cannot distinguish between even largely varying particle sizes in the relevant size range.

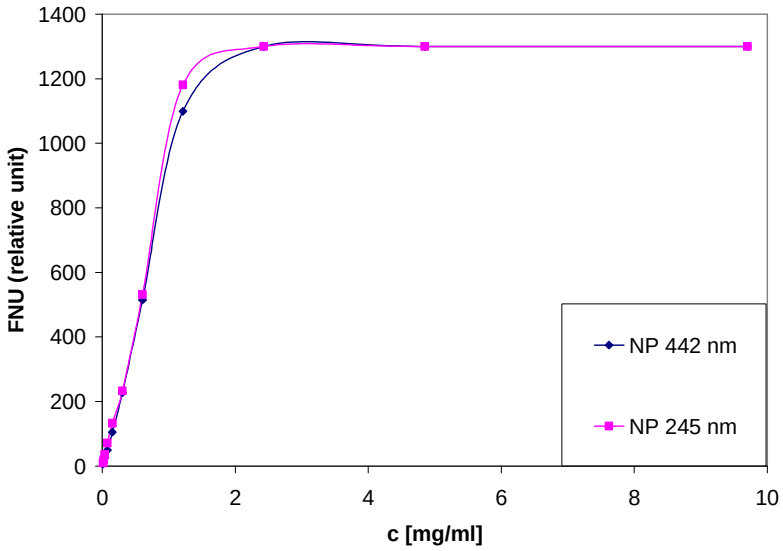

Fig. 2: *Concentration curve obtained by turbidity measurement of two GNP batches sized 245 and 442 nm over a concentration range from 0.1 to 10 mg/ml showing limited linearity (n=3).*

When monitoring the compressibility of a dispersion by measuring the ultrasonic velocity, the influence of the density has to be investigated and be determined in advance. Therefore, density measurements of GNPs in HPW were carried out. The density of the dispersions increased linearly with concentration from 0.99720

to 0.99975 g / cm3. (R^2 = 0.9981).

The increase in density results, according to the Newton Laplace equation, in a reduction of velocity. This shows that a decrease in compressibility of the dispersions is responsible for the overall increase in sound velocity.

The latter signifies that the particles overall enhance the propagation of sound in the dispersions. The effect may be attributed to an increase in hydrated surfaces. However, this model neglects the intrinsic compressibility of the particles and should therefore be considered with caution.

To demonstrate the linear relation between sound velocity and concentration over a wider range than the turbidity measurement, three dilution series concentrated up to 5, 10 and 15 and mg / ml (as determined gravimetrically beforehand) of three differently sized GNP batches (165, 280, and 630 nm diameter) where prepared, respectively. Additionally, the dilutions were investigated with the intent to distinguish between the dU values of differently sized particles. The difference in velocity (dU) between HPW and the particle dispersions with increasing concentrations of GNPs was measured and plotted against concentration.

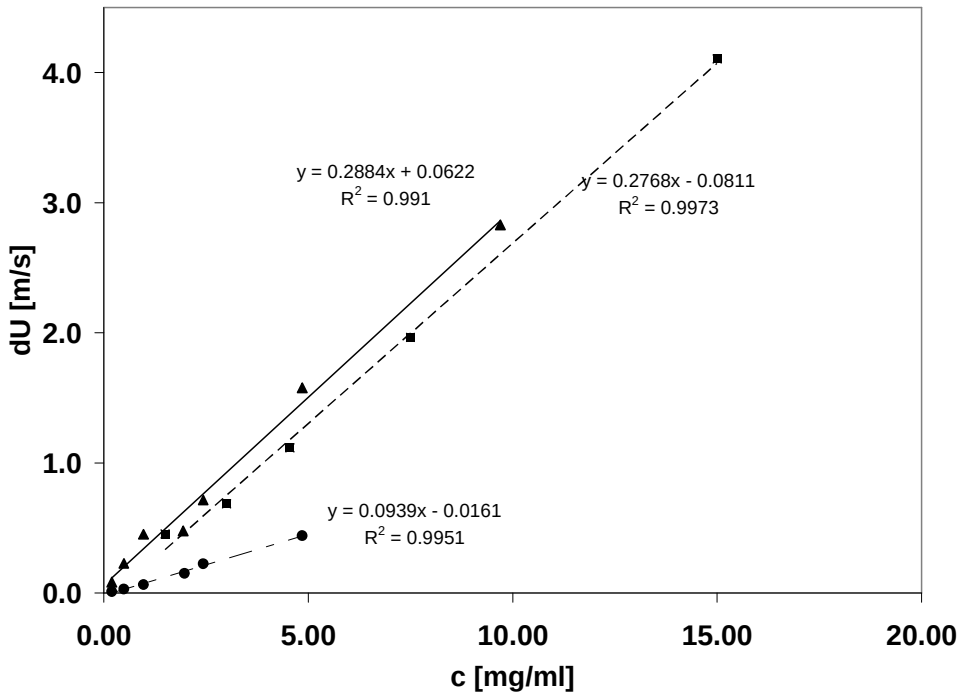

Fig. 3: *Difference in ultrasonic velocity (dU) of GNPs with three different diameters plotted against concentration: 165 nm (▲), 280 nm (■) and 630 nm (●). n=3 for each data point with* $R^2_{1\text{-}3} > 0.99$

For all particle sizes the ultrasonic velocity (dU) increased linearly ($R^2 > 0.991$ in all cases) with the particle concentration (Figure 3). Direct measurements were possible from low (0.25 mg / ml) to high concentrations (5, 10 or 15 mg / ml, respectively) extending the linear range up to ten-fold compared to turbidity measurements without need for dilution. Linearity was reached up to a concentration of 40 mg / ml (data not shown). Furthermore, the slope decreased with the particle size. It is postulated that with known concentrations previously determined gravimetrically it is possible to make deductions on particle size distributions by analysis of dilution series of a given and even very turbid batch of GNPs.

However, intensive validation work would be required prior to size estimation by URT of each single particle batch being under investigation. On the one hand the particles' total surface area accounts for the size representing slope. On the other hand URT cannot differentiate whether this surface is of evenly sized or highly disperse particles. Yet, as monodispersity was demonstrated in this trial by PDI values below 0.15 for the examined GNPs, the slopes of the batches can be compared among themselves for size correlation.

Predominantly, as a consequence of the lower compressibility of the hydration shell in a GNP dispersion, sound velocity is increased in comparison to free water. Therefore sound velocity U rises linearly with higher particle concentrations and smaller particle sizes which likely build larger hydration shells compared to larger particles at the same concentration (Figure 3) (Gekko 2002).

The delivery of ODNs is one of the main purposes of GNP usage. Therefore, the employed cationized form of GNPs allows ODN loading onto the surface via electrostatic interactions. Furthermore, the positive charge of the carrier facilitates the cellular uptake of the bound DNA, which, due to its negative charge, cannot penetrate cell membranes on its own (Fraley 2006).

Because GNPs are designed not to act in HPW but in physiological conditions featuring an ionic strength of about 299 mosm / kg and at a pH of 7.4, the dU of non cationized GNPs sized 180 nm dispersed in PBS (imitating physiologic conditions) was furthermore compared to corresponding dU results in HPW. Two batches of cationized GNPs (with average diameters of 167 and 297 nm) were analyzed, accordingly (Figure 4).

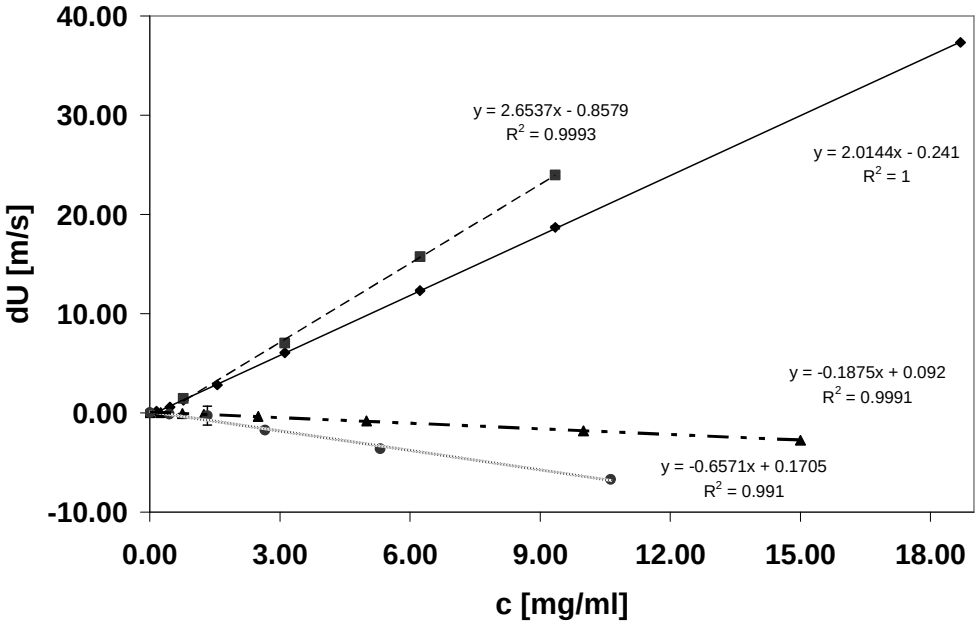

Fig. 4: *Linear concentration curve obtained by URT measurement showing dependence of dU on GNP diameter and dispersion medium with 180 nm non cationized GNPs in PBS (◆), 180 nm sized non cationized GNPs in HPW (■), 167 nm sized cationized GNPs in PBS (▲) and 297 nm sized, cationized GNPs in PBS (●), respectively (n=3, ± S.D.).*

Non-cationized GNPs dispersed in HPW display a small but significant higher dU value than in PBS. In contrast, negative dU/dc values were found for both cationized batches. The slope of the larger particles sized 297 nm was steeper than the slope of the GNPs sized 167 nm (Figure 4). The positively charged amine groups are presumably neutralized by the chloride and phosphate ions present in the PBS (zeta potential is about 30 mV lower than GNPs in HPW). This partly explains the reduction of the hydration effect.

Assuming a density increase with increasing concentration as found for the non cationized GNPs with an average diameter of 214 nm (data not shown), this would mean that the influence of the hydration layer is much reduced compared to the density effect. It is known that addition of electrolytes compress the double layer around the particles.

Examining the Laplace equation, the observed declining dU values of cationized GNPs correlate to rising compressibility, likely related to the particle size. To assess this newly observed particle phenomenon, PCS and laser diffraction were used as essential cross references for particle size monitoring.

Therefore, 15 µl stock dispersion of cationized and non-cationized GNPs originating from the same batch were added each to 1 ml solution blends of HPW and increasing percentile amount of PBS, glycerol 2.5% (m/m) or glucose 5% (m/m) ranging from 100% HPW to 100% additive.

In this setup, cationized GNPs (> 7 mV measured in PBS) lost up to 17% of their diameter in PBS measured by PCS. In contrast, cationized GNPs in the other two isotonic media and non-cationized GNP (< -2 mV measured in PBS) in all three examined media, including PBS did not significantly change the particle diameter (Figure 5).

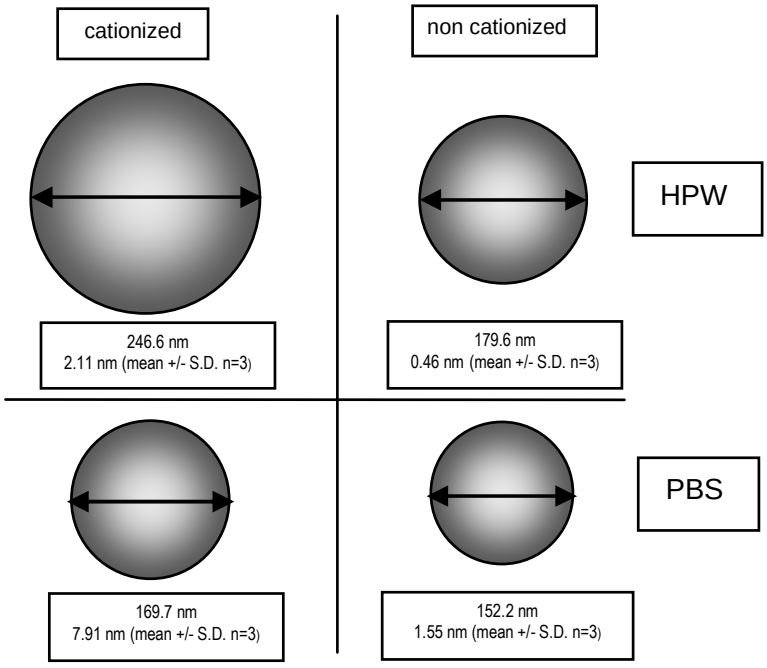

Fig. 5: *Hydrodynamic diameter development upon surface charge and dispersion medium of Gelatin nanoparticles all made of the same batch.*

These findings were confirmed by laser diffraction analysis where the same cationized GNPs decreased in size even by 35 % while non-cationized remained constant in size (data not shown). To get more insight into the swelling and shrinking behaviors of GNPs upon ionic change, a further setup employed a side by side PCS measurement with the non-cationized and cationized GNPs sized slightly larger than the previously tested batch. 15 µl GNP stock dispersions were diluted and sectioned into 1 ml batches, each with HPW and PBS respectively, for PCS measurement.

The cationized GNPs of the same batch show a 45% larger diameter in HPW than

in PBS. If exposed to the almost zero osmotic pressure ambience of HPW (0.4 mosm / kg), cationized GNP swell by this value. For non-cationized particles this effect is significantly reduced as their size is only increase by 18%, compared to PBS). (Figure 5)

This swelling experiment was repeated with the same cationized GNP batch to investigate the reversibility and time course of the size effect. Three samples of GNPs were stored in PBS for one week at 25 °C. Three further GNP samples in PBS were purified by centrifugation (18000 g, ’20, 25°C), redispersed in HPW and stored alike.

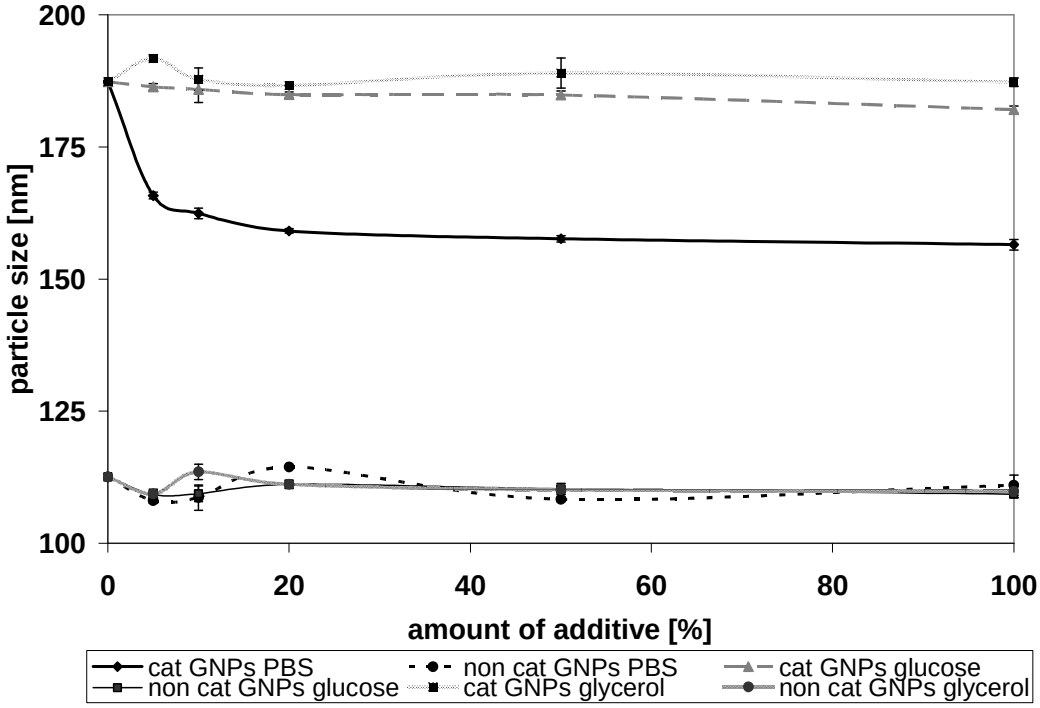

Fig. 6: *Curves obtained by PCS measurement of cationized and non-cationized GNPs revealing size-dispersion media (PBS, glycerol, glucose) dependence (n=3, ± S.D.).*

PCS analysis revealed that small percentages (below 10%) of PBS in the dispersion have an immediate effect on the size of the particles (Figure 6). This is similar for the GNPs that underwent medium exchange to HPW. After exchanging PBS for HPW medium the cationized GNPs swell to an extent which is comparable to GNPs stored in HPW form the beginning (Table 2).

	cationized GNP in PBS initial value	cationised GNP in PBS 1 week storage at 25 °C	PBS treated GNP redispersed in HPW initial value	PBS treated GNP redispersed in HPW 1 week storage at 25 °C
[nm]	159.68	157.68	221.78	220.80
S.D.	0.81	0.99	1.90	1.05

Table 2. *Cationized GNP sizes upon storage in PBS and after medium exchange in HPW.*

The 10% difference in diameter might originate from residual PBS after centrifugation. As shown in Figure 6, small amounts of PBS lead to shrinking. Therefore, the shrinking and swelling processes are reversible. Due to the fact that non-ionic but isotonic dispersions show no significant impact on the particle size (Figure 5), the osmotic pressure can be ruled out as the main driving force. This effect would presumably lead to a less compressible structure and an increase in dU/dc which is not evident in this case. Instead, it is hypothesized that anions of the PBS medium electrostatically interact with the cationized GNP surface. Apparently, GNP positive surface charge is compensated and, as counter ions the anions reduce the electrostatic repulsion within the polymer matrix and partly condensation is no longer prevented. This principle was previously described by Bloomfield et al. detailing DNA condensation by polyelectrolytes based on Manning's counter ion condensation theory (Bloomfield et al 1980).

2.3.2 **Determination and evaluation of ODN loading onto GNPs**

After clarifying plain particle properties accessible by URT in relevant media, the binding of ODNs to GNPs of known concentration by URT was subsequently investigated. Previously, to draw conclusions on changes in compressibility from velocity measurements the density of ODN solutions dependent on concentration was investigated. Exemplarily, for a 22 base pair ODN in HPW (0 to 0.35 mg/ml) it was found that the density increased linearly (R^2=0.9811) over the given concentration range (supplementary material). Therefore, plotting of dU data against ODN concentration is appropriate as well.

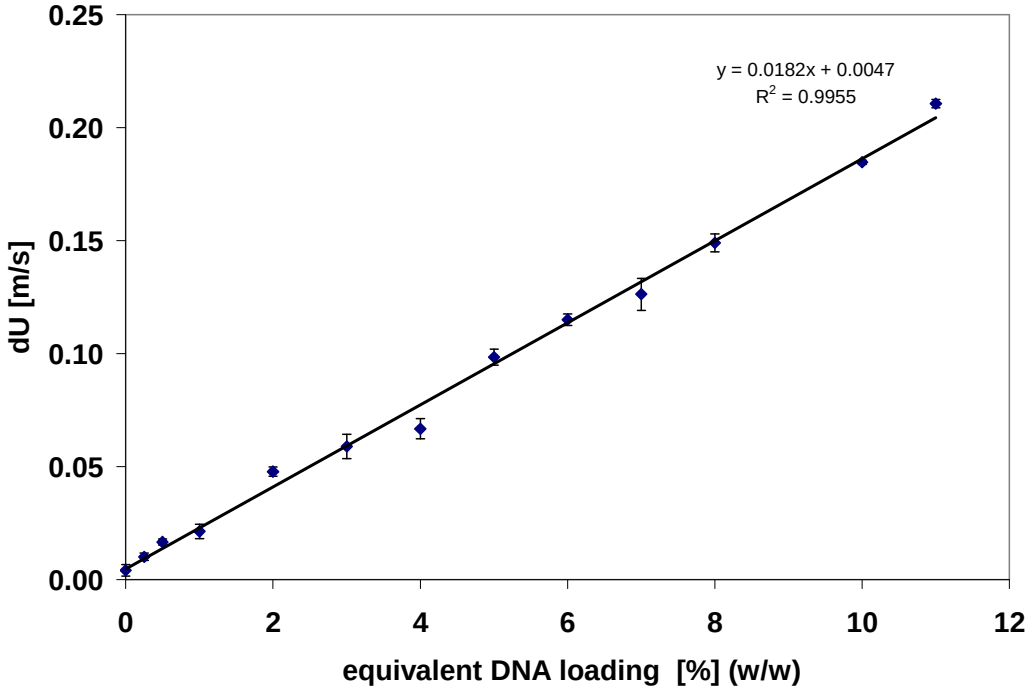

Fig. 7: *dU of a diluted 22 base pairs ODN as a function of concentration from 0.005 to 0.2 mg / ml representing 0.25 to 11 % (w/w) in following loading experiments. Cell 1 = HPW, cell 2 = ODN. (n=3, ± S.D.)*

The URT measurements were performed with a 22 base pair double stranded (ds) ODN (Figure 7). The difference in velocity dU between HPW and the 22 base pair ds ODN with increasing concentrations is shown in Figure 7 where dU increases linearly with percentile ODN loading onto GNPs (0 to 11 % (w/w)) representing a ODN concentration from 0 to 0.2 mg / ml. These data and the density measurements indicate that the compressibility increases linearly with concentration.

The graph's x-axis shows the percentile (w/w) ODN loading based on the weight of GNP in the respective dispersion. The constant GMP concentration is 2 mg / ml. This allows the calculation of each ODN concentration step in mg / ml.

High linearity over the entire concentration range is demonstrated. Single stranded ODN reveals higher dU values (data not shown). This is likely due to the fact that the longer single strand can build up more encompassing hydration shell. The double stranded ODN has less free surfaces for hydration because of the intra ODN interaction. Therefore, an increase in dU over time of a ds ODN solution of known concentration could indicate a strand separation and therefore negative stability affections. However, this idea was not further pursued in this study.

Instead, the supplementary use of URT was focused on the interaction of ODNs with GNPs to gain information about optimal loading parameters and to monitor inconsistencies related to a suboptimal loading of ODN onto GNP. A first experiment with GNPs in the presence of 10% (w/w) of a 30 bases ss ODN led to an overall instable formulation. Visible flocculation and sedimentation of macroscopic GNP-ODN aggregates occurred. This can be explained by a complete compensation of the GNP surface charge by binding of ODNs. It could be shown by a reduction of the zeta potential of the formulation in PBS from +7 mV to 0 mV in the presence of ODN.

The dU value in the presence of 10% (w/w) 30 bases ss ODN measured directly after mixing decreased sharply (Fig. 8). Repeated redispersion by a micropipette in the sample cell led to a short interruption of this trend of approximately 100 seconds. Using the simple hydration model explained above, the decrease in velocity can be explained by the aggregation and following sedimentation of particles, thereby removing surface area from the solution and reducing the overall water bound in hydration shells. A decrease in hydration means an increase in compressibility and consequently a decrease in ultrasonic velocity assuming that changes in density can be neglected.

In addition, subsequently occurring sedimentation will affect the propagation of sound. Since the sediment collects at the bottom of the cell, where the sound generating piezoelectric crystals are located the effect on sound propagation is difficult to predict. Sedimenting particles will collect in areas of the cell that are outside the sound path, further reducing the sound velocity. However, as soon as more and more particles build up in the bottom the cell this may lead to an increase in velocity due to an increase in concentration between the sound generating crystals. On the other hand an increase in large macroscopic particles will lead to an increase in scatter of the sound wave that will lead to a decrease in sound velocity due to non-adiabatic scattering (Pinfield et al 1997). Consequently, excessive sedimentation halts the dU signal completely.

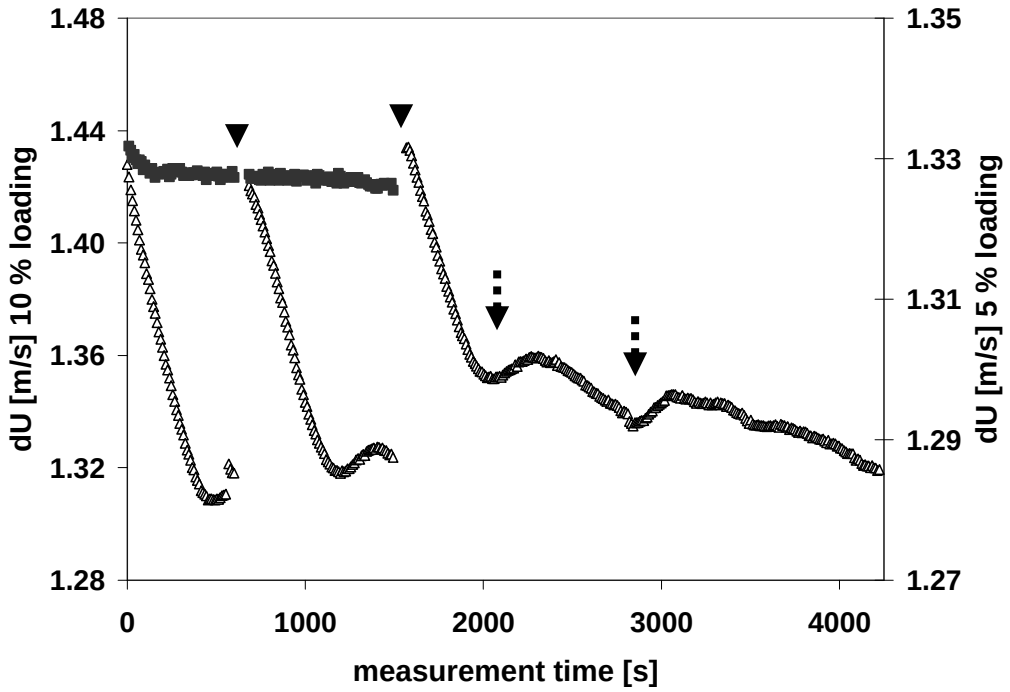

Fig. 8: *dU values plotted against the reaction time for three subsequently cell fillings of samples with 10% (w/w) (△) and 5% (w/w) (■) 30 bases ss ODN loaded GNP. Cell 1 = HPW; cell 2 = ODN-GNP sample. Arrows represent refilling (▼) or redispersion (⇢) respectively.*

As GNP aggregation and subsequently sedimentation occurs, the dU signal concurrently decreases. Without further experiments it cannot be derived to what extend both events contributed to the signal. However, conversely this phenomenon can be of use to confirm formulation quality: the absence of a falling dU signal indicates the absence of sedimenting aggregates. Figure 8 also shows the difference in ultrasonic velocity between HPW and a stable 5% (w/w) ODN-dispersion over time. The ultrasonic velocity is constant over the analysed period. URT can therefore be proposed for monitoring stability of pre-characterized colloidal systems.

The final goal of this study was to demonstrate URT as a suitable tool to determine ODN loading and to distinguish it from non-successful loading of ODN onto GNP surfaces.

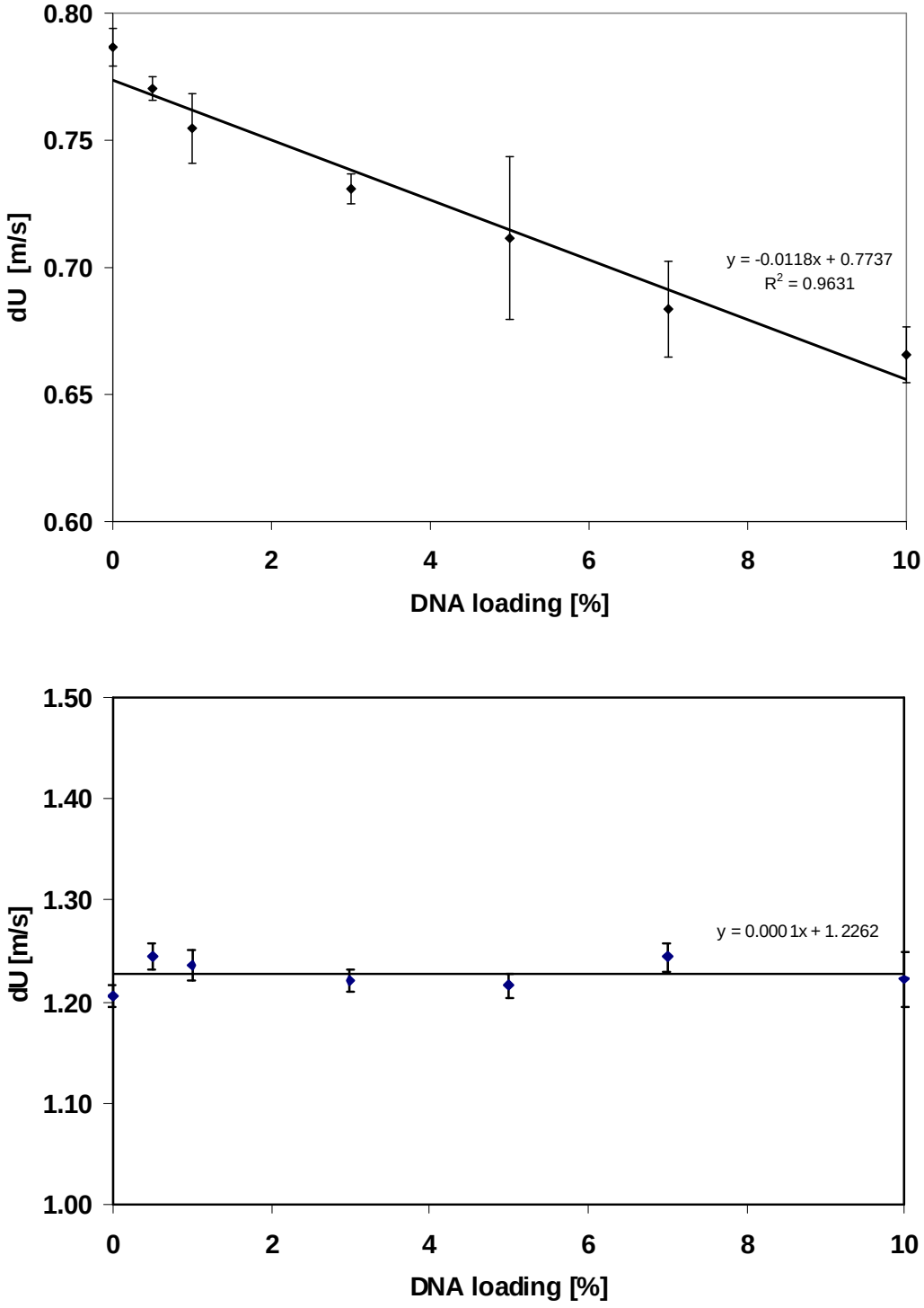

Fig. 9: *dU in dependence of (a) cationized GNP and (b) non-cationized GNP incubated with increasing amounts of ODN. (GNP concentration constant at 2 mg/ml. cell 1: ODN equivalently concentrated, cell 2: ODN loaded GNP 0.5 -10% (w/w, ODN/GNP) (n=3, ± S.D.).*

Since URT technology is unspecific and detects all changes in dispersion (e.g. concentration of any component) a protocol which minimizes effects from

volumetric and concentration errors was devised. Cationized and non-cationized GNPs (in the sample cell 2), which were previously incubated with ODN, were measured each against the ODN solution (in the reference cell 1) in the same concentrations (w/w) (ODN/GNP) as employed for the loading. The difference between the references and the sample is therefore a fixed amount of GNPs present in the sample cell. If there is no interaction between the ODN and the GNPs, the GNPs should lead to a constant difference in ultrasonic velocity independent of the ODN concentration. If an interaction occurs the difference in ultrasonic velocity will change with increasing ODN concentrations.

Figure 9a shows the signal for cationized GNPs. The difference in ultrasonic velocity decreases with increasing ODN concentration. Using the hydration model this can be explained by a reduction of GNP and ODN surfaces exposed to the buffer by binding of the ODN to the particles. Figure 9b shows the signal of the non-cationized GNPs. There is no effect on the difference in velocity with increasing ODN concentration. This is an indication that there is no interaction between the particle and the ODN. To conclude, for GNP preparations well characterized in concentration and size, the ODN loading can be estimated after calibration and subsequently used in routine analysis.

As a final comparison, the extent of loading was further followed by monitoring the zeta potential values measured in HPW of loaded cationized versus non-cationized particles and in 10 mM NaCl as a control (data not shown). As mentioned in the introduction, measuring the surface charge was described in literature as a possible loading surveillance method. In the present setting, cationized particles in HPW exhibit a reduction in zeta potential from 36.2 mV with a 1 % (w/w) ODN loading to 19.2 mV with a 10 % (w/w) ODN loading (Table 3). Non cationized GNPs show a reduction from 22.3 mV to 10.6 mV for the same loading conditions. Linear plotting of the data leads to a coefficient of correlation (R^2) of 0.9229 while plotting the zeta potential data of non-cationized GNPs leads to a regression with $R^2 = 0.7778$. These two R^2 values differ significantly because the p-value is 0.01 as determined by one factorial ANOVA analysis from comparison of all R^2 values from all single measurements. This indicates a different ODN – particle surface interaction most likely due to a different level of ODN loading onto the GNP surface.

	non-cationized GNPs		cationized GNPs	
loading [%] (w/w)	Zeta [mV]	S.D.	Zeta [mV]	S.D.
1	22.30	1.66	36.20	2.76
2	19.20	1.32	34.80	2.73
3	19.30	1.40	33.90	2.08
4	17.10	2.57	27.50	2.16
5	14.10	1.11	28.20	1.05
6	16.20	1.31	24.20	0.81
7	17.00	0.45	24.30	1.68
8	16.40	0.44	24.30	0.51
9	12.40	0.20	22.80	1.04
10	10.60	0.98	19.20	1.86

Table 3. *Zeta potentials of ODN loaded cationized and non cationized GNPs.*

Therefore, the zeta potential method backs URT findings, yet seems to be less convenient and accurate (linear decrease with rising loading, see Table 3), while conversely URT provides linear and consistent results in our examples.

As the standard control method, UV-spectrometric analysis of the two GNP samples was used and revealed the ability of URT to distinguish clearly between successful and non successful loading. According to the spectroscopic method, only 2% of the total ODNs were found in the supernatant of the cationized GNPs, which supports the URT data of successful loading. Concerning the non-cationized GNPs, 40% of the ODN were found in the supernatant. Remarkable 60% were presumably bound to the GNPs by unspecific and weak interactions and/or trapped in the pellet by the fast sedimentation of the particles during centrifugation.

To summarize, on the one hand URT depends as a relative method on existing absolute methods like PCS, gravimetry and UV-spectrometric analysis of previously centrifuged samples. As described, these methods partly feature disadvantages e.g. for formulations sensitive to centrifugation. On the other hand, once these methods have been successfully employed to validate a specific URT setup they are no longer necessary for this very process and could advantageously be stinted in routine analysis.

2.4 Conclusions

URT is ranked a potential quick, non-destructive method with a high dynamic measuring range to determine GNP concentrations of known size as well as the surface loading status of hydration shell building agents like ODNs of GNPs.

However, URT needs to be calibrated for each nanoparticle system by comparison with described methods like PCS and spectroscopy. Therefore, the method is feasible and well applicable for QC of nanoparticle but not of microparticle procedures in the course of formulation development of clinical supplies.

3. Evaluating salts of the Hofmeister series regarding their impact on GNP particle size alteration and initial immunostimulatory trials

3.1 Introduction and objectives

Findings of the media-depending GNP sizes within the URT study promoted the question whether there was a systematic impact of the dispersant media composition on swelling and shrinking of the colloidal carrier system. Previously, PBS turned out to influence the particle size. Because PBS consists of a multitude of salts, a more in-detail study on which particular salts contribute to which extend to the changes in apparent GNP properties. The most prominent approach for protein swelling experimentation, the Hofmeister series was used as a systematic basis for media-associated size alterations. The Hofmeister concept describes the impact of several salts on precipitation of proteins and swelling of biological material ending up with a “typical ordering” as depicted in Fig. 1 (Kunz 2010). Yet, it has to be mentioned that the initial series was based on salts and not on individual ions. Moreover, several series were developed over the past 120 years and the relative importance of direct ion-ion interactions versus ion-water interactions are matter of ongoing debate (Kunz 2010). In the present study, cationized and non-cationized particles were diluted in relevant salt solutions over a low to high concentration range. On the high end, the employed concentrations represented the double osmolarity compared to physiologic milieu referring to a high value of 0.3 M. The extend of size alteration was expected to be in accordance with salting-in or salting-out properties of the applied ions (Fig.1).

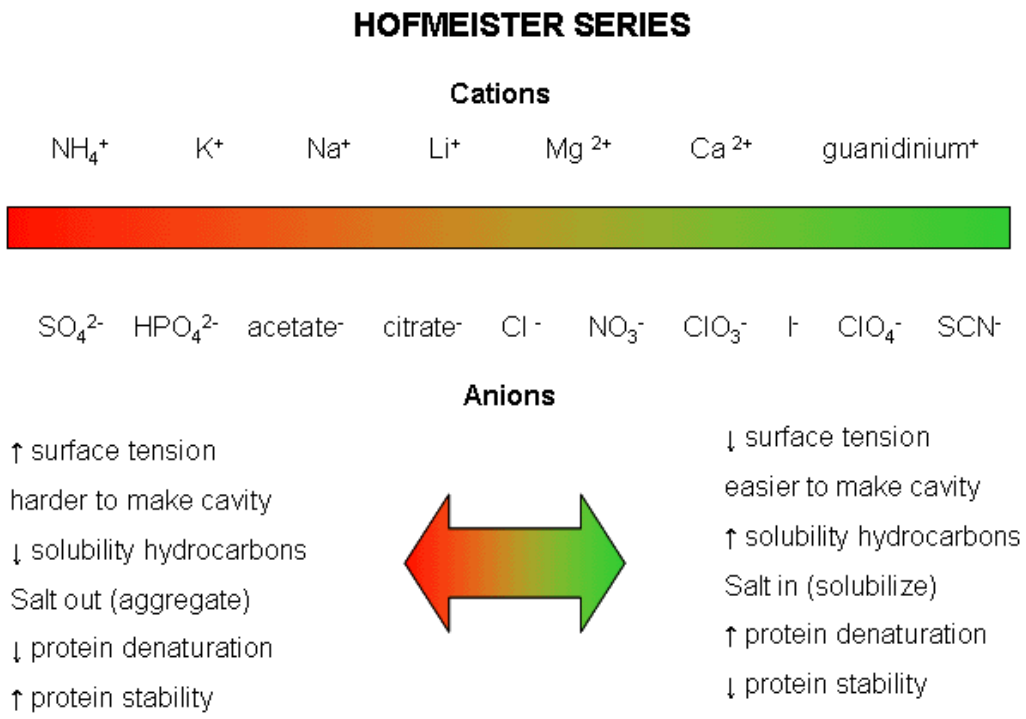

Fig. 1: *Sequencing ions in the Hofmeister series according to their salting-in and salting–out effects (Kunz 2010). A selection of representative salts was employed in the present study.*

3.2 Materials and Methods:

The GNPs were produced according to the original procedure (Coester et al. 2000). However, the change of manufacturing site from Munich to Denver, CO, irequired to adapt some standard production parameters or tools employed.

As acetone tended to boil already below 50°C at 1609 meters altitude, the two desolvation steps in the nanoparticle formation process had to be carried out at about 40-45°C which resulted in so far unassessed potential particle property deviations. Furthermore, deviations in flask and stirring bar size and/or surface characteristics, as well as in the temperature of added reagents speed and control of heating and stirring varied from validated protocols. Centrifugation tubes had to be reused over the relevant time period for particle purifications as all commercially availably single-use sterile 50 ml tubes would not fit into the available Beckman JA-17 rotor while the original Beckman containers were incompatible with acetone.

3.2.1 **Deviations in GNP preparation from the standard protocol**

Particles were made from porcine gelatin A (Sigma, St. Louis, USA) under aseptic conditions in a safety hood with desolvant agent acetone (Fisher, USA) and cross linked with thawed glutaraldehde 25% (V/V, Sigma). Adjustments of pH values were conducted with 0.1 N NaOH and HCl with a pH meter (Denver instruments, Denver, USA). A Beckmann Centrifuge with JA-17 insert was used for particle purification by ultracentrifugation at a force of 14000 – 22000 g depending on the applicable particle size. 50 ml centrifugation tubes (Millipore, USA) were washed and autoclaved for reuse.

All particle sizes were determined by a PCS device (PAS particle sizing system, Santa Barbara, USA) and calculated involving a Nicomp 388 software. Particle sizes are given as a mean of three subsequent measurements each involving at least 10 -20 subruns. Standard deviations (SDs) are given as means of the SDs calculated by Nicomp 388 software in the Gaussian particle distribution analyzing mode.

Particles were measured in an aqueous dispersion of 2.5 µl particle dispersion in 600 µl HPW if not indicated otherwise.

3.2.2 **Methods regarding Hofmeister series**

Solutions of relevant salts representing prominent points in the Hofmeister series were diluted in HPW according to table 1 in order to create solutions in a 0 to 0.3 M molar concentration range. Stock solutions of each salt were prepared according to the instruction in table 1.

Type of salt	Salt dry substance [g]	HPW [ml]
Na_2SO_4	2.131	50
Na-citrate	1.548	20
NaCl	0.350	20
$NaClO_3$	0.638	20
NaI	0.899	20
NaSCN	1.216	50

***Table 1**: Composition of applied salt stock solutions making concentrations of each 0.3 M, listed top down from low to high salting-in salt properties.*

2 µl of non-cationized and 4 µl of cationized GNP dispersion was diluted to a total volume of 600 µl and transferred into a round single-use borosilicate cuvette for subsequent PCS measurement. An anticlimactic dilution series of the media were carried to obtain a dilution row of each individual salt solution with molarities of 0.3, 0.2925, 0.2875, 0.275, 0.25, 0.2, 0.15, 0.1, 0.05, 0.025, 0.0125 and 0.0075 mol/l. Solutions were filtered by 0.22 µm cellulose acetate filters and checked for particle precontamination by PCS. GNPs were added to the ready solution (n=3) instead of adding salt to a salt-free GNP solution to guarantee complete salt dissolution.

3.3 Results and Discussion

The selection of salts represents the extremes of salting-in and salting-out as well some intermediates. Only common sodium salts were assessed at this initial stage as anions are supposed to be the driving force in making proteins to aggregate or to be solubilized according to the Hofmeister series (Zhang 2006).

First, particles were subjected to size measurements on a pH scale from 3.3 (in HPW) which represented the storage pH of freshly prepared GNPs up to 10.4. No significant size change was observed for the non-cationized GNPs while cationized GNPs exhibited a size reduction of up to 5% at the higher pH values. However, as the employed salts feature pH values in the 4 – 6 range, this does not apply to the subsequent size measurement results. Next, non-cationized GNPs' sizes were examined in presence of the selected salts as given in the figures below (Fig. 2-6) in the sequence from salting out towards salting in salts.

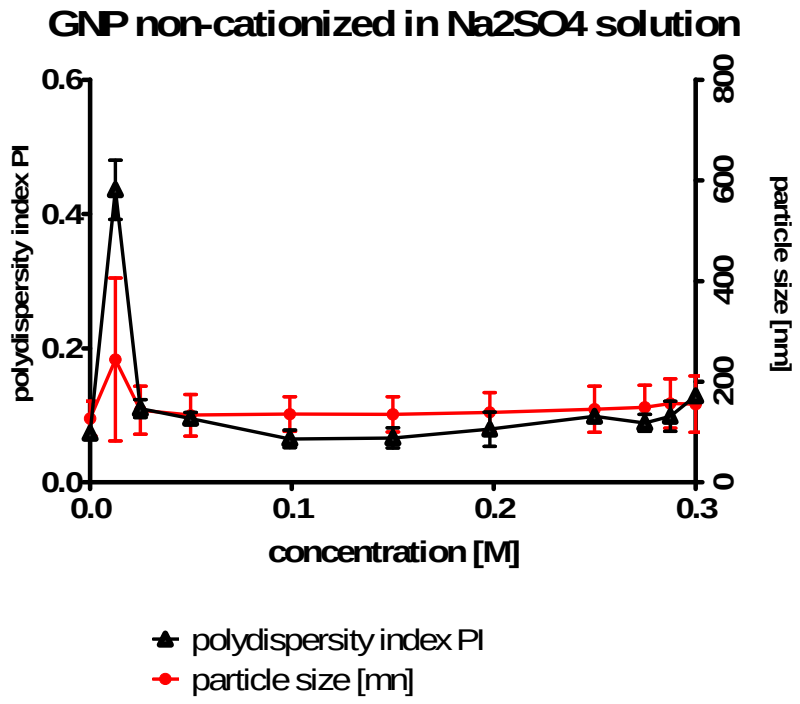

Fig. 2: *size and variance of size distribution of non-cationized GNPs in Na_2SO_4 (n=3 ± SD)*

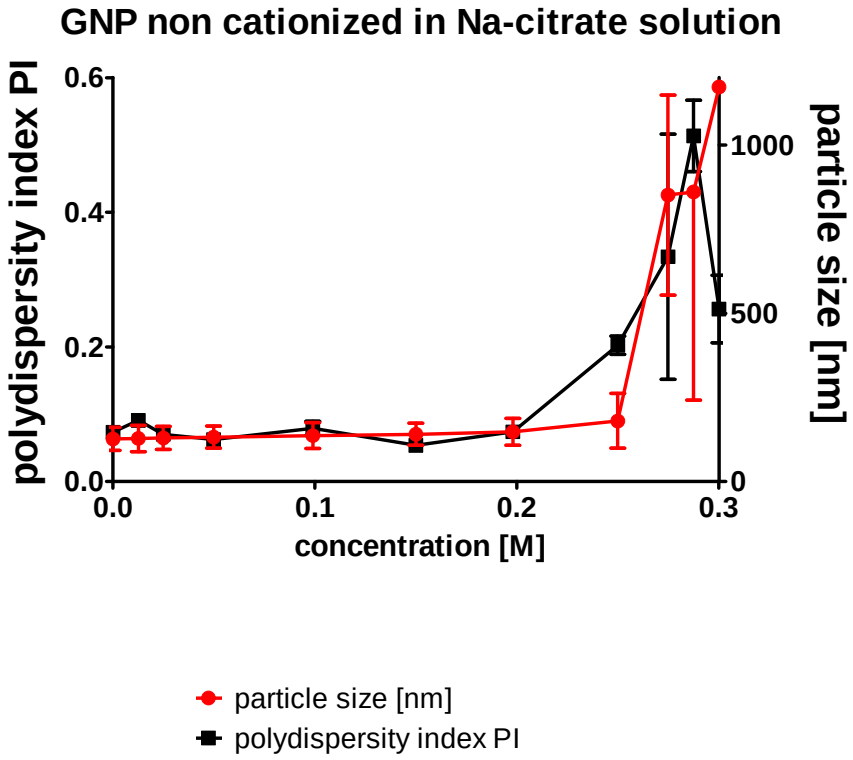

Fig. 3: *size and variance of size distribution of non-cationized GNPs in Na-citrate (n=3 ± SD)*

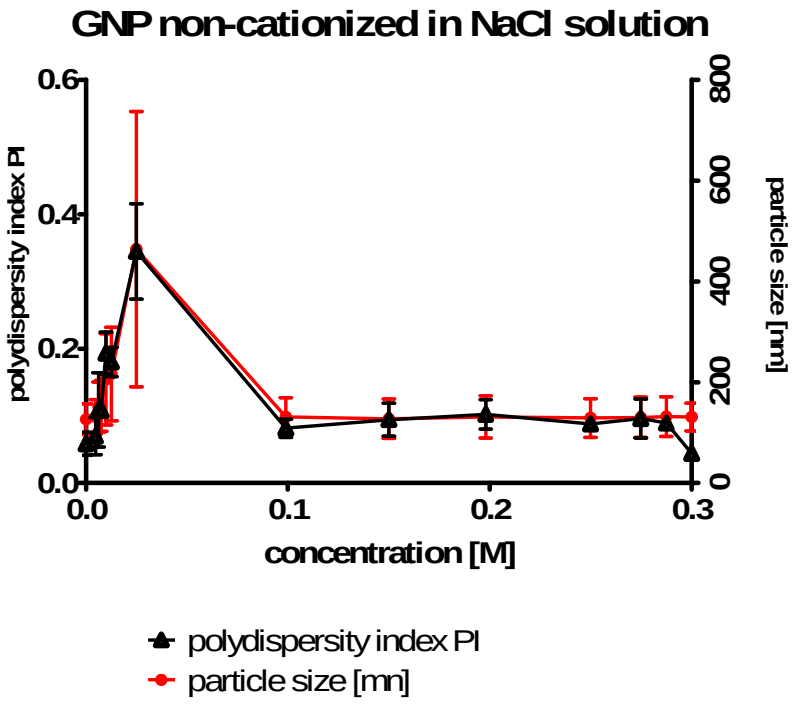

Fig. 4: *size and variance of size distribution of non-cationized GNPs in NaCl (n=3 ± SD)*

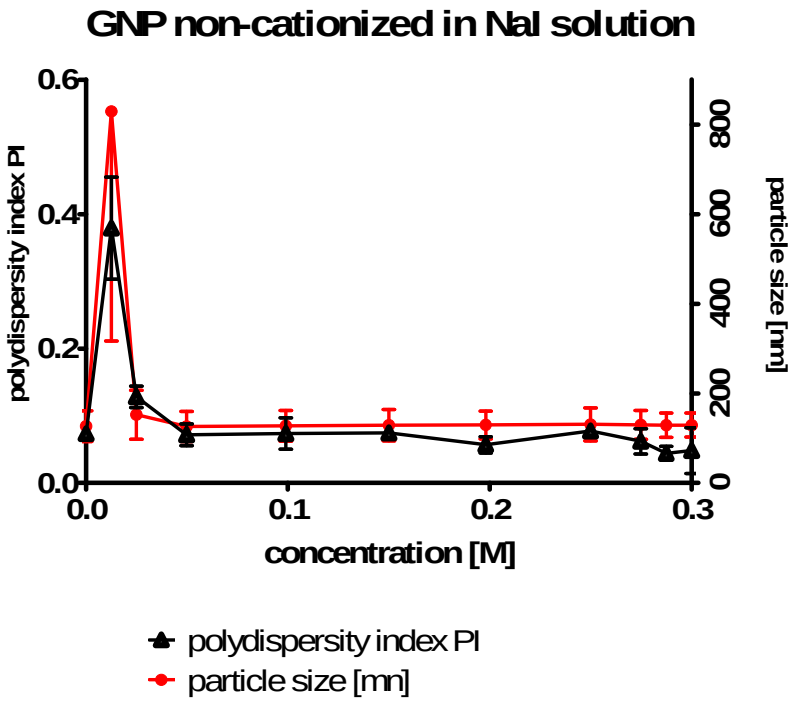

Fig. 5: *size and variance of size distribution of non-cationized GNPs in NaI. (n=3 ± SD)*

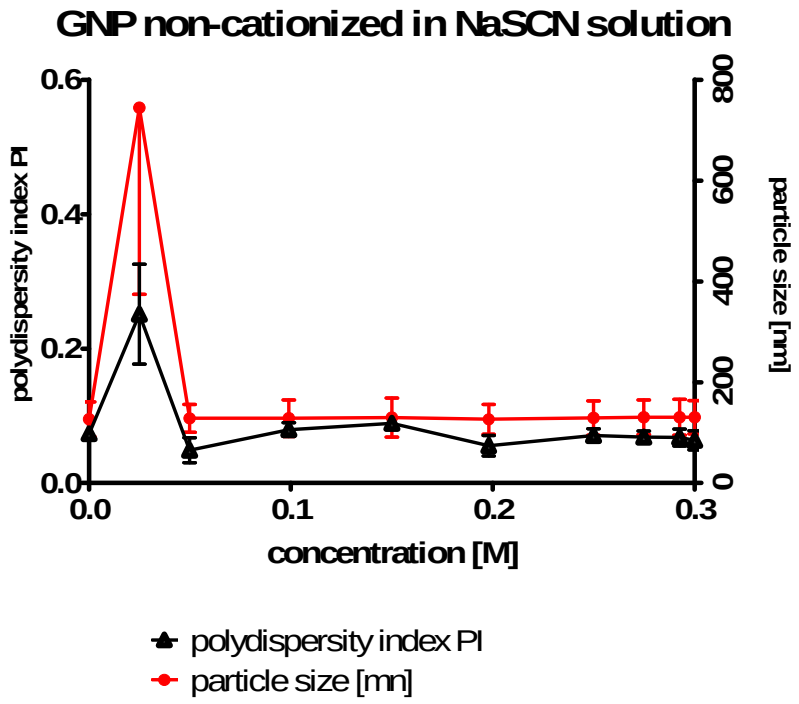

Fig. 6: *size and variance of size distribution of non-cationized GNPs in NaSCN. (n=3 ± SD)*

Regarding the above demonstrated results, it can be stated that the type of anion has a significant impact on the particle size and its distribution. With the exception of sodium citrate (Fig. 3) all salts lead to an "initial peak" of increased size below 0.05 M salt concentration. The extent of this peak increases with the salt's "salting in" properties within the Hofmeister series. This positioning indicates that besides the salting in effect, reduced surface tension, less protein stability and an increased risk of aggregation is prevalent (Kunz 2010). It is not yet understood why this phenomenon is restricted to the very low part of the applied concentration range. Obviously, it is always the first and lowest measured amount of salt that results in the peaks. Viscosity and osmolarity alterations are supposed to be the lowest here, but due to less hindrance diffusion processes of the anions into the GNP matrices are probably most efficient in this low concentration range. Therefore, viscosity and osmolarity measurements need to be performed along with this consistent finding in order to clarify the anions positioning and impact.

Furthermore, the cationized GNPs were subjected to the same salt solutions as the non-cationized GNPs and measured alike.

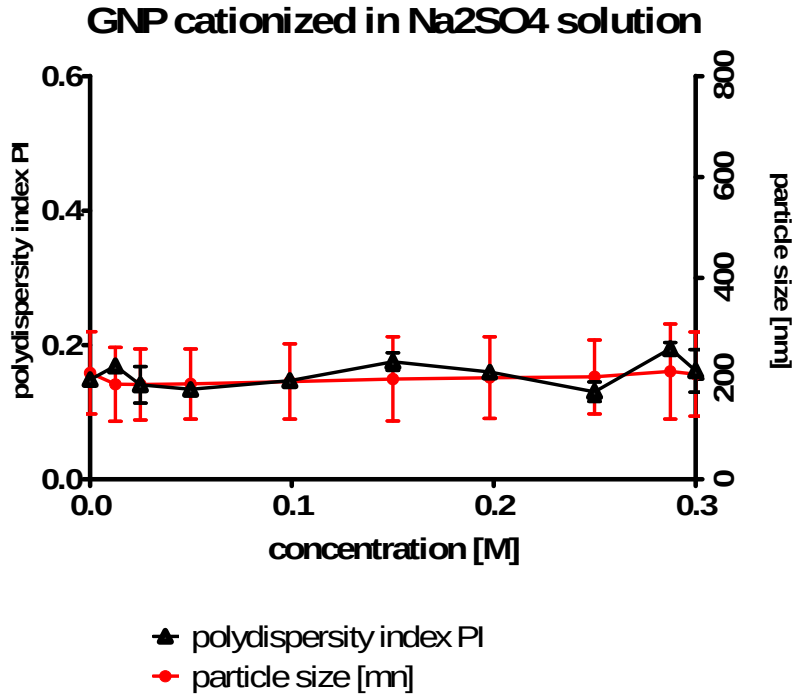

Fig. 7: *size and variance of size distribution of cationized GNPs in Na_2SO_4. (n=3 ± SD)*

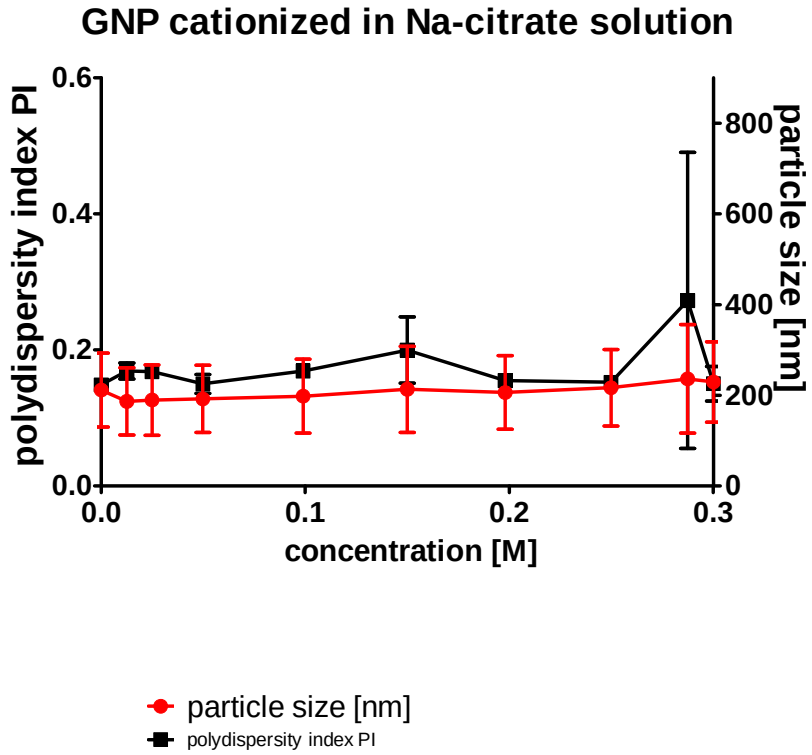

Fig. 8: *size and variance of size distribution of cationized GNPs in Na-citrate. (n=3 ± SD)*

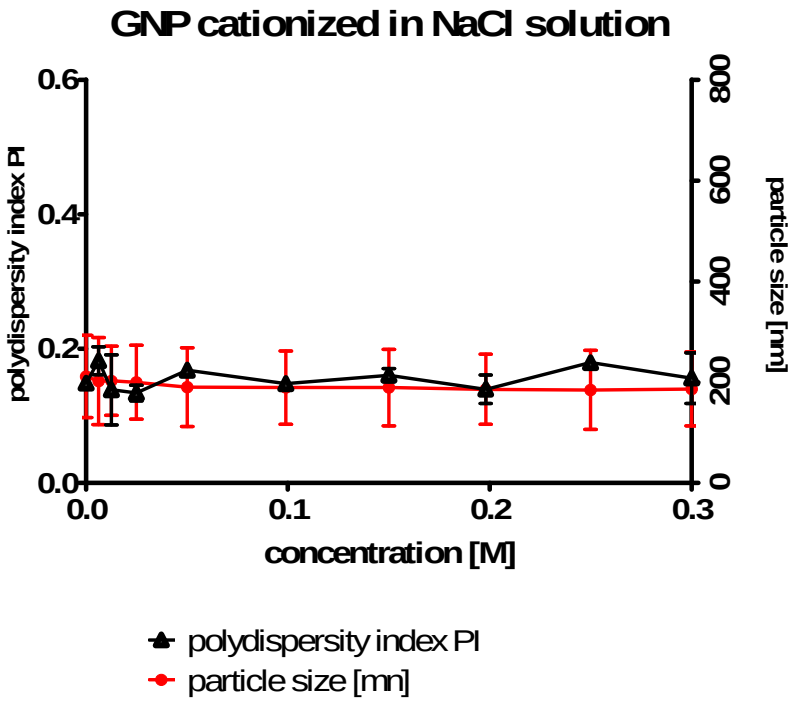

Fig. 9: *size and variance of size distribution of cationized GNPs in NaCl. (n=3 ± SD)*

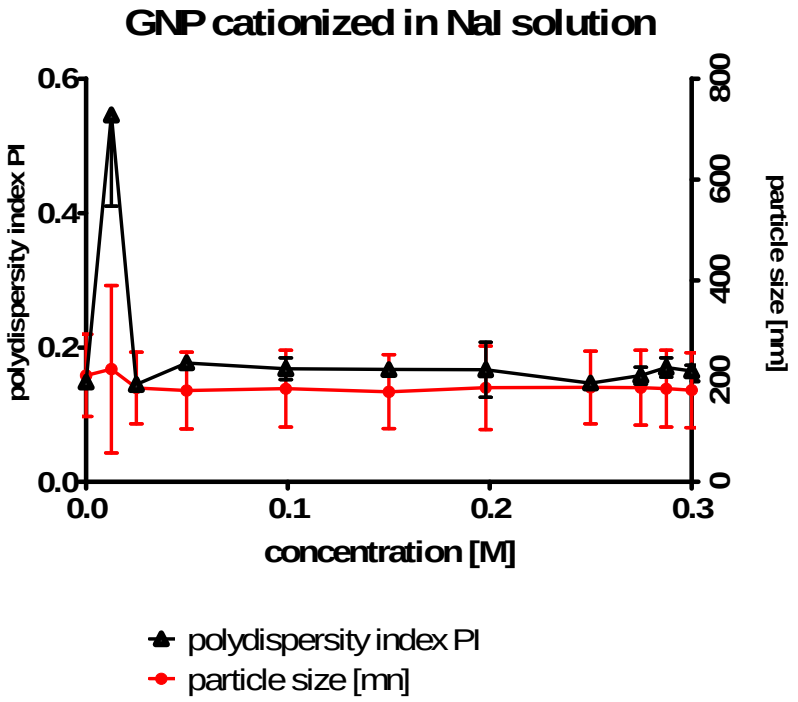

Fig. 10: *size and variance of size distribution of cationized GNPs in NaI. (n=3 ± SD)*

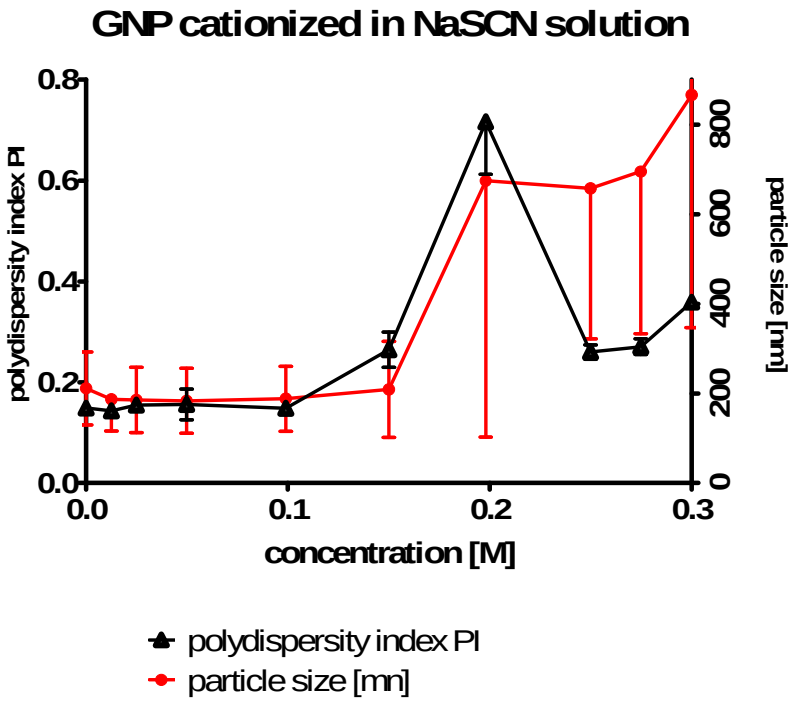

Fig. 11: *size and variance of size distribution of cationized GNPs in NaSCN. (n=3, ± S.D.).*

The size and size distribution measurement results of cationized GNPs differ from those obtained from non-cationized ones. An “initial peak” is not occurring with the one exception of NaI where size is increased at a concentration of 0.0125 M to a smaller extend of about 5% compared to up to 200% with the non-cationized particles. A possible reason for this finding is that cationized GNPs “absorb” the medium anions by ion pairing and prevent them to have a surface tension and subsequent aggregation inducing effect as being solvated. However, as the concentration of the salting-in salt is increased heavily, aggregation tendencies are dominant as soon as the “absorbance” reservoir is depleted. The only exception is NaSCN showing heavy size increase most likely due to aggregation (Fig. 11). This finding is again in accordance with the Hofmeister series as NaSCN is the most salting-in one on the list. However, the nature of aggregation of this finding needs to be proven in an additional trial on the reversibility of size change. If the size change is completely reversible, this is the proof for swelling instead of aggregation. If a combination of swelling and aggregation is the reason, an incomplete size remission in combination with an elevated PI is expected.

3.4 Conclusion

Finally, it can be stated that the anion type strongly influences the particle size and size distribution while - based on this preliminary data- the pH alone does not. It is proposed to conduct follow up experiments to check consistency of the newly found size changes and aggregation tendencies over various batches produced under standard conditions and to rule out interfering oxidative and reductive processes. Nevertheless, the present data is in accordance with the initial findings on the existence and reversibility of ion-induces GNP size changes (Fuchs et al. 2010). Methods such SEM for absolute size conformation would be desirable in future. However, careful validation would be required to assure that the obtained GNP sizes in dispersion translate to dry samples which are required in SEM.

4. Imaging techniques for nanocarriers

4.1 Survey on options to track nanoparticle biodistribution

A successful therapy is globally characterized by reaching the pathogenic target *in vivo* (Debbage 2009). Nanoparticles offer a multitude of available techniques not only to target but also to effectively monitor the system's *in vivo* fate (Pauwels and Erba 2007). Imaging can generally be provided by a signal emitted by a modification responding to external excitement -such as fluorescence or ultrasound resonance- or an intrinsic signal like magnetic or radioactive radiation. Especially fluorescence imaging is a very quickly evolving field in *in vivo* analysis with a focus on oncology (Weissleder and Pittet 2008). But certainly fluorescence contributed to cellular imaging as well, clarifying cellular uptake and intracellular localization both in fixed and living cells (Thurn et al. 2007). For instance, the fluorescence signal of tetramethylrhodamine conjugated dextran labeled GNPs allowed the endolyzosome localization in murine dendritic cells by confocal laser scanning microscopy (Coester et al. 2006). This was the precondition for further endosome-based TLR-9 targeting for immunostimulating strategies (Zwiorek et al. 2008). The same technique revealed the uptake of Alexa labeled GNPs by isolated liver resident Kupffer cells as decisive for decoy oligonucleotide delivery (Hoffmann et al. 2009; Zillies 2007).

Knowledge about the intracellular location of the administered drug delivery system in total is crucial to correlate its effects with the observed physiologic outcome. In this case, the immunostimulatory action of NP-bound isRNA presumably needs interaction with the pharmacodynamic target receptor, the endosome-based TLR-7. Previously, Coester et al. first demonstrated a possible endosomal targeting of plain, unloaded GNPs in dendritic cells generated from murine bone marrow cells (Coester *et al.* 2006). Therefore, murine DCs were incubated for 24h with TMR-dextran GNPs and followed by fluorescence-labeling with FITC-concanavalin A for cytoplasm membrane staining and with lysotracker blue DND-22 for endosome staining.

Based on the general understanding that colloidal drug carrier systems taken up by phagocytosis remain in the endosomes (Maitra 2005), a complete co-localization of the TMR–dextran labeled GNPs with the lysotracker stained endosome. But a closer look at the CLSM overlay also reveals a clear blue fluorescence that is not co-localized with the red stained nanoparticles. This information confirms that not

all endosomes are involved in the uptake process of plain GNPs.

Of subsequent interest was if oligonucleotide (ODN)-loaded GNPs (see chapter IV, 1.1) can be localized as well in cells capable of phagocytosis. Therefore, GNPs were labeled with Texas red and loaded (2.5% [w/w]) with Alexa Fluor 488 labeled ODNs. Kupffer cells generated from rat liver were incubated with these GNPs and subsequently stained for nucleus (Hoechst 33342) and endosomal membrane (Vibrant^{TM} Did cell staining). From the overlay of single CLSM channels a co-localization of GNPs, ODNs and endosomes was derived (Zillies 2007).

Furthermore, fluorescence microscopy could provide information beyond static cell evaluation, but also in an *in vitro* flow model where bloodstream-like sheer forces can be simulated (Schultes 2009). In such conditions, endothelial cells adherent to the capable microscopic slide express different surface protein patterns compared to static conditions. Therefore, cell-GNP interactions can be more realistically evaluated which is of particular importance for endothelium targeting in nanoparticle-mediated anti-neovascularization strategies (Schultes 2009).

For *in vivo* fluorescence imaging, macroscopic systems such as fluorescence reflectance imaging devices for surface use (up to 3-5 mm depth resolution) and tomographic fluorescence devices such as FMT which can reconstruct three dimensional maps of fluorochromes are available (Weissleder and Pittet 2008). The latter is quantitative and can be combined with CT for better *in vivo* localization (Weissleder and Pittet 2008). However, from a regulatory point of view, radionuclide labeling is the only technique that can give full quantitative mass-balance information after administration *in vivo* (Hargreaves 2008). Its major ability is to account for the full administered dose and its fate which is detrimental for drug safety (Brindle 2008). Radio-labeling of nanoparticles requires a chemical conjugation of appropriate emitters. Technically, either a radioisotope is introduced into the biological structure such as [^{18}F]-Fluor-Deoxy-Glucose and coupled to the nanoparticle or a metal radionuclide is bound via a chelator to the carrier.

So far, biodistribution studies were mostly carried out on small animal models (Schnockel et al. 2008). Traditionally, the dose of radionuclide-based nanoparticulate formulation was administered, tissues were sectioned post mortem

and tissue gamma counting was performed. For different time points of interest, sets of new animals had to be scarified (Franc et al. 2008). While this method is accurate to reflect the distribution at a specific moment, it does not allow studying distributions over time within the same living animal. Therefore, positron emission tomography (PET) as well as PET combined with computer tomography (PET-CT), a technique already in use for human diagnostics in oncology was applied for small animal use as a non-invasive system for online whole body monitoring (Riemann et al. 2008). This system uses radionuclides that undergo a β^+ decay such as ^{18}F in deoxy-glucose or ^{64}Cu, ^{68}Ga or ^{111}In as metal radionuclides which emit a positron. This positron gets annihilated when inevitably encountering its ubiquitary antiparticle electron in the tissue. In the annihilation event, two gammaphotons are created and depart the place of origin in a 180° angle. The PET scanner subsequently detects this pair of photons simultaneously and correlates this double event of detection to the single place of origin. Readout electronics assist in creating a 3D picture out of the sum of all detected events at a time. Resolutions reach below 1 mm.

Zwiorek et al. employed both the PET and the *ex vivo* tissue sectioning as a quantitative reference to track nanoparticles *in vivo* (Zwiorek 2006).

The strategies for optimized radiolabeling of nanoparticles by grafting specially designed ligands capable of binding radionuclides by coordination for *in vivo* PET imaging were shown by (Sun et al. 2007).

Kaul et al found prolonged blood circulation times of GNPs when decorated with 5 kDa PEG (Kaul and Amiji 2004). Furthermore, higher *in vivo* β-galactosidase gene expressions and consequently superior tumor transfection as per colorimetric enzymatic activity assays were found in a GNP-based gene delivery attempt to target tumors when the carrier was PEGylated (5 kDa) which led to their conclusion of a PEG-related better passive tumor targeting. Kommareddy linked the anhydride of diethylenetriaminepentaacetate (DTPA) as a chelator to both thiolated and 2 kDa-PEGylated GNPs for ^{111}In radiolabeling (Kommareddy and Amiji 2006). Moreover, PEG-modified thiolated GNPs were found to show sensitivity towards reducing environments and thus featured a tumor-selective accumulation. Summarizing, half-lives upon i.v. administration exhibited to be higher for the PEGylated and thiolated protein nanoparticles in comparison to PEG-only modified or plain particles. In parallel, high percentages of injected

dose per gram organ tissue were reduced in spleen and liver depicting a lower undesired accumulation of the carrier here. However, a proof for the coexistence of particle and radionuclide *in vivo* as a fundamental precondition for activity data interpretation was not given yet. This should be implemented by the present study involving double-labeled GNPs both with a radionuclide and fluorescent dye. Furthermore, the benefit of PEGylation for enhanced nanoparticle biodistribution was not yet confirmed to be a general rule and should be assessed for GNPs hereby. Besides these points, this study was to clarify whether the starting macromolecular of gelatin or the nanoparticulate shape contributed predominantly to GNP circulating properties after i.v. administration.

4.2 Materials and Methods

4.2.1 Preparation and characterization of PEGylated gelatin nanoparticles

4.2.1.1 Preparation of PEGylated gelatin nanoparticles

First, a 0.2 M borate buffer was prepared as follows: 2.50 g of boric acid were dissolved in 200 ml of HPW under stirring. The pH was adjusted to 8.5 with a 40% solution of NaOH. Afterwards, about 250 µl of a 1 % (w/v) solution of α-methoxy-ω-aminopoly(ethylene glycol) (13 000 Da) in borate buffer pH 8.5 were prepared (PEG solution). Then, the aqueous GNP dispersion and the PEG solution were mixed in Eppendorf™ tubes in three different weight to weight ratios: 1:0.3, 1:0.2 and 1:0.1. 24 µl, 16 µl and 8 µl of the PEG solution were employed, respectively. Each tube was finally filled up to 800 µl with borate buffer pH 8.5 (in a variant approach each tube was filled up to only 200 µl). Incubation was performed under constant shaking (800 rpm) for at least two hours at 35 °C.

4.2.1.2 Characterization of PEGylated gelatin nanoparticles via PEG assay

At first, two basic solutions were prepared as follows: 5.00 g of $BaCl_2$ were dissolved in 100 ml of 0.1 M HCl by shaking ($BaCl_2$ solution). Furthermore, 1.25 g of I_2 and 2.00 g of KI were dissolved in 100 ml completely desalted water under overnight stirring (iodine solution). About 250 µl of a 1 % (w/v) solution of α-

methoxy-ω-aminopoly(ethylene glycol) (13 000 Da) in 0.2 µm filtered HPW were then prepared. 50 µl of this solution and 450 µl of borate buffer pH 8.5 were mixed in an Eppendorf™ tube (PEG solution, 0.1 % (w/v)). Afterwards, the following solutions were each pipetted in an extra cap:

	borate buffer pH 8.5 [µl]	PEG solution, 0.1 % (w/v) [µl]
1	720.0	-
2	718.2	1.8
3	716.4	3.6
4	714.6	5.4
5	712.8	7.2
6	711.0	9.0
7	707.4	12.6

Table 1: *Scheme for the preparation of a PEG standard curve.*

As a reference to the PEGylated GNP, the same volume of GNP dispersion already used for the preceding PEGylation was pipetted in an Eppendorf™ tube and mixed with 720 µl of borate buffer pH 8.5. After the centrifugation (25 155 g for 15-30 min) of the reference and PEGylation caps, 36 µl of each supernatant were transferred into Eppendorf™ tubes and mixed with 684 µl of borate buffer pH 8.5. Then, 180 µl of $BaCl_2$ solution and another 180 µl of iodine solution were added. The solutions for the standard curve were also treated in this way. At last, 300 µl of the reference, PEGylation and standard curve caps were each triply plated on a 96 well plate and immediately red out with a photometer (Tecan Systems Inc, San José, USA) at 590 nm.

4.2.2 Preparation and characterization of PEGylated and glycine-linked GNPs

4.2.2.1 Preparation of PEGylated and glycine-linked GNPs

The starting PEG solution was prepared as 600 µl of a 0.3 % (w/v) solution of α-t-butyloxycarbonylamino-ω-carboxy succinimidyl ester poly(ethylene glycol)

(11700 Da) in borate buffer pH 8.5 were prepared. About 1 ml of a 0.1 % (w/v) solution of glycine in 0.2 µm filtered HPW was also confected as an amino-group-carrying model for this coupling trial. 19 µl of this solution were then pipetted into the PEG solution so that a molar excess of glycine was existent. Incubation took place for 60 minutes at 28 °C and under constant shaking (750 rpm). Afterwards, 40 µl of 2 M HCl were added and shaking was continued for another 30 minutes. The pH was finally adjusted to 8.6 with 1 M NaOH and the solution was diluted to 0.1 % (w/v) of PEG. So, it was used to PEGylate fluorescent-labeled GNP analogous to the standard preparation protocol. However, this time volumes of 240 µl, 160 µl and 80 µl of the glycine-linked PEG solution were necessary.

4.2.2.2 Characterization of PEGylated and glycine-linked gelatin nanoparticles via TNBS assay

First, a 0.1 M borate buffer pH 9.2 was prepared by dissolving 2.00 g of borax in approximately 90 ml of HPW by heating and under stirring. When this solution was completely cooled down to room temperature, further HPW was added until the 100 ml mark was reached. Thereafter, about 1 000 µl of a 0.1 % (w/v) solution of glycine in 0.2 µm filtered HPW were prepared. 100 µl of this solution and 900 µl of 0.2 µm filtered HPW were mixed in an Eppendorf™ tube (glycine solution, 0.01 % (w/v)). Afterwards, the following solutions were each pipetted in an extra cap:

	borate buffer pH 9.2 [µl]	glycine solution, 0.01 % (w/v) [µl]
1	640.0	-
2	633.6	6.4
3	627.2	12.8
4	620.8	19.2
5	614.4	25.6
6	608.0	32.0

Table 2: *Scheme for the preparation of a glycine standard curve.*

After the centrifugation (25 155 g for 10 min) of the sample caps, 288 µl of each supernatant were transferred into Eppendorf™ tubes and mixed with 352 µl of borate buffer pH 9.2. Then, 200 µl of the sample and standard curve caps were each triply plated on a 96 well plate. Right before the photometric analysis at 405 nm, 2 µl of 2.5 % (w/v) 2,4,6-trinitrobenzene sulfonic acid (TNBS) solution were added to each well.

4.2.3 **Preparation of DOTA- and RGD-linked radio labeled gelatin nanoparticles**

All experimental work related to radioactivity and was conducted in cooperation with the group of Prof. Wester, Department of Nuclear Medicine, Technical University Munich. The DOTA-Ga-labeling concept was conceived together with Dr. J. Auernheimer. Injections, sectioning and PET imaging of animals were performed by veterinarian K. McGuire and admitted staff.

At first, about 1.1 ml of a 0.1 % (w/v) 1,4,7,10-tetraazacyclododecane-1,4,7,10-tetraacetic acid (DOTA) isothiocyanate (NCS) solution in dimethyl sulfoxide (DMSO) were prepared (DOTA-NCS solution). About 1 ml of a 0.1 % (w/v) arginine-glycine-aspartic acid (RGD) solution in DMSO was also confected (RGD solution). Both solutions were stored at - 20 °C. Furthermore, a third solution consisting of 1650 µl of 0.1 M HCl and 150 µl of 2.5 M 4-(2-hydroxyethyl)-1-piperazineethanesulfonic acid (HEPES) buffer was prepared (reaction solution). Thereafter, a volume of aqueous fluorescence labeled and PEGylated GNP dispersion according to 1 mg of completely dried particles was twice pipetted into an Eppendorf™ tube and mixed with 20 µl of DOTA-NCS solution and another 20 µl of RGD solution (in a variant approach no RGD solution was added). Then, both reaction tubes were filled up at 400 µl with 0.2 M borate buffer pH 8.5. Alternatively, RGD was first coupled to PEG and subsequently the construct was coupled by at pH 8.4 to the GNPs (Fig. 1). Incubation took place for 4.5 hours at 36 °C and under constant shaking (750 rpm). Finally, the particles were purified by centrifugation (20 000 g for 8 min) and redispersion in 400 µl of 0.2 µm filtered HPW. They were stored as dispersion in darkness at 4 °C. Right before application, this dispersion was

centrifuged again at 13 000 rpm for ten minutes (Heraeus, Langenselbold, Germany). Then, the sediment was dissolved in 150 µl of reaction solution. After the addition of 1650 µl of Ga-68 eluate and 150 µl of 2.5 M HEPES buffer, both samples were incubated for ten minutes at 80 °C in an oil bath. Afterwards, they were centrifuged again at 13 000 rpm for nine minutes (in a variant approach two purification steps by centrifugation were employed). Each sediment was dissolved in 200 µl of 0.9 % (w/v) NaCl solution. The resulting dispersions were finally filtrated through a 5 µm filter and 100 µl were each filled into a syringe. Radioactivity was measured with a CRC 15-R dose calibrator (CAPINTEC, Ramsey, USA).

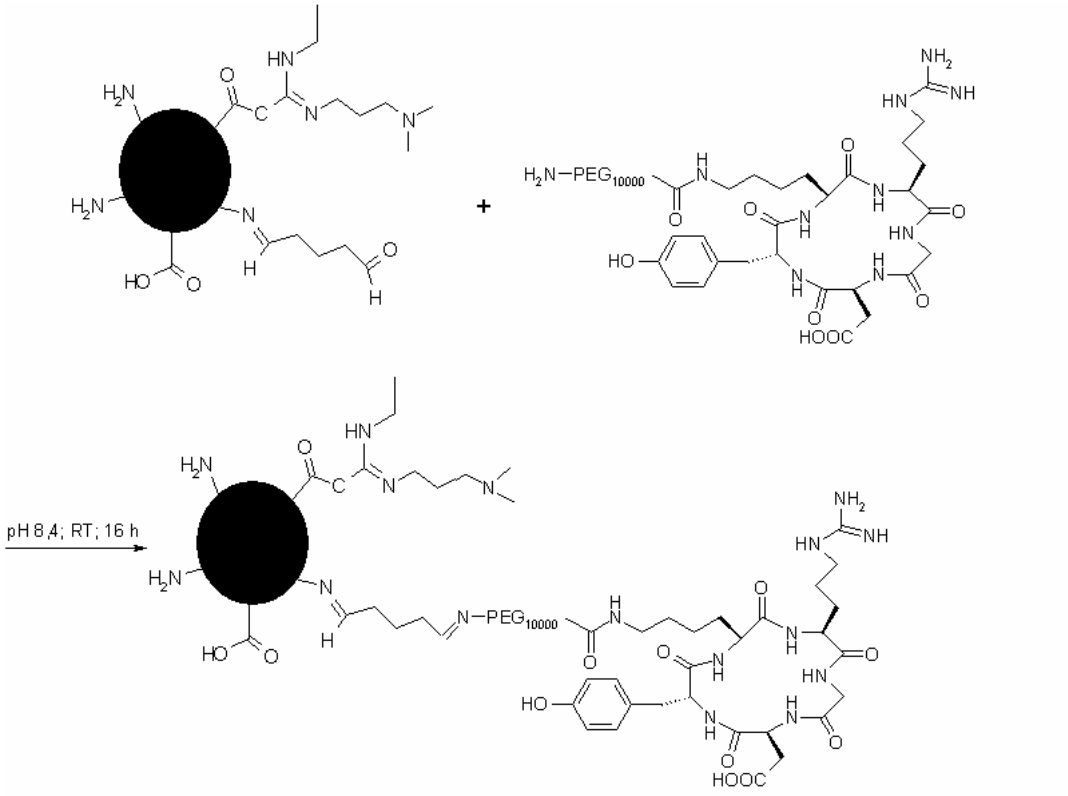

Fig. 1: *Reaction scheme for a RGD-PEG construct coupled to the GNP surface.*

4.2.4 **Preparation of Alexa 633 and ^{111}In-labeled gelatin in solution**

Fluorescent labeling by covalent coupling of Alexa 633 (Invitrogen, Carlsbad CA, USA) to gelatin molecules was carried out after the first desolvation step according to the standard protocol. Afterwards, the gelatin gelatin solution freed

from the low molecular weight fraction was allowed to react with DOTA-NCS 100:1 (w/w) in borate buffer 0.2 M at pH 8.4 for 2 h. After covalent binding of the chelator to the macromolecule, the radiolabeling was performed by the addition of 0.2 M NH_4Ac buffer till pH 4.5 was reached and 40 µl of ^{111}In solution for radionuclide introduction at 80°C for 10 min. Total volume did not exceed 1.5 ml. After radiolabeling, fractionation and separation from free ^{111}In was performed. Finally, 12 fractions of 1.0 ml each were collected after introducing the 1.5 ml reaction volume and 12 ml of HPW onto disposable PD-10 desalting columns (medium: Sephadex^{TM}G25; GE Healthcare Europe, Munich, Germany). The fractions were subsequently analyzed for contained activity by the CRC 15-R dose calibrator and further used depending on their measured activity.

4.2.5 **Biodistribution study via non-invasive positron emission tomography (PET)**

GNPs tumor-bearing CD-1 nude mice (Charles River, L'Arbresle, France; M21 melanoma cells injected s.c. in house) were first anesthetized with 2 % (v/v) isoflurane and fixed on the PET examination table. 200 µl of ^{68}Ga-labeled GNP dispersion (were then injected subcutaneously 0.5 cm away from the tumor. PET pictures (small animal PET MOSAIC, Philips Healthcare, Eindhoven, Netherlands) were taken over a period of two hours.

4.2.6 **Conventional biodistribution study via γ counter**

Bulb/c mice and tumor-bearing CD-1 nude mice were anesthetized with diethyl ether. After 100 µl of GNP dispersion or gelatin solution were either injected into the tail vain (bulb/C mice for biodistribution studies) or subcutaneously 0.5 cm away from the tumor or on the opposite body site (CD-1 nude mice for tumor targeting study), the mice awoke from narcosis and survived further 2 – 24 hours before they were scarified by CO_2. PET mice were scarified the same way. Then, the following organs and were explanted and examined using a γ counter (Wallac 1470, Turku, Finland): heart, lung, liver, pancreas, spleen, kidney, adrenal gland,

bladder, muscle (tumor and opposite body site), stomach, small and large intestine, tail and not least tumor. Also blood and urine were investigated.

4.2.7 Confocal laser scanning microscopy (CLSM) of tumor tissue

After the organs were explanted and radioactivity was determined via γ counter, tumor tissue frozen sections of 10 µm of thickness were prepared and stained with Hoechst 33342 to identify nuclei. Consecutively, they were examined with a Zeiss 510 LSM NLO confocal laser scanning microscope (Carl Zeiss Microscope Systems, Jena, Germany).

4.3 Result and Discussion

4.3.1 The impact of particle size and concentration on biodistribution

Intravenous administration of nanoparticles deserves careful evaluation of possible risks by particle accumulation in sensitive organs and aggregation in spots of the circulation system that might cause undesired side effects. Zwiorek observed a massive lung accumulation of positively charged ^{18}F-labeled GNPs (Zwiorek 2006).

Consequently, a new challenging scenario with a concentration of 2 mg/ml and large ^{68}Ga-labeled GNPs of 390 nm was approached in the experiment reported in Fig. 2.

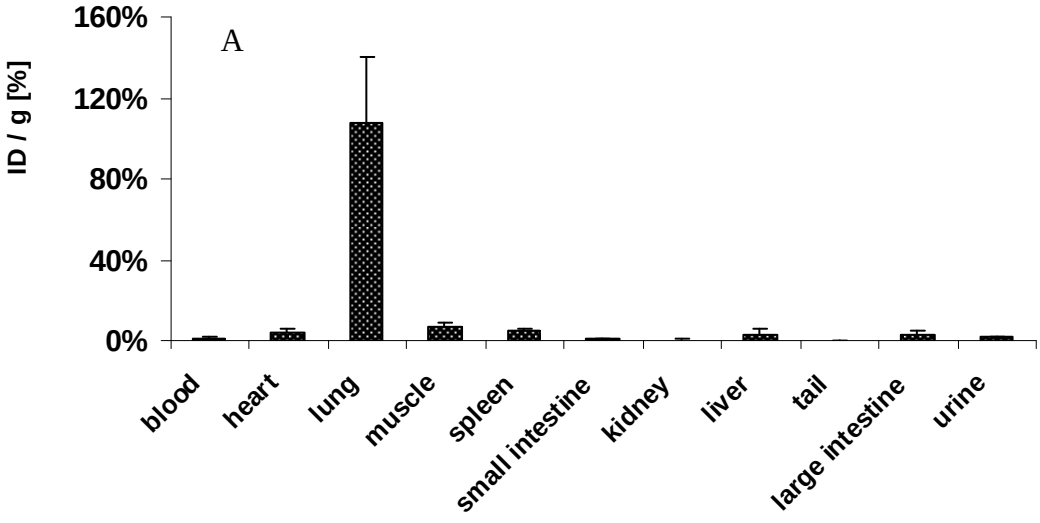

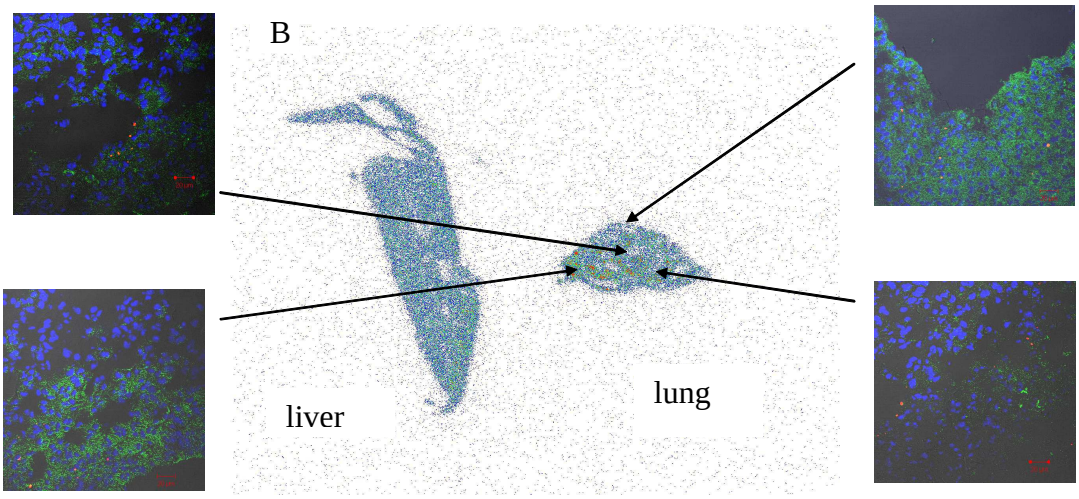

Fig. 2: (A) *Ex vivo biodistribution of ^{68}Ga-labeled GNPs of 390 nm after 4 h of i.v. injection in bulb/C mice (n=3, ± S.D.). The sum of individual organ values exceeded 100% to some organs' weight below 1.0 g. (B) Matched CLSM and autoradiography pictures confirm GNP accumulation in the lung but not in liver tissue.*

Clearly, after 4 h almost the whole injected dose ended up in the lung. Although the animal survived till the time point of sacrifice without any clinical symptoms, this situation constituted a potential danger. Therefore, concentrations were kept below 1 mg/ml in all further applications and injected volumes did not exceed 250 µl even for the PET examinations to ensure not more than 250 µg of GNPs enter the bloodstream at a time.

4.3.2 **Quantification of PEGylated gelatin nanoparticles via PEG assay**

PEG-coated nanoparticles are expected to exhibit a prolonged circulation in blood so that a better targeting effect towards tumor cells can be achieved (Torchilin 2007). As PEGylation of drug carrier systems was discussed to provide further advantageous effects, this study focused on PEGylated GNP both for s.c. and i.v. administration.

Before the first *in* and *ex vivo* experiments with PEGylated GNP were started, we tried to establish a method for the indirect quantification of successfully bound PEG based on the Childs assay (Childs 1975). Therefore, an aliquot of aqueous

GNP dispersion was incubated with a solution of α-methoxy-ω-aminopoly(ethylene glycol) in borate buffer so that the residual aldehyde groups on the GNP surface reacted with the terminal PEG amino groups (Fig. 3). GNPs were then separated via centrifugation. Finally, the supernatant theoretically consisting of only non-bound excessive PEG in borate buffer was further diluted and photometrically analysed after the addition of both, $BaCl_2$ and iodine solution. With the aid of a standard curve (data not shown), the amount of non-bound PEG was determined. This rendered possible to make a statement concerning PEGylation success.

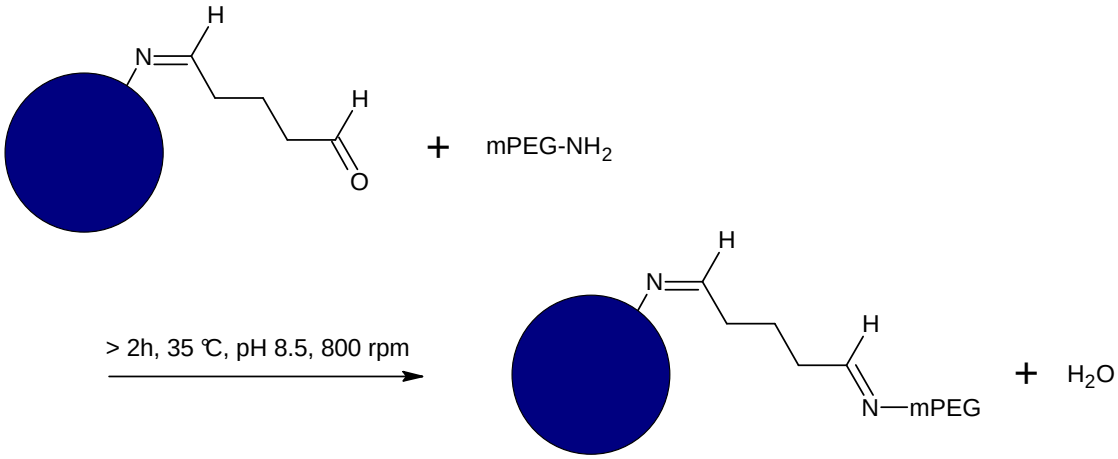

***Fig. 3**: Reaction scheme for the PEGylation of GNP; mPEG-NH_2: CH_3O-$(CH_2CH_2O)_n$-CH_2CH_2-NH_2.*

Fig. 4 shows the percentage of non-bound excessive PEG in six different PEGylation approaches. Three different PEG:GNP weight to weight ratios were investigated as well as two different total PEGylation volumes. Every data point in the figure below displays the mean of three individual samples. Measurement data was obtained in time intervals of one minute.

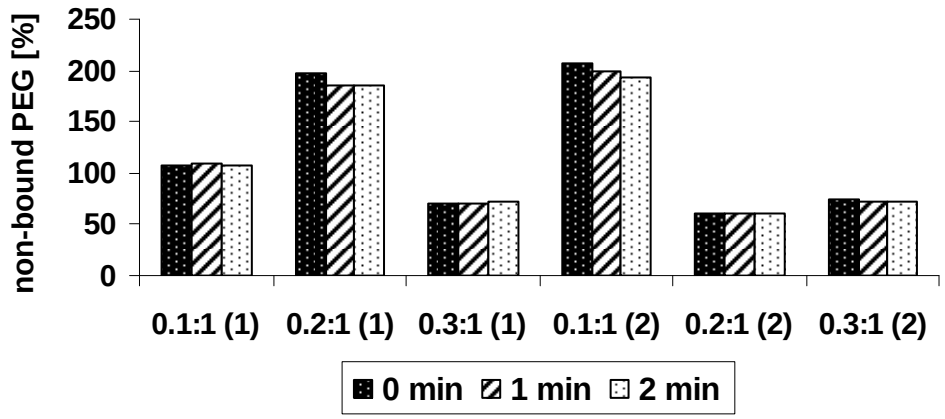

***Fig. 4**: Percentage of non-bound excessive PEG in six different PEGylation approaches; 0.1/0.2/0.3:1: weight to weight ratio of PEG:GNP, (1): 800 µl of total PEGylation volume, (2): 200 µl of total PEGylation volume; each point represents the mean of three individual samples (n=3).*

As values indicate, far more than 100 % of non-bound PEG [see 0.2:1 (1) and 0.1:1 (2)] was found as artefacts. Consequently, this quantification method should be considered critically. False positive values obviously contribute to non-representative results. Due to the fact that the causes for these results still remain unclear, future quantifications of successfully bound PEG should be carried out by another method. Asymmetrical flow field-flow fractionation combined with refractive index detection for example is an established method for the quantification of PEGylated GNP drug carrier systems (Zillies et al. 2007). Nevertheless, this assay permits to make some qualitative statements. Thus, a smaller total PEGylation volume seems to be more capable for a successful PEGylation than a larger one. Also PEG:GNP ratios of more than 0.1:1 in 200 µl of total volume lead to better PEGylation results. Not least, the assay does not depend on time as we first expected because of decreasing absorption values. Further experiments (data not shown) confirmed this hypothesis by showing that the results for the amount of non-bound PEG were almost constant over a time period of at least half an hour.

However, a further PEG assay experiment showed a PEGylation success of approximately 91 %. This time, α-t-butyloxycarbonylamino-ω-carboxy succinimidyl ester poly(ethylene glycol) was used instead of α-methoxy-ω-aminopoly(ethylene glycol). Future experiments will show if this approach is generally superior to the one generally employed before. Reproducibility for

example needs to be tested in more detail.

4.3.3 Quantification of PEGylated and glycine-linked gelatin nanoparticles via TNBS assay

The use of peptides as targeting agents leads to an increased intracellular drug delivery in different murine tumor models. In this study, GNPs were therefore coupled to RGD which is the ligand of cell adhesion integrins on endothelial cells (Peer et al. 2007).

It was aimed to quantify successfully bound RGD by using the TNBS assay, we first had to find a model peptide or amino acid that reacts the same way RGD does but is less expensive. It was finally decided in favor of glycine.

At first, a molar excess of glycine was incubated with a solution of α-t-butyloxycarbonyl-amino-ω-carboxy succinimidyl ester poly(ethylene glycol) in borate puffer so that the glycine amino groups were allowed to react with the terminal carboxyl succinimidyl ester groups. Thereafter, 2 M HCl was added to free the boc-shielded PEG amino groups. The resulting solution was finally alkalized again and diluted so that it could be used for the PEGylation of GNP analogous to the reaction scheme described in Fig. 3. Afterwards, GNPs were separated via centrifugation. The supernatant was further diluted and photometrically analysed after the addition of TNBS solution. As TNBS generally binds to free amino groups, not only residual glycine molecules are detected. Glycine-linked PEG molecules that did not bind to the aldehyde groups on the GNP surface also give positive results due to their free PEG amino group. This renders it possible to make a statement concerning the success of GNP glycine-linkage. Whether glycine was directly bound to the GNP surface or via a PEG spacer can not be determined with this assay. Therefore a combination of both, PEG and TNBS assay is recommended for further experiments.

Tab. 3 shows the amount of non-bound excessive glycine and glycine-linked PEG per well in three different PEGylation approaches. Thus, PEG:GNP weight to

weight ratios of 0.1:1, 0.2:1 and 0.3:1 were investigated. Every calculated value displays the mean of three individual samples.

PEG:GNP ratio	0.1:1	0.2:1	0.3:1
non-bound glycine and glycine-linked PEG per well [µg]	-0.170	0.072	0.183

***Tab. 3**: Amount of non-bound glycine and glycine-linked PEG per well [µg] in three different PEGylation approaches; 0.1/0.2/0.3:1: weight to weight ratio of PEG:GNP; every calculated value displays the mean of three individual samples (n=3).*

Although the amino acid was initially added in a molar excess, no residual glycine or glycine-linked PEG could be determined when the PEG:GNP weight to weight ratio was 0.1:1. Glycine that was not coupled to PEG was presumably directly bound to the GNP surface. In the next investigated weight to weight ratios of 0.2:1 and 0.3:1 residual glycine or glycine-linked PEG could be detected, respectively. In both cases, the possible amino group binding sites on the GNP surface seemed to be saturated. According to this, the weight to weight ratio of 0.3:1 led to a larger amount of excessive glycine or glycine-linked PEG than the weight to weight ratio of 0.2:1 did. Due to several dilution and pH adjustment steps during the preparation procedure, we were unfortunately not able to retrace the concentration of glycine in the PEGylation solution. Therefore, the results could not be presented in percentages.

4.3.4 *In vivo* and *ex vivo* studies of s.c.-administered modified GNPs

In the following experiments, we continuously employed fluorescence and radioactive labeled GNP to track biodistribution in tumor-bearing CD-1 nude mice. That way, the success of an active tumor targeting could be proved. Our main results are presented below.

4.3.4.1 Biodistribution study via non-invasive positron emission tomography (PET)

In comparison to *ex vivo* experiments, PET offers the possibility to follow biodistribution in living individuals. PEGylated and fluorescence labeled GNPs were therefore coupled to DOTA-NCS and RGD. The former was absolutely necessary because it directly binds deprotonated amino groups on the GNP surface and complexes later added radioactive Ga-68 that can be detected by PET. RGD was incidentally added due to its supposed active tumor targeting properties. Finally, 100 µl of the radio-labeled GNP dispersion purified from free, uncomplexated radionuclides were administered subcutaneously to a tumor-bearing CD-1 nude mouse. Injection took place 0.5 cm away from the tumor. Thereafter, PET pictures of the anaesthetized mouse were taken over a period of two hours.

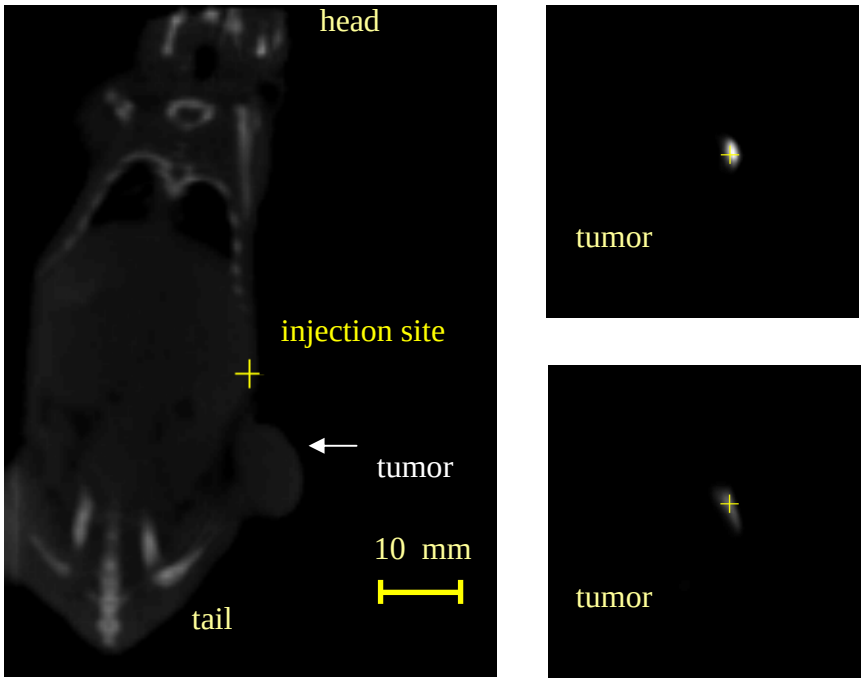

***Fig. 5**: CT picture (left) of a tumor-bearing CD-1 nude mouse (posterior view) and PET pictures (right) indicating GNP biodistribution one minute post injection (top) and 120 minutes post injection (down); the pictures aren't identical in scale.*

Fig. 5 firstly shows a computer tomography (CT) picture (left) of a tumor-bearing CD-1 nude mouse in posterior view. The tumor as well as the injection site are marked. Further, PET pictures (right) indicating GNP biodistribution one as well

as 120 minutes after s.c. GNP application are mapped. They confirm that GNP remain at the injection site where they form a depot or partially immigrate into tumor tissue. Due to the half-life of Ga-68 (68.3 min), the PET picture down right shows a lower signal than the one above.

4.3.4.2 **Conventional biodistribution study via γ counter**

In this study, we examined murine GNP biodistribution by measuring radioactivity with a γ counter in several organs explanted 120 minutes after s.c. injection of a radio labeled GNP dispersion.

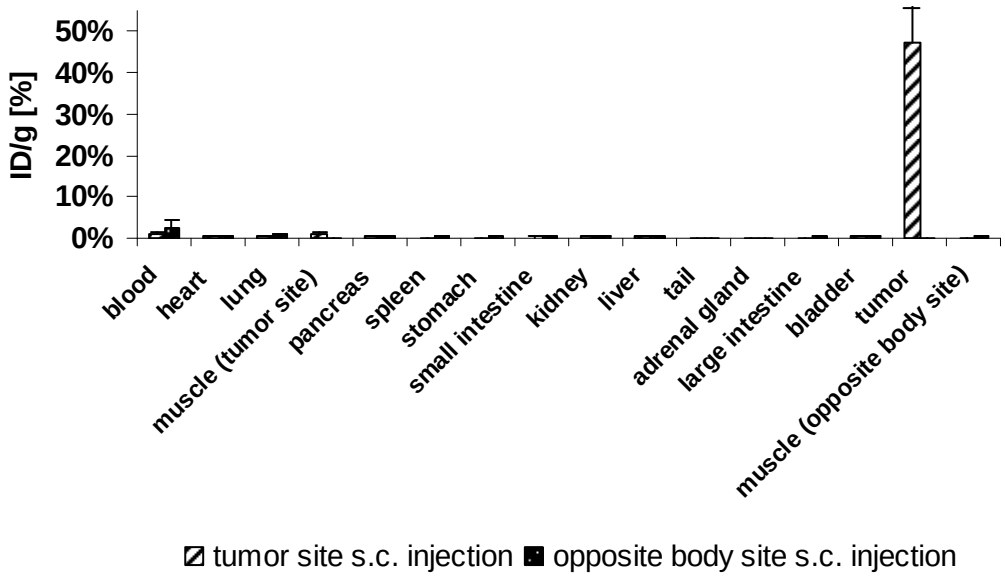

***Fig. 6**: Biodistribution of Ga-68 labeled but non-RGD-linked GNP (180 nm) in tumor-bearing CD-1 nude mice 120 min after s.c. injection either on tumor side (blue) or on the opposite body side (purple; % ID/g). Each point represents the mean of three investigated mice (n=3 ± S.D.).*

Fig. 6 shows the biodistribution of Ga-68 labeled but non-RGD-linked GNP of 180 µm in diameter in tumor-bearing CD-1 nude mice. The GNP dispersion (radioactive yield: 65 %) was either injected subcutaneously 0.5 cm away from the tumor or on the opposite body site. Each point in the figure above displays the mean of three investigated mice.

This study clearly demonstrates that GNP tumor uptake is only successful when the GNP dispersion is injected subcutaneously close to the tumor. Injection on the

opposite body side obviously does not lead to higher GNP concentrations in the tumor than in all the other examined organs. However, biodistribution was only investigated over a period of two hours before the mice were scarified and the organs were explanted. As this time-frame was very tight, the major part of GNP remained in blood or in the depot at the injection site. Probably, an active tumor targeting also of the particles that were injected on the non-tumor-bearing side could be observed by elongating biodistribution time. Nevertheless, such a high GNP tumor site accumulation was not expected due to an increased GNP uptake in other organs such as the kidney.

Fig. 7 also shows the biodistribution of Ga-68 labeled GNP in tumor-bearing CD-1 nude mice. This time, the GNP dispersion was injected subcutaneously 0.5 cm away from the tumor. We employed either a dispersion of RGD-linked GNP (250 nm; radioactive yield: 52 %) or a dispersion of non-RGD-linked GNP (180 nm; radioactive yield: 65 %). Each point in the figure below displays the mean of four and three investigated mice, respectively.

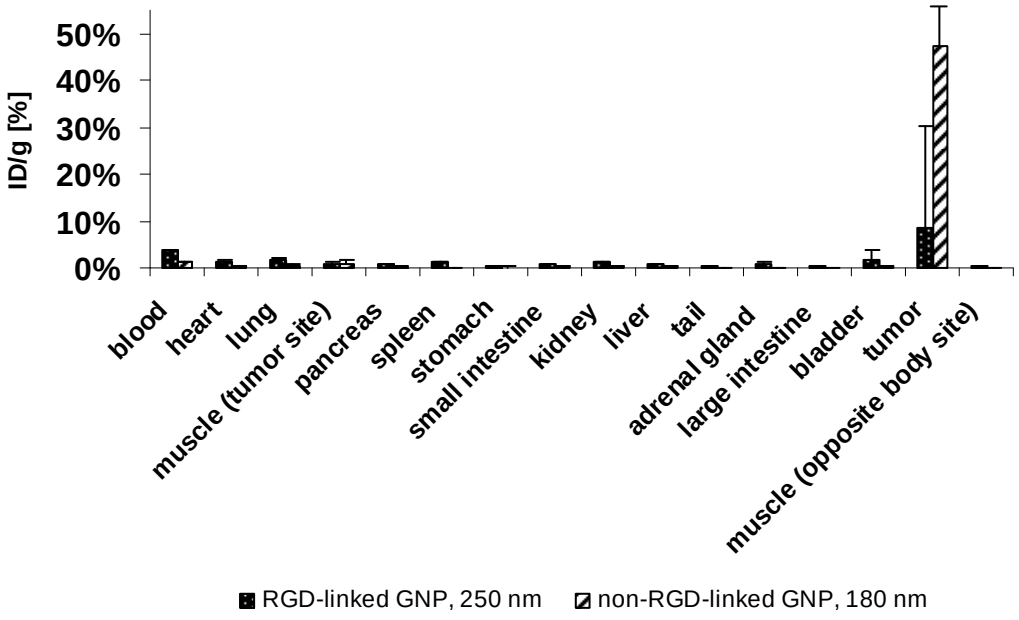

***Fig. 7**: Biodistribution of Ga-68 labeled GNP in tumor-bearing CD-1 nude mice 120 min after s.c. injection on tumor site (% ID/g); green: RGD-linked GNP, 250 nm, n = 4, blue: non-RGD-linked GNP, 180 nm, (n = 4, ± S.D.).*

This experiment indicates that GNP accumulation in the tumor is dependent from particle size and/or possibly from RGD-linkage. We were able to observe that

non-RGD-linked smaller particles considerably led to higher tumor uptake rates than RGD-linked larger particles. This is surprising because RGD is generally known for its active tumor targeting properties. However, particle size should not be underestimated. Maybe, higher GNP tumor uptake occurs due to smaller particles and is not influenced by RGD-linkage. Continuative experiments possibly using RGD-linked and non-RGD-linked particles of the same size could clarify this circumstance. We further found out that RGD-linked larger GNP led to higher uptake rates in the other organs than non-RGD-linked smaller particles did. This is probably due to the fact that RGD does not specifically bind to cancer cells but also to other integrin expressing cells (Peer et al. 2007).

4.3.4.3 **Confocal laser scanning microscopy (CLSM) of tumor tissue**

Aside from radioactive labeling, GNPs were additionally fluorescence labeled. Consequently cell trafficking could easily be tracked in tumor tissue frozen sections of 10 µm of thickness. To avoid interference with tissue autofluorescence, Alexa® 633 that is known for red light emission was used instead of standard Alexa® 488 for labeling GNPs. The dye directly bind to amino groups on the GNP surface and can be detected by CLSM.

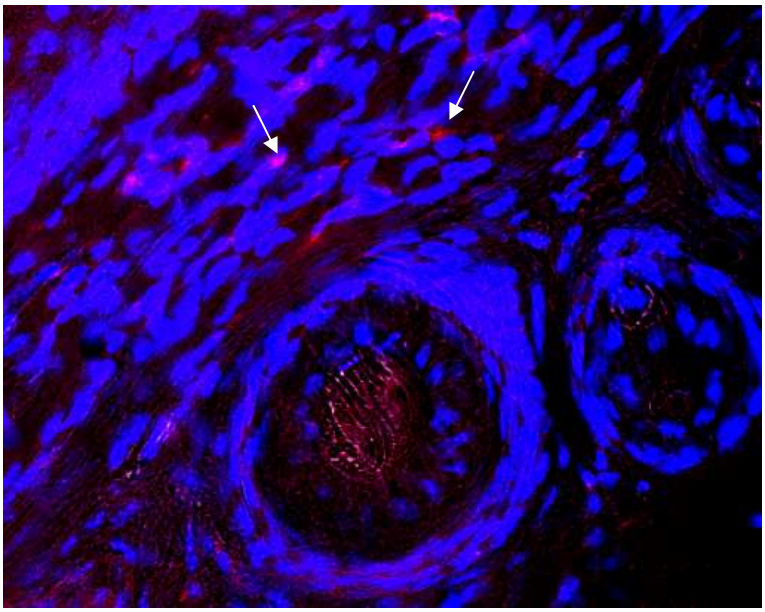

***Fig. 8**: Hoechst-stained frozen section (10 µm) of M21 tumor tissue comprising truncated vessels; blue: nuclei, red: GNP (see arrows). Inner diameter of*

centrally pictured vessel about 20 µm.

Fig. 8 shows a Hoechst-stained frozen section of M21 tumor tissue explanted 120 minutes after s.c. GNP (180 nm) injection on tumor site. Hoechst 33342 is a fluorescence dye emitting blue light upon laser excitation. As it intercalates DNA, it is generally used for marking nuclei. Hence, cell nuclei appear blue in the CLSM shoot above whereas GNP emit red light (see arrows). This experiment finally confirms the preceding biodistribution results. Thus, PEGylated (13 kDa, Fig. 2) GNP are able to escape into tumor tissue and to accumulate there.

4.3.5 *In vivo* and *ex vivo* studies of i.v.-administrated plain and PEGylated GNPs

In this study, it was attempted to gain more insight about the impact of PEGylation on the circulation properties of GNPs. This was of special interest as recently Cho et al. could not confirm a higher blood circulation time or superior passive tumor targeting of all PEGylated GNP-doxorubicin formulations in general (Cho et al. 2006; Cho et al. 2007). This backs previous findings of our group (Zwiorek 2006), as no significant difference in prolonged circulation time or increased passive tumor accumulation between PEGylated and non-PEGylated GNPs could be found.

In brief, GNPs were grafted with 5 kDa PEG via an imine bond between the PEG-polymer and the GNP surface as described earlier (Zillies et al. 2007) and labeled by ^{123}I radioiodination (Zwiorek 2006). 15 and 60 min post injection organ inspection by a γ-counter, GNP concentrations did not differ in all examined organs including the blood (Zwiorek 2006).

Additionally, when coupling larger 13 kDa PEG covalently to the GNP surface by stronger amid bonds as described above for the s.c.-related administration, no increased blood circulation times were found (Fig. 9). The latter setup ruled out that an early hydrolysis of a too weak linkage was the reason for the missing differentiation of PEGylated versus non PEGylated GNPs. As a conclusion from these findings, it can be hypothesized that colloidal carriers that already feature high hydrophilic properties such as gelatin and an in situ steric heterogeneous

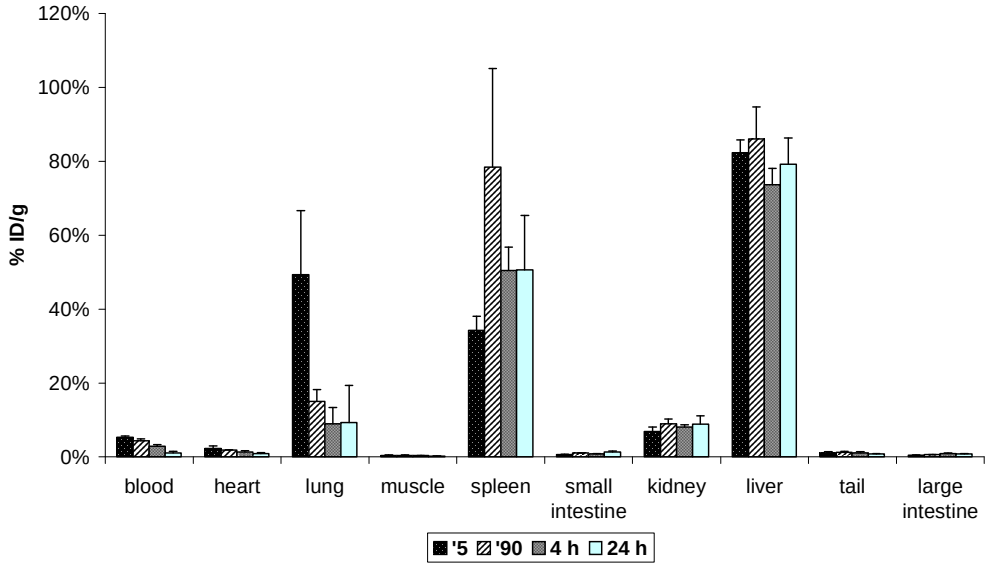

Fig. 9: *Ex vivo biodistribution and PEGylated (13 kDa) ^{111}In-labeled GNPs of 250 nm in balb/C mice (n=4, ± S.D) after injection into the tail vain. Radioactivity Concentrations are given as per cent of the injected dose per g (%ID/g).*

surface with hindrance properties are less accessible for the proven and undoubtful PK enhancements attributed to PEG when combined with hydrophobic delivery systems or therapeutic proteins (Jevsevar et al. 2010).

Evaluating the full blood recovery of GNP-linked activity of another batch confirmed the finding depicted in Fig. 10.

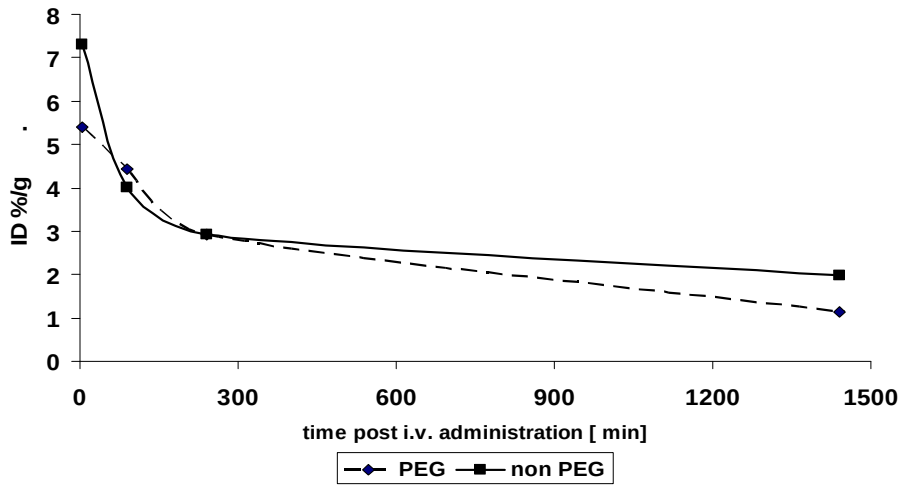

Fig. 10: *Full blood recovery of ^{111}In-labeled PEGylated and non-PEGylated GNPs over a time period of 24 h (n=3, ± S.D.).*

Here it is shown, that the PEGylation (13 kDa) had no significant influence on the

circulation time of GNPs.

Another finding from the *ex vivo* sectioning was that GNPs biodistribution is size depending at least in part, as the lung accumulation rises with the mean diameter and vice versa. This was in accordance with previously reported size effects on distribution and even intracellular effects (Jiang et al. 2008; Minchin 2008).

While radiolabeling was widely conducted with protein nanoparticles for conservative biodistribution studies and PET was applied for a variety of nanoparticle-based trials (Cheon et al. 20091112) no successful employment of PET studies was yet carried out on protein-based nanoparticles. Therefore, one attempt used N-succinimidyl-[^{18}F] fluorobenzoate PET-suitable prosthetic group to be linked to the GNPs. While the labeling process was successfully performed, too high *in vivo* concentrations were needed for adequate imaging (Zwiorek 2006). However, a safe formulation suitable for PET imaging was obtained when using DOTA as a chelator and $^{68}Ga^{3+}$ as radionuclide (Fuchs et al. 2008). Here, radiochemical yield was up to 75% and radiochemical purity in the final preparation reached 98.5%.

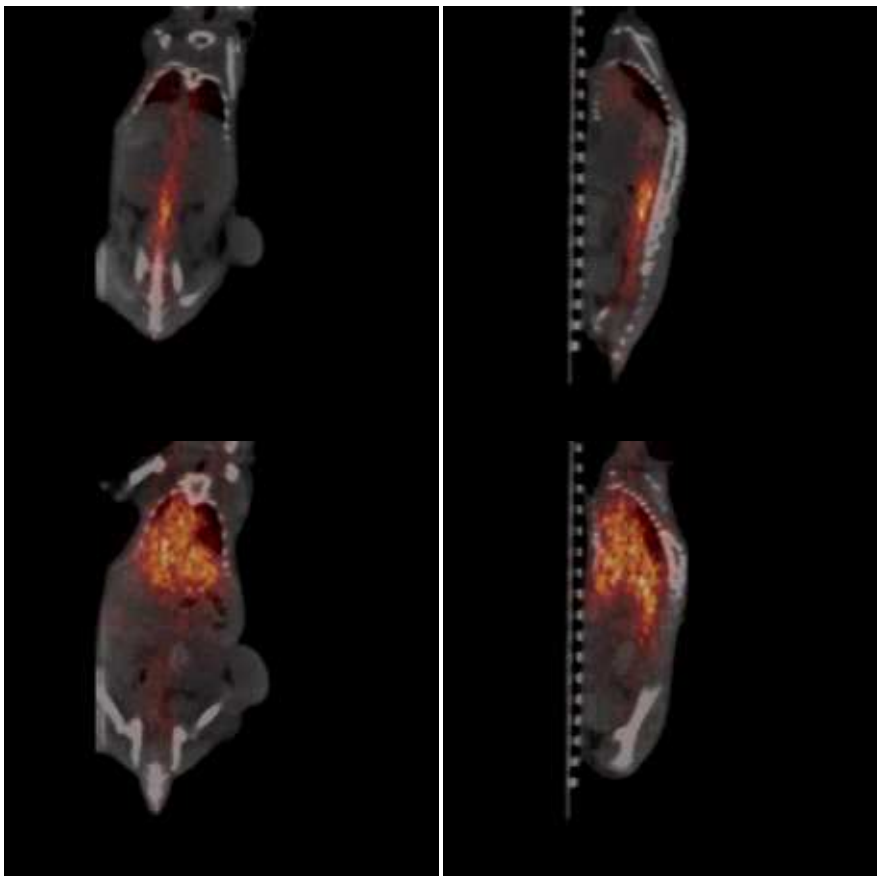

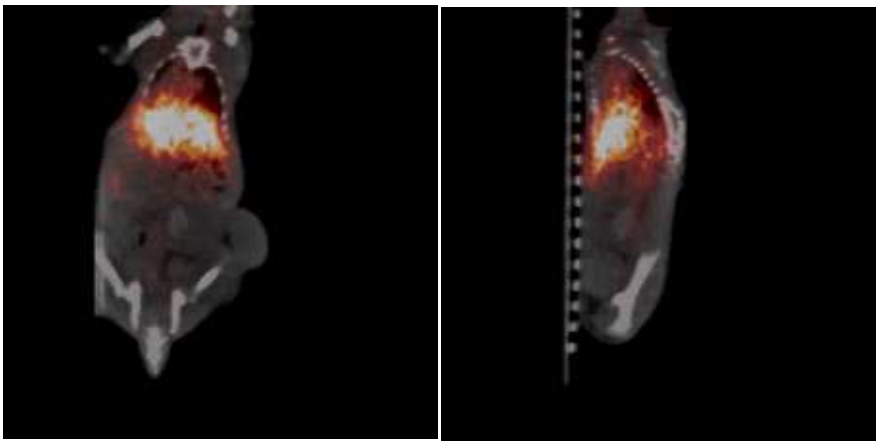

Fig. 11: *Combined PET/CT online imaging of ^{68}Ga-labeled GNPs 10, 50 and 100 seconds post injection into the tail vain with the left column representing coronal plane view (head upwards) and the right column representing sagital plane view. Brighter color represents respectively higher particle accumulation.*

The biodistribution of this protein nanoparticulate formulation could be tracked online for the first time by combined small animal PET/CT (Fig. 11). Furthermore, *ex vivo* sectioning of organs after administration of dually fluorescence and $^{68}Ga^{3+}$ labeled GNPs revealed the co-localization of activity marker and particles. Therefore, the particle double-checked distribution data based on radiolabeling alone could be seen as robust. Furthermore, flanking *ex vivo* trials proofed the difference in biodistribution for the pure macromolecular gelatin and GNPs (Fig. 11).

4.3.6 **Differentiation of biodistribution profiles of soluble gelatin in from GNPs: particles matter.**

To evaluate the biodistribution properties of GNPs upon i.v. administration, it is essential to adequately attribute the acquired data to the particle quality. Gelatin as a hydrophilic macromolecular should decisively contribute to the particle surface characteristics such as the similarity to other PEGylated particles in hydrophilic properties. However, the proof that the GNP biodistribution properties were linked more to their particulate nature than to their constituting material alone was not yet provided. Therefore, a suitable ^{111}In-labeld gelatin fraction was gained by employing a PD-10 desalting column to separate unbound nuclide (which was trapped in the column) from successfully labeled gelatin macromolecule (see 4.2.4).

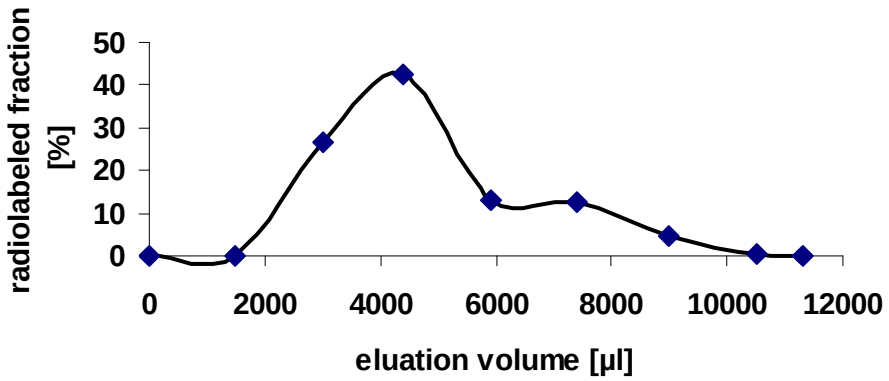

Fig. 12: *Histogram of 1 ml fractions of 111In-labeled gelatin solution, fractionized by a PD-10 desalting column with a size cut off of approx. 5 kDa.*

The forth fraction (3000 – 4000 µl) featuring the highest activity was chosen (Fig.12) to obtain high signal responses. Furthermore, this relatively early eluated fraction should represent a high molecular weight fraction which also served as starting material in the manufacturing process of GNPs. However, MWs could not be determined within this study.

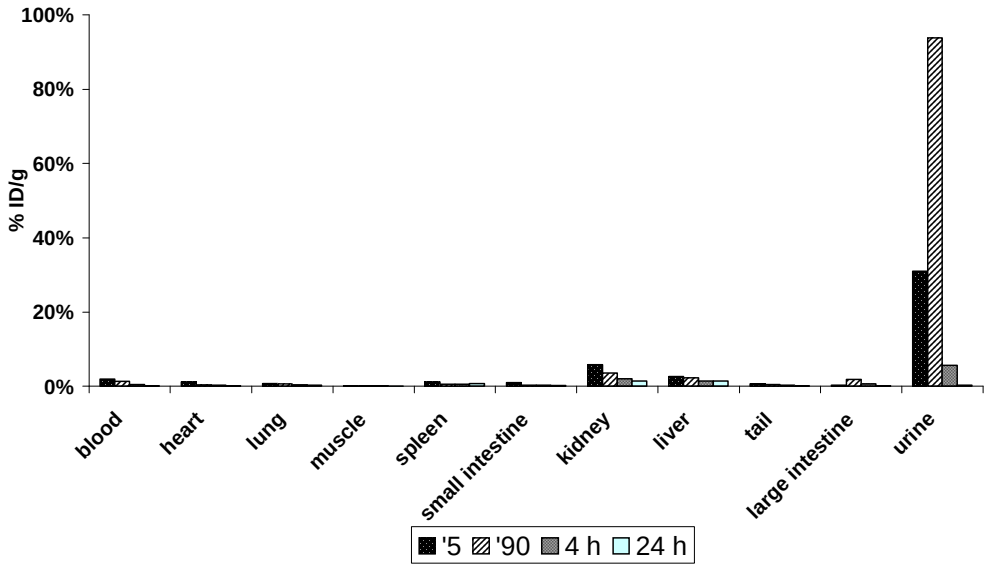

Fig. 13: *Ex vivo biodistribution of ^{111}In-labeled soluble gelatin in balb/C mice after injection into the tail vain. Radioactivity concentrations are given as per cent of the injected dose per g (%ID/g) (n=1).*

In contrast to GNPs (Fig. 9), gelatin as a soluble molecule did not accumulate in lung, spleen or liver. On the contrary, it was renally eliminated rapidly as revealed by the activity peak in the urine after 90 min (Fig. 13). While the non-accumulation could be seen as positive from a toxicological point of view -if

gelatin was toxic at all- the non-retention in the blood appeared as striking. Injected doses did not peak beyond 2% ID/g while GNPs initially could reach up to 10% despite PEGylation.

Moreover, lower particle sizes such as 250 nm (Fig. 9) revealed beginning of lung clearance already between the 5 and 90 minutes measuring point. In the corresponding extend, accumulation progressed in the liver, although this process is size depending, too. Nevertheless, it could be concluded that the i.v. administration as for many other nanocarriers is not the first choice when a specific targeting beyond the preferential MPS organs is of interest. Surface grafting of targeting structures -in the present case the RGD tripeptide- may not always compensate the particle-associated undesired biodistribution patterns. Therefore, further studies concentrated on immunotherapy via alternative routes of administration such as s.c. and inhalative. They were chosen to ensure a sufficiently long time of pharmacodynamic action before degradation or elimination of the drug-loaded nanocarrier system could occur to a larger extend.

IV Gelatin nanoparticles as a valuable tool in immunotherapy

1. Immunotherapy by nucleic acids – why?

1.1 Historical perspective

The idea to trigger the immune system for antitumoral action looks back on a long development originally coming from the observed interrelation of infections and tumor regression (Thotathil and Jameson 2007). Coley was the first to systematically introduce related research and reported a coherence between erysipelas and cancer remission (Coley 1893). Furthermore, he made a liquid preparation containing bacterial lysates of Streptococcus pyogenes and Serratia marcescens which was known for decades to elicit fever and immune activation in general. However, the biomolecular mechanisms and possible implications on more specified therapeutic applications were revealed only in the last 15 years. Specific short DNA strands were identified as the main trigger of immunostimulation within the bacterial lysate (Tokunaga et al. 1984). These short methylated oligonucleotides featured palindromic CpG-motifs responsible for B-cell activation (Krieg et al. 1995). Furthermore, contained lipopolysaccharides (LPS) were shown to be involved in IL-12 induction, a cytokine which is known for its Th1 pathway inducing properties (Tsung and Norton 2006). Most recently, involvement of the CpG-ODN as pathogen associated molecular pattern (PAMP) recognizable by a pattern recognition receptor (PRR) was confirmed in Coley's toxin (Hobohm et al. 2008). Today, synthetic CpG-motifs containing ODNs represent a potential new group of therapeutics involved in several clinical trials. The expected growth here is underlined by the fact that the CpG-manufacturing Coley Pharmaceutical Group was acquired by Pfizer in 2008. However, no CpG-based product has yet reached the market beyond clinical phase III and a suitable carrier seems to be of advantage in related efforts (see Chapter I).

1.2 The principle of CpG-mediated immunostimmulation

Artificial CpG oligonucleotides are agonists for a member of the PRR family signalling through an endosomal membrane based type receptor, the Toll-Like Receptor 9 (TLR9) (Angel et al. 2008; Wernette et al. 2002). The name "Toll-like receptor" was not derived from the English word toll in the meaning of fee but instead was coined by Nobel price laureate Nüsslein Vollhard of Tübingen who

described the molecular biologic discovery as “toll” referring to “great” in German. The discovery was rather accidental by realizing that a knock out of TLRs resulted in increased sensitivity of Dosophila flies to fungical infection (Lemaitre et al. 1996). Subsequently, these structures were identified as highly conserved in higher species to include humans.

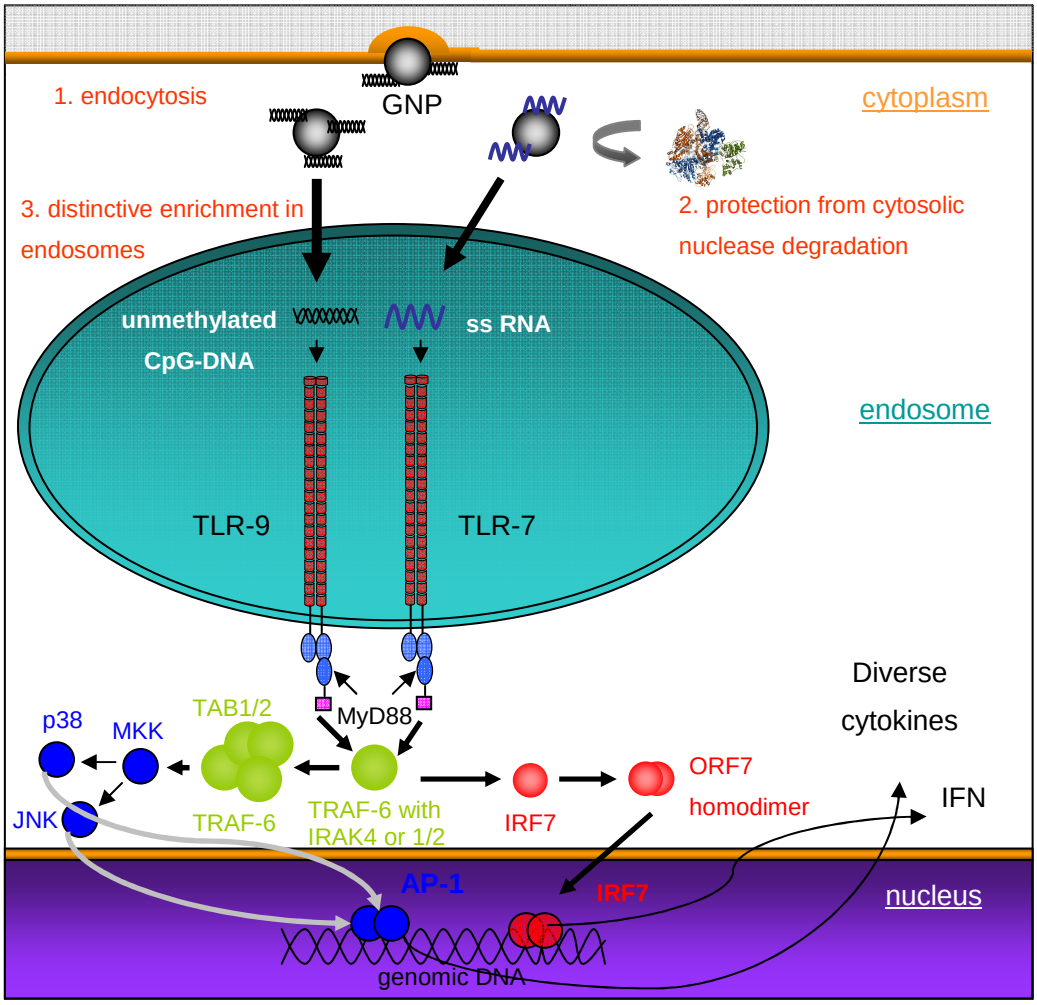

Fig. 1: *Survey on intracellular TLR-7 and TLR-9-mediated signalling MyD88-dependent pathways and the role of GNPs as a potent TLR-agonist delivery device. MyD88 is an essential Toll/IL-1 receptor (TIR) domain-containing adaptor for the induction of inflammatory cytokines via all the TLRs. Upon stimulation, MyD88 recruits IL-1 receptor-associated kinase (IRAK) to TLRs through interaction of the death domains of both molecules. IRAK is activated by phosphorylation and then associates with the TNF receptor associated factor (TRAF6), leading to the activation of two distinct signaling pathways, and finally to the activation of c-Jun N-terminal kinases (JNK) and nuclear factor kappa-light chain-enhancer of activated B cells (NF-kB) transcription factors for the translation of effector proteins such as cytokines.*

CpGs were shown to influence several signalling pathways in a variety of immune

cells, leading to cytokine production in many mammalian species (Zwiorek et al. 2004; Zhao et al. 2010) (Fig. 1). It appears that the specific purines and pyrimidines surrounding the CpG motif, phosphothioated backbone, as well as the spacings between CpG motifs may influence both the level and the type of immune stimulation (Krieg et al. 1995; Mutwiri et al. 2003). CpG motifs improve the antigen presenting function of dendritic cells (DCs), monocytes and macrophages, induce the proliferation of B lymphocytes, stimulate the immunoprotective activity of natural killer (NK) cells, and recruit T cells to the site of ODN administration (Coester et al. 2006; Torchilin 2007; Zwiorek et al. 2008). Recent studies showed that the immune system responds to CpG motifs by activating potent Th1-like immune responses which can be harnessed for immune therapy of cancer, allergy, infectious diseases (Krieg 2002), autoimmune diseases, and sterile inflammation (Kanzler et al. 2007). Consequently, CpGs may also be used as potent adjuvant for vaccines which was a central delivery application for the present GNPs (Bourquin et al. 2006; Bourquin et al. 2008) also by directly activating plasmoidal dendritic cells (pDCs) and subsequently B-cells without the involvement of T-cells (Poeck et al. 2004). As illustrated in Fig. 1 (chapter V, 3.1), the Th1 pathway activation elicits T cell (CD8) response (Bourquin et al. 2006) e.g. via IL-12. This was proven in prophylactic anticancer studies involving GNP-bound CpG (Bourquin et al. 2008).

1.3 Other nucleic acid-derived therapeutic strategies

Molecular DNA or RNA therapy is an upcoming approach to controvert difficult to treat diseases by engaging in transcriptional processes. Transcriptional factors are nucleus based proteins that can have a boosting or alleviative effect on gene expression. These TFs recognize their own short binding region even in absence of neighbouring genomic DNA. This makes synthesized ODN with consensus base sequences a possible therapeutic option to manipulate gene expression (Mann and Dzau 2000).

Decoy ODNs inhibit the binding of a TF, for example the promoter region of the cytoplasm based NF kappa B receptor. Thereby they prevent this transcription factor from inflammatory interactions with its target genomic DNA in the nucleus. Other transcriptional interfering strategies all target the mRNA level like antisense ODNs, ribozyme ODNs and RNAi. First therapeutic successes were achieved in

the fields of retinopathy, restenosis, glomerulonephritis and rheumatoid arthritis (Morishita et al. 2004).

1.4 Nucleic acid-based immunotherapeutic strategies against cancer

As mentioned above, Coley found prolonged resistance against cancer upon treatment by his bacterial-derived toxin. Since TLR-9 activation by CpG motifs was identified as decisive for antitumoral action, the insight into related immunologic fundamentals pathed the way towards CpG-based immunotherapy against cancer (Krieg 2002; Krieg 2006). Of central importance was the ability, to overcome T-cell anergy by the adjuvant properties of CpGs. However, this essential adjuvant ability was proven not to be applicable exclusively for TLR-9-mediated CpG action (Hornung et al. 2002; Heil et al. 2004), but moreover for TLR-7-mediated RNA effects which is demonstrated in the following. In order to achieve a specific immune reaction against a cancer target, immune cells need to be primed against relevant cancer-specific antigens. In the current studies, Ovalbumine (OVA) was used as an established and potent model antigen. However, for future targeted therapeutic strategies, real tumor-expressed antigens need to be included such as pancreas cancer-expressed surface protein survivin (SVV) also referred to as BIRC5 (Altieri 2003). The importance of this field of tumor-specific antigen-directed anti-cancer immunotherapy is stressed by the fact that the FDA approved the first therapeutic cancer vaccine Provenge® (sipuleucel T) in April 2010 for the treatment of hormone-refractory prostate cancer (Bordon 2010).

2. Antitumoral response triggered by GNP-bound RNA to agonist TLR7

Introduction

The capacity of GNPs to function as RNA carrier is demonstrated in the following insert which cites a joint pre-review manuscript for publication by the Center for Integrated Protein Science Munich and Divison of Clinical Pharmacology, Department of Internal Medicine (*), Ludwig Maximilan University Munich, on the one hand and the Department of Pharmacy, Pharmaceutical Technology and Biopharmaceutics (†), Ludwig Maximilan University Munich, on the other hand.

Delivery of immunostimulatory RNA oligonucleotides by gelatin-based nanoparticles triggers an efficient antitumoral response

Carole Bourquin, Cornelia Wurzenberger*, Sebastian Fuchs†, David Anz*, Sarah Weigel*, Nadja Sandholzer*, Gerhard Winter†, Conrad Coester† and Stefan Endres* (CB and CW contributed equally to this work.)*

Introduction

Upon viral infection, a strong immune response is elicicited through recogniciton of viral components by specific receptors of the innate immune system. Molecular patterns within viral nucleic acids are recognized by the pattern-recognition receptors TLR7 (single-stranded RNA sequences), TLR9 (CpG DNA sequences) RIG-I (5'-triphosphate RNA) and MDA-5 (double-stranded RNA) (Heil et al. 2004, Hemmi et al. 2000, Hornung et al. 2006, Kato et al. 2006). A highly selective immune response can be induced by Synthetic DNA and RNA oligonucleotides containing these molecular patterns are a powerful tool to simulate an immune response in a highly selective manner. It is for instance well established that binding of synthetic CpG ODNs to TLR9 both promotes innate immunity and triggers the generation of a protective Th1-type immune response (Krieg 2007). In experimental models and in cancer patients, CpG ODNs enhanced cytotoxic T cell responses to tumor antigens upon vaccination (Brigger et al. 2002; Wurzenberger et al. 2009; Brazolot Millan et al. 1998; Brazolot Millan et al. 1998; Speiser et al. 2005). Furthermore, we have recently shown that RNA oligonucleotides can stimulate innate immunity through both the Toll-like receptor 7 and RIG-I receptors (Hornung et al. 2006; Hornung et al. 2004) and thereby induce efficient antitumoral responses (Bourquin et al. 2009, Poeck et al. 2008).

TLR7-activating RNA oligonucleotides act on several components of both the murine and the human immune systems: they trigger T and B cell responses to antigen (Bourquin et al. 2007), activate neutrophils (Janke et al. 2009) and antitumoral NK cells (Bourquin et al. 2009) and block the suppressive function of regulatory T cells experimental models and in cancer patients (Anz et al. 2010). We have demonstrated previously that these effects on different immune cell populations are directed by TLR7-expressing dendritic cells that control immune

activation through the production of a panel of cytokines (Anz et al. 2010; Bourquin et al. 2007). The therapeutic potential of TLR7 agonists is supported by encouraging results with a recently developed class of antitumor agents, the imidazoquinoline, that act in part through the activation of TLR7 (Hemmi et al. 2002). The lead compound, imiquimod, is however only approved for the treatment of skin tumors by topical use and is effective against solid tumors only when applied locally (Broomfield et al. 2009). RNA ODNs thus form a new class of TLR7 agonists with promising therapeutic potential. Furthermore, RNA ODNs can be designed to include other antitumoral properties in the same molecule. The introduction of an inhibitory siRNA sequence permits silencing of tumor-promoting genes that synergizes with the immunostimulatory activity of the RNA oligonucleotides to block tumor growth (Poeck et al. 2008).

A key challenge for the therapeutic application of RNA ODNs is the need for efficient *in vivo* delivery to protect RNA ODNs from degradation, to promote cellular uptake and to target the RNA to the desired intracellular compartment (Whitehead et al. 2009). In this study we have investigated the efficacy of previously described cationized GNPs (Zwiorek et al. 2008) for the delivery of immunostimulatory RNA ODNs. Gelatin represents the advantage of being biodegradable and non-toxic and has been used in patients as a plasma expander for decades (Ward et al. 1977b). GNPs are stable during storage, show high stability after administration and can be easily scaled-up for manufacturing processes. Highly homogeneous GNPs of well-defined diameter can be generated by a two-step desolvation method (Coester et al. 2000). Furthermore, we have previously demonstrated that GNPs delivery enhances the CD8 T cell response triggered by CpG DNA oligonucleotides (Bourquin et al. 2008).

Here we examined the immunostimulatory capacity of GNP-delivered RNA ODNs both *in vitro* and *in vivo*. We show that nanoparticle-delivered RNA ODNs strongly activate immune responses in a TLR7-dependent manner. GNPs enhance the uptake of RNA ODNs by immune cells and protect them from degradation. In addition, immunization with nanoparticle-bound RNA ODNs and a model antigen protected from tumor growth. We thus characterize a new formulation for immunostimulatory RNA ODNs that enhances their ability to induce a strong Th1-type immune response to antigen and trigger efficient antitumoral responses.

Materials and Methods

Mice

Female C57BL/6 mice were purchased from Harlan-Winkelmann (Borchen, Germany). Mice were 6 to 12 weeks of age at the onset of experiments. TCR transgenic OT-I mice were kindly provided by Dr. T. Brocker (Institute of Immunology, Munich, Germany). Animal studies were approved by the local regulatory agency (Regierung von Oberbayern, Munich, Germany).

Reagents and cell lines

The fully phosphorothioated 20-mer RNA oligonucleotides 9.2dr (5'-UGUCCUUCAAUGUCCUUCAA-3') (Hornung et al. 2004) and polyA were purchased from CureVac (Tübingen, Germany). For some experiments, fluorescein-5'-tagged RNA oligonucleotides were used (Metabion, Martinsried, Germany). The unmodified 9.2 triphosphate RNA (PPP-5'-GCAUGCGACCUCUGUUUGA-'3) was produced by *in vitro* transcription in our laboratory (Hornung et al. 2006). Gelatin type A from porcine skin (175 Bloom) and chicken egg ovalbumin (OVA) were purchased from Sigma-Aldrich (St Louis, MO). The OVA-transfected B16-F10 cell line was kindly provided by Dr. T. Brocker.

Preparation of cationized gelatin nanoparticles

Gelatin nanoparticles were prepared in the Division of Pharmaceutical Technology and Biopharmaceutics at the University of Munich as previously described (Coester et al. 2000). Subsequently, cationization of the nanoparticles was achieved through introduction of a permanent quaternary amino group by covalent coupling of cholaminechloride hydrochloride onto the particle surface, as previously described (Zwiorek et al. 2008). Cationized particles prepared by this protocol were shown by *Limulus* amoebocyte lysate assay to be endotoxin-free (Coester et al. 2006). Unloaded particles were stable in size and ζ potential when stored as stock dispersion at 4°C for several months. For formulation with RNA oligonucleotides, particles were loaded with 5% (w/w) RNA oligonucleotides by shaking for 2 h at 800 rpm at room temperature. To evaluate the physical stability

of RNA oligonucleotide attachment to the cationic nanoparticle surface, dispersions were incubated in PBS at a final pH of 7.4 or 4.9 for up to one week. Dispersions were then centrifuged at 25000 g for 30 min and the supernatant was analyzed spectrophotometrically at 260 nm for free RNA. Controls consisted of either RNA or gelatin nanoparticles in the equivalent buffer. Results of percentile successful loading were calculated as follows:

$$\text{RNA loading} = \left(1 - \left(\frac{\text{OD of GNP-RNA supernatant} - \text{OD of GNP control supernatant}}{\text{OD of RNA control supernatant}}\right)\right) \times 100\,[\%]$$

Bone marrow cell culture

Bone marrow cells were harvested from murine femur and tibia and erythrocytes were lysed with ammonium chloride buffer (BD Biosciences, Heidelberg, Germany). Cells were cultured in RPMI 1640 medium supplemented with 10% FCS, 2 mM L-glutamine, 100 µg/ml streptomycin, and 100 IU/ml penicillin and activated with 10 µg/ml RNA oligonucleotides complexed to 200 µg/ml gelatin nanoparticles. Alternatively, 10 µg/ml RNA oligonucleotides were complexed to 50 µg/ml DOTAP (N-[1-(2,3-dioleoyloxy)propyl]-N, N, N-trimethylammonium methyl-sulfate; Roche, Mannheim, Germany) or 2.5 µg/ml lipofectamine (Lipofectamine 2000; Invitrogen, Carlsbad, USA) according to the manufacturers' instructions. Polyethylenimine (PEI) was kindly provided by Dr. M. Ogris (Department of Pharmacy, Munich, Germany). 10 µg/ml RNA oligonucleotides were complexed to 7.5 µg/ml PEI directly before stimulation.

Fluorescence microscopy

Bone marrow cells were stimulated for 3 h with fluorescein-5'-tagged RNA oligonucleotides and carriers as described above, washed three times and adhered to poly-l-lysine-coated microscope slides. Cells were then fixed in 100% acetone for 10 min. Topro-3 (Invitrogen) was used for nuclear counterstaining. Stained cells were visualized using a fluorescence microscope (Carl Zeiss) and Adobe Photoshop was used for adjustment of contrast and picture size.

Quantification of cytokines and flow cytometric analyses

Concentration of IL-12p70 and IL-6 in culture supernatants was determined by ELISA according to the manufacturer's instructions (BD Biosciences). IFN-α was measured according to the following protocol: rat monoclonal antibody to mouse IFN-α (clone RMMA-1) was used as the capture antibody, rabbit polyclonal antibody to mouse IFN-α for detection (both from PBL Biomedical Laboratories, Piscataway, NJ) together with HRP-conjugated donkey antibody to rabbit IgG as the secondary reagent (Jackson ImmunoLaboratories, Bar Harbor, ME). Recombinant mouse IFN-α (PBL Biomedical Laboratories) was used as standard (IFN-α concentration in IU/ml). For flow cytometric analyses, cells were stained with fluorochrome-conjugated monoclonal antibodies (B220, CD11b, CD11c, CD69, and isotype controls) and propidium iodide from BD Biosciences. Data were acquired on a FACSCalibur or a FACSCanto (BD Biosciences) and analyzed using FlowJo software (Tree Star, Ashland, OR).

Induction of OVA-specific CD8 T cell proliferation

For the *in vivo* induction of antigen-specific CD8 T cell proliferation, splenocytes from OT-I mice were labeled with 15 nmol/ml carboxyfluorescein succinimidyl ester (CFSE; Molecular Probes, Eugene, OR) after erythrocyte lysis. 5 x 10^6 labeled OT-I cells were adoptively transferred into wild-type mice on day 0. On day 1, mice were immunized s.c. with 75 µg OVA together with 100 µg free RNA oligonucleotides or 100 µg RNA oligonucleotides complexed to 2 mg gelatin nanoparticles. Two days later, freshly isolated splenocytes and cells from draining and contralateral lymph nodes were analyzed by flow cytometry. Antigen-specific T cell proliferation is expressed as percentage of dividing cells ($CFSE_{lo}$) within all CFSE-positive CD8 cells.

Immunization with OVA

For immunization of mice, 75 µg OVA were injected s.c. together with 100 µg free RNA oligonucleotides or 100 µg RNA oligonucleotides complexed to 2 mg nanoparticles two or three times at a 14-day interval. For the detection of OVA-specific antibodies, serum was collected one week after the second immunization and serum IgG concentrations were determined by ELISA: plates were coated

overnight with 10 µg/ml OVA in PBS and blocked 1 h with 1 % BSA in PBS. After incubation of serum samples for 1 h at a dilution of 1:200, plates were washed with PBS/0.05% Tween 20. Goat-anti mouse IgG conjugated to HRP (SouthernBiotech, Birmingham, AL) was added at 1 µg/ml for 1 h. Plates were again washed and ELISA was developed by o-phenylenediamine (Sigma-Aldrich). Reaction was stopped by 1 M H_2SO_4 and OD was read by photometer at 490 nm.

Tumor monitoring

One week after the third immunization, 10^6 B16-OVA cells were injected s.c. in the right flank. Tumor growth was monitored three times a week and is expressed as the product of the perpendicular diameters of individual tumors. Mice were sacrified at day 35 after tumor induction.

Statistics

Statistical analyses were performed by unpaired, one-way analysis of variance (ANOVA) with the Newman–Keuls multiple comparison test. Significance was set at $P < 0.05$. Comparisons among groups regarding day of onset of tumors were made using the log-rank test. Statistical analyses were performed using SPSS software (SPSS, Chicago, IL, USA).

Results

Nanoparticle-delivered RNA oligonucleotides efficiently trigger an innate immune response

We have recently described that immunostimulatory sequences within RNA oligonucleotides activate both innate and adaptive immune responses through TLR7 (Bourquin et al. 2007; Hornung et al. 2004). To assess the delivery potential of cationized gelatin nanoparticles for these immune-activating RNA oligonucleotides, murine bone marrow cells were stimulated with nanoparticle-bound RNA 9.2dr oligonucleotides. Oligonucleotides contained a phosphorothioate-modified backbone (PTO) to enhance immunostimulatory activity (Bourquin et al. 2007). Nanoparticle-bound RNA induced production of

the pro-inflammatory cytokines IL-12p70, IL-6 and IFN-α in the culture (Figure 1A). In contrast, no cytokine production was detected upon stimulation with free RNA oligonucleotides. Nanoparticles alone induced no IL-12p70 or IL-6 and only low levels of IFN-α. Cytokine induction by nanoparticle-bound RNA oligonucleotides was abolished in bone marrow cells from TLR7-deficient mice, confirming that the immunostimulatory activity was mediated by TLR7 (Figure 1A).

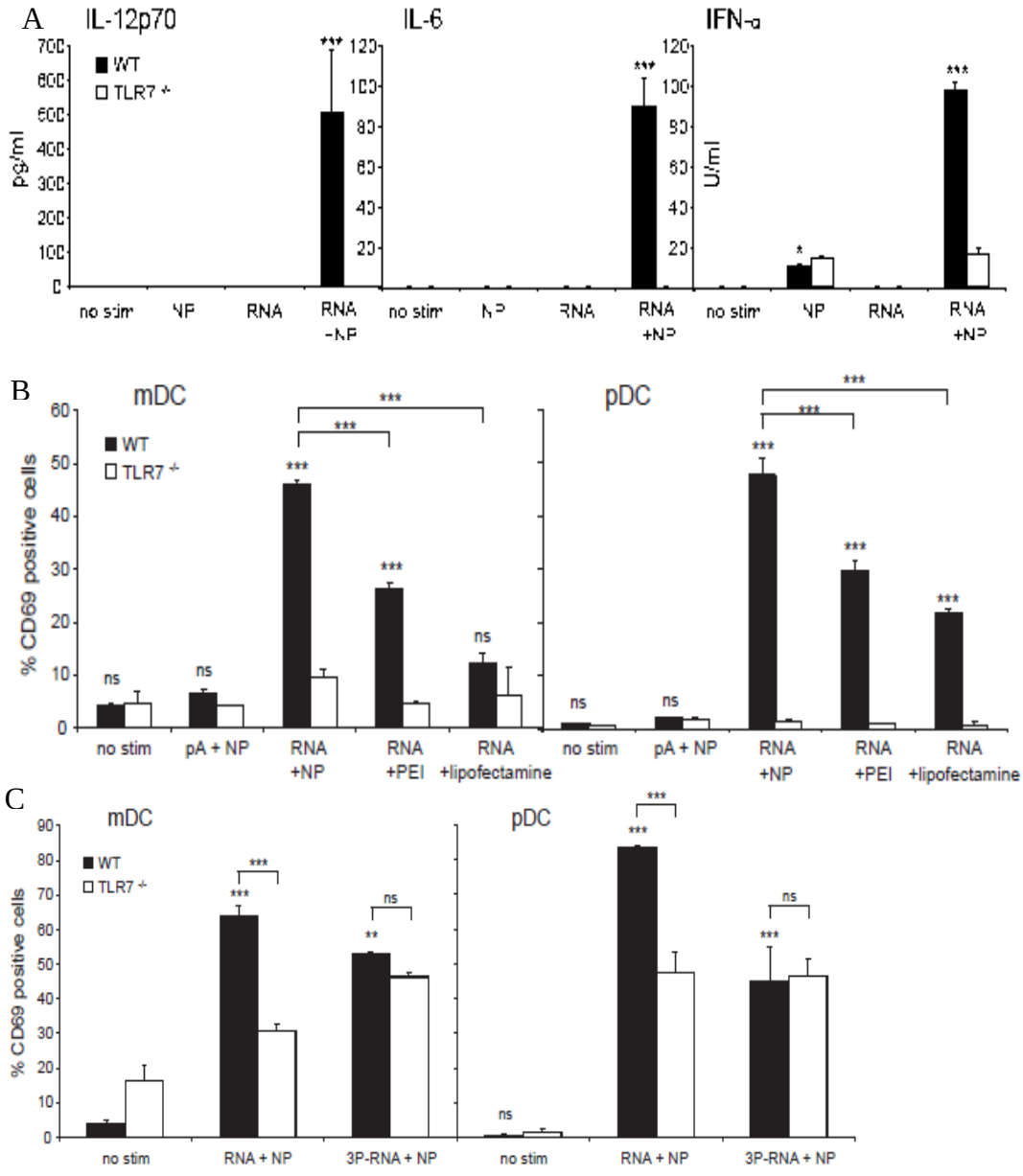

Fig. 1: **Nanoparticle-bound RNA ODNs activate innate immune responses**

Murine bone marrow cells from wild-type or TLR7-deficient mice were activated for 18 h with RNA ODNs complexed to different carriers as indicated. (A) Culture supernatants were analyzed by ELISA for IL-12p70, IL-6 and IFN-α production.

*(B and C) Surface expression of the activated marker CD69 on CD11c+ B220- myeloid DC (mDC) and CD11c+ B220+ plasmacytoid DC (pDC) within the culture was alayzed by flow cytometry. Data are expressed as % CD69-positive cells within the indicated populations. All results show the mean of triplicate samples +/- SEM. Data are representative of four independent experiments. Asterisks without brackets indicate comparison with unstimulated cells ***p < 0.001, ns not significant.*

Dendritic cells within the culture were activated by nanoparticle-bound 9.2dr PTO RNA with over 40% of both myeloid and plasmycytoid dendritic cells expressing the early activation marker CD69 (Figure 1B). Indeed, nanoparticle-delivered RNA induced a more potent activation of dendritic cells than RNA bound to the transfection reagents polyethylenimine (PEI) or lipofectamine (Figure 1B). As shown for cytokine induction, CD69 upregulation by RNA oligonucleotides was TLR7-dependent. Furthermore, cell activation was dependent on the RNA sequence since no activation was detected after stimulation with a PolyA oligonucleotide of the same length (Figure 1B). It has previously been shown that 5'-triphosphate-modified RNA oligonucleotides target the cytosolic receptor RIG-I (Hornung et al. 2006). Interestingly, nanoparticle-bound 5'-triphosphate RNA oligonucleotides also induced an activated phenotype in dendritic cells but did not induce cytokine secretion (Figure 1C). Stimulation by 5'-triphosphate 9.2dr oligonucleotides was independent of TLR7 (Figure 1C).

Nanoparticle formulation of immunostimulatory RNA oligonucleotides promotes their uptake into intracellular compartments

We have previously shown that efficient endosomal delivery of RNA oligonucleotides is required to induce TLR7-mediated immune activation (Anz et al. 2010). Here we examined the efficacy of cationized GNPs for the intracellular delivery of fluorescently labeled RNA oligonucleotides in direct comparison with the transfection reagents DOTAP, PEI and lipofectamine. RNA oligonucleotides bound to GNPs were rapidly taken up by bone marrow cells with over 80% of cells staining positive for labeled RNA after 6 h (Figure 2A). Free RNA oligonucleotides were not taken up by bone marrow cells (less than 1% 9.2dr RNA-positive cells). Uptake of RNA oligonucleotides complexed to the transfection reagents DOTAP, PEI or lipofectamine was less efficient with a

maximum of 38% of bone marrow cells staining positive for the fluorescently labeled RNA complexed to PEI (Figure 2A). Confocal microscopy revealed that nanoparticle-delivered RNA oligonucleotides can be observed as distinct dots after internalization, suggesting an endosomal uptake (Figure 2B). Complexation of RNA oligonucleotides to DOTAP resulted in a similar localization pattern, while RNA oligonucleotides bound to PEI or lipofectamine were evenly distributed in the cytoplasm of the transfected cells. Thus, nanoparticle-bound RNA oligonucleotides are efficiently taken up by immune cells and accumulate in intracellular compartments.

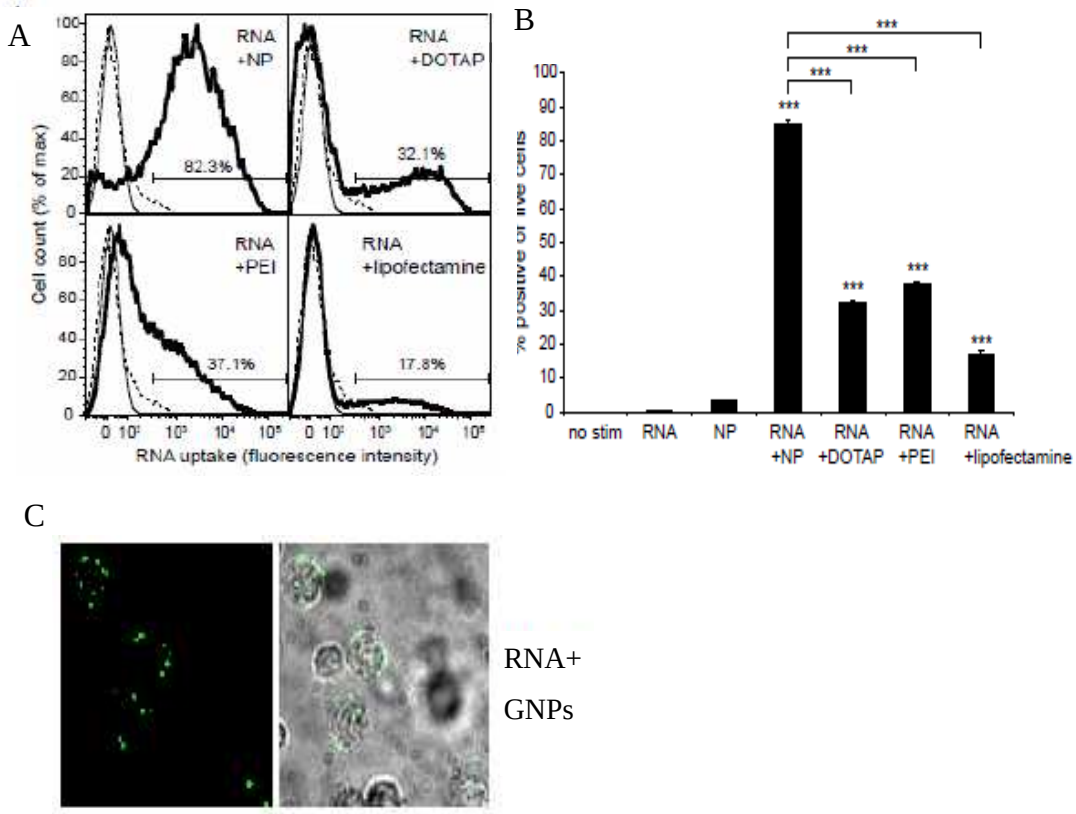

Fig. 2: **Nanoparticle formulationof immunostimulatory RNA ODNs promotes their uptake into intracellular compartments.**
*Murine bone marrow cells were stimulated with 10 µg/ml fluorescein-labled RNA ODNs compexed to different carriers. (A) Histograms illustrate uptake of fluorescently labeled RNA by bone marrow cells analyzed by flow cytometry, (bold line: RNA with indicated carrier; line line: free RNA; dashed line: no RNA) (B) Graph shows percentage of RNA ODN-positive cells as mean +/- SEM of triplicate samples. Asterisks without brackets indicate comparisons with unstimulated cells and cells stimulated with either ORN or NP alone. *** P < 0.001. (C) Confocal microscopy of RNA ODN-stimulated cells shows intracellular localization of the fluorescently labeled RNA (green) after 3 h. Left panel shows a fluorescence image, right panel shows a differential interference contrast (DIC) picture merged with fluorescence. Results are representative of two independent experiments.*

Nanoparticle formulation protects immunostimulatory RNA oligonucleotides from degradation by RNases

In addition to facilitating the uptake of RNA oligonucleotides into the appropriate intracellular compartment, an effective delivery system must protect nucleic acids from degradation. This is an important requirement for the application of immunostimulatory RNA oligonucleotides in a therapeutic setting, as the widespread distribution of RNases results in a very short lifespan for unprotected RNA which was demonstrated *in vitro* earlier (Elmen et al. 2005).

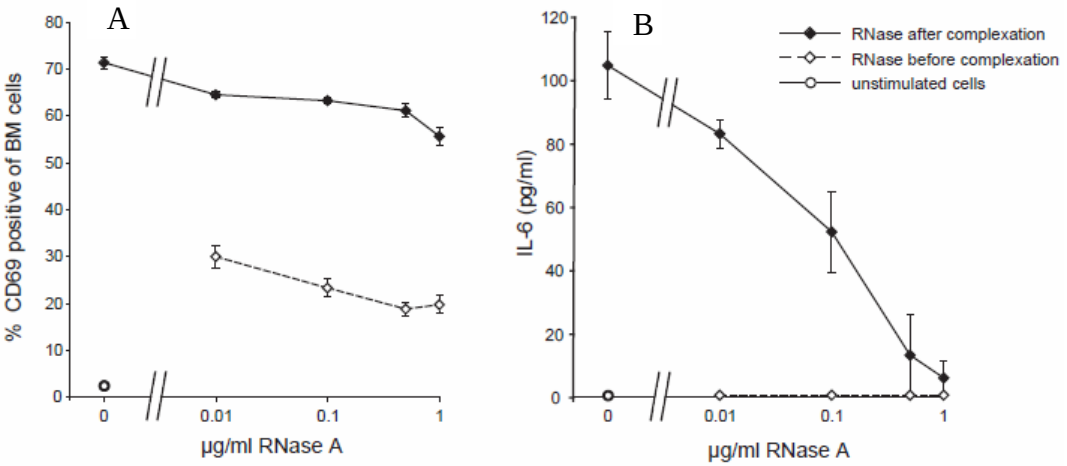

Fig. 3: **Nanoparticle-bound immunostimulatory RNA ODNs are protected from RNase degradation.** *Bone marrow cells were activated with GNP-bound 9.2dr PTO RNA ODNs digested with RNase A in the indicated concentrations either before or after the complexation of RNA to GNPs. Surface expression of the activation marker CD69 was analyzed by flow cytometry (A) and IL-6 concentration in the supernatants was analyzed by ELISA (B). Data show mean and SEM of triplicate wells and is representative of five independent experiments.*

The complexation of RNA oligonucleotides to GNPs was assessed whether it provided protection from degradation by RNases. We observed that RNA loading onto the cationic GNP surface was stable for at least one week at both cytosolic (7.4) and endosomal pH (4.9) (Figure 3A). Immunostimulatory RNA oligonucleotides were then exposed to partial digestion by RNAse A either before or after complexation with GNPs (Figure 3B). Prior incubation with cationized gelatin nanoparticles protected RNA oligonucleotides from degradation by RNase A, as they still induced an activated CD69+ phenotype and cytokine production in a bone marrow cell culture after a one-hour RNase treatment (Figure 3B). In contrast, RNA oligonucleotides that were incubated with GNPs after the RNase treatment had lost their immunostimulatory potential.

Nanoparticle-bound RNA oligonucleotides trigger antigen-specific CD8 T cell and antibody responses

To investigate the effect of nanoparticle-bound RNA oligonucleotides on the development of an immune response to antigen, CFSE-labeled OVA-specific T cells from OT-I mice were adoptively transferred into wild-type mice. 24 h later, mice were immunized s.c. with OVA protein together with free RNA oligonucleotides or nanoparticle-bound RNA oligonucleotides. Three days after immunization, proliferation of CFSE-labeled cytotoxic T cells (CTL) in draining lymph nodes and spleen was analyzed by flow cytometry. Proliferation was enhanced in mice immunized with OVA plus nanoparticle-bound RNA oligonucleotides. In contrast, free RNA oligonucleotides did not promote OVA-specific proliferation. To examine the effect of immunization with nanoparticle-bound RNA oligonucleotides on the development of an antibody response, mice were immunized with the model antigen ovalbumin (OVA) together with free RNA oligonucleotides or nanoparticle-bound RNA oligonucleotides twice at a 14-day interval. One week after the second immunization, serum levels of OVA-specific antibodies were measured. In mice immunized with OVA and nanoparticle-bound RNA oligonucleotides, levels of OVA-specific IgG were significantly increased compared to mice immunized with either OVA alone or OVA with free RNA oligonucleotide. Nanoparticle-bound RNA oligonucleotides did not induce a generalized immune activation, as we detected neither unspecific activation of immune cells in the spleen nor elevated serum cytokine levels after s.c. injection of nanoparticle-bound RNA (data not shown). Thus, nanoparticle-bound RNA oligonucleotides act as potent adjuvants and elicit efficient antigen-specific immune responses when administered with antigen while at the same time preventing an indiscriminate systemic activation of the immune system.

Nanoparticle-bound RNA oligonucleotides induce an efficient antitumoral response

The ability to stimulate cytotoxic T cell responses is a prerequisite for obtaining an efficient antitumoral immune response. To assess whether the antigen-specific responses induced by nanoparticle-bound RNA oligonucleotides protected from the development of a tumor, wild-type mice were immunized with OVA together with free RNA oligonucleotides or nanoparticle-bound RNA oligonucleotides

before s.c. challenge with OVA-expressing B16 melanoma cells.

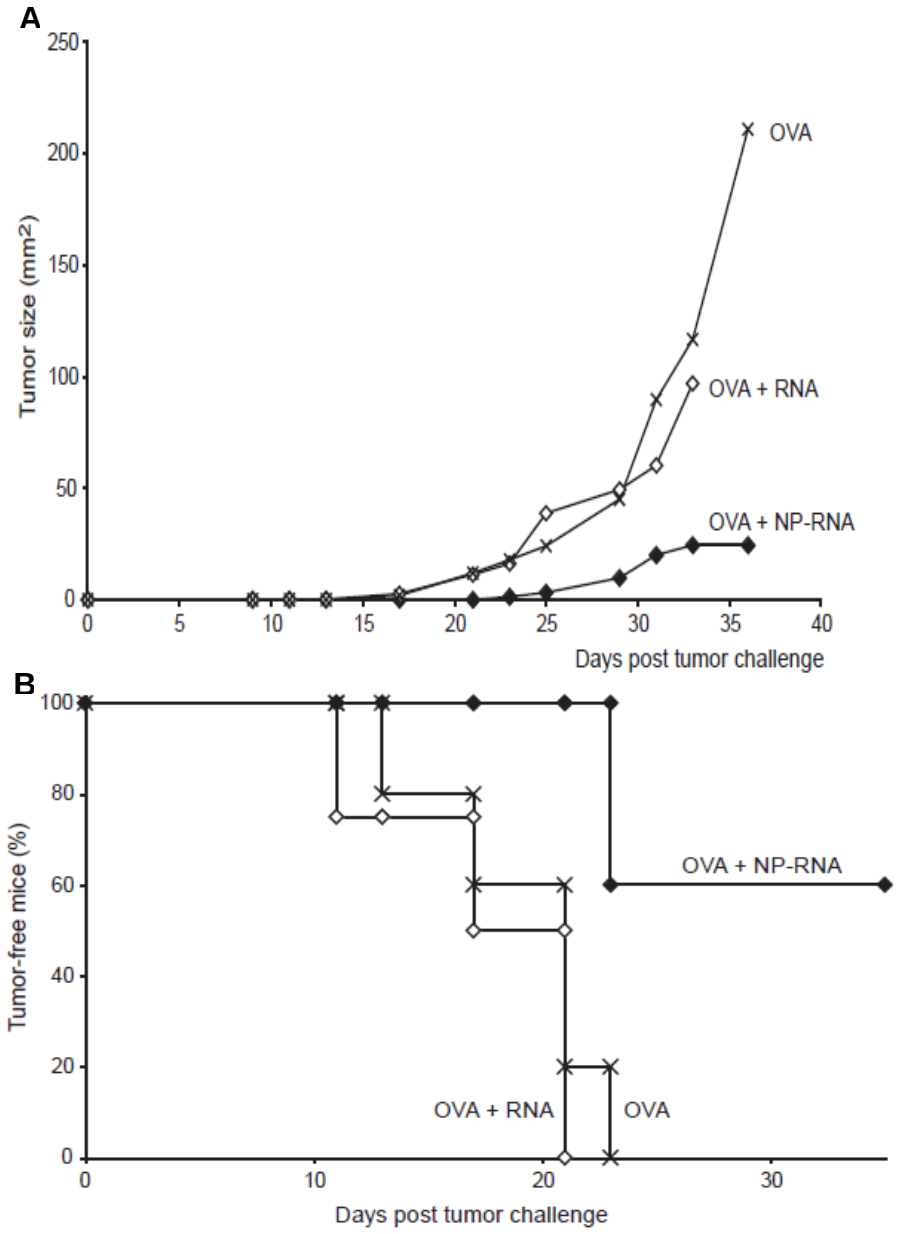

Fig. 4: Nanoparticle-bound RNA ODNs induce an antigen-specific antitumor immune response

Mice were immunized three times with OVA together wit hfree RNA ODNs or RNA ODNs bound to GNPs. One week after the last immunization, mice were injected with OVA-expressing B16 melanoma cells and tumor growth was monitored. Results are shown as (A) mean tumor sizes per group and as percental tumor-free mice (B). Immunization with OVA together with GNP-bound RNA ODNs significantly increased (the onset point of) tumor-free survival compared to OVA together with free RNA ODNs or OVA alone (P=0.004). Similar results were obtained in two independent experiments.

While all mice immunized with OVA or OVA plus free RNA ODNs developed a measurable tumor from day 11 onwards, only two of five mice immunized with OVA and GNP-bound RNA oligonucleotides developed a tumor and this treatment group showed an improved tumor-free survival ($P = 0.004$; Figure 4A and B). Thus, immunization with GNP-bound RNA ODNs induces a potent antitumoral response that protects from a subsequent tumor challenge.

Discussion

RNA oligonucleotides containing specific molecular patterns trigger immune activation though a broad range of mechanisms and can potentiate antigen-specific immune responses, block immunosuppressive mechanisms and inhibit tumor growth. Furthermore, RNA ODNs have emerged as a powerful tool to silence expression of specific genes, raising high expectations for the development of novel therapeutics (Castanotto and Rossi 2009). The combination of both gene-silencing and immunostimulation in one RNA molecule may further enhance the therapeutic potential of RNA ODNs (Poeck et al. 2008). A major issue for the application of RNA ODNs in the clinic is however the development of suitable drug delivery systems that are both safe and effective (Whitehead et al. 2009).

An efficient delivery system must protect RNA ODNs from degradation, facilitate uptake into target cells and deliver the RNA to the appropriate intracellular localization (Whitehead et al. 2009). Dendritic cells play a critical role in directing the immune response to RNA ODNs and therefore represent an important cellular target (Anz et al. 2010). We show here that gelatin nanoparticle-delivered RNA ODNs activate dendritic cells more efficiently than RNA delivered by frequently used transfection reagents such as lipid-based formulations or PEI. Indeed, GNPs greatly enhance uptake of immunostimulatory RNA ODNs into dendritic cells with over 80% of cells positive for fluorescently labeled RNA. This highly efficient uptake was not achieved by the other transfection reagents examined. We further show that complexes of gelatin nanoparticles and RNA ODNs are highly stable and that gelatin nanoparticles protect RNA from degradation by nucleases.

The mode of delivery of RNA ODNs plays an important role in the type of immune response induced and directs the subsequent cytokine response (Ablasser

et al. 2009). For optimal efficacy, targeting of the appropriate intracellular compartment is essential. GNP-delivered RNA accumulates in endosomal compartments where TLR7 is located (Diebold et al. 2004), whereas RNA ODNs delivered by lipofectamine or PEI are found diffusely in the cytosol. DOTAP, a lipid-based transfection reagent, also enhances delivery to the endosome (Yasuda et al. 2005). Indeed, it was previously shown that RNA ODNs delivered by DOTAP induce TLR7-dependent immune responses *in vitro* and *in vivo* (Bourquin et al. 2007). However, DOTAP is highly toxic and forms unstable complexes that preclude an application in a clinical setting (Bouxsein et al. 2007). Interestingly, it was observed that 5'-triphosphate RNA bound to GNPs activates dendritic cells independently of TLR7, suggesting stimulation of the cytosolic RIG-I receptor. Thus, this may open the door for further beneficial GNP applications as carrier systems as they may also deliver RNA ODNs to the cytosol in amounts sufficient for immune activation of RIG-I. Moreover, they might be suitable for other RNA carrying tasks they demonstrated their ability to protect RNA from degradation *in vivo* and *in vitro*.

Systemic administration of colloidal carriers often results in accumulation in the liver, kidneys and lungs (Whitehead et al. 2009). Importantly, it was shown here that antitumoral protection can be achieved by subcutaneous injection of nanoparticle-bound isRNA together with antigen, bypassing the need for systemic delivery. This proof of principle target was previously demonstrated oligonucleotides almost exclusively to the draining lymph nodes following subcutaneous injection, thus directing the oligonucleotides to the initiation site of the immune response (Bourquin et al. 2008). This enables the selective triggering of antigen-specific T and B cell responses without resulting in systemic immune activation.

In addition to their essential role for the *in vivo* delivery of nucleic acids, gelatin nanoparticles may have an adjuvant effect of their own. Indeed, particulate adjuvants such as alum, poly(lactide-co-glycolyde) (PLG) and polystyrene microparticles enhance TLR-induced secretion of proinflammatory cytokines by dendritic cells through stimulation of the NALP3 inflammasome receptor complex (Sharp et al. 2009; Eisenbarth et al. 2008). It is thus possible that GNPs may themselves activate the NALP3 inflammasome. The induced immune

response may synergize with TLR7 activation by RNA oligonucleotides and contribute to the adjuvanticity of gelatin nanoparticle-delivered RNA oligonucleotides.

In conclusion, it was shown that GNPs are an efficient delivery system for TLR7-activating RNA oligonucleotides both *in vitro* and *in vivo*.

Acknowledgements

This study was supported by grants from the German Research Foundation (DFG En 169/7-2 and Graduiertenkolleg 1202 to C.B. and S.E., the excellence cluster CIPSM 114 to S.E. and the SFB-TR 36 to S.E.), from LMUexcellent (research professorship to S.E.) from the Else-Kröner Fresenius Foundation and from BayImmuNet to C.B. and S.E. This work is part of the doctoral thesis of S.F and S.W. at the Ludwig Maximilian University Munich.

Outlook starting from the above study

However, the immunologic antitumoral effects in Figure 4A and B was not yet optimal taking the large difference between soluble RNA and GNP-bound RNA observed in Figures 1-3 into account. Therefore, optimization of the setup conditions is a matter of ongoing follow-up experiments. In addition, the effector/memory T cell responses induced by OVA alone or OVA on 9.2dr nanoparticles will be addressed. Finally, to achieve crucial importance to clinical utility by this isRNA immunologic antitumoral concept, current follow-up studies explore the possibility of a treatment of existing tumors instead of the so-far employed prophylactic strategy. Therefore, OVA-expressing Pac02 pancreatic tumor cells are used to establish an eligible murine model instead of B16 myeloma cells. Thereby, immune response can be built up within the established two-week-period of three-fold immunization while the individuals do not potentially die before that period due to a very aggressive tumor type (B16). In the future, loading of immunostimulatory ODNs together with antigen onto the same particles may further improve immunization outcome, as recent studies have shown that conjugation of TLR ligands and antigen result in superior activation of T cell responses. Thus, an all-in-one vaccine formulation in which GNP simultaneously deliver antigen and adjuvant may represent an advantageous delivery system.

3. *In vitro* effects of CpG oligodeoxynucleotides delivered by gelatin nanoparticles on canine peripheral blood mononuclear cells of atopic and healthy dogs

3.1 Introduction

Canine atopic dermatitis (AD) is very similar to the human equivalent and thus considered a relevant model for human atopic dermatitis (Marsella and Girolomoni 2009). It possesses characteristic clinical features and is associated in most but not all cases, with the formation immunoglobulin E (IgE) against environmental allergy (Olivry and Sousa 2001). The pathophysiology is due to an interplay of genetic, environmental and immunologic factors (DeBoer and Marsella 2001; Olivry et al. 2010; Schnabl et al. 2006). A defective epidermal barrier and cutaneous infections influence the course of the disease (DeBoer and Marsella 2001).

Allergen-specific immunotherapy is a recommended therapeutic option for canine AD and was reported to be effective in controlling clinical signs in approximately 60% of treated dogs (Olivry et al. 2010; Schnabl et al. 2006). In addition it is recommended to control infections if present and to restore skin barrier function. Glucocorticoids or calcineurin inhibitors may be needed in some patients, antihistamines and essential fatty acids may be beneficial in preventing recurrence of clinical signs and/or decreasing the dose of glucocorticoids needed. However, cases of refractory canine AD are an unfortunate fact in small animal practice. Thus, research on new immunomodulatory therapies and studies investigating the etiology and pathogenesis of this disease are obligatory.

Novel therapeutic strategies for AD include cytosine-phosphate-guanine (CpG) oligodeoxynucoleotides (ODN), signaling through an endosomal membrane based type of pattern recognition receptor (PRR) the Toll-Like Receptor 9 (TLR9) (Angel et al. 2008; Wernette et al. 2002). CpGs were shown to influence several signaling pathways in a variety of immune cells, leading to cytokine production (Lee et al. 2009; Zhao et al. 2010) in many mammalian species (Fig. 1) (Olivry et al. 2010).

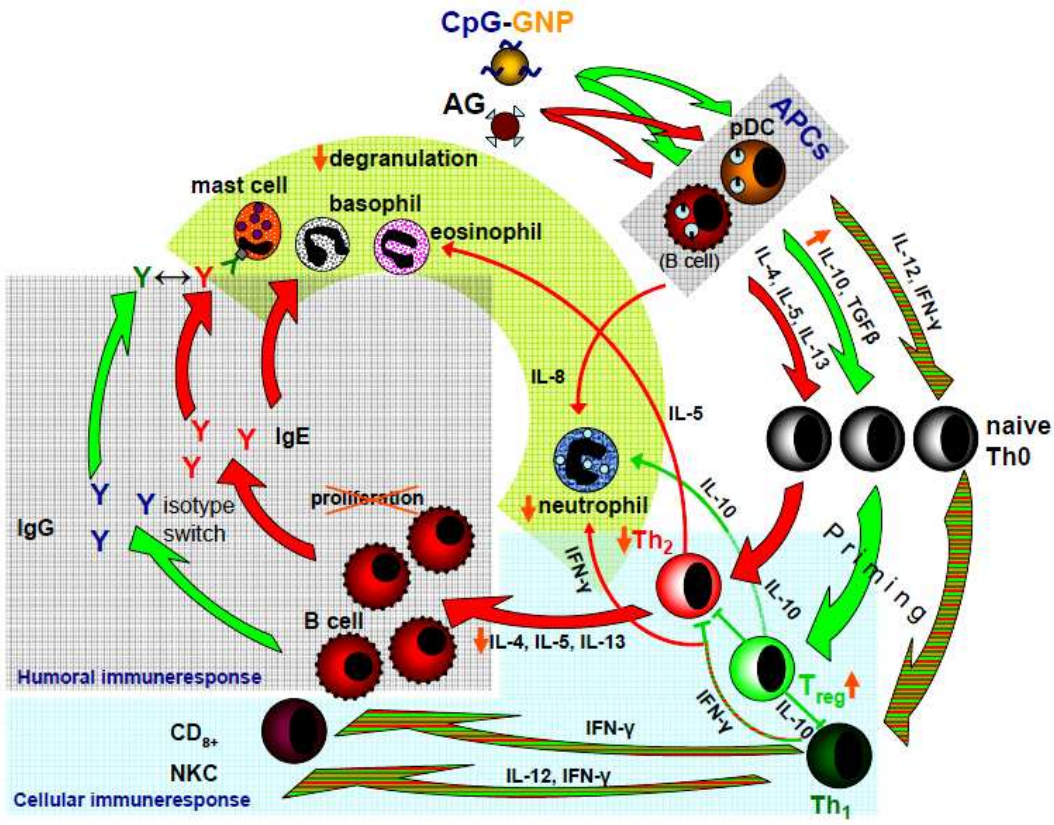

***Fig. 1**: CpG (class-A) GNPs directly stimulate pDCs which prime naive Th_0 cells to CD4+ CD25+ T reg cells and subsequently lead to increased IL-10 release while Th2 responses are reduced and IgE release is suppressed. Red arrows represent pro-allergic and green arrows regulatory pathways. Orange arrows indicate the anti-allergic interactions by CpG-GNPs.*

It appears that the specific purines and pyrimidines surrounding the CpG motif, the phosphothioated backbone, as well as the spacings between CpG motifs may influence both the level and the type of immune stimulation (Krieg et al. 1995; Mutwiri et al. 2003). CpG motifs improve the antigen presenting function of dendritic cells (DCs), monocytes and macrophages, induce the proliferation of B lymphocytes, stimulate the immunoprotective activity of NK cells, and recruit T cells to the site of ODN administration (Coester et al. 2006; Torchilin 2007; Zwiorek et al. 2008). Recent studies showed that the immune system responds to CpG motifs by inducing potent Th1-like immune responses which can be harnessed for immune therapy of cancer, allergy, infectious diseases (Krieg 2002), autoimmune diseases, and sterile inflammation (Kanzler et al. 2007). As explained in 1.1, CpGs are also promising adjuvant for vaccines (Angel et al. 2008; Bourquin et al. 2008). *In vitro* testing of CpG showed that CpG ODN are powerful stimulators for dog and cat immune cells (Wernette et al. 2002). In humans, TLR9

was identified in DCs, B cells and other cell types (House et al. 2009; Hashimoto et al. 2005). Canine TLR9 mRNA expression was identified in macrophages (House et al. 2009) and in PBMCs, lymph nodes, spleen and kidneys (Hashimoto et al. 2005). Adverse effects following CpG ODN treatment are possible. However, there is no evidence that modest doses of CpG ODN are directly toxic or cause autoimmune disease in healthy animals (Zwiorek et al. 2004).

Colloidal particulate delivery systems fall within the same size range as microbes and thus are preferentially phagocytosed by DCs and are considered advantageous for subunit vaccines based on proteins, peptides and DNA (Hornung et al. 2002; Keppel et al. 2008). It was previously shown that gelatin nanoparticles (GNPs) are effectively taken up by TLR9 possessing cells (Coester et al. 2006). The GNP carrier system for ODNs in this study prevents enzymatic degradation, transports CpG to the desired site of action, and is biodegradable and biocompatible (Torchilin 2007). The combination of reduced dosing and more specific carrier-induced targeting contributes to one of the major goals attributed to nanocarriers - less side effects (Zwiorek et al. 2008). Recent studies revealed that GNPs were superior to other established carriers such as DOTAP, PEI or lipofectamine in targeting the intracellular compartment endosome in DCs, where the target receptor TLR9 of CpG ODN is located (Bourquin et al. 2010, in revision).

Our study aims were to demonstrate cellular uptake of CpG-GNP by canine PBMCs and to evaluate its direct influence on cytokine production by PBMCs of atopic and healthy dogs. Indirect influence of CpG and CpG-GNP on PBMCs thru stimulated macrophages was also investigated.

3.2 Materials and methods

This study was conducted at the Department of Veterinary Medicine, Small Animal Clinic, LMU Munich. All experiments were jointly performed by veterinarian Dr. A Rostaher and the author.

3.2.1 Animals

Dogs suffering from AD (n=8) and concurrent hypersensitivity to house dust mites on intradermal testing or serum testing for allergen-specific IgE were included. Control samples were taken from healthy control dogs (n=8) without history or

evidence of cutaneous or systemic illness. All dogs of both groups did not receive any form of immunosuppressive agents for at least 6 weeks prior to blood collection.

3.2.2 **CpG sequence**

ODNs with the sequence GGTGCATCGATGCAGGGGGG (Kurata et al. 2004) were employed with a full phosphotioate backbone (Biomers GmbH, Ulm, Germany). For demonstration of intracellular localization by confocal laser scanning microscopy (CLSM), a batch of CpGs was labeled with fluorescent dye Atto 540 (Biomers GmbH, Ulm, Germany).

3.2.3 **Preparation of GNPs**

The unloaded GNPs were prepared by a two-step desolvation method (Coester et al. 2000) as previously described in chapter II, 1.2.1. Fluorescence labeling comprised the covalent attachment of Alexa 633 dye (Invitrogen, Carlsbad, USA). Cationization was carried out as established earlier (Zwiorek et al. 2004). All involved chemicals were obtained from Sigma-Aldrich (Taufkirchen, Germany). GNP concentration was determined gravimetrically by a microbalance (Mettler Toledo UMX2, Greifensee, Switzerland). Intensity weighted particle sizes were obtained by dynamic light scattering (positron correlation spectroscopy, PCS) using a Zetasizer ZS Nano (Malvern Instruments, Worcestershire, England). To exclude the viscosity impact on PCS particle size results, the viscosity of particle samples was determined with an Anton Paar automated microviscosimeter (Anton Paar, Graz, Austria). For Zeta potential measurement before and after loading, GNP stock dispersions were diluted in 10 mM NaCl at a 1:10 ratio (V/V) and measured in folded capillary cells (Malvern Instruments, Worcestershire, England).

3.2.4 **ODN loading of cationized GNP**

Five mg of aseptically prepared nanoparticles were incubated with 250 µg of ODN in a total volume of 3339 µl filled up by PBS of pH 7.4 (5% w/w) for 2 h at 22°C and under gentle shaking using a Thermomixer™ (Eppendorf, Hamburg, Germany) device. As quality control, loading efficiency was analyzed photometrically at 260

nm (UV1, Thermo Fisher Scientific Inc., Waltham, USA) in the samples' supernatant after centrifugation and accepted, if loading was at least 97% (w/w).

3.2.5 **Blood sampling and PBMC isolation**

20 ml of blood were collected from the jugular vein using EDTA containing tubes on day 0 and day 10. Canine PBMCs were isolated by density gradient centrifugation of peripheral blood according to the Ficoll-Hapaque method as previously reported (Stehle M. 2008). Briefly, 15 ml centrifugation tubes were filled with 7 ml Ficoll® separation solution (Biochrom, Berlin, Germany) featuring a density of 1.077 g/ml and covered with 7 ml blood previously diluted 1:1 with phosphate buffered saline (PBS). After centrifugation without brake (40 min, 1200 g, room temperature), the concentrated PBMCs located at the white interface between plasma and separation solution were removed by pipetting. The cells were washed and re-suspended thereafter in 10 ml RPMI-1640 cell culture medium (Biochrom, Berlin, Germany) completed with 10 % bovine calf serum (Biochrom, Berlin, Germany) and 1 % penicillin-streptomycin (Biochrom, Berlin, Germany). PBMC viability and number were determined by trypan blue staining (Biochrom, Berlin, Germany) and by cell counting in a Neubauer chamber. In all experiments, 98% to 100% of cells were viable. The isolated cells were stored at 4°C and used within 1 hour.

3.2.6 **Monitoring CpG-GNP uptake by cultured PBMCs of healthy dogs**

2.5 x 10^5 PBMCs were transferred into µ-slide 8 well ibiTreat microscopy chamber slides (Ibidi, Integrated BioDiagnostics, Martinsried, Germany), covered with 300 µl composite medium and cultured for 10 days. The cell culture medium was changed every 2-3 days. Ten days old PBMCs were incubated with fluorescence labeled CpG-GNP for 2 h. The supernatant was carefully removed and the cells washed using 300 µl PBS. Thereafter, the PMBC membranes were labeled with 100 µL Concanavalin A / Alexa 488 (Invitrogen, Carlsbad, USA) solution for 1 min and washed three times with PBS. PBMC nuclei were stained with 50 µl Hoechst 33342® dye (Invitrogen, Carlsbad, USA) for 5 min. After the final washing step, cells were fixed with 4% paraformaldehyde (Roth, Karlsruhe, Germany). As reported earlier (Coester et al. 2000), chamber slides were finally

prepared with a cover medium consisting of 10% Mowiol 488 and 2.5% diazabicyclooctan (DABCO) (Sigma, Taufkirchen, Germany), and visualized employing a Zeiss 510 LSM NLO confocal laser scanning microscope (CLSM,Carl Zeiss Microscope Systems, Jena, Germany).

3.2.7 **PBMC cultivation and immunostimulation**

2 x 10^6 PBMCs were cultured in 24-well flat bottom Nunc® plates (Thermo Fischer Scientific, Wiesbaden, Germany) in a total volume of 1 ml of standard cell culture medium for 10 days at 5% CO_2 and 37°C, which was exchanged every 2-3 days. During cultivation, adherent cells acquired a macrophage-like phenotype.

1.5 µg of the positive control Concanavalin A (Con A, Biochrom, Berlin, Germany), 75 µg CpG and 1500 µg of CpG-GNP containing 75 µg CpG were added to the wells containing cultured PBMCs and incubated for 2 h, respectively (Fig. 2).

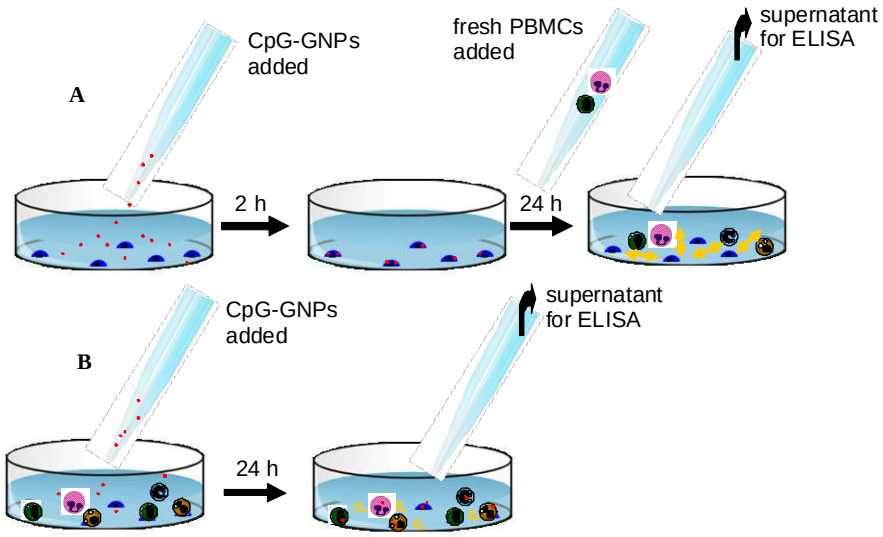

Fig. 2: *Scheme of incubation setup: Either cultured canine PBMCs get incubated for 2 h by CpG-GNPs with subsequent fresh PBMC addition and supernatant evaluation after 24 h stimulation or direct stimulation of fresh canine PBMCs by CpG-GNPs for 24 h.*

Un-stimulated cells in cell culture medium only and cells incubated with GNPs alone served as negative controls. The supernatant was removed and the cells were washed twice. To prove an indirect effect of CpG and CpG-GNP on PBMCs through stimulated macrophages, 2 x 10^6 PBMCs from the same dogs were added

to the wells containing macrophages and incubated for 24 h at 5% CO_2 and 37ºC (Fig. 2). The direct effects of CpG and CpG-GNP on PBMCs were explored by stimulating 2 x 10^6 PBMCs from the same dogs without presence of cultivated cells. The culture supernatants were collected after 24 h incubation (Fig. 2) and then stored at -80ºC until use.

3.2.8 **Quantification of cytokines**

Cell culture supernatant concentrations of interferon gamma (IFN-γ), interleukin (IL)-4, IL-6 and IL-10 were measured by Canine Cytokine Milliplex (C CYTO 90K-04, Millipore, Billerica, USA) according to manufacturer instructions. The cytokines were quantified by a Bio-Plex 200 reader (Bio-Rad, Hercules, USA) equipped with the Luminex® xMAPTM technology detection system. Result calculation was performed with the Bio-Plex Manager Software The used MILLIPLEX ® Map is based on Luminex® xMAP technology which is characterized by the feasibility to measure the four selected analytes in one sample well at a time. In brief, 5.6 µm microspheres internally color-coded with two fluorescent dyes are used to create a set of 100 distinctly colored beads by a specific concentration relation of the two dyes in each bead. Every single bead is coated with a capture antibody specific for an analyte. Here, anti-IFN-γ capture antibody is located in the 07 bead region, IL-4 in the 41, IL-6 in the 47 and IL-10 66 bead region (Fig. 3). The bioassay steps to capture and detect the cytokines of interest take place on the bead surface instead of the plate surface or well bottom as it is with common ELISAs. The capture antibodies are bound covalently by amid-bonds to the microsphere surface.

If these coated beads encounter their specific analyte in the reaction mixture, binding occurs which is followed by the introduction of the biotinylated detection antibody and the incubation with the reporter molecule Strepavidin-PE conjugate (Fig. 4). After completion of the bead surface reactions quantification analysis can be performed.

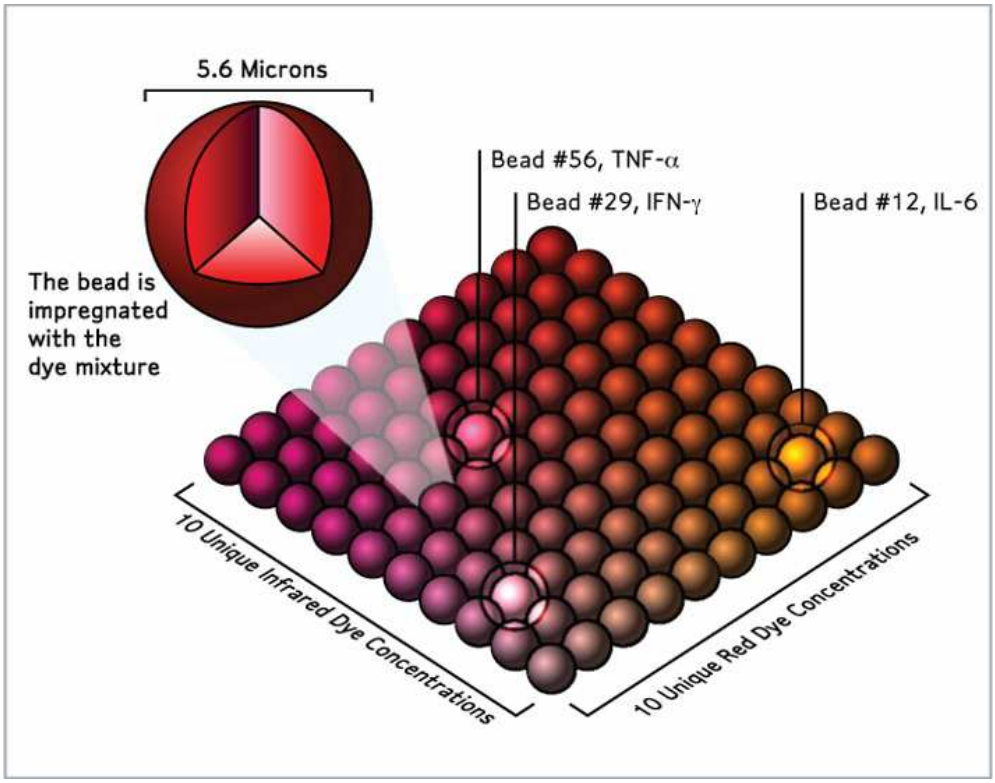

Fig. 3: *Milliplex ® microspheres: 100 separately addressable microsphere sets. So theoretically 100 different sets are obtainable, each representing a single well of a plate (www.millipore.com).*

Next, the samples are taken up by the Luminex® detection system as a particulate suspension and lined up in single before passing through the detection chamber. In there, two lasers are applied to identify the bead and there fore the analyte on the one hand, and the PE label of the conjugate to quantify the relevant cytokine on the other hand: The red laser to excite the internal microsphere dyes and the green laser to excite the report dye associated to the cytokine conjugate. (Fig. 4)

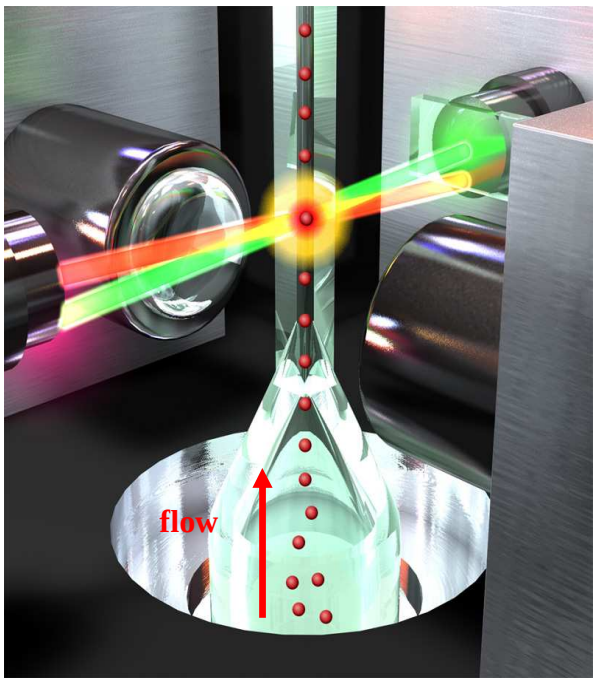

Fig.4: *Dual laser detection to classify and quantify cytokines in FACS-like analysis chamber (www.millipore.com).*

Each individual signal is finally processed to a quantitative bioassay result giving the concentration of each cytokine in the original solution. The four detection antibody conjugated beads can be added to each single sample to obtain four results from each sample.

3.2.9 Statistical Analysis

An analysis of variance with a Tukey post test (or with non-parametric data a Kruskal Wallis test with Dunn post test) was used to compare the cytokine production in the various groups. The level of significance was set to $p<0.05$.

3.3 Results

3.3.1 Formulation quality control

GNPs featured a hydrodynamic diameter of 247 nm (S.D. ±1.13 nm) before and 243.1 nm (S.D. ±2.51 nm) after loading. The zeta potential measured in 10 mM NaCl remained constant at +18.0 mV and at a conductivity of 1.18 mS/cm. CpG surface loading remained at 98% (m/m) or higher 2 h post complexation (II, 2.1).

3.3.2 CpG-GNP uptake by cultured PBMCs of healthy dogs

Fluorescent labeled plain GNPs were taken up by cultured PBMCs and accumulated in distinct intracellular regions. In a next step, CLSM confirmed cellular uptake of the CpG loaded GNP formulations in cultured PBMCs (Fig. 5). The fluorescent labeled CPG-GNPs appear as yellow spots within the cells but outside the nucleus stained blue.

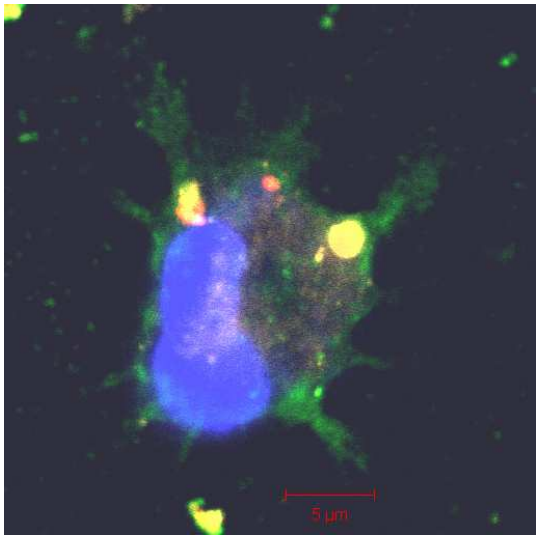

Fig. 5: *Exemplary CLSM picture illustrating cellular uptake of CpG-GNPs (yellow, Alexa 594 staining) by cultured PBMCs (nucleus blue, Hoechst 33342 staining and cell membrane green, Concanavalin A / Alexa 488 staining) after 120 min of incubation.*

3.3.3 Cytokine quantification

There was no significant increase triggered by any formulation in IL-4 concentration in any group (Fig. 6a and 6b). While supernatants of untreated macrophages of atopic and non-atopic dogs featured 137 pg/ml and 171 pg/ml and those of untreated fresh PBMCs of atopic and non-atopic dogs 182 pg/ml and 194 pg/ml, respectively, IL-4 concentrations of all other treated groups lay below. IL-6 concentration was below the detection threshold in all groups and consequently could not be evaluated.

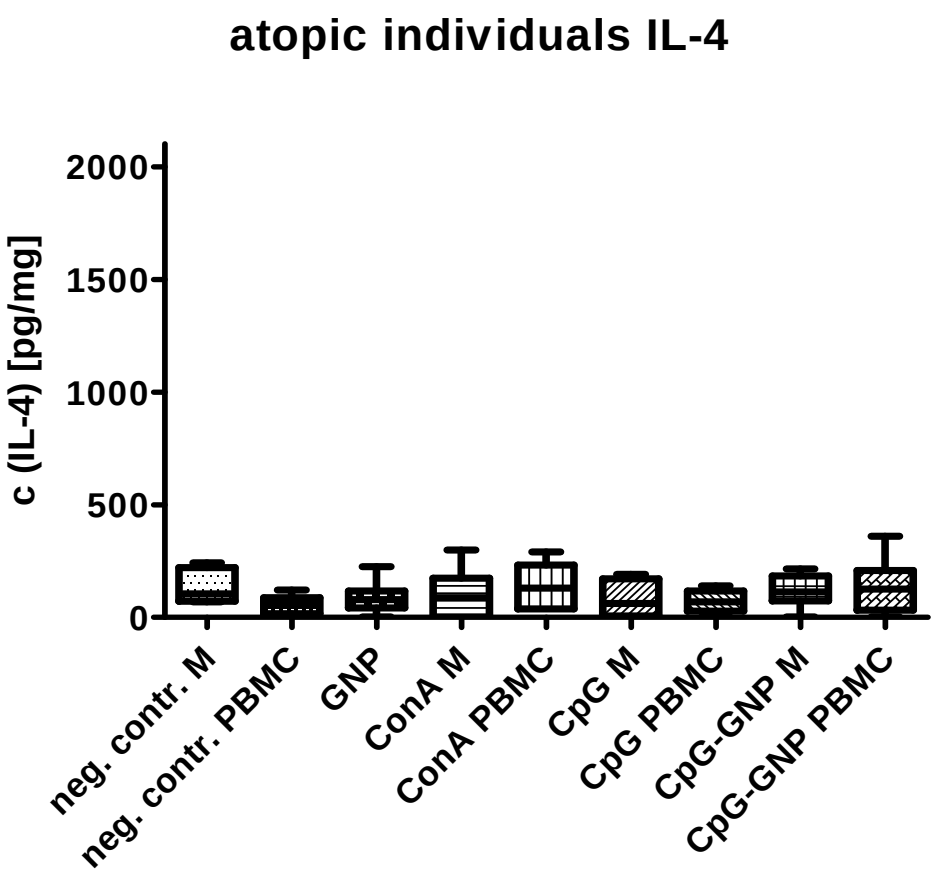

Fig. 6a: *IL-4 release of fresh PBMCs (PBMC) and 10-day cultured macrophages (M) of atopic individuals upon stimulation by GNPs alone, Concanavalin A (ConA) as a positive control, CpG alone or CpG loaded GNPs (CpG-GNP) or without stimulation (neg. contr.) (n=8, ±S.D.).*

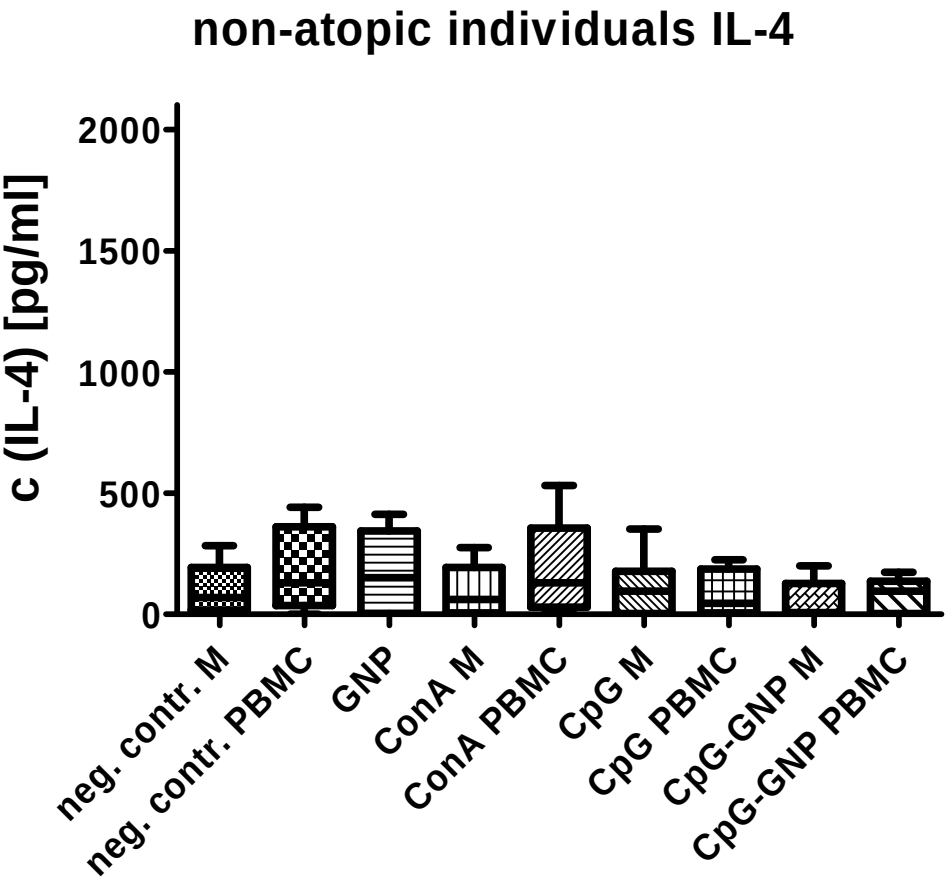

Fig. 6b: *IL-4 release of fresh PBMCs (PBMC) and 10-day cultured macrophages (M) of* ***non-atopic*** *individuals upon stimulation by GNPs alone, Concanavalin A (ConA) as a positive control, CpG alone or CpG loaded GNPs (CpG-GNP) or without stimulation (neg. contr.). The y-axis scale was chosen for better comparison to expression of other cytokines (n=8, ± S.D.).*

In contrast, direct CpG-GNP stimulation of PBMCs in atopic and healthy individuals resulted in significantly higher concentrations of IL-10 compared both to negative control and to CpG alone. In addition, Con A significantly increased IL-10 in comparison to the negative control and to CpG alone, but not compared to CpG-GNPs (Fig. 7a).

For healthy dogs, IL-10 release upon Con A stimulation did not differ significantly from CpG alone (Fig. 7b), the latter did not significantly differ from the negative control. However, indirect stimulation of PBMCs through macrophages did not exhibit any IL-10 increased release upon any stimulus compared to negative control both in atopic and healthy dogs.

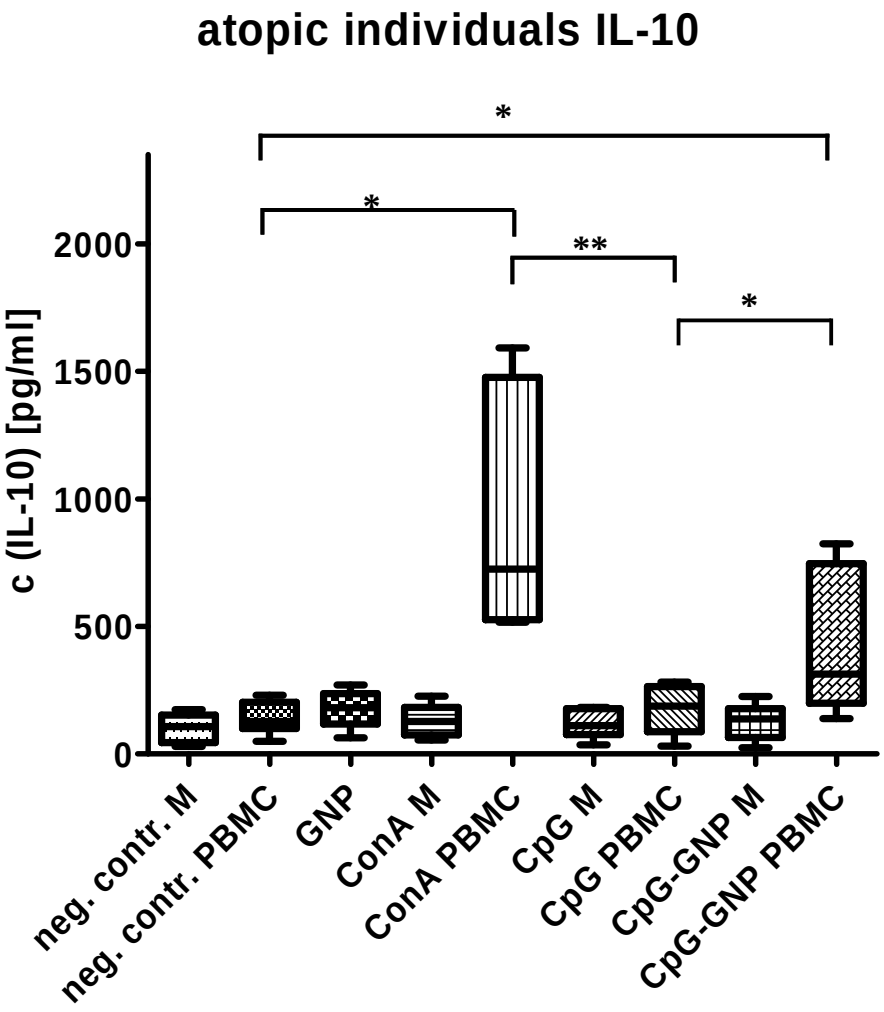

Fig. 7a: *IL-10 release of fresh PBMCs (PBMC) and 10-day cultured macrophages (M) of atopic individuals upon stimulation by GNPs alone, Concanavalin a (ConA) as a positive control, CpG alone or CpG loaded GNPs (CpG-GNP) or without stimulation (neg. contr.). Relevant interrelations' levels of significance are indicated by * for $p < 0.05$ and ** for $p < 0.01$ ($n=8$, ± S.D.).*

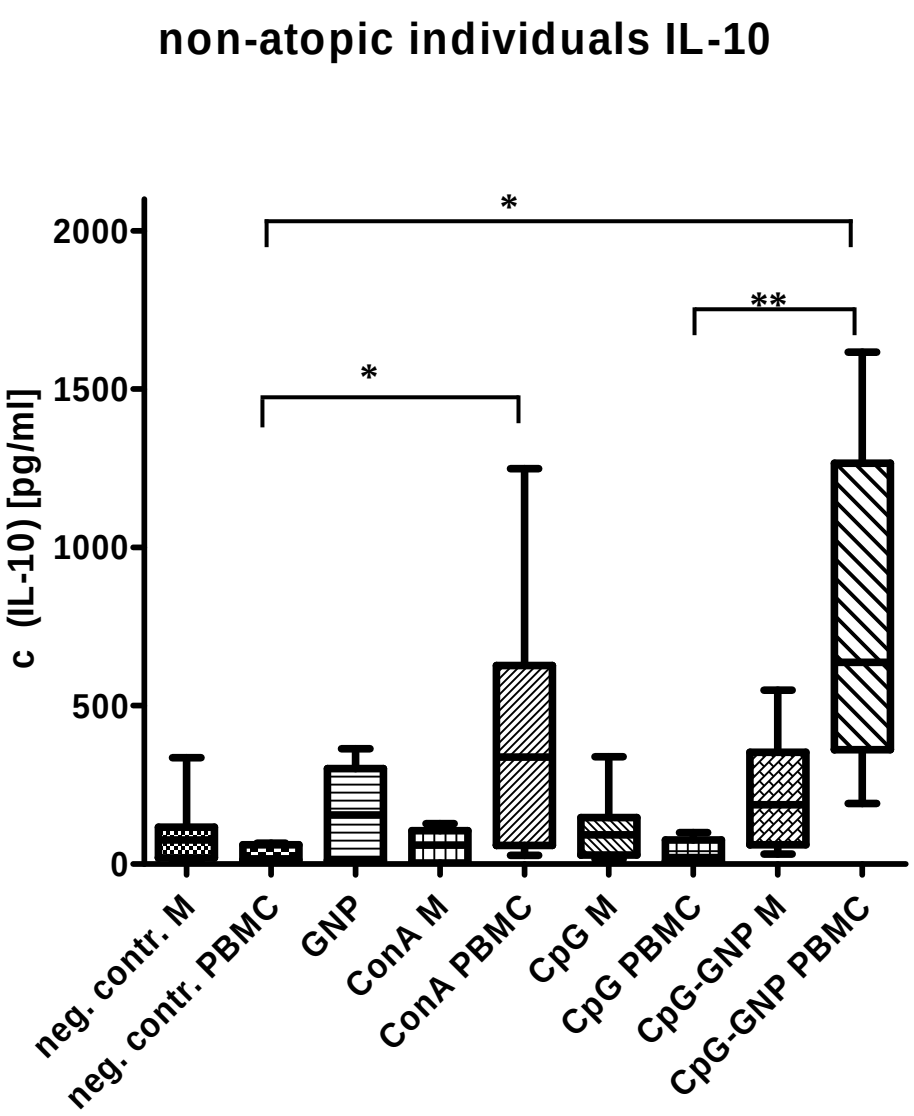

Fig. 7b: *IL-10 release of fresh PBMCs (PBMC) and 10-day cultured macrophages (M) of non-atopic individuals upon stimulation by GNPs alone, Concanavalin a (ConA) as a positive control, CpG alone or CpG loaded GNPs (CpG-GNP) or without stimulation (neg. contr.). Relevant interrelations' levels of significance are indicated by * for p< 0.05 and ** for p< 0.01 (n=8, ±S.D.).*

IFN-γ was released by macrophages (198 pg/ml) and fresh PBMCs (237 pg/ml) in atopic and non-atopic dogs only upon Con A stimulation and not after incubation with CpG or CpG-GNPs (Fig. 7). Standard deviations of mean were observed as very high. Thus, no levels of significance could be obtained.

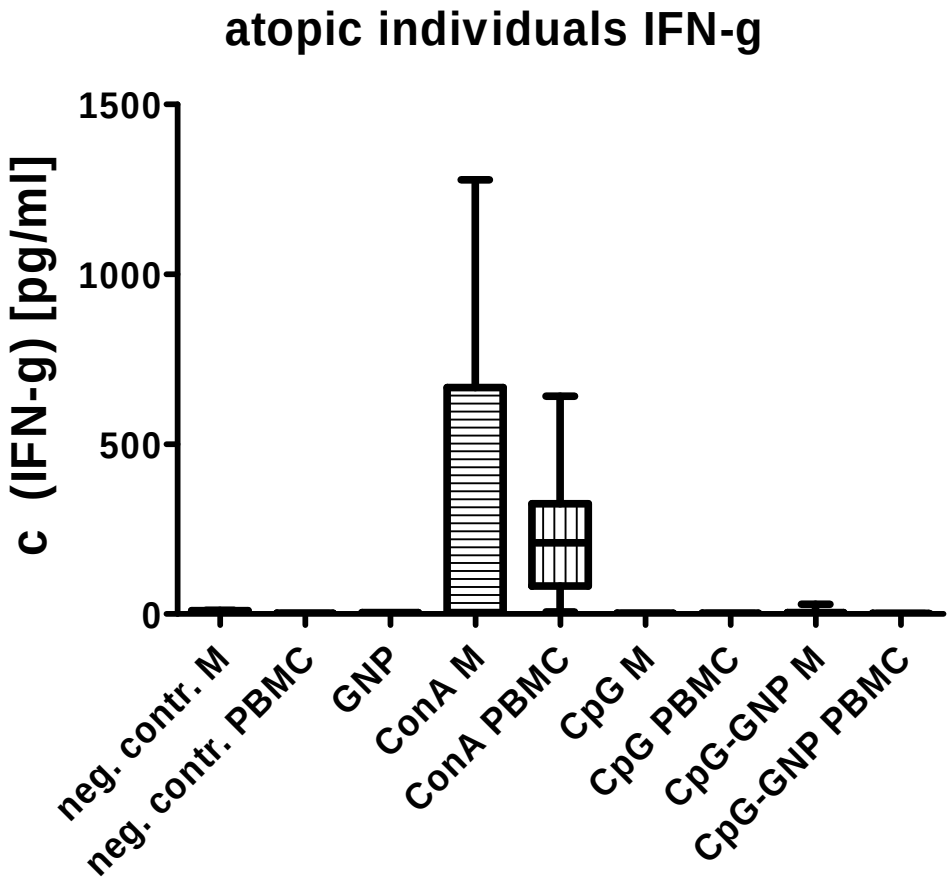

Fig. 8a: *IFN-gamma release of fresh PBMCs (PBMC) and 10-day cultured macrophages (M) of atopic individuals upon stimulation by GNPs alone, Concanavalin a (ConA) as a positive control, CpG alone or CpG loaded GNPs (CpG-GNP) or without stimulation (neg. contr.) (n=8, ± S.D.).*

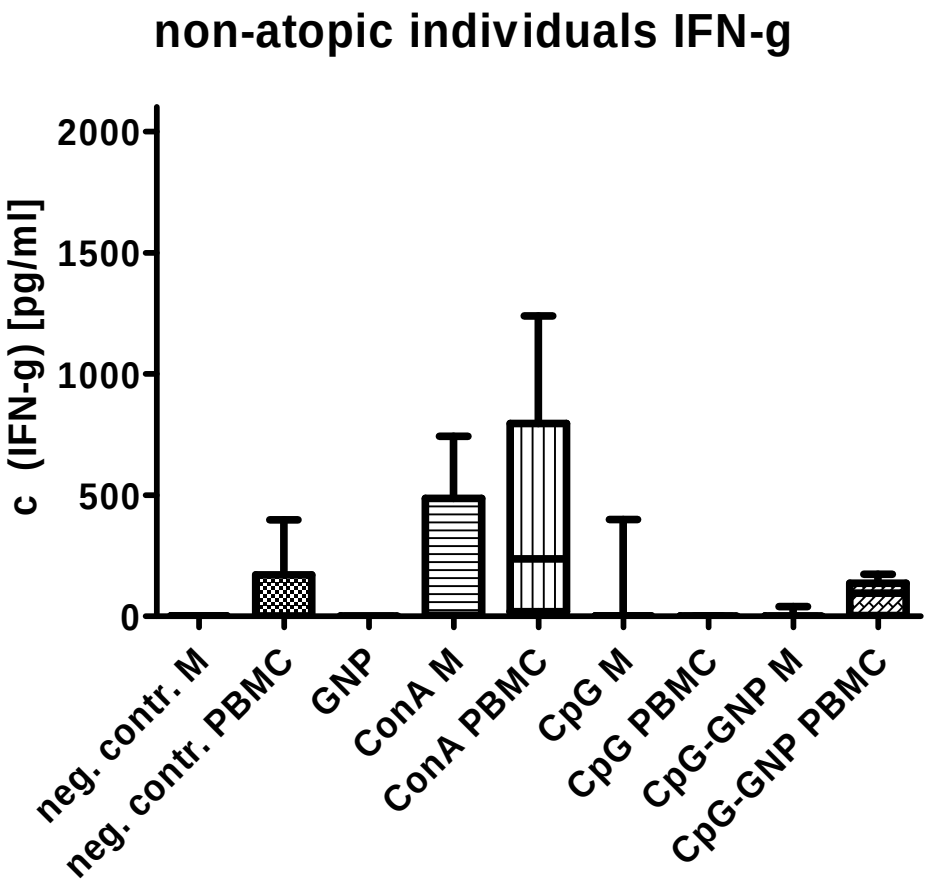

Fig. 8b: *IFN-gamma release of fresh PBMCs (PBMC) and 10-day cultured macrophages (M) of non-atopic individuals upon stimulation by GNPs alone, Concanavalin a (ConA) as a positive control, CpG alone or CpG loaded GNPs (CpG-GNP) or without stimulation (neg. contr.) (n=8, ± S.D.).*

3.4 Discussion

In this study, CLSM demonstrated successful uptake of stable CpG-GNPs by canine cultured PBMCs within 2 h. In addition, direct stimulation of PMBCs with CpG-GNP resulted in a significant increase of IL-10 production.

It was previously shown in proliferation assays, that CpGs alone are taken up by canine immune cells (Wernette et al. 2002). In this study, CpG uptake was visualized directly by ultrastructural analysis for the first time to the authors' knowledge. This demonstrated uptake is a precondition for CpG and/or CpG-GNP related immunologic effects. *In vitro* immunologic effects of CpG-GNP or CpG alone were compared to controls. The bead-based flow cytometric method used in this study facilitates simultaneous quantification of different cytokines within one sample (Lee et al. 2009; Zhao et al. 2010).

There was no significant increase in any of the analyzed cytokine concentrations

after stimulations with CpG-GNP or CpG alone in canine macrophages. This can be explained by the fact that TLR9 is not the primary PRRs pathway in canine macrophages, as was previously shown (House et al. 2009). The production of cytokines is controlled by RNA and proteolytic processing (Abbas AK et al. 2010). Therefore, degradation of pre-existing cytokines in the 24 h incubation time is possible but rather unlikely as cytokine production was shown in PBMCs subjected to the same incubation conditions. The stimulation time may have been too short. However, based on the demonstrated uptake of CpG and CpG-GNP after 2 h, this time period should be sufficient for macrophage stimulation. It is unlikely that a low viability of cells in the macrophage cultures was responsible, as in the atopic group there was a high production of Th1 cytokine IFN-γ after stimulation with Con A. Therefore, the present observation is in accordance with the previous finding that macrophages require other partner cells for effective response to the CpG challenge such as pDCs contained in the fresh PBMCs preparation (Hornung et al. 2002).

A shift towards a Th1 and T regulatory immune response during allergen specific immunotherapy (Keppel et al. 2008; Shida et al. 2004) for treatment of canine AD was shown *in vivo* and *in vitro*. The same was found for CpG employment in cats (Reinero et al. 2008) and CpG-allergen conjugates in humans (Simons et al. 2004). Clinical efficacy of CpG-allergen conjugates (Creticos et al. 2006) and CpG-virus-like-particle formulations administered together with allergens were demonstrated in humans (Senti et al. 2009).

No *in vitro* production of IL-4 was observed in the atopic or healthy group. This is in concordance with previous studies. The first *in vivo* study in canine atopic patients using liposome-plasmid DNA complexes showed a significant decrease in serum IL-4 and pruritus scores (Olivry et al. 2010). Although IL-4 is a key mediator in pathogenesis of AD it cannot always be detected in atopic individuals (Kim et al. 2003). IL-4 was also not detectable in a study evaluating rush immunotherapy with CPG in a colony of asthmatic cats, consistent with the present results (Reinero et al. 2008).

The most essential finding was a significant increase in IL-10 in atopic and healthy dogs after direct PBMC stimulation with CpG-GNP compared to CpG alone and negative control. These differences in IL-10 production suggest that GNPs can enhance the immunomodulatory effects of CpG and provide

preliminary evidence for the use of GNP formulated CpG in dogs. The source of IL-10 could be B cells, dendritic cells and/or CD4+CD25+ T_{reg} cells (Krieg 2006). Kurata et al (Kurata et al. 2004) used the same ODN sequence which was employed here. However, in this study a fully phosphorothioated backbone was used which probably enhanced the CpG action on B cells in this study and which consecutively produced more IL-10 (Krieg et al. 1995). This backbone modification was also selected to achieve an increased resistance to endonucleases, longer half-life and thus greater immunomodulatory effect. Moreover, the higher charging of this modification might have let to repulsion effects and consequently to a lower tendencies of self-association. Instead, these CpG strands were more easily fixed to the GNP surface and thus the immunomodulative impact might have been enhanced. Interestingly, elevated IL-10 mRNA transcription after *in vitro* stimulation of canine PBMCs with ODN rich in CpG34 and elevated IL-10 protein levels after stimulation with synthetic agonists of TLR935 were reported earlier. In contrast, the *in vivo* use of CpG in adjuvant rush immunotherapy in experimental feline allergic asthma did not reveal any changes in IL-10 in bronchoalveolar fluid (Reinero et al. 2008).

IL-6 release by any cellular setup was not detected in this study. This finding is concordance with a study evaluating synthetic agonists of TLR9 where only a mild increase in IL-6 was detected (Im Hof et al. 2008). This is of particular importance as IL-6 was shown previously to have a suppressive effect on Treg cells (Pasare and Medzhitov 2003). Due to the fact that Treg cells are the primary mediators of peripheral tolerance playing a pivotal role in modulating chronic inflammatory diseases (Vignali et al. 2008), a downregulation by released IL-6 would have been detrimental to the desired development of immunotolerance in the treatment of dogs with AD.

IFN-γ, the Th1 signature cytokine, was not detected after stimulation with CpG in contrast to the findings of Kurata et al (Kurata et al. 2004) and others (Krieg 2002). This needs to be elucidated in further studies, but could be due to inhibition of IFN-γ production by high IL-10 concentrations. IL-10 reduces proliferation of DCs, blocks IL-12 secretion and thus suppresses IFN-γ indirectly (Pasare and Medzhitov 2003; Im Hof et al. 2008).

In summary, the concurrent use of CpG with a GNP carrier increased IL-10

production by PBMCs in both, atopic and healthy dogs. Macrophages seemed not to be the primary CpG canine cell target. Clinical studies in humans suggest that allergens in combination with CpGs are an efficacious and safe treatment option for asthma and allergic disease. Such studies in canine patients with AD are currently in preparation as this treatment may result in higher clinical efficacy and possibly less adverse effects.

4. Nucleic acid-based immunotherapy against hypersensitivity – preformulation studies for an inhalative CpG-GNP formulation for RAO therapy in horses

4.1 Recent developments in nanoparticle administration by inhalation

Pulmonary delivery as a non-invasive route of drug administration still constitutes a vivid research field in the treatment and diagnosis of respiratory and non-respiratory diseases (Smola *et al.* 2008). Within, nanoparticulate delivery is a clear but dynamic quota offering an advantageous perspective e.g. for a lung application of GNPs in future immunotherapeutic settings.

GNPs have demonstrated their feasibility as a carrier in several settings to include mediating antitumoral immunotherapy by adjuvant CpG deoxyoligonucleotides (Bourquin *et al.* 2008). By addressing toll-like 9 receptors (TLR9) on plasmoidal dendritic cells, T effector cells are subsequently activated by interleukins (IL) such as IL-12 to overcome agony and CD8 T cells engage in the desired cytotoxic action. However, besides immune activation, a reduction of immune response in events of hypersensitivity can be generated via TLR9 agonists as well (Jurk and Vollmer 2007; Krieg 2006). Equally, a promising field is the treatment of hypersensitivity such as allergies and asthma. Recurrent airway obstruction (RAO), also referred to as chronic obstructive bronchitis (COB), is a common equine incident which is to date not yet completely curable (Horohov *et al.* 2005; (Kunzle et al. 2007). Therefore, an administration of GNP formulated CpG to the lung seems to be a valuable direct delivery attempt without painful parenteral injection. In order to conduct related *in vivo* studies, the impact on GNP integrity must be evaluated for appropriate aerosol-forming devices. They should provide adequate droplet sizes with embodied GNPs for successful lung deposition, preferably ranging from 1 – 5 µm known as the fine particle fraction (FPF) (Ghazanfari et al. 2007).

The lower airways with respiratory brochioles and alveolar sacs (WEIBEL and GOMEZ 1962) offer a large surface area for drug interaction. Most common are local therapeutic strategies involving steroids or bronchodilators in the treatment of COB, asthma or cystic fibrosis as well as antimicrobial agents against infectious diseases such as tuberculosis (Purewal 1998; Rytting et al. 2008).

Direct targeting of the area of therapeutic interest enables a reduction in administered drug amount compared to e.g. oral or i.v. route (Vaughn et al. 2006) leading to reduced side effects (Keller 1999). Systemic delivery is facilitated by the alveolar sacs morphology including an extraordinary thin epithelial barrier of 0.1-1 µm, high blood flow, low enzymatic activity and finally the avoidance of the first past effect (Butz et al. 2002; Rytting et al. 2008). However, despite intense research, which concentrated mostly on the applications of antibiotics and insulin, systemic access via the inhalative route has suffered a major drawback since the withdrawal of inhalative insulin Exhubera® in late 2007.

The abolishment of ozone depleting chlorofluorocarbons (CFC) following the Montreal protocol led both to its replacement by hydrofluoroalkanes (HFA) in pressurized metered dose inhalers (pMDI) and to an increased use of non-pressurized systems (Kawashima et al. 1999). Pressurized pMDIs were among the earliest and are still among the most established systems in use for the delivery of dissolved or suspended active ingredients to the respiratory tract (Brown and George 1997). They were successfully employed in the aerosolization of protein formulations such as insulin-containing nanoparticles or emulsions (Butz et al. 2002; Nyambura et al. 2009; Butz et al. 2002; Nyambura et al. 2009). Non-pressurized systems comprise dry powder inhalers (DPIs), pneumatic jet inhalers, ultrasound nebulizers and most recently vibrating mesh (VM) devices (Waldrep and Dhand 2008). DPIs were meanwhile widely employed for standard asthma medication but were also used to deliver complex formulations such as dry powder microparticle-bound nanoparticles. Examples were polyacrylate NP-bound Salbutamol sulfate (Hadinoto et al. 2007) and Chitosan-NP-bound Insulin (Grenha et al. 2005). However, pure nanoparticle formulations cannot be delivered in that manner due to too small particle size (< 1µm) and thus missing lung deposition and consequently exhalation of the formulation (Sung et al. 2007). Therefore, excipients like micronized lactose were identified as beneficial (Finlay et al. 20050127) and e.g. GNP aerosols were successfully formulated as DPI after spray drying loaded with a placebo drug (Sham et al. 2004).

Pneumatic jet nebulizers were available since the 1950ies and possess the ability to nebulize preparations of high viscosity such as suspensions. Negative attributes were their limited portability, high residual dead volumes making dosage of drugs featuring critical therapeutic ranges difficult. Moreover, high shear forces

represented another problematic factor impacting the drug formulation during the application process (Waldrep and Dhand 2008; Ghazanfari *et al.* 2007). Still, Insulin solid lipid nanoparticles were delivered to the lung by this means and resulted in prolonged plasma glucose and insulin profiles (Liu et al. 2008). The newer type of ultrasound nebulizers suffered from heat generation during the nebulization process which negatively affected sensitive materials such as protein and nucleic acids while suspensions cannot be processed due to their viscosity (Lentz et al. 2006; Ghazanfari et al. 2007). Hence, ultrasonic nebulizers could not be successfully introduced for nanoparticulate or liposomal applications (Elhissi and Taylor 2005). For instance, Dailey et al. received sufficient mass median aerodynamic diameters (MMAD) by ultrasonic nebulization but reported inconsistent output and increased particle aggregation (Dailey et al. 2003). On the contrary, VM devices proved their feasibility to nebulize both delicate and slightly viscous formulations (Ghazanfari *et al.* 2007; Lentz *et al.* 2006; Waldrep and Dhand 2008; Elhissi and Taylor 2005). Among them fall passively VM devices such as the Omron Microair nebulizer which can be distinguished from active VM devices such as the AeroNeb Go of Nektar (Ghazanfari *et al.* 2007). The first group featured a perforated plate with approximately 3 µm-diameter holes. The plate was passively induced by an attached piezo crystal via a transducer horn. The fluid got extruded through the microholes and consequently, the aerosol was formed. As a result, very high nebulized drug output efficiency was achieved while output rates tended to be relatively low and ceased early when viscous formulations were involved. Conversely, the actively VM devices featured a plate with dome-shaped apertures which are moved up- and downwards 10^5 times per second in a micrometer range by an electric vibrating element. This micropump extruded the fluid and thus created the aerosol (Ghazanfari *et al.* 2007). Described advantages of the active VM device were a more rapid aerosol generation and a relatively high nebulized output over 70%. Approximately 50% of the nebulized droplet output were sized as FPF below 5.21 µm and therefore reached the lower airways' area of interest without inactivation or denaturation of delicate active pharmaceutical ingredients (API) (Haroon et al. 2005). A comparable VM device was employed recently to successfully nebulize complex PLGA-PVA nanoparticles loaded with a model drug (Beck-Broichsitter et al. 2009).

Compressor or jet nebulizers apparently were not suitable in our application of

fragile CpG. Nevertheless, jet nebulized GNPs gave promising results such as enabling targeted lung cancer delivery of chemotherapeutic agent cisplatin (Tseng et al. 2007; Tseng et al. 2009). While the median droplet size was determined and lung deposition was proved *in vivo*, no further characterization of the data of the nebulization process itself was given. Therefore, two established devices with different VM techniques were compared in addition to the pMDI for GNP integrity, its impact on various parameters' influence of viscosity, its importance of administration time and recovered concentration after quantitative recondensation. *In vitro*, the ability of nebulized CpG loaded GNPs was tested in comparison to original non-nebulized ones to trigger IL-10 release from relevant cultured equine lymphocytes gained from bronchoalveolar lavage fluid (BALF). Bronchoalveolar lavage is an established method to recover respiratory secretions in peripheral airways and alveoli by a flexible fiberbronchoscopy and make them available for subsequent cytological investigations (Bernstein 1984; Hoffman 2008). The presented findings constituted a prerequisite for further equine *in vivo* studies.

4.2 Materials and Methods

4.2.1 Materials

The immunomodulative single stranded mixed phosphothioester/-diester backbone CpG-ODN 2216 class A with the sequence 5`-G*G*GGGACGATCGTCG*G*G*G*G*G*-3` was received as lyophilisate from biomers (Ulm, Germany), diluted in sterilely filtrated highly purified water (HPW) produced by a purelab plus device (Elga labwater, Celle, Germany) to a final concentration of 1 mg/ml and stored at -80°C till final use. IL-10 quantifying equine Duo set ELISA was purchased from R&D Systems (Minneapolis, USA). Liquefied gas propellant HFA 134a was obtained from Schick GmbH (Stuttgart, Germany).

4.2.2 Preparation of the CpG-GNPs

Plain, cationized and fluorescent labeled GNPs were prepared as described in chapter II, 1.2.1 according to the established protocols (Coester *et al.* 2000; Zwiorek *et al.* 2008). 20 bases long CpG-ODN 2216 (Biomers, Ulm, Germany)

was loaded onto the GNP surface in HPW by electrostatic attraction. To ensure colloidal stability, the CpG concentration was set to 5 % (m/m) based on the GNP mass. For this, the aseptically prepared samples of cationized GNPs were subsequently incubated for 1 h at 22 °C and 300 rpm using a Thermomixer™ device (Eppendorf, Hamburg, Germany). The concentration of the GNP dispersion was set to 0.5, 1.0 or 1.5 mg/ml for subsequent different nebulization setups.

4.2.3 **Determination of nanoparticle properties and dispersion viscosity**

Particle sizes were determined by PCS using a Zetasizer Nano ZS (Malvern Instruments, Worcestershire, England) as described above in chapter II. Intensity weighted particle mean diameter (Z-average) and PDI as the width of the fitted Gaussian distribution were calculated by the DTS V. 5.10 software from at least 15 subruns. For Zeta potential measurement before and after loading GNPs were diluted in 10 mM NaCl to maintain a sufficient but not too high ionic strength in terms of conductivity and electrode corrosion. GNP concentration was determined gravimetrically (Mettler Toledo UMX2, Mettler, Greifensee, Switzerland).

Viscosity of GNP formulations was determined prior nebulization by an automated microviscosimeter (AmV) device by Anton Paar GmbH (Graz, Austria). Percentile loading efficiency was proven indirectly by UV-spectroscopy at 260 nm wavelength (UV1, Thermo Fisher Scientific Inc., Waltham, USA) Therefore, the supernatant(s) of CpG-GNP samples, supernatants of GNP controls (without CpG) and supernatants of CpG controls (without GNP) were taken into account as given below:

$$CpG\ loading = \left(1 - \left(\frac{OD\ of\ s(CpG - GNP) - OD\ of\ s(GNP\ control)}{OD\ of\ s(CpG\ control)}\right)\right) \times 100\,[\%]$$

4.2.4 **GNP aerosolization**

For aerosolization by pMDIs, 12 ml aluminium pMDI containers were filled with 3, 5 or 10 g of a 1 mg / ml GNP dispersion and a cap with dosing chamber and purging valves was positioned on top of the container. Crimping and subsequent

liquefied propellant filling trough the dosing chamber was conducted by a hand operated laboratory plant 2005/2 (Pamasol, Pfaeffikon, Switzerland). The filling weight of propellant was kept constant at 1.5 g / pMDI resulting in 2:1, 4:1 and 8:1 GNP dispersion : propellant ratios. To estimate consistency of dosing, a sequence of 30 spraying passes was performed for each formulation and the pMDI was weighted after each pass. Aerosols and droplets were collected in suitable 50 ml tubes for subsequent GNP characterization.

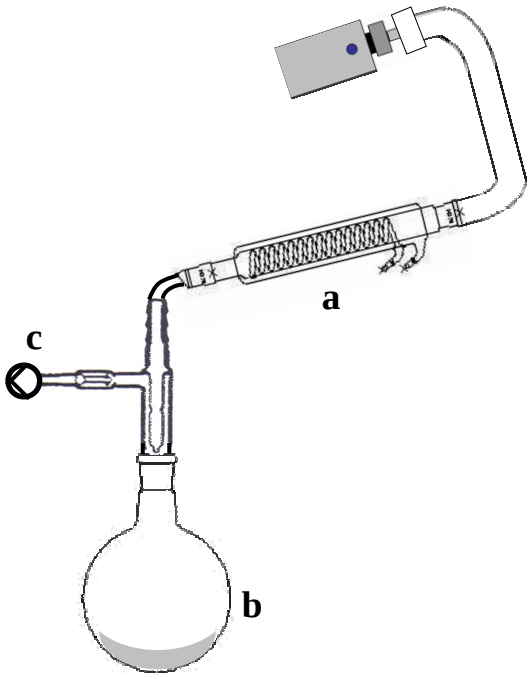

Fig. 1: *Experimental setup of the 4 ±1°C chiller (a), collecting flask (b) and vacuum pump (c) to determine GNP concentration of precipitated vapors generated by the nebulizer Microair.*

VM-nebulization was performed by a passively vibrating NE-U22V Microair (Omron, Matsusaka, Japan) and an actively vibrating AeroNeb Go (Aerogen, Galway, Ireland) device. The Microair instrument was employed with the manufacturer-provided rubber supplement mouth piece (Fig. 1) while the AeroNeb Go was either (a) used with the manufacturer-provided “nebulizer body” connected to the essential medication cup/aerosol generator part or (b) with a 90° glass connector with joints that suitably matched the medication cup/aerosol generator part’s outlet side. Nebulization efficiency (NE) was determined for all three instrumental setups by weighing the VM device before nebulization and after operation to dryness. The latter was considered apparent when visibly no more vapor escaped from the aerosol generator. After division of the weights, the

results were given in percent. To determine the post-nebulization weight, the whole instrument with all practically relevant adapters or nebulizer bodies was put on a lab balance (College, Mettler Toledo, Greifensee, Switzerland). Therefore, only those portions of the nebulized formulation that completely escaped the apparatus (nebulizer plus auxiliary parts) and consequently contributed to the deposition study were considered relevant for the NE calculation.

For size and concentration evaluation of post-nebulized GNPs, the resulting aerosol was collected in a closed glass system equipped with a water cooled chiller at 4°C to quantitatively condensate vapors. Either the Mircoair VM device (Fig. 1) or the AeroNeb Go VM device with attached glass connecter was fitted to the closed glass system. An applied vacuum of 700 mbars which translated to a flow rate of approximately 30 l/min (Vaccubrand CVC200, Wertheim, Germany) was introduced to assure high yields of GNP dispersion in the collection round bottom flask.

Subsequently, intercepted samples were analyzed for size, size distribution and concentration. Results were compared to the pre-nebulized ones, respectively.

4.2.5 **Droplet size analysis**

Droplet sizes of dispersions nebulized by the two VM devices were assessed by laser diffraction. Therefore, 0.5 ml of a GNP dispersion (1 mg/ml) were nebulized and the vapor was directed through the 633 nm laser beam of a Mastersizer X long bench (Malvern Instruments, Malvern, UK) in 4.5 cm distance to a 300 mm lens. Droplet sizes were calculated by the version 2.19 Mastersizer software using an implemented model based on a particle refractive index of 1.45 and a dispersion optical density of 0.276 at 633 nm. Results are the mean diameter of three runs each with 1000 measuring events. Corresponding FPFs defined as the particle fraction below 5.21 µm were given in percent.

4.2.6 **Deposition study**

For deposition studies, fluorescence labeled GNPs with covalently bound Alexa 633 dye were employed at a concentration of 1 mg / ml and characterized according to Ph. Eur. by apparatus type A twin-stage glass impinger apparatus (Copley Scientific Ltd., Nottingham, UK, Fig. 2). HPW was introduced in the

upper (7 ml) and lower (30 ml) stages of the impinger and a steady flow rate of 60 l / min was maintained during the aerosolization process by a Glax. Sing. Sta. pump (Erweka GmbH, Heussenstamm, Germany) to mimic physiologic breathing air flow. Additionally, a 500 ml aerosol spacer (GSK, Brentford, UK) was introduced as a pre-separator between the VM-nebulizer or pMDI and the impinger.

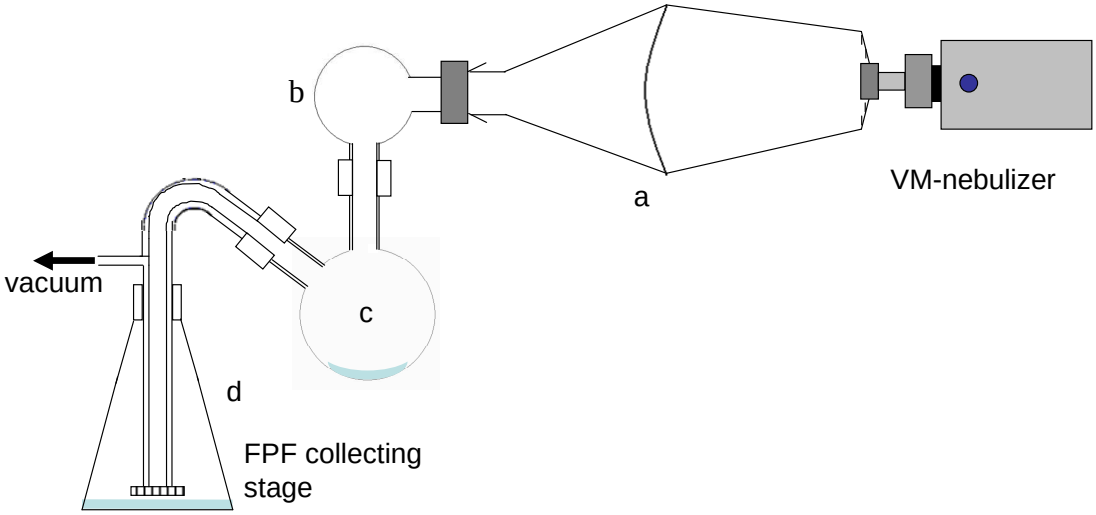

Fig. 2: *Experimental setup of the nebulizer – here Omron's Microair- connected to the spacer (a) which was attached to the twin-stage impinger (Ph. Eur. device type A) with mouthpiece (b), stage one (c) and stage two (d).*

FPF to be found in stage 2 of the impinger was considered the respiratory fraction (RF) as part of the whole nebulized fraction. Results of single fractions were calculated (standard curve) by referring the mass per stage calculated from the detected fluorescence intensity of Alexa 633 labeled GNPs to the whole applied mass of GNPs in the nebulizer and given in percent.

4.2.7 **Cell culture and immunostimulation**

Bronchoalveolar lavage fluid (BALF) was collected from a 20 years old male horse of 520 kg body weight with RAO condition sedated by detomedine (0.01 mg/kg) and butorphanol (0.01 mg/kg) i.v. as previously described . An endoscope was passed nasotracheally for visual inspection of the trachea (Hoffman 2008; Jackson *et al.* 2004). For local anaesthesia, 10 ml of a 2% mepivacaine solution were passed through the endoscope channel and afterwards the endoscope was pulled back up towards larynx. Subsequently, a BALF catheter (Bivona Inc.,

Gary, USA) was inserted as far as the bifurcation tracheae, firmly adjusted by a balloon and then employed to introduce two 100 ml aliquots of sterile 0.9% NaCl solution. The 200 ml were immediately aspired again by new sterile syringes and transferred to sterile 50 ml centrifugation tubes. Samples were refrigerated at 4°C shortly until subsequent centrifugation at 1200 g for 6 minutes to spin down contained cells. The pellet was resuspended in RPMI medium (Biochrom AG, Berlin, Germany) supplemented with 10% FCS and 67.8 µg/ml penicillin and 113 µg/ml streptomycin. Cell numbers were counted using a Neubauer chamber (Laboroptik GmbH, Friedrichsdorf, Germany). 2 x 10^5 cells per well were transferred to a 96 well polystyrene cell culture plate (Techno Plastic Products, Trasadingen, Switzerland). Per individual well, 0.275 mg were GNPs loaded with 13.5 µg (5% (w/w) CpG, they were (a) transferred directly without further processing to a cell culture 2 x 10^5 cells of BALF cells per well or (b) first nebulized by the active VM-device, completely regained from the vapor and added to the cell culture.. Incubation was set to 24 h at 37°C in a 5% (V/V) CO_2 atmosphere. Afterwards, culture plates were centrifuged at 1200 g for 6 min. and cytokine IL-10 was quantified from collected supernatants by an equine IL-10 ELISA (Duoset, R&D systems, Minneapolis, USA) according to manufacturer's instructions. Detection wavelength was 450 nm. Remaining cell pellets in the well plate were immediately resuspended in 300 µl of 3-(4,5-Dimethylthiazol-2-yl)-2,5-diphenyltetrazolium bromide (MTT) working solution consisting of 82% PBS, 9% FCS and 9% of a 5 mg/ml MTT stock solution. Hence, 0.135 mg MTT reagent was applied per 2x10^5 cells. After two hours of incubation at 37°C and in 5 % (V/V) CO_2 culture plates were centrifuged at 1200 g for 6 min., supernatants were discarded and the remaining pellets resuspended in 200 µl DMSO and subsequently analysed at 590 nm. All samples and related analysis were conducted in triplicate.

4.3 Results

4.3.1 Particle characterization upon nebulization by pMDI and VM-devices

First, the impact of nebulization by pMDI was assessed. Therefore, vapor fractions were collected, and PCS measurements revealed initial high particle sizes and size distributions (PDI values) that diminished in the course of application (Fig. 3). Over a storage time of 48 h, pMDI formulation exhibited no negative impact on unloaded GNPs' stability. As per differential weighing, maximum achieved NE with the pMDI was 77.4% for the 4:1 GNP dispersion : propellant ratio formulation while the others (2:1, 8:1) remained slightly below. After this degree of drawdown, pressure was too low to ensure aerosolization upon liquid's exit from the container via the purging valve. Average dosing was 68 mg formulation per pass. However, the S.D of 20 mg indicated a high variability translating to a relative standard deviation of 29.4%.

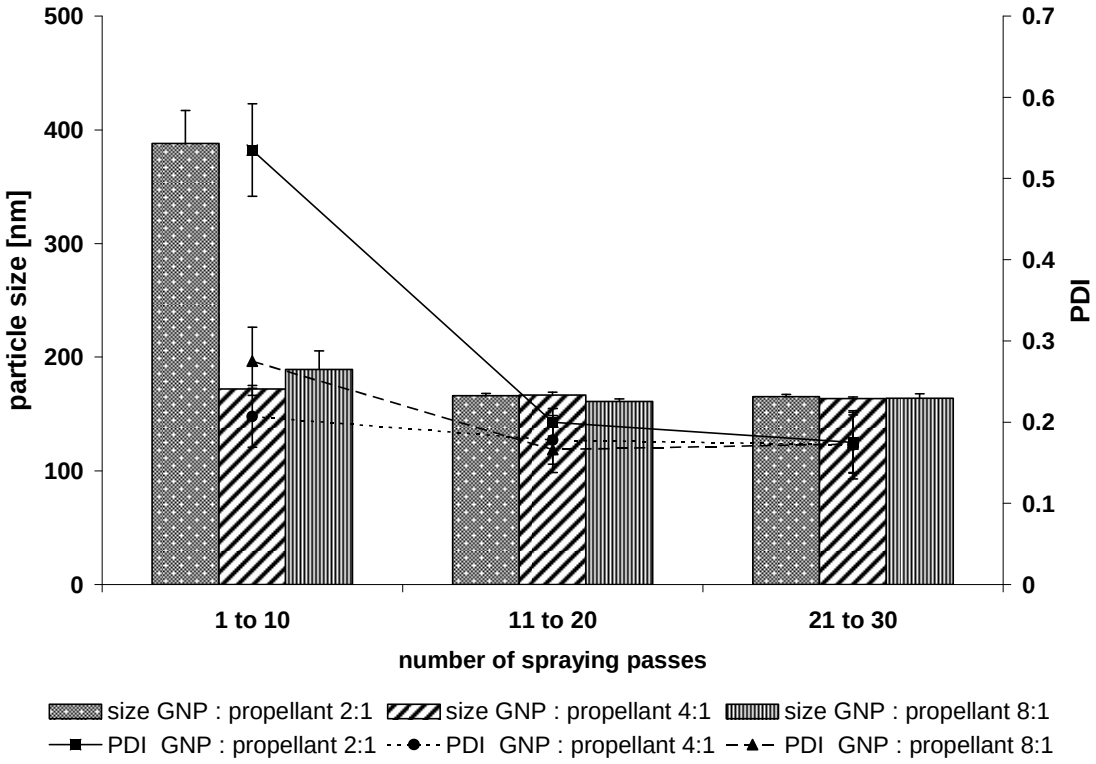

Fig. 3: *Particle size and size distribution characterized by the PDI value of GNPs nebulized by pMDI in dependence of the aqueous GNP to propellant ratio and of the number of praying passes (n=3, ± S.D.).*

GNP integrity was indeed not altered over time by the formulation with HFC propellant as most likely no interaction occurred between the hydrophilic GNPs and the inert simultaneously hydrophobic and lipophobic liquid gas (Table 1).

time point [h]	size [nm]	S.D.	PDI	S.D.
0	163.8	3.8	0.173	0.036
1.5	150.2	1.3	0.072	0.007
3	152.7	1.8	0.063	0.028
48	153.9	2.4	0.076	0.015

Table 1: *Particle size and size distribution characterized by the PDI value of GNPs nebulized by pMDI in dependence of the storage time within the pMDI container (n=3).*

For unloaded, fluorescing GNPs with an original size of 145.5 nm (±1.76 nm) and a very low PDI of 0.038 (±0.025), neither VM-nebulization process altered the assessed parameters significantly (Table 2).

Omron's Microair®				
c [mg/ml]	size [nm]	S.D.	PDI	S.D.
0.5	149.9	1.373	0.027	0.017
1.0	147.4	2.061	0.059	0.035
1.5	146.2	1.601	0.024	0.015
Nektar's AeroNeb Go®				
c [mg/ml]	size [nm]	S.D.	PDI	S.D.
0.5	144.9	1.084	0.037	0.025
1.0	144.6	0.989	0.021	0.014
1.5	145.6	0.734	0.032	0.023

Table 2: *Sizes and size distributions of plain GNPs after nebulization (n=3, ± S.D.).*

As shown before (Fuchs et al. 2010), particle sizes determined by PCS grow after cationization. Accordingly, above mentioned particles of 145.5 nm were considerably larger (250 nm) after cationization compared to the state before the modification. This size did not change considerably by CpG loading to the GNP

surface which was important to guarantee overall colloidal stability. However, CpG-loaded GNPs of being sized 256.2 nm (±3.63 nm) pre-nebulization turned out to be significantly smaller at 222.3 (±1.42 nm) after nebulization by the Microair while not being significantly different at 248.2 (±7.34 nm) with the AeroNeb Go device.

4.3.2 **Nebulization efficiency of VM-devices**

NE remained consistent within the repeated measurements for each single device as demonstrated by low S.D. values. Furthermore, the GNP concentration has hardly any impact on the NE. A negligible tendency of higher percentile NE values with rising concentration is visible as it is 93.8, 97.0 and 95.9% and 94.4, 97.0 and 97.8% for the Microair and for the glass adapter-supplemented AeroNeb Go, respectively (Fig. 4). However, the applied VM system has an impact. While the above given values peak near 100%, using the commercial nebulizing body, the AeroNeb Go's NE ranks only half at about 50% while the rest is trapped in the device (Fig. 4). Recovered masses of re-precipitated samples in the round flak collector were 70.2, 71.7 and 79.1% (m/m), respectively.

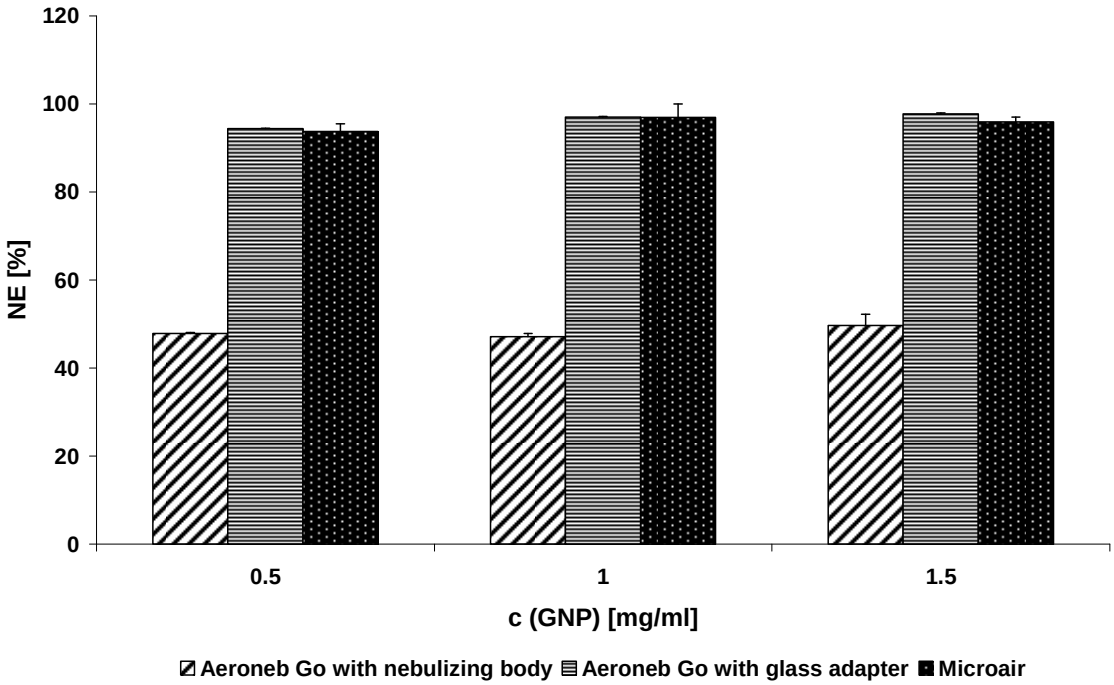

Fig. 4: *Nebulization efficiency (NE) of GNP dispersions concentrated 0.5, 1.0 and 1.5 mg/ml in dependence of the applied nebulizer and/or the applied adapter (n=3, ± S.D.).*

4.3.3 **Output rates of VM-devices**

The passive VM-device required a significantly longer period of time to nebulize constantly employed volume of 1 ml of GNP dispersion completely to "dryness" compared to the active VM-device (Table 3). Viscosity rose linearly with GNP concentration and accordingly output rates dropped.

	Nektar's AeroNeb Go®		Omron's Microair®			
c [mg/ml]	time [min:sec]	S.D.	time [min:sec]	S.D.	viscosity [mPa*s]	S.D.
0.5	01:43	0.001	08:21	0.013	0.9137	0.0003
1.0	01:46	0.003	08:49	0.005	0.9201	0.0008
1.5	01:53	0.002	10:57	0.024	0.9283	0.0024

Table 3: *Required nebulization times for three GNP concentrations by the active (ledt) and the passive (right) VM device and related viscosity (n=3).*

With rising GNP concentration, the output rates by the passive VM device were only 0.12, 0.11 and 0.09 mg/min, respectively. In comparison, the active VM device achieved 4.9 to 5.8 times higher output rates of 0.58, 0.57 and 0.53 ml/min, respectively.

4.3.4 **Consistency of concentration after nebulization**

All three employed GNP concentrations were determined gravimetrically before and after nebulization. Post-nebulized concentrations were gained from dispersions precipitated by the nebulizers as shown in Figure 1. Results and corresponding deviations of the post-nebulized concentration values to the pre-nebulization values are given in Table 4. Negative deviations indicating lower GNP concentrations are found for all three Microair runs. For the AeroNeb Go, two deviations were positive indicating a concentration increase and only one was negative. As a trend, deviations got smaller with rising GNP concentration for both VM devices.

	Nektar's AeroNeb Go®			Omron's Microair®		
concentration prior nebulization [mg/ml]	concentration after nebulization [mg/ml]	S.D.	deviation through nebulization [%]	concentration after nebulization [mg/ml]	S.D.	deviation through nebulization [%]
0.5	0.534	0.057	6.8	0.458	0.003	-8.5
1	0.956	0.131	-4.4	0.974	0.102	-2.6
1.5	1.516	0.202	1.1	1.448	0.182	-3.5

Table 4: *Comparison of the recovery (absolute and percentile) of three GNP concentrations before and after nebulization by a Microair and an AeroNeb GoVM-device.*

4.3.5 **Aerosol particle size characterization**

Analysis of nebulized droplet sizes revealed slightly higher diameters for droplets created by the Microair device. Here, the mean diameter of the AeroNeb Go-generated droplets accounted for 6.60 ± 0.03 µm while those by the Microair was determined at 7.46 ± 0.10 µm (n=3, ± S.D.). Accordingly, the FPF defined below 5.21 µm (Ghazanfari et al. 2007) was 37.13% (± 0.57) and 30.24% (± 0.97) for the two VM devices, respectively. When nebulizing HPW alone by the AeroNeb Go, a mean droplet sizes of 6.34 µm and a FPF of 36.28% were received.

4.3.6 **Deposition study**

Deposition characteristics were assessed by an impinger to estimate the feasibility of each aerosol-producing device to deliver GNPs in a high RF to the therapeutically relevant lower airways. GNPs delivered by an pMDI generated aerosol showed a bad deposition related to lower airway targeting as 65.66% (±0.84%) of the nebulized GNP mass were trapped in the spacer and only 0.76% (±5.46%) could be found on the last stage representing the RF (Fig. 5). The passive VM-device featured a prospective lung deposition of 47.65% (±18.04%) with 1.95% (±0.91%) ending up in the spacer while the active VM-device exhibited the highest RF value of 65.68% (±11.20%) with 3.43 (±0.40%) to be found pre-separated in the spacer (Fig. 5).

Some particles were deposed on the glass connections and could not be

quantitatively assigned to single distinguished stages. They constituted the amount lacking to 100%.

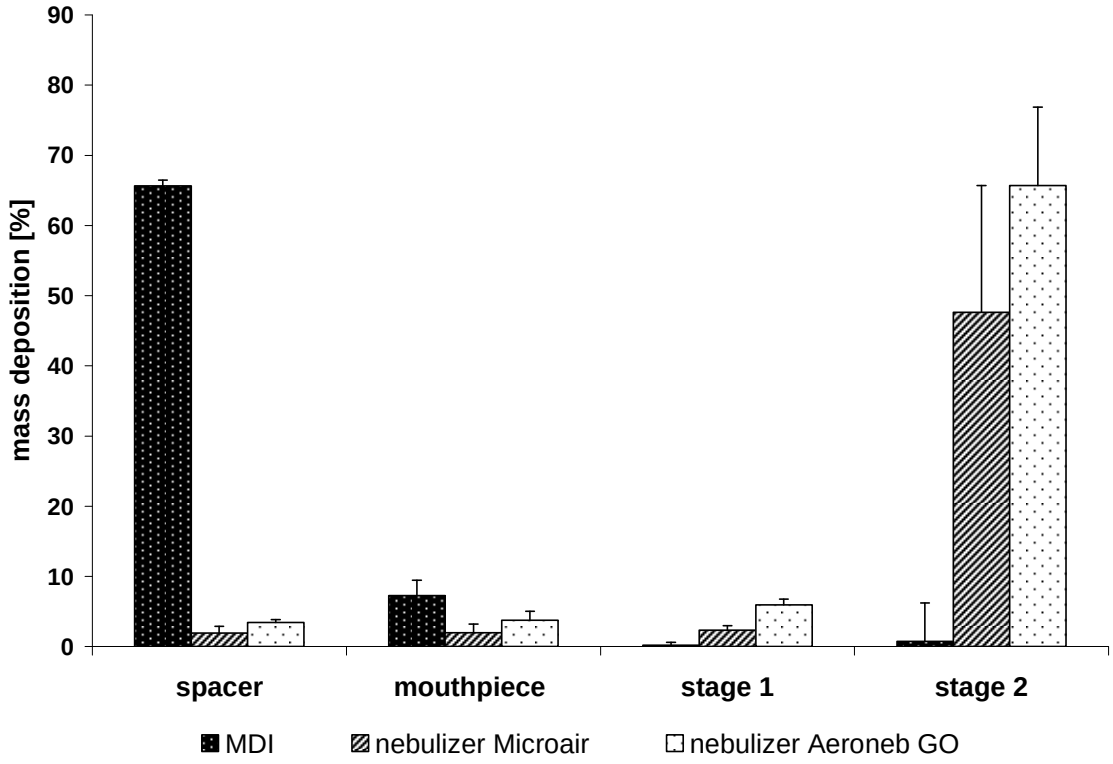

Fig. 5: *Mass deposition of fluorescent labeled GNPs in the twin-stage impinger in dependence of the applied aerosolization device (n=3, ± S.D.).*

4.3.7 **Stimulation of IL-10 release *in vitro***

CpG-ODN loading onto the GNPs' surface was 98.51% (±1.29) according to the gravimetrical differential determination. The Zeta potential was determined to be 23.0 mV (±0.4 mV) before and 21.7 mV (± 1.0 mV) after the loading. Conductivity dropped accordingly from 0.943 mS/cm (± 0.002) to 0.884 mS/cm (± 0.003) due to the reduced amount of chargings present in the dispersion. Analysis for the central immunomodulating cytokine IL-10 revealed significant higher release for both the nebulized and the non-nebulized formulation compared to the control, untreated BALF cells' supernatant. Difference in release between the two applied GNP groups was not significant and accounted for 225.2 pg/ml (± 56.3 pg/ml) and 230.7 pg/ml, respectively (n=3, ± S.D.). Additionally, cell viability was very high in both cases, reaching 102.2% (± 3.8%) compared to the negative control of amount of untreated viable cells as per MTT assay. Plain, non-

loaded GNPs did not trigger IL-10 release in a quantifiable manner and had no negative effect on viability over 24 h (data not shown).

4.4 Discussion

In this study, we evaluated for the first time the most suitable administration technique for pulmonal GNP delivery. In the perspective of ongoing *in vivo* studies involving the immunotherapeutic application of CpG-GNPs in equine RAO, the basis of a reliable dosage form is given hereby.

First, the possibility to generate an aerosol of aqueous GNP dispersions by pMDI was tested. Nanoparticle size and size distribution after aerosolization, consistency of dosing and deposition characteristics were of central interest to assess this dosage form's feasibility. Although a standard proof dosing chamber was used for the pMDI, a constant aerosol dosing was not given with RSD of up to 29%. The collected vapors contained GNPs of appropriate size and size distribution after the early spraying phase was completed (Fig. 3) and GNP quality was constant over the observed time of 48 h (Table 1). Remarkably, particles' PDIs were lower for high GNP to propellant ratios in the early spraying phase but equalized after an increased amount of spraying passes (Fig. 3). But visibly, aerosols featured heterogeneous droplet size distributions as larger droplets were trapped on the mouthpiece's inner surface of the pMDI. Accordingly, most of the generated aerosol was held back as coarsely dispersed fraction in the spacer and only a small amount was subsequently found on the final impinger stage (Fig. 5).

Apparently, the FPF was too low to contribute to a high RF. The likely reason was the high surface tension of the aqueous phase which hindered the propellant to enable sufficient aerosolization. Therefore, surfactants would have been required to reduce the hindering high surface tension. However, their amount, their possibly negative impact on CpG activity and their physiologic harmlessness needed to be determined in this case. Furthermore, pMDIs required pressurized propellant filling with a special apparatus. As CpG-GNP formulations needed to be prepared freshly, a pMDI filling system might not always be available. Therefore, as long as a storage stable formulation is not at hand, pMDIs remain inappropriate for practical use in addition to their so far poor FPF generation from GNP dispersions.

On the contrary, VM-nebulizers showed an overall good performance which was in accordance with previous studies on their employment in nebulization of delicate dispersion. Furthermore, once the CpG-GNP formulation was prepared it could easily be transferred to the VM-device's medication cup without the need of any special instrument such as a pressurized propellant filling station. As a central finding, particle sizes and size distributions both of loaded and loaded GNPs were not significantly affected by the nebulization process (Table 1). This was observed for both devices and for all applied therapeutically feasible concentrations.

Ghazanfari et al. (2007) revealed in detail how the liquid's properties such as viscosity, surface tension and ionic background influenced the NE and FPF. The latter was defined as droplet sizes below 5.21 µm in diameter and was decisive for a resulting preferably high RF for potential alveolar deposition. As present GNP dispersions were determined in a viscosity range close to water, it is referred to the FPF and average droplet size cited in literature. Viscosity was proven by Ghazanfari et al. to be a critical factor for the overall generation of vapor by VM-devices. Related values above 2.45 mPa/s resulted in absence of aerosol generation. In this study, a GNP concentration of 1.5 mg/ml constituted the upper chosen limit for a reasonable and stable formulation for loaded GNPs. Consequently, the corresponding viscosity, rising linearly with GNP concentration, did not extend beyond 0.9283 mPa/s and aerosol generation was feasible without obstacles related to the formulation's viscosity (Table 3). However, although NE was very high both for the actively and the passively VM-device (Fig. 4), a huge difference was observed between the output rates. They were 4.9 to 5.8 times higher with AeroNeb Go compared to the Mircoair (Table 3). This trend was also observed for various solutions by Ghazanfari accounting for factors from 1.4 to 3.3. The viscosity was coined to be the crucial parameter in output rates for the Microair. This is in accordance with our findings where output rates dropped by 6.29% and by 24.74% for the 1 mg/ml and 1.5 mg/ml formulation when nebulized by the passive VM-device compared to the 0.5 mg/ml dispersion (Table 3). On the contrary, output rates were reduced for the equivalent GNP concentrations by only 3.83% and 9.85% when nebulized by the active VM-device, respectively. The latter is supposed to occur due to the higher energy input by the active VM micropump which overcame resistance of fluids to shear forces more easily (Elhissi et al. 2006).

Furthermore, with regards to the present deposition study, the maximum RF was proven to be produced by the active VM-device (Fig. 5). Equalizing this RF with the droplet sizes determined by laser diffraction and with previous FPF results by Ghazanfari (2007), this RF value is considerably higher. However, the present deposition results in Fig. 5 refer to the fluorescent NP signals themselves and not to directly to the generated droplets in the micrometer range. As droplets might burst in flight and release contained nanoparticles, a higher lung deposition than expected due to the droplet size-associated deposition is likely. Furthermore, the fact that the highest FPF was generated by the active VM device was revealed by all analytic methods alike. Moreover, the potential *in vivo* target of the CpG-GNP formulation is not restricted to the alveoli but rather comprises the segmental, terminal and respiratory bronchioles as well because RAO affects the complete lower airways e.g. by brochospasm of smooth muscles and excessive mucus production. Thus, a deposition both in alveoli and bronchioles facilitated by droplet sizes of 5 µm (± 2 µm) are desirable and were achieved in the present setting. As a decreasing surface tension was determined to correspond to a higher FPF outcome (Elhissi and Taylor 2005; Ghazanfari et al. 2007), this parameter has to be considered for the GNP formulations as well.

Gelatin is known to reduce the surface tension significantly from 72 dyn/cm (water) down to about 55 dyn/cm in concentrations above 0.25 mg/ml depending on temperature and prevalent pH value (Sato and Ueberreiter 1979). It was shown that gelatin molecules are surface active and accumulate at interfaces due to their hydrophobic segments rich in proline, hydroxyproline, alanine, valine and leucine (Sato and Ueberreiter 1979). Here, the surface reducing effect might be mediated both by residual soluble gelatin in the dispersion as well by the nanoparticles themselves, featuring the gelatin amphipilic properties on the surface.

This is in accordance with findings on reduced surface tensions and consequently higher FPF produced by VM-devices when liposomal formulations were employed (Aboudan et al. 2004; Elhissi and Taylor 2005).

Furthermore, nanoparticles themselves were previously proven to enrich in liquid-gas interfaces (Vafaei et al. 2009). This inclusion led to a reduction of effective surface energy because related values for nanoparticles-water, nanoparticles-air and resulting air-water interfaces are lower than for the original air-water interface (Vafaei et al. 2009). Therefore, a combination of the gelatin properties and the

nanoparticulate properties combined seem to contribute to a reduction in surface tension and consequently to the final desired augmented FPF. As the active VM-device showed the overall best performance in output rate and RF generation, it was exclusively used to generate nebulized CpG-GNPs for the *in vitro* cytokine stimulation test.

Finally, it was shown that after nebulization CpG-GNPs are still capable of inducing the same immune response in BALF cells as if they were not nebulized. Comparing IL-10 releases over 24 h, no significant changes were quantified between nebulized and non-nebulized formulations. This demonstrated the gentle character of the employed aerosolization technique and proofed the feasibility of intact nebulized CPG-GNPs to be later used in inhalative immunotherapy. The manufacturing of CpG loaded GNPs was meanwhile well established and could be quickly performed in a clinical lab equipped with sterile working facilities. Yet, the formulations needed to be employed within hours to avoid the remaining risk of aggregation which was associated with CpGs class A earlier (Kerkmann et al. 2005). Therefore, DPIs could constitute an advanced strategy to provide a long-term stable application form of CpG-loaded GNPs. Freeze drying of ODN-loaded GNPs was introduced before (Zillies et al. 2008) and could be used to develop an inhalative powder formulation. Consequently, sealed single doses such as introduced in commercial disk haler could constitute a feasible and storable alternative to so far successful nebulization of aqueous CpG-GNP dispersions in future every-day use.

4.5 Conclusion

A protein-based carrier system, gelatin nanoparticles, was developed to deliver immunostimulatory CpGs in an aerosol for the first time. Characterization revealed no negative impact onto the colloidal stability of the formulation when nebulized by vibrating mesh devices. Concentration remained unaffected by this process, thus enabling predictive dosing. Nebulization could be accomplished within reasonable timing in clinical terms and consequently led to a generation of a fine respirable fraction of up to 65.7% as shown by impaction studies. Furthermore, nebulized CpG-GNPs elicited significant IL-10 release from equine BALF cells *in vitro* to the same extend as non-nebulized did and are therefore considerable in immunotherapy. The hereby available formulation holds great

potential e.g. for the treatment of RAO in the premier equine *in vivo* study involving nanocarriers.

5. Immunostimulation of bronchoalveolar lavage cells from recurrent airway obstruction-affected horses by different CpG-classes bound to gelatin nanoparticles

This work was conducted in close and essential cooperation with the Equine Clinic, LMU Munich. All experiments -besides gaining of BALF- were conducted together with veterinarian John Klier.

5.1 The significance of RAO and the potential of CpG immunotherapy in horses

In the last decades, allergic airway diseases have dramatically increased in the northern hemisphere of industrialized countries in horses and humans (Kline 2007; Braun-Fähränder 2009). Equine recurrent airway obstruction (RAO) has become one of the most common airway diseases (Fey 2006). Housing of horses in stables with permanent exposure to potentially allergenic organic and inorganic particles was reported to be a major trigger factor (Schmallenbach et al. 1998; Robinson 2001; Millerick-May 2009). Keeping horses on pasture leads to improved clinical signs, however, complete avoidance of allergens is not always possible (Robinson 2001). The permanent inhalation of various antigens from moldy hay, mite dust as well as endotoxin, β-glucan and other organic and inorganic particles causes airway neutrophilia and inflammation with a mixed Th1/Th2 immune response (Horohov et al. 2005; Cordeau et al. 2004). Although the clinical signs of RAO were well defined (Robinson 2001), immunological mechanisms are still controversy discussed. However, a predominant Th2 allergic response was recently presumed (Horohov et al. 2009). In several studies, signs of predominant Th2 response such as high IL-4, IL-5 in bronchoalveolar lavage fluid (BALF) of RAO horses exposed to antigens were reported (Lavoie et al. 2001; Cordeau et al. 2004). Due to persistent chronic inflammatory reaction in small airways of the affected horses, Th1 participation was also confirmed (Ainsworth et al. 2003). Recently, proinflammatory and chemotactic IL-17 from Th17 cells has been demonstrated to be involved in the progression of RAO pathology (Debrue et al. 2005; Ainsworth 2009) Thus, IL-17 pathway is of special interest in the progress of chronic airway inflammation (Iwakura and Ishigame 2006).

As a potential therapeutic option for RAO, unmethylated Cytosin-Phosphate-

Guanin-Oligodeoxynucleotides (CpG-ODN) have been explored (Fonseca and Kline 2009). CpG-ODNs were introduced as effective immune stimulating agents to cause a Th2/Th1 immune shift (Kline 2007). This shift further promoted an immunoglobuline isotype switch from IgE to IgG2 (Bohle 2002). The prevalence of IgE is a matter of ongoing debate (Halliwell et al. 1993; Marti 2009). In addition, a shift from pro-allergy mediating IL-4, IL-5 and IL-13 Th2 cytokines towards pro-inflammatory IFN-γ and IL-12 Th1 cytokines was observed. Anti-inflammatory and antiallergic properties of Th2 cytokine IL-10 turned out to be of interest. Particularly, IL-10 producing T regulatory cells (Tregs) and its balance towards Th2 cells seemed to play an important role in immune homeostasis in the lung and thus could be used for therapy of RAO (Akdis et al. 2004; Lloyd and Hawrylowicz 2009). Consequently, besides a conventional symptomatic therapy the possibility to modulate cytokine level in order to avoid development of an allergic hypersensitivity may be a better therapeutic option.

Three distinctive CpG classes (A-, B- and C-class) with varying immunologic effects were previously investigated (Krieg 2002; Krieg 2002). The key pattern-recognition receptor for these “danger signals” is the Toll-Like receptor 9 (TLR-9) which is located in endosomes (Krieg 2002; Krieg 2002). Recently, equine TLR-9 was detected in monocytes, airway epithelial cells, capillary endothelium in the lungs and pulmonary intravascular macrophages (Schneberger et al. 2009). Furthermore, species-specific immune stimulation depending on CpG motifs has been determined (Hartmann and Krieg 2000; Rankin et al. 2001).

The beneficial use of delivery systems like lipid nanoparticles or gelatin nanoparticles (GNPs) to protect ODNs from degradation by nucleases and to enhance cellular uptake was recently demonstrated (Wilson et al. 2009; Zwiorek et al. 2008). GNPs from gelatin type A obtained from porcine skin were found to be immunologically inert and the use of GNPs showed amplified CpG-related TLR-9 activation (Zwiorek et al. 2008). Consequently, the aim of this study was to identify the optimal CpG motif to stimulate equine BAL cells *in vitro* for the first time and to detect specific immunomodulating effect (Th2/Th1 shift) on the cells derived from RAO and healthy horses treated with GNP-delivered CpG-ODN.

5.2 Materials and methods

All works of this study have been conducted in close collaboration with the, Department of veterinary medicine, Equine clinic LMU, Munich. BAL was gained by veterinarian John Klier, all other experiments were performed alternating or together.

5.2.1 Horses and physical lung examination

Based on published schemes (Gerber et al. 2004) a lung scoring system was developed to assess critical clinical parameters (nasal discharge, coughing, breathing rate and thoracic percussion), blood gas chemistry, exercise examination, endoscopic exploration, cytology of tracheobronchial secret (TBS) and bronchoalveolar lavage fluids (BALF). In the present study eleven horses (eight trotter, one pura raza espanol, one warmblood and one knabstrupper) with an age range of 6-22 years and a weight range of 470-560 kg were scored and enrolled in the study. The scoring system allowed grouping patients into four categories of healthy horses and horses with mild, moderate and severe RAO. Two groups were established, whereby the first group consisted of seven horses with moderate RAO (mean age = 14.6 years) and the second group had four healthy horses (mean age = 12.3 years).

5.2.2 Oligodeoxynucleotides

To evaluate the optimal stimulating CpG motif in cultured equine BAL cells, three different CpG classes with previously employed motifs in horses in general were compared. Five different CpG ODNs and one non-CpG ODN were used (Biomers GmbH, Ulm, Germany). Each class was represented by two different sequences except the A-class where only one sequence was available. All CpG classes were single stranded ODN with a length of 20 to 30 bases. ODN 2041 (5`-CTG GTC TTT CTG GTT TTT TTC TGG-3`) was used as control. The A class differs in backbone structure from the other classes. It consists of a backbone chimera of phosphorothioate* (PS) and phosphodiester (PD) modified deoxyribose: CpG A ODN 2216 (5`-G**\***G**\***G GGA CGA TCG TCG* G**\***G**\***G **\***G**\***G- 3`). Two different B-classes were compared: CpG B ODN 2142 (5`-TCG CGT GCG TTT TGT CGT TTT GAC GTT- 3`) and CpG B ODN 2006 (5`-TCG TCG TTT TGT CGT TTT GTC GTT- 3`). The C-class was represented by CpG C

ODN 2395: (5`-TCG TCG TTT TCG GCG CGC GCC G- 3`) and CpG C ODN M362: (5`-TCG TCG TCG TTC GAA CGA CGT TGA T- 3`).

5.2.3 **Preparation of ODN loaded GNP**

Cationized GNPs were prepared according to the standard protocol (Coester et al. 2000; Zwiorek et al. 2008) as described in chapter II, 1.2.1. For cationization, the pH of solution was adjusted to 4.7. For purification, particles were centrifuged at 18000 g for three times, washed and subsequently filtered through a membrane with a pore size of 1.2 µm (Pall Life Sciences, Lab Products, Ann Arbor, USA). Then, ODNs were bound onto prepared positively charged GNPs by electrostatic interaction as described earlier (Zwiorek et al. 2008). Particle size and surface charge (Zeta potential) were quantified in 10 mM NaCl by a Zetasizer ZS Nano (Malvern Instruments, Malvern, UK). A ratio of 5% (w/w) of ODN to GNPs was chosen to ensure colloidal stability (Zwiorek et al. 2008).

A working concentration of 2.5 mg/ml for GNPs and 1.0 mg/ml for ODNs was used. Therefore, 76.5 µl of GNP stock solution were diluted by 230 µl highly purified water (HPW) and 43.8 µl of respective CpG ODN stock solution were mixed by gentle stirring to obtain a final ODN concentration of 0.125 mg/ml. As references, 0.125 mg/ml CpG ODN solution of each class (306.5 ml HPW, 43.8 µl CpG ODN stock solution) and 2.5 mg/ml GNP dispersion (274 µl HPW, 76.5 µl GNP stock solution) were prepared. All the samples were incubated for 90 minutes at room temperature with constant stirring at 300 rpm in a Thermomixer (Eppendorf, Hamburg, Germany). The samples were stored at 4°C and used within 48 hours.

5.2.4 **Preparation of cells and cell culture**

From every horse BALF was taken by using 50 ml of sterile and 37°C temperated 0.9% NaCl solution per 100 kg) packed on thermal packs and centrifuged immediately by 1200 g for 6 minutes. Supernatants were stored at -80 °C to conserve actual cytokine concentration. Total cell count was determined by manual counting using trypanblue with a Neubauer counting chamber (Laboroptik GmbH, Friedrichsdorf, Germany). 2 x 10^5cells (mixture of neutrophile granulocytes, alveolar macrophages and lymphocytes) in 230 µl RPMI medium

(Biochrom AG, Berlin, Germany) per well in a 96 well plate (Techno Plastic Products, Trasadingen, Switzerland) were incubated for 24 hours at 37 °C in 5% (V/V) CO_2 atmosphere. The RPMI cell culture medium was supplemented with 10% (V/V) FCS, 67.8 µg/ml penicillin and 113 µg/ml streptomycin.

5.2.5 **Immunostimulation by ODN and cytokine quantification (ELISA)**

Five different CpG sequences of three different classes and one ODN lacking a CpG motif, as described above, were incubated with the equine BAL cells in triplicates. In detail, 0.275 mg GNPs loaded with 13.5 µg (5% (w/w)) ODN or 13.5 µg of soluble ODN were added per well to compare the effects of unbound ODNs and ODNs bound to GNPs. To estimate the immunostimulating response of ODNs in cell culture, supernatant was taken after 24 hours of incubation and analyzed by equine ELISAs (Duoset, R&D Systems, Minneapolis, USA). Three key-cytokines namely IL-4, IL-10 and IFN-γ were evaluated. The ELISAs were performed according to the manufactures protocol. The limits of detection of the applied ELISA assays were 15.6 – 2000, 156.25 – 20000 and 31.2 - 4000 pg/ml, respectively. Results were throughout corrected by subtraction of relspective concentrations in supernatants of untreated BAL cells, which served as negative control.

5.2.6 **Cell viability by MTT-assay**

MTT assays were performed to evaluate cell viability following incubation with CpG and CpG-GNP. Cell pellets after removal of supernatant were immediately resuspended in 300 µl MTT (3-(4,5-Dimethylthiazol-2-yl) -2,5-diphenyltetrazolium bromide) working solution consisting of 82% PBS, 9% FCS and 9% of a 5 mg/ml MTT stock solution. Thus, 0.135 mg MTT reagent was added per 2 x 10^5 cells. After two hours of incubation at 37°C and in 5% (V/V) CO_2 the culture plates were centrifuged at 1200 g for 6 min. Then, the supernatant was discarded and the remaining pellets resuspended in 200 µl DMSO to solubilize violet formazan crystals. The absorbance of each well was measured at 530 nm using multiwellplate reader (Wallac). Untreated BAL cells served as a reference for 100% viability. All the measured experiments were conducted in triplicate.

5.2.7 Statistical analysis

Data from cytokine quantification by ELISAs and MTT assays were analyzed using the Prism 5 software (Graphpad software Inc., La Jolla, USA). An unpaired student t-test was employed to estimate significant differences between two independent groups such as stimulation of cells gained from RAO-affected versus healthy horses. $P < 0.05$ was considered as statistical significant data from experiments and the data reported as mean ± S.D.

5.3 Results

5.3.1 Quality control and formulation study of CpG-GNP

Particle sizes and size distribution determined before and after loading exhibited a mean particle diameter of 250 nm and homogenous size distributions with polydispersity index values throughout below 0.15. CpG loading onto the GNP surface was at least 98% (w/w).

After 48 hours GNP-bound CpG-ODN formed visible aggregations and cytokine stimulation was reduced significantly. Therefore, all GNP formulations were freshly prepared and used immediately for the experiments.

5.3.2 Cytokine release in cell culture upon stimulation by CpG/CpG-GNP

5.3.2.1 IL-10 release

In order to compare the effect of CpG-GNP versus soluble CpG on cytokine release from BAL cells, six sequences of ODNs (to include five CpGs) were tested. IL-10 showed the highest release in absolute concentration values of the three quantified cytokines on average. As a general observation, cells from healthy horses secreted significantly ($P = 0.0047$) higher amounts of IL-10 than those of RAO affected horses regardless of the employed ODN.

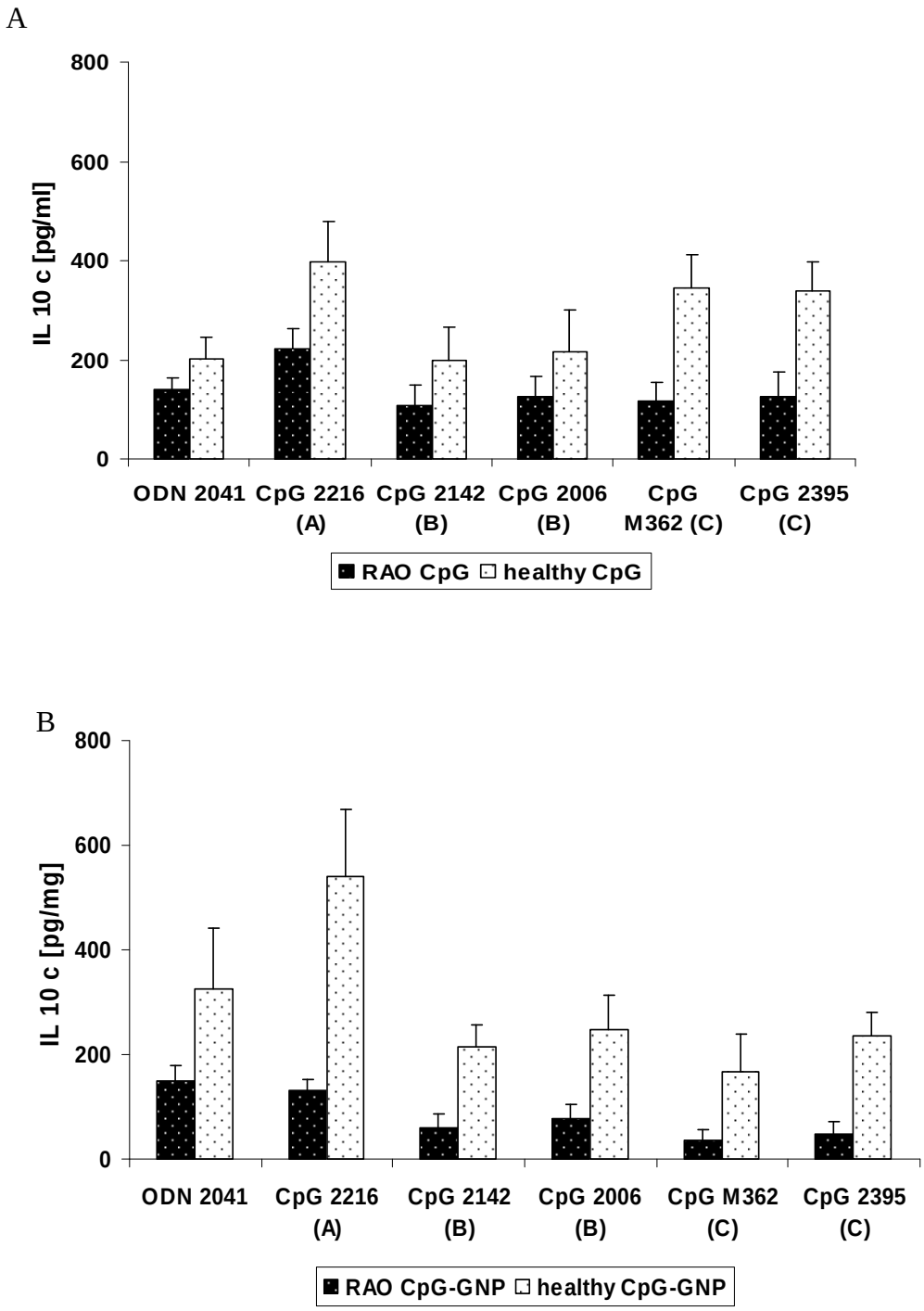

Fig. 1: IL-10 expression from BALF cells from healthy and RAO-affected horses with different CpG classes. *BAL cells derived from RAO (black bars) or health horses (white bars) were incubated with 13.5 µg of soluble ODN (**A**) or GNP-bound ODN (**B**). Cells from healthy horses secreted significantly higher amounts of IL-10 than those of RAO affected horses (P = 0.0047). CpG A triggered the highest IL-10 release for both cells groups. Depicted values are group means ± S.D and corrected by subtraction of the negative control. (Klier 2010)*

Fig. 1a shows IL-10 stimulation efficiency of soluble CpG. Out of the six different ODNs, CpG 2216 (A-class) showed the highest IL-10 release for both examined groups. IL-10 release was 400 pg/ml in cells from healthy horses and 220 pg/ml in those from RAO horses. However, CpGs of the B and C class did not trigger release in RAO derived cells, with relatively low concentrations of about 125 pg/ml. C-classes appeared to result in higher stimulation (350 pg/ml) than B-class (200 pg/ml) in cell culture for healthy horses. Consequently the employed B-classes (ODN 2142 and ODN 2006) and C-classes (ODN M362 and ODN 2395) showed almost identically release behavior for RAO horses. In Fig. 1 b IL-10 stimulation by CpG-GNPs is shown. Most noticeable is the significant higher release of IL-10 of the cells from healthy horses ($P = 0.0051$). Furthermore the GNP-bound CpG 2216 induced the highest IL-10 concentration (540 pg/ml) which surpassed the release value by soluble CpGs as shown in Fig 1 a. On the contrary the stimulation by all particle-bound CpGs are lower than those by soluble.

5.3.2.2 **IL-4 release**

In contrast to IL-10, IL-4 release upon stimulation by six soluble CpG did not differ *(P* = 0.614) between RAO and healthy horses derived cells (Fig. 2 a).

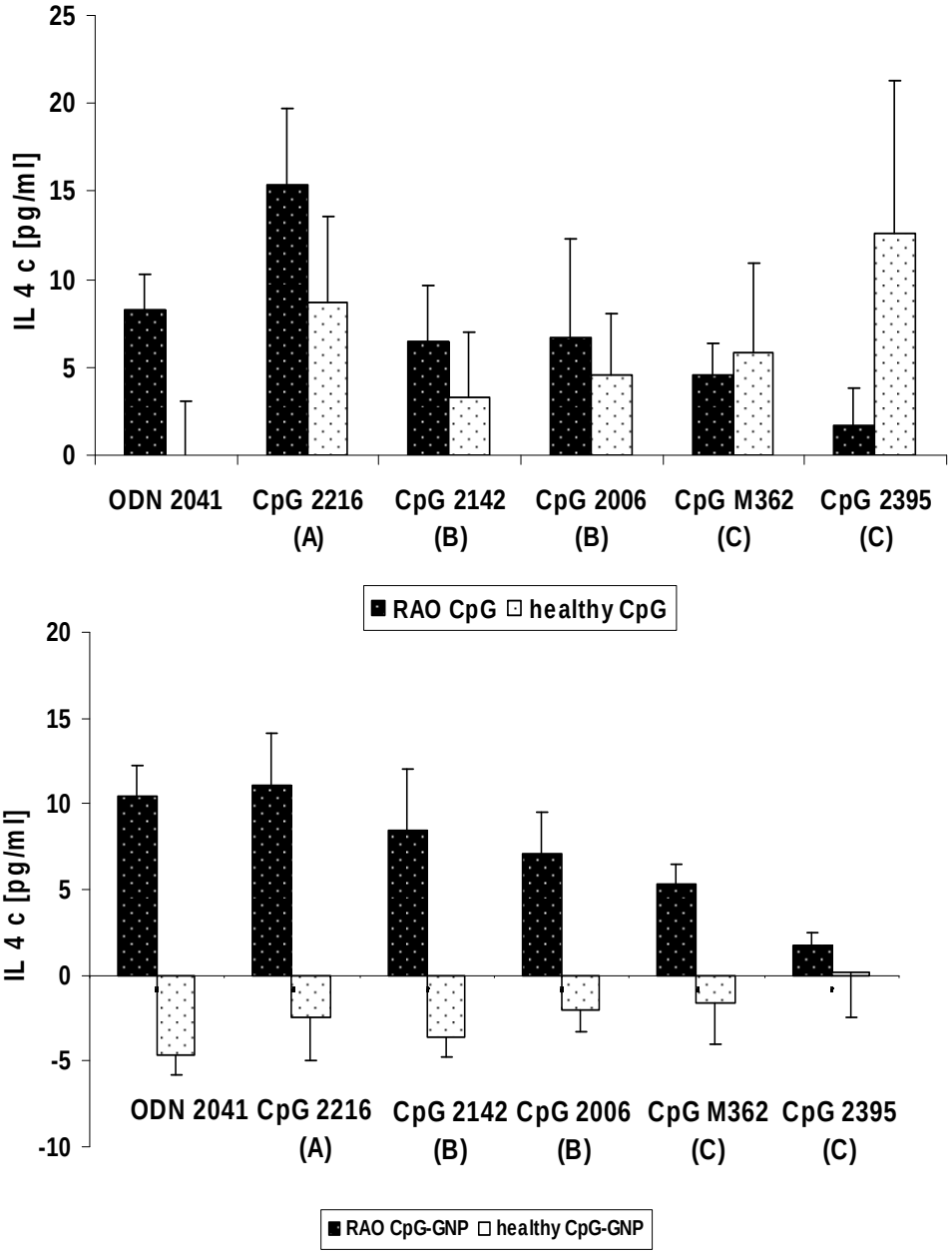

Fig. 2: ***IL-4 expression from BALF cells from healthy and RAO-affected horses with different CpG classes.*** *BAL cells derived from RAO (black bars) or health horses (white bars) were incubated with 13.5 µg of soluble ODN (**A**) or GNP-bound ODN (**B**). Cells from healthy horses secreted significantly lower amounts of IL-4 than those of RAO affected horses (P = 0.001) when treated with GNP-bound ODNs (B). Incubation with soluble ODNs did not result in such significantly distinguishable release (A). Depicted values are group means (n=3, ± S.D.) and corrected by subtraction of the negative control. (Klier 2010)*

Both absolute values were low and inter and intra variations were high. However, as shown in Fig. 2 b difference of high significance (P = 0.001) was found when comparing GNP-bound CpG stimulated cell cultured from RAO and healthy horses for IL-4 release. The latter resulted negative values (Fig. 2 b) while those

of RAO were positive and comparable to those provoked by soluble CpG (P = 0.9469). Furthermore GNP-bound CpG lowered IL-4 release of cells of healthy horses considerably more than soluble CpG (Fig. 2 a) (P = 0.0018).

5.3.2.3 **IFN-γ release**

In Fig. 3 an IFN-γ release from RAO and healthy horses-derived cell cultures is displayed after stimulation by soluble CpGs. On average, no significant difference could be observed between the mean values of both groups (P = 0.3514). However, the six employed ODNs revealed distinctive effects. As seen for IL-10, the highest release was induced by CpG 2216 A-class and accounted for 94 ±10 pg/ml in RAO and 135 ±19 pg/ml in healthy derived cell cultures. All other ODNs induced lower amounts between 15 and 50 pg/ml (Fig. 3 a). A tendency towards higher release by healthy horses-derived cells could be presumed but was not statistically significant (Fig. 3 a). In contrast, GNP-bound ODNs led to a clear discrimination between RAO and healthy derived cells in terms of IFN-γ in Fig. 3 b (P = 0.008). Here, CpG 2216 A-class stimulated the highest IFN-γ secretion as well, accounting for 76 ± 14 pg/ml (healthy) and 25 ± 10 pg/ml (RAO).

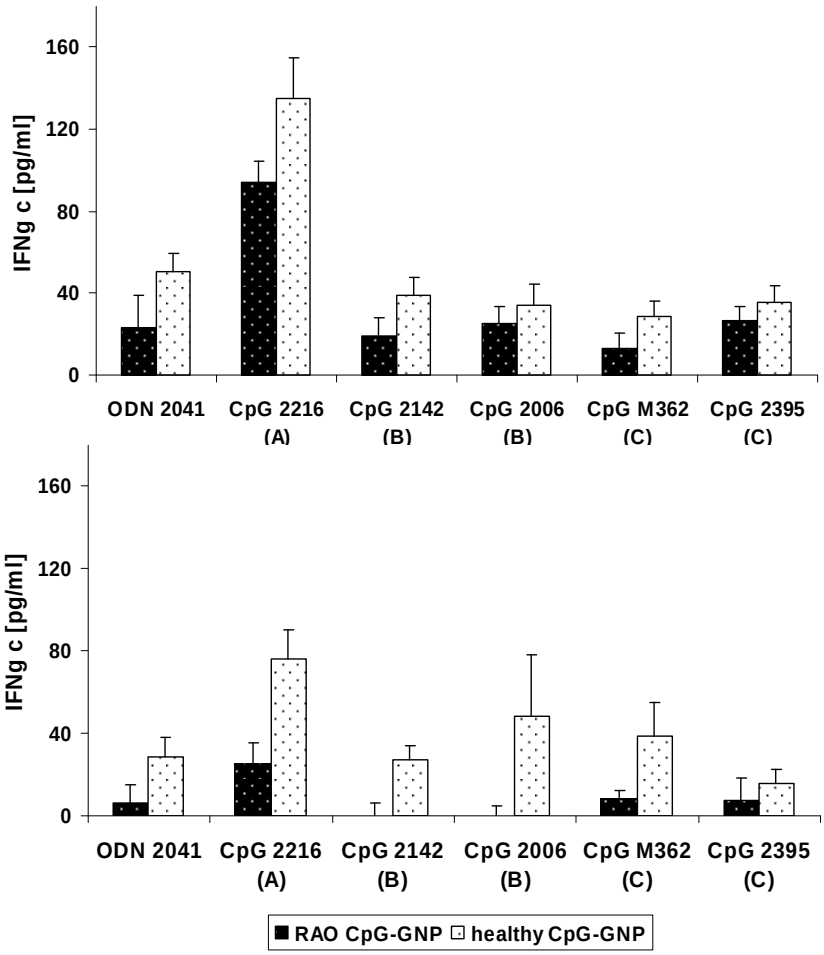

Fig. 3: ***IFN-γ expression from BALF cells from healthy and RAO-affected horses with different CpG classes.*** *BAL cells derived from RAO (black bars) or health horses (white bars) were incubated with 13.5 µg of soluble ODN (**A**) or GNP-bound ODN (**B**). Depicted values are group means (n=3, ± S.D.) and corrected by subtraction of the negative control. (Klier 2010)*

In this individual example (CpG 2216) marginally statistically significant difference was found (P = 0.05). Besides, no or slight release from RAO cell cultures was found (Fig. 3 b), while no statistical significance occurred between the healthy derived cell cultures treated by CpG in comparison by CpG-GNP (P = 0.45).

5.3.3 **MTT assay**

BAL cells from RAO affected and healthy horses were employed to investigate *in vitro* cell viability after 24 h of incubation with regard to detectable differences after administration of soluble ODN compared to GNP bound ODNs. Four mean values (cells from (a) RAO-affected horses on the one hand treated either with

CpG or with CpG-GNP and cells from (b) healthy horses on the other hand treated with CpG or CpG-GNP), were averaged out of the individual viability results of the sixth employed ODNs (Fig. 4). In the healthy group no significant differences were detectable in viability between soluble CpG or CpG-GNP administration. No significant differences were seen between the six individual examined ODNs. Of all evaluated means of the four groups, lowest viability was observed in cells from RAO affected horses treated with soluble CpG (69.7% ± 6.6%). In contrast, cells from RAO horses treated with CpG-GNP showed the highest viability on average 104.3% ± 6.4% which was a statistically significant higher value ($P < 0.0001$). As an example, the difference between cells treated with CpG-ODN 2216 A-class and cells treated with GNP-bound CpG-ODN 2216 A-class was found significant ($P = 0.0405$).

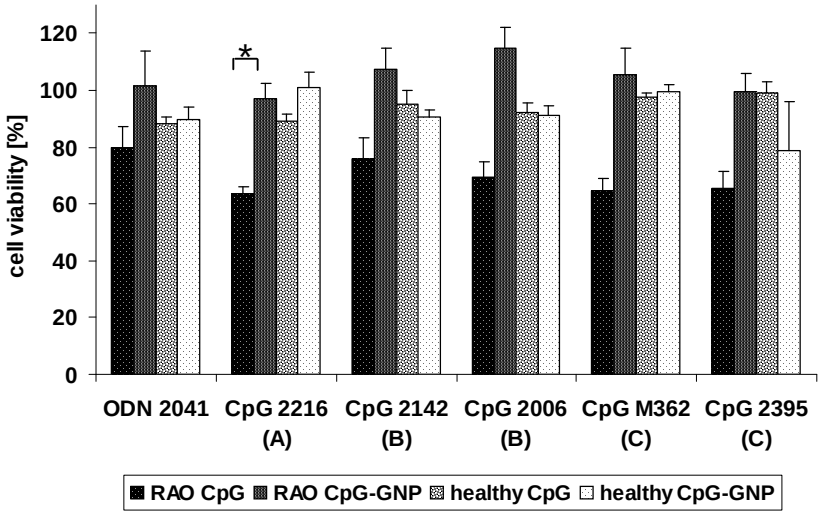

Fig. 4: *Percentile cell viability of BALF cells from healthy and RAO-affected horses challenged with six different CpG classes as per MTT assay. (Klier 2010)*

However, mean viability of cells from healthy horses exposed to soluble CpG was 94.2% ± 4.0% and with CpG-GNP administration 91.7% ± 8.0%. No significant differences were observed between these two mean values ($P = 0.512$). Accordingly, no significant difference was identified in the example of CpG-ODN 2216 A-class ($P = 0.5319$). Moreover, cells derived from RAO and healthy individuals did not differ in viability when challenged with GNP bound CpG-ODN 2216 A-class ($P = 0.808$). Summarizing, BAL cells gained from RAO horses showed significant higher cell viability in MTT assay when incubated with CpG-GNP in comparison to soluble CpG. This difference was not seen in assays

with cells gained from healthy horses.

5.4 Discussion

The major aim of this study was to identify optimal stimulating CpG motifs in horses, concerning Th2/Th1 shift via TLR-9 activation. Optimal TLR-9 agonist sequences were reported to be 5`-GACGTT-3` (Bauer et al., 2001) and 5`-GTCGTT-3` (Hartmann and Krieg, 2000) for murine and human use, respectively. The same motif was found to be beneficial for different animal species including the horse (Rankin et al., 2001). In contrast, ODN sequences containing this motif (2142 and 2006 B-class) were not most effective in stimulating BAL cells in the present study. This contrary could probably be due to different prevalent cell populations between PBMCs and BAL cultures. For horses, Olafsdottir et al. (2004) described an ideal sequence 5`-CTCGTT-3` which indeed hasn't been confirmed by other groups yet. Due to deficiency of knowledge in the action of various CpG motifs on equine BAL cells, motifs with a record of any equine employment were chosen and their distinctive effects were compared. Previously, CpG B 2142 and CpG C 2395 as well as ODN 2041 were used *in vitro* only in equine PBMCs cultures which is a known and well established model (Liu et al., 2008 and 2009). However, as RAO is located in small airways in this study cells were harvested from this specific region to investigate effects on this specialized group of lung cells.

This is the first study which compared the effects of all three CpG classes *in vitro* on equine BAL cells. Furthermore, two different motifs per class except the A class were investigated to gain more insight into motif depending CpG immunostimulation on equine BAL cells. First studies on equine BAL cells were often based on cytokine quantification by mRNA detection instead of translational products themselves by ELISAs. The advantage of measuring proteins directly instead of mRNA is the possibility to exclude posttranscriptional modifications which could influence results quantitatively.

With regard to the results, the optimal stimulating sequence among five explored CpG-ODN in equine BAL cells was the A-class 2216. The detectable IL-10 up regulation was higher than expected as CpGs were previously known for potent IFN-γ release in general and CpG A-class for IFN-α release in particular (Krieg

2002). Characteristics of the A-class which could influence the efficacy are its exceptional backbone structure (backbone chimera), palindrome motif and poly guanine tail which all contributes to a special structure-effect interaction (Krieg 2006). The actual IL-10 cytokine release profile was related to heterogeneous cell composition in BAL (macrophages, neutrophile granulocytes and lymphocytes). TLR-9 receptors were identified as the primary target of CpG-ODNs (Krieg, 2002). Among other cells human plasmacytoid dendritic cells (pDCs) are known to express constitutionally TLR-9 in the endosome. Furthermore pDCs build the first line of antigen presenting cells at the interface between the body surface and the environment and are expected to take up CpG formulations. Human pDCs were shown to form a tight network in the epithelium of conducting upper and lower airways (Garnier and Nicod, 2009). Similarly, it can be assumed that pDCs are located in equine lungs and serve the same functions as in humans. Via the TLR-9 pathway CpG 2216 induced human pDCs which activated $CD4^+$ CD 25^- towards IL-10 producing $CD4^+$ CD 25^+ T-regs by direct cell contact (Moseman et al. 2004).

The potency of employed ODN 2041 (which was lacking a CpG motif) in stimulation of IL-10 probably showed a CpG independent TLR-9 activation mechanism and the importance of sugar backbone on TLR-9 activation (Haas et al., 2008). Synthetic CpG-ODN possesses a modified phosphorothioate sugar backbone which acts as strong TLR-9 antagonist by competitive inhibition (Haas et al., 2008). CpG motifs inverse the antagonistic effect towards a desired TLR-9 stimulation. The high efficiency of phosphorothioate modified CpG-ODN is explicable by 100-fold higher affinity towards TLR-9 in contrast to the original phosphodiester structure in natural prokaryotic DNA as basal TLR-9 agonist (Haas et al., 2008). With regard to participation of IFN-γ in chronically airway inflammation *in vivo* this observation is interesting as a possible therapeutic alternative.

All six ODNs treated cells in BAL from healthy horses showed higher releases of IL-10 and IFN-γ as compared to RAO horses. This was observed regardless of the formulations (CpG, CpG-GNP). The most likely explanation is a difference in cell types. As RAO is expected to be associated with Th2 upregulation less stimulation of Th1 and Treg effects is likely to happen. On the contrary, healthy individuals should have normal regulatory T cell capability which is demonstrated

here by high level of the cytokine IL-10.

All three cytokines detected in cells obtained from healthy horses could serve as important parameter for non allergic lungs under homeostatic immunologic conditions without excessive Th2 response. Therefore, detected cytokine concentrations in healthy individuals could be regarded as benchmarks for a CpG-based immunotherapy of RAO-affected individuals.

With regard to the observation that no significant difference of IL-10 release by cells from RAO-affected horses within CpG classes B and C was detectable, it could be hypothesized that the class is more determining than the individual CpG sequence.

IL-10 decreases IL-4, IL-5 and IFN-γ release (van Scott et al., 2000; Taylor et al., 2006) and could therefore be beneficial to interfere with pathophysiology of RAO. With regard to an expected up regulation of proinflammatory Th1 cytokines by CpG-ODN, IFN-γ release was interestingly relatively low. A possible explanation could be the high amounts of IL-10 which could have inhibited IFN-γ release.

The absolute values of IL-4 concentration were considerably low and below the detection limit of 15.6 pg/ml as given by the ELISA standard curve. However, raw data values were higher before being corrected by subtracting the untreated BAL cell result considered as a negative control. Therefore the observed trends that those cells obtained from healthy horses exhibited lower IL-4 release was considered convincing with regard to earlier findings (Cordeau et al., 2004; Horohov et al., 2005). This is in accordance with the presumption of Th2 downregulation, according to expected Th2/Th1 shift and probably also due to high IL-10 amounts with negative feedback on IL-4 release. These results support the idea of CpG-ODN prominent role in the down regulation of allergic Th2 cytokines (Bohle 2002; Vollmer and Krieg, 2009). Furthermore, GNPs obviously discriminated CpG action towards IL-4 release in cells derived from healthy horses.

CpG-ODN also induces B cells to produce IL-10, which acts in a counter regulatory fashion to limit the inflammatory response to CpG (Kline and Krieg, 2001). This would be beneficial in chronic inflammatory responses like RAO. It is known that a pure Th1 response with IFN-γ could contribute to exacerbation of allergic disease (Umetsu and DeKruyff, 2006). IFN-γ is also produced in lungs of patients with asthma and seems to contribute to severity of the allergic reaction

(Umetsu and DeKruyff, 2006). Th1 cells on their own do not counterbalance Th2 cells but even could augment inflammatory reactions in lungs in an *in vivo* model (Umetsu and DeKruyff, 2006). On the contrary, IFN-γ was found to contribute to inhibitory effects in asthma and allergy in combination with suppressive IL-10 from T-regs (Stock et al., 2004).

Moreover, the IL-4 receptor α (IL-4Rα) gene on chromosome 13 was identified as a candidate gene responsible for RAO (Gerber et al., 2008). IL-4Rα is also associated with asthma and atopy as well as with parasitic defense in humans and animals (Gerber et al., 2009). Gerber et al. found a coherency between intestinal helminthes burden and RAO wherein RAO affected horses showed a significant lower helminthes burden than healthy horses. The same group described the phenomenon as inverse relationship between asthma and the resistance to parasites which seems to correlate with IgE levels (preliminary data). Thus, the abolishment of intestinal helminthes in horses as in humans is supposed to contribute to a rising rate of allergic diseases. Altogether, environmental influences, genetic and epigenetic impacts, feeding and microbial infections which impair body's defense increase the risk to develop allergic airway diseases. This applies to horses as well as humans.

The MTT assay revealed that the various formulations had distinctive impacts on viability of tested BAL cells. The most important observation was the significant difference between CpG and CpG-GNP treated cells from RAO affected horses. The GNP formulated CpGs were less cytotoxic on average for the cell population present in the RAO BAL which is in accordance with earlier findings (Bourquin et al., 2008). In summary, GNPs were shown as an effective and biocompatible nucleotide delivery system in equine *in vitro*. Furthermore, GNPs are expected yet to protect short active A-class from otherwise early degradation. The assignment of A-class CpGs *in vivo* has been limited because of its susceptible backbone structure but its use was recently reported in a clinical study (Senti et al., 2009).

Soluble CpGs result in a significantly higher viability in healthy cells as compared to RAO cells, but still lower than the CpG formulation. This is evident from the IL-10 release profiles where release by healthy horses derived cells are significantly higher than by RAO cells. On the contrary, higher viability of CpG-GNP treated cells does not correspond to higher IL-10 or IFN-γ release. One

explanation could be an overstraining phenomenon of the regulatory cytokine producing cells which were supposed to be present in lower number in BAL from RAO-affected horses than in BAL of healthy horses. The difference in treatment response could be a proof of distinction of RAO and healthy cells on cytokine level *in vitro*. Due to the fact that cell isolation kits for equine BAL cells are not commercially available, it was not possible to stimulate separately isolated cell types for quantification of cytokines. Although, the isolation of individual cells and their quantitative contribution to cytokine release as well as their viability following stimulation are desirable. This may be a necessary precondition for successful future *in vivo* applications. Here, comparable experimental conditions as *in vivo* are given where a heterogenic composition of relevant cells is present. Therefore, intercellular interaction could probably be better reflected to finally predict *in vivo* therapeutic effects. Interestingly, previous human pediatric studies found that numbers of $CD4^+CD25^+$ T-reg cells appeared in decreased amounts in children suffering from asthma (Hartl 2007). Extrapolating this finding to the present equine scenario, a lowered number of $CD4^+CD25^+$ Treg cells in BALF of RAO-affected horses could have caused the observed depletion in IL-10 expression.

In conclusion, CpG-ODN 2216 A-class was identified as most efficient stimulating motif out of the six examined here to trigger IL-10 and IFN-γ in horses. As a potent delivery system GNPs were partially able to enhance CpG impact (IL-4 and IL-10 in cells from healthy horses) and was found to be biocompatible. With regard to RAO, local administration of CpG-ODN/GNP by inhalation has been found to be promising. Besides the conventional symptomatic treatment either by systemic or aerosol administration of β_2-sympathomimetic agents, mucolytic agents and corticosteroids this new approach need to be explored further as interfering with the immunologic pathogenesis could offer an effective anti-hypersensitivity therapy.

6. A nebulized gelatin nanoparticle-based CpG formulation is effective in immunotherapy of allergic horses.

6.1 Introduction

The previous sub-chapters IV.4 and IV.5 rendered obvious that GNPs are suitable for nebulization by active vibrating mesh devices to be administered to the lung. Moreover, this application process did not negatively affect a delicate payload such as CpG-ODNs which remained effective after nebulization. This was confirmed by *in vitro* assays beforehand. Furthermore, an A-class CpG-ODN sequence was identified which exhibited good activation of peripheral tolerance in horses as concluded from the induction of key cytokine IL-10 *in vitro*. Consequently, the next step was to establish a clinical application to proof the tolerability and the effectiveness of the new formulation and application route *in vivo*. Therefore, an aerosol formulation of biodegradable, biocompatible and non-toxic (Bourquin et al. 2008, Zwiorek et al. 2008) GNP-bound CpG-ODN 2216 was used to treat equine RAO in a clinical study. Accordingly, a novel technical combination of an equine spacer for eased application of aerosols and a suitable VM device needed to be introduced. Like human asthma, RAO in horses was considered common multifactor allergic airway hypersensitivity reaction elicited by environmental exposure to potential allergens (Robinson 2001) and heritable components (Gerber et al. 2009). A promising immunotherapeutic strategy against allergic conditions already entering human clinical phase IIa studies involved CpG-ODN (Senti et al. 2009) as synthetic analog of natural microbial CpG-DNA (Krieg 2002). This TLR9 agonist demonstrated efficiency in allergic diseases due to its immunomodulating potential to cause a Th2/Th1 shift (Vollmer and Krieg 2009, Kline 2007, Krieg 2002) which was associated with a downregulation of proallergic Th2 cytokines (IL-4, IL-5, IL-13) and an upregulation of antiallergic Th1 cytokines (IFN γ, IL-12) and an immunoglobulin isotype switch from allergy mediating IgE to IgG (Bohle 2002; Bohle 2002). Before, electrostatically GNP-bound CpG-ODNs were proven to be protected against early degradation by nucleases via steric shielding. Furthermore, cellular uptake of CpG-ODN into target cells was enhanced by nanoparticulate delivery (Zwiorek et al. 2008). In the present study, bronchoalveolar lavage fluid was obtained from healthy and allergic horses to quantify Th1/Th2 cytokine levels before and after novel inhalation regimen to estimate regimen effectiveness on cytokine level. Of equal

importance, clinical symptoms were assessed to obtain information on a possible curative effect. Thus, this study was the first one to provide a proof effectiveness of colloidal nanocarrier-mediated immunotherapy in food-producing animals and constitutes the most advanced project within this thesis.

6.2 Materials and methods

This work was conducted in close and essential cooperation with the Equine Clinic, LMU Munich. Gaining of BAL and diagnosis of clinical symptoms was conducted by veterinarian John Klier. All other experiments were performed alone or in cooperation with him, depending on the individual case.

6.2.1 **Nanoparticle production and loading.**

GNPs were manufactured according to the standard protocol (Coester et al. 2000) as described in chapter II, 1.2.1 using porcine-derived gelatin type A Bloom 175, glutaraldehyde 25% solution, cholamine and 1-Ethyl-3-(3-dimethylaminopropyl)carbodiimide (EDC). All starting materials were purchased from Sigma (Taufkirchen, Germany). The cationization of GNPs and electrostatic binding of CpG-ODN onto the particle surface was described before (Zwiorek et al. 2008). Particle size and surface charge were quantified in 10 mM NaCl before and after loading by a Zetasizer ZS Nano (Malvern Instruments, Malvern, UK). The target surface loading of 5% (w/w) was checked photometrically to ensure colloidal stability of applied dispersions.

6.2.2 **Oligodeoxynucleotides.**

Five different CpG-ODNs and one ODN without CpG motifs were synthesized by Biomers GmbH (Ulm, Germany). All ODNs were single stranded with a length of 20 to 30 bases. The following sequences covered all major three CpG-ODN classes (A-, B- and C-class): ODN 2041 without CpG motif (5`-CTG GTC TTT CTG GTT TTT TTC TGG-3`), CpG-ODN A 2216 (5`-G**\***G**\***G GGA CGA TCG TCG* G**\***G**\***G **\***G**\***G-3`) with its specific chimera backbone structure consisting of phosphorothioate* (PS) and phosphodiester (PD) modified deoxyribose. The latter sequence was the only one to be chosen for direct *in vivo* application (IV, 5)

All other employed sequences were throughout phosphorothioate backbone structured. Moreover, two different B-classes and two different C-classes were matched: CpG B ODN 2142 (5`-TCG CGT GCG TTT TGT CGT TTT GAC GTT-3`), CpG B ODN 2006 (5`-TCG TCG TTT TGT CGT TTT GTC GTT-3`), CpG C ODN 2395 (5`-TCG TCG TTT TCG GCG CGC GCC G-3`) and CpG C ODN M362 (5`-TCG TCG TCG TTC GAA CGA CGT TGA T-3`).

6.2.3 **CpG-GNP formulation.**

A working concentration of 3 mg/ml for GNPs and of 1.0 mg/ml for ODNs was adjusted. For *in vitro* cell cultures, 278 µg of GNPs loaded with 14 µg of ODN were applied per well which corresponded to 0.87 mg/ml GNP and 0.044 mg/ml of ODN. As references, CpG-ODN solutions of every class with a concentration of 0.044 mg/ml and GNP dispersion concentrated 0.87 mg/ml were added per applicable well. For inhalation studies, 3.75 mg GNPs were loaded with 187.5 µg ODN in a total volume of 2.5 ml highly purified water (HPW) were used per individual inhalation.

6.2.4 **Nebulization.**

For inhalation studies, an Equine Haler™ spacer (Equine HealthCare Aps, Hoersholm, Denmark) and an AeroNeb Go™ vibrating mash nebulizer (Aerogen, Galway, Ireland) were combined by a 90° glass connector with ground joints that suitably matched the aerosol generator part's outlet diameter and the spacer's inlet (Fig. 1).

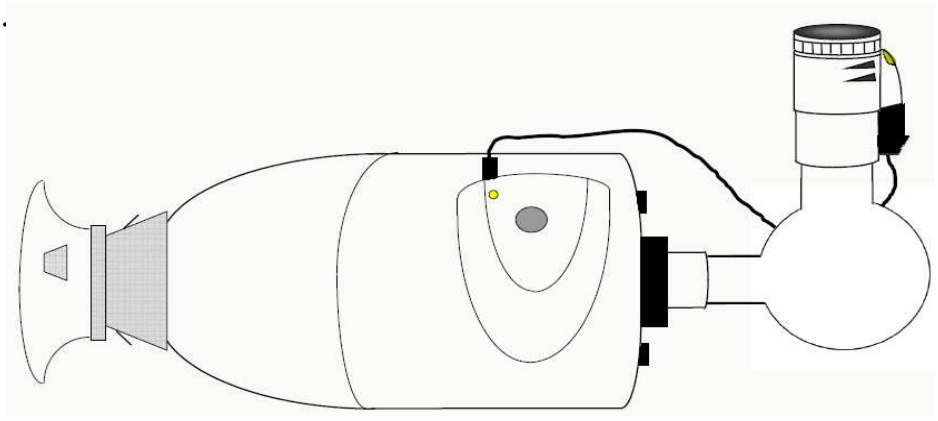

Fig. 1: *Technical setup of the combined VM-device with the equine inhalation spacer.*

The identical protocol was run for negative control placebo trial and for the medication trial. The negative control exclusively contained an aqueous (HPW)

GNP dispersion (1.5 mg/ml) while the medication was a combination of GNP (1.5 mg/ml) and CpG-ODN 2216 (0.075 mg/ml). Healthy and RAO-affected horses were inhaled three times alike with two-day intervals between individual administrations followed by a control BAL. Two additional subsequent inhalations and one final BALF examination for disease development monitoring were added if significant changes occurred after the third inhalation. Clinical examinations, blood gas analysis, endoscopic exploration and cytology of TBS were performed at the beginning, after three and finally after five inhalations.

6.2.5 **Clinical examination and lung scoring.**

A lung scoring system (Gerber et al. 2004) was further developed comprising clinical parameters (nasal discharge, breathing rate), blood gas chemistry, endoscopic exploration, cytology of tracheobronchial secret (TBS) and of bronchoalveolar lavage fluid (BALF). Accordingly, 14 horses of a mean weight of 477.7 kg and aged 12.0 years on average were scored. The applied scoring system allowed grouping the patients into four categories (healthy, mild, moderate and severe RAO). For the clinical trial, three groups of horses were established, with the first group (n = 4) consisting of healthy horses (mean age of 8.8 years) for the placebo negative control, the second group (n = 4) consisting of healthy horses for compatibility study (mean age of 10.4 years) and the third group (n = 4) of moderate RAO-affected horses for therapeutic efficiency verification (mean age of 16.8 years). TBS scoring (grades 0-5) was performed according to Gerber et al. (2004): 0 = none, clean, singular TBS; 1 = little, multiple small blobs; 2 = moderate large blobs; 3 = marked, confluent/stream-forming; 4 = large, pool-forming; 5 = extreme, profuse amounts. The key arterial blood gas parameter of partial pressure of oxygen (PaO_2) was measured by a Radiometer Copenhagen NPT 7 series (Radiometer GmbH, Willich-Schiefbahn, Germany). Physiological values for PaO_2 were set to 100 mmHg (±5 mmHg). Moreover, percentages of neutrophile granulocytes out of total cell count from TBS cytology were calculated after staining by Diff-Quick® staining set (Medion diagnostics, Düdingen, Switzerland). Physiological range of breathing rate was defined as 8 to 16 breaths per minute while higher values were considered as pathological.

6.2.6 **Cell culture and *in vitro* cytokine quantification.**

BALF was taken from every horse before and after inhalation regime (50 ml/100 kg body weight sterile, warm, isotonic NaCl solution). Gained cell suspension was centrifuged by 1200 g for 6 minutes. Supernatants were stored immediately at -80 °C on dry ice in the stable for cytokine conservation. Then, supernatants were analyzed for IL-4, IL-10 and IFN-γ by equine duo set ELISA kits according to the manufacturer's protocol (R&D Systems, Minneapolis, USA) (Fig. 2).

Total cell count was determined and subsequently cells were seeded, stimulated by six ODNs and checked for cytokines as described above in 5.2.4 and 5.2.5. The *in vitro* stimulation before and after *in vivo* inhalation was assessed due to the pictured design of experiment (Fig. 2). The study was approved and was designated the No 55.2-1-54-2531-31-10 by the legal agency for animal experiments (Regierung von Oberbayern, Munich, Germany).

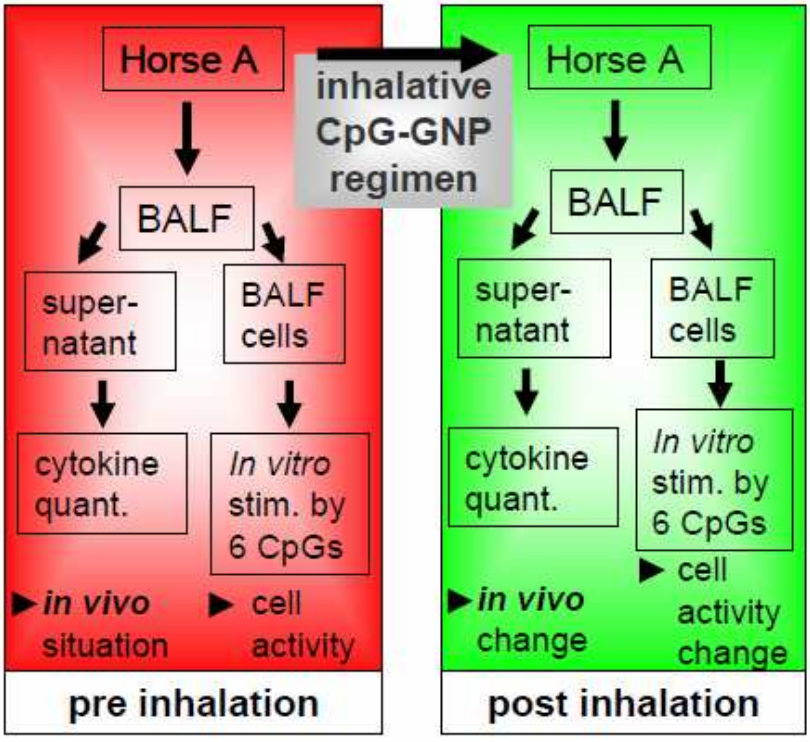

Fig. 2: *Overview on the combined in vitro and in vivo study design to investigate the inhalative regimen's influence both on changes in BALF cytokine composition and on changes in cell composition and activity after an additional CpG stimulation in vitro. As an example, the full set of experiments for a single horse is pictured.*

6.2.7 **Statistical analysis.**

Comparisons between groups (normally distributed) were carried out using the unpaired Student`s *t*-test. N is shown in parenthesis for each calculation in Figure legends. All statistical analysis was performed using Prism Graph (Version 5.0, GraphPad software Inc., La Jolla, USA).

6.3 Results and Discussion

6.3.1 **Tracking the regimen's therapeutic effect *in vitro***

To evaluate the efficiency of envisaged inhalation therapy, BALF was obtained both from RAO-affected and healthy horses before and after the inhalation regimen GNP-bound CpG-ODN 2216. Data from healthy individuals served as physiological reference. First, BALF cells of RAO-affected horses were stimulated *in vitro* by six different ODNs as described in chapter IV.5 (scheme Fig. 2). Averaged results depicted in Fig 3a and 3b imply a major impact of the inhalation therapy in RAO-affected individuals. Fig. 3a shows *in vitro* IL-10 expression of cells derived from RAO-affected horses treated by ODNs and GNP-bound ODNs both before and after inhalation.

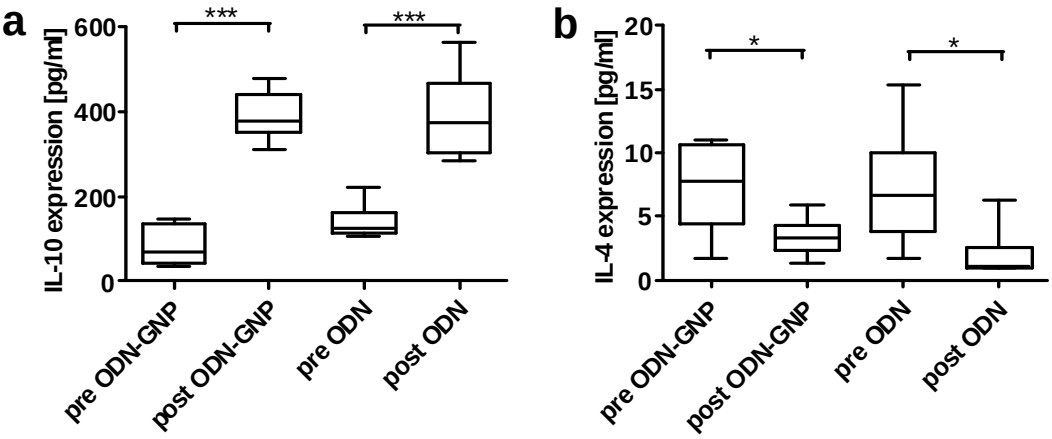

Fig. 3: ***Release of key cytokines from BALF cells gained from RAO-affected horses stimulated in vitro by ODN and ODN-GNP before (pre) and after (post) in vivo inhalation therapy, respectively. a,*** *IL-10 release from cell cultures stimulated by soluble ODN and ODN-GNP is increased by inhalation therapy of GNP-bound ODN and subsequent in vitro stimulation (n=18, ± S.D) by 6 different GNP-bound ODNs or by 6 different soluble ODNs on average.* ***b,*** *IL-4 release is accordingly decreased.*

After inhalation treatment, a significantly ($P < 0.0001$) higher IL-10 release (390 pg/ml) in BAL cell cultures stimulated by GNP-bound ODNs was observed

as compared to the state before inhalation treatment (83 pg/ml) (Fig. 3a). Similar trend of IL-10 release was observed after stimulation (389 pg/ml) by soluble ODNs (Fig. 3a) compared to the value of 139 pg/ml before inhalation regime ($P = 0.0002$). This could be due to the fact that the inhalation therapy triggered antiallergic IL-10 producing cells in BAL. Accordingly, IL-4 *in vitro* expression was decreased significantly after inhalations of both soluble ($P = 0.0298$) and GNP-bound ($P = 0.0282$) ODNs although the absolute values were comparably low (Fig. 3b). These findings indicated that Th2-mediated proallergic immune response was reduced. In contrast to high IL-10 values *in vitro*, especially after inhalation treatment, low amounts of both IFN-γ and IL-4 could be regarded as a negative feedback mechanism by IL-10 (Taylor et al. 2006; Van Scott et al. 2000). In contrast, Th_1 upregulation (IFN-γ) was expected after treatment with CpG-ODN. Yet, measured IFN-γ values (data not shown) could not confirm the Th1 upregulation and might have been influenced by high IL-10 values. However, low IFN-γ levels could be considered as beneficial in chronic inflammatory processes (Umetsu and DeKruyff 2006).

Overall, IFN-γ release *in vitro* was low and did not reveal a general trend after treatment by GNP-bound ODNs ($P = 0.1414$) or by soluble ODNs ($P = 0.4870$) before (pre) versus after (post) inhalation treatment of RAO affected horses. However, CpG A-class exhibited higher stimulation before and after inhalation treatment as compared to all the other CpG-classes (data not shown).

6.3.2 **Therapeutic effect on cytokine level *in vivo***

As a key cytokine to mediate tolerance, IL-10 was our primary interest in the evaluation of cytokine expression after administration of GNP-bound CpG-ODN *in vivo*. Fig. 4a clearly depicts the *in vivo* increase of IL-10 expression detected in BALF supernatant in RAO-affected horses. While three inhalations led to a significant 3.8-fold increase ($P = 0.0473$) in IL-10 expression, a 6.9-fold increase was found after five inhalations (Fig. 4a). Therefore, the average IL-10 levels differ significantly ($P = 0.034$) before starting and after finishing the full five inhalation regimen applied to RAO-affected horses. Healthy horses exhibited a 2.14 fold augmentation in IL-10 expression after pulmonal administration of GNP-bound CpG-ODN confirming the principle of action (Fig. 4a).

However, differences in expression levels before and after inhalation were marginally statistically significant (P = 0.089). In contrast, no significant difference (P = 0.289) was found when comparing healthy horses before and after three inhalative administrations of blank GNPs which was given as placebos (Fig. 4a).

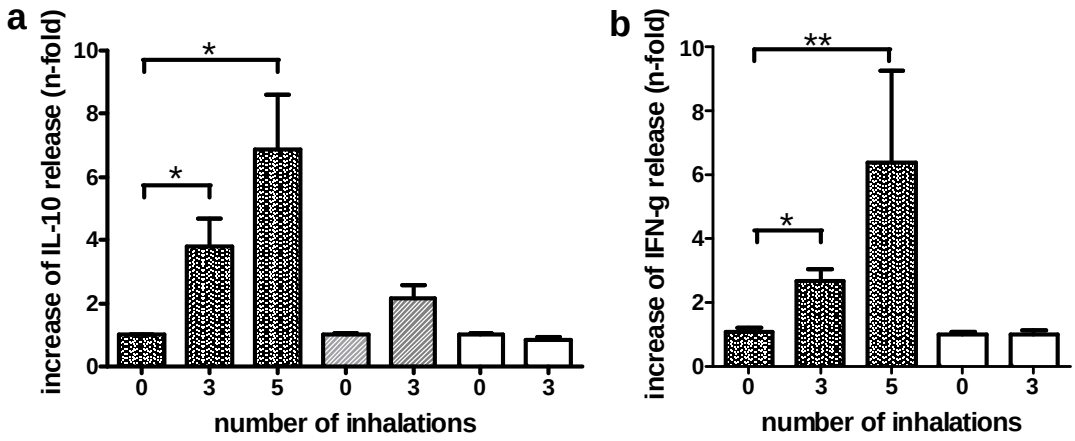

Fig. 4: ***Effect of GNP-bound CpG-ODN and plain GNPs on cytokine release in vivo before and after inhalation therapy. a,*** *IL-10 release is expressed as n-fold increase based on 1 as initial value before inhalation. IL-10 release from RAO-affected horses (n=4, ± S.D.) before and after three and five inhalation of GNP-bound CpG-ODN (black bars), from healthy horses (n = 4, ± S.D.) before and after three inhalations of GNP-bound CpG-ODN (grey bars) and from healthy horses (n=4, ± S.D.) before and after three inhalations of plain GNP (white bars).* ***b,*** *IFN-g(amma) release from RAO-affected horses before and after three and five inhalation of GNP-bound CpG-ODN (black bars) and from healthy horses before and after three inhalations of plain GNP (white bars).*

Therefore, it was concluded that IL-10 could be induced following administration of CpG-GNP through inhalation in RAO affected horses. The studies of previous chapter V.5 led to the decision to employ CpG-ODN 2216 (A-class) *in vivo* due to superior IL-10 inducing properties from equine BAL cells compared to representatives of the B- and C-class. Likely, IL-10 could be beneficial in avoiding allergic inflammatory immune response towards allergen contact and could therefore prevent tissue injury by neutrophile degranulation. In humans, increase in IL-10 by established antiallergic medication such as glucocorticoids or allergen immunotherapy was frequently attributed to the activation of T-reg cells (Ryanna et al. 2009). Asthmatic human patients showed lower amounts of T-regs

in BAL compared to healthy ones which corresponds to the lack of peripheral tolerance (Hartl et al. 2007). Therefore, it was hypothesized that the found increased IL-10 expression could be related to higher or nearly physiologic (equivalent to healthy) Treg cell numbers in the lower airways. Furthermore, it is known that CpG-ODN activates plasmoidal dendritic cells (Moseman et al. 2004) which reside the lower airways (von Garnier and Nicod 2009). In addition, it was shown earlier that CpG-ODN promoted both IL-12 and IL-10 release by dendritic cells which led to increased IL-12 mediated Th1 and IL-10 mediated Treg induction (Jarnicki et al. 2008). Thus, it can be concluded from the present study that GNP-bound CpG-ODN induced release of IL-10 contributed to Treg cell-mediated peripheral tolerance which would be beneficial as an innovative and alternative treatment of allergic airway diseases (Umetsu et al. 2006, Ryanna et al. 2009, Moseman et al. 2004).

In vivo secretion of IL-4 and IFN-γ was analyzed in BALF supernatants before and after inhalation regimens. IL-4 levels were below detection threshold *in vivo*. For IFN-γ, a significant impact of GNP-bound CpG-ODN was observed. Fig. 4b reveals a constant increase after three and five consecutive inhalations compared to IFN-γ levels in BAL supernatants before the regimen ($P = 0.0034$). Placebo administration did not result in altered cytokine expression ($P = 0.8322$) (Fig. 4b) while IFN-γ data could not be obtained from healthy individuals treated with GNP-bound CpG-ODN. However, increased IFN-γ expression by GNP-bound CpG-ODN met the expectation of CpG-ODN-driven Th1 activation. Furthermore, the parallel increase of IFN-γ in combination with suppressive cytokine IL-10 was reported to be beneficial in challenging allergic conditions (Stork et al. 2004). This finding also supports the previously discussed Th2/Th1 shift away from Th2 associated proallergic pathways (Jurk and Vollmer 2007).

6.3.3 **Curative effectiveness of the GNP-based formulation**

Beside cytokine-based immunologic parameters, the clinical impact of the hereby proposed therapy was assessed. First, the breathing rate per minute was assessed as an easily accessible clinical parameter to discriminate healthy and RAO affected individuals. RAO affected horses exhibited a breathing rate of

19.6 (± 1.47) breaths per minute (bpm) before treatment (Fig. 5a) which was significantly higher than the measured bpm value 13.6 (± 0.98) of healthy horses (P = 0.0094). The regimen (five doses) lowered the rate significantly down to 12.8 (± 0.80) bpm (P = 0.0036). After treatment the breathing rate no longer differed significantly from physiological values (8- 16 bpm) of healthy horses (P = 0.5447) (Fig. 5a). Therefore, it can be concluded that the regimen potentially contributes to a normalization of bpm of RAO affected horses.

The determination of blood gas was used to evaluate the extent of gas exchange and the response to treatment (Robinson 2001). The magnitude of gas exchange abnormality correlates with the severity of bronchiolitis and clinical signs (Robinson 2001). In this study, it was observed that healthy horses had a PaO_2 of 94 mmHg (± 2.07) (Fig. 5b). In contrast, RAO-affected horses showed a PaO_2 of 86.75 mmHg (± 2.29) (Fig. 5b). This mean value was significantly improved (P = 0.0153) towards 95.6 mmHg (± 1.69) by the full regimen of five inhalations (Fig. 5b). Thereafter, no statistically significant difference was observed compared with the healthy animals (P = 0.5384). Although not significant, variability in this study before and after treatment was considerable in healthy individuals. Therefore, this clinical parameter should not be regarded as robust as previously discussed criteria.

Healthy individuals exhibit airways which are free of mucus deposition. A typical clinical sign of RAO is the appearance of excessive mucus accumulation within the trachea by dyscrine and hypercrine pathological action known as tracheobronchial secretion (TBS).

This clinical sign was positively affected by the treatment of five inhalations as the graded TBS score decreased (P = 0.1078) from 2.7 (± 0.436) to 1.7 (± 0.34) (Fig. 5c). However, TBS values of RAO-affected horses did not dwindle to physiological levels which accounted for 0.3 (± 0.20) on average but remained significantly higher (P = 0.0019) than those of healthy subjects (Fig. 5c). Additional studies need to clarify whether a longer regimen can ameliorate the already observed positive trend in TBS reduction.

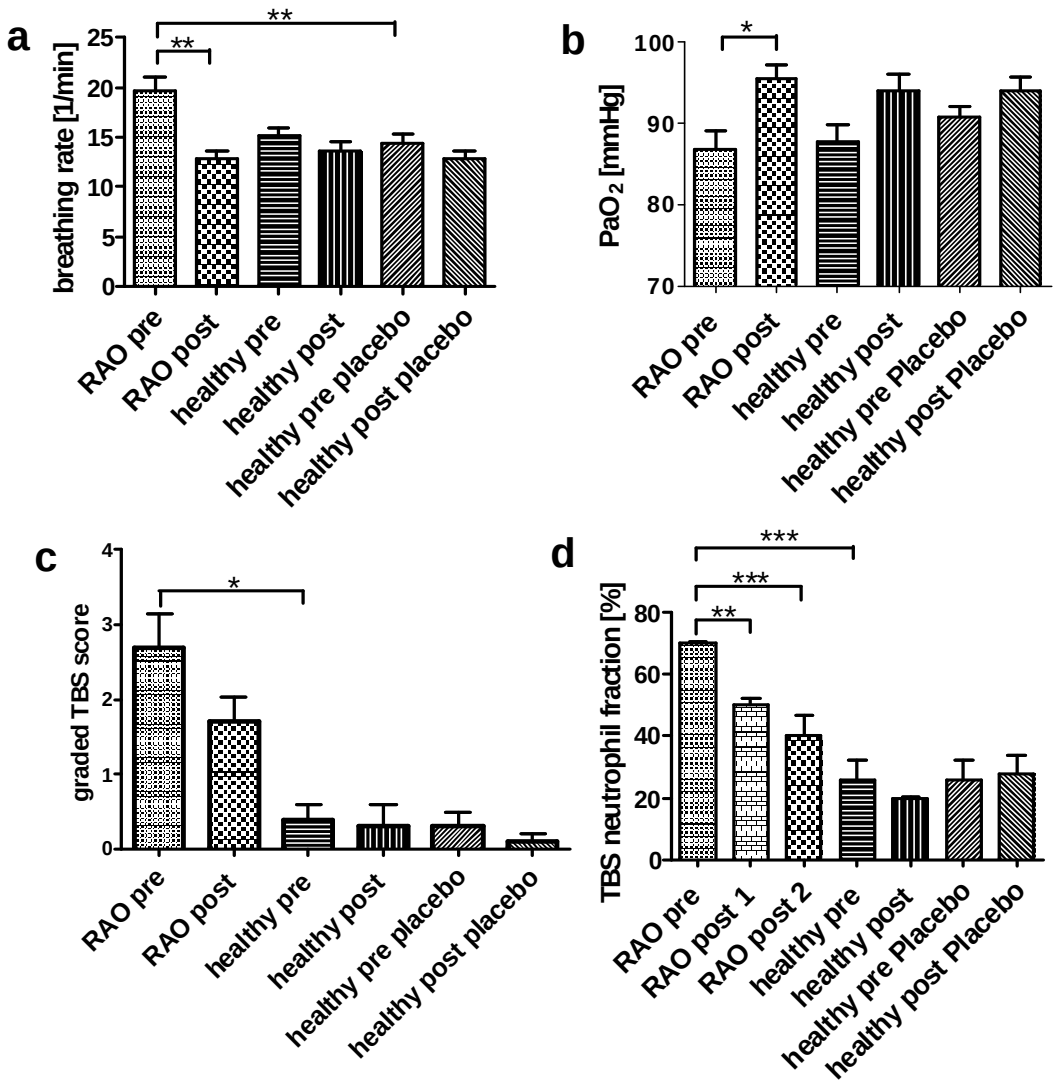

Fig. 5: ***Therapeutic effect of GNP-bound CpG-ODNs versus plain GNPs (placebo) on important clinical parameters. a,*** *Breathing rate before and after treatment by GNP-bound CpG-ODN in RAO-affected horses (n=4, ± S.D.), before and after treatment by GNP-bound CpG-ODN in healthy horses (n=4, ± S.D.) and before and after treatment by GNPs (placebo) in healthy horses (n=4, ± S.D., left to right).* ***b,*** *Oxygen partial pressure in arterial blood before and after respective treatments.* ***c,*** *Occurrence of tracheobronchial secrete before and after respective treatments.* ***d,*** *Percentile of neutrophil granulocytes in the TBS before and after respective treatments.*

Within TBS, the percentage of neutrophile granulocytes represents a strong indicator for RAO (Lavoie et al. 2001). Moreover, it is regarded as one of the most decisive parameters to evaluate RAO. Consequently, determined levels were high (70% ± 0.50) in RAO individuals before treatment and differed significantly from values of healthy horses exhibiting 26% (± 6.0) ($P = 0.0004$) (Fig. 5d). Treatment by GNP-bound CpG-ODN contributed to a significant decrease down

to 50% (± 2.04) by three inhalations ($P < 0.0001$) and down to 40% (± 6.52) by five inhalations ($P = 0.0048$), respectively (Fig. 5d). The percentage of neutrophiles within the TBS was directly related to the severity of the RAO condition. Therefore, it can be deducted that the severity of the pathogenesis was significantly reduced after five applications of GNP-bound CpG-ODN as no statistically significant difference could be observed compared to healthy horses ($P = 0.195$). Furthermore, Fig. 5d shows that in healthy horses neither the GNP-bound CpG-ODN ($P = 0.3472$) nor the placebo ($P = 0.8171$) resulted in a significant change of neutrophile percentages, respectively. Previously, T-reg activation was related to a reduction in activity and the number of neutrophile granulocytes by promoting their rate of apoptosis (Lewkowicz et al. 2006). Human neutrophiles are responsible to express all known TLRs except TLR3 (Lewkowicz et al .2006). Moreover, TLRs were shown to possess a crucial impact on T-reg stimulation and function (Lewkowicz et al. 2006). Beyond, TLRs were referred to play an integral part in the organisation of innate immune responses and indirect control of the adaptive immunity by activating antigen presenting cells (Pasare and Medzhitov 2003). Previous investigations confirmed that T-reg cells inhibit neutrophiles other than by direct cell-cell contact mechanism (CTLA-4/B7-1 mechanism) and especially through IL-10 action (Montagnoli et al. 2006). Furthermore, this mechanism was advantageous in the treatment of allergic diseases (Umetsu and DeKruyff 2006).

6.4 Conclusion

Above all, the GNP-based formulation was shown to be well tolerated *in vivo*. The observed impressive IL-10 induction by the hereby proposed treatment could directly be related to the clinically apparent decreasing neutrophile percentage. Therefore, IL-10 induction most likely contributed to the regimen's anti-RAO effectiveness. Consequently, further studies with higher patient numbers and dose escalation are in planning state to elucidate the full potential of this first applied inhalative nanoparticle based immunotherapy in food producing animals.

V Final conclusion and outlook

1. Enhanced production opportunities

Up-scaling of the original manufacturing setup was technically possible and performed up to ten-fold increased batch sizes. Systematic correlation studies enabled the establishment of a set of equations to predict necessary GNP preparation parameters for each relevant batch size. This shall contribute to future higher GNP demand in clinical manufacturing.

Moreover, the feasibility of replacing well-established but initially toxic starting material glutaraldehyde as a cross-linking agent by the enzymatic alternative Transglutaminase was demonstrated.

2. Analytics

Ultrasonic resonator technology was demonstrated as a capable tool in relative GNP size analysis and ODN surface binding detection which could serve in future as a non-destructive tool for online in-process control in continuous GNP production. Within this study, a variable response of cationized and non-cationized GNPs towards distinctive buffers was observed. The swelling and size reduction was in accordance with the salts of the Hofmeister series.

Of special importance was the successful radio-labeling of GNPs by radionuclides $^{111}In^{+}$ or $^{68}Ga^{3+}$ respectively, to monitor their biodistribution after s.c. or i.v. administration both by conservative sectioning and PET. PEGylation was conducted and proofed for several molecular weights. However, no enhanced circulation properties could be obtained due the prevalent hydrophilic properties of the starting molecule gelatin. Nevertheless, the radio-labeling technique could be beneficial in new applications such as the monitoring of inhaled GNPs and in the quantification of the resulting lung deposition.

3. Immunotherapy

3.1 Adjuvant cancer immunotherapy

In continuation of promising *in vitro* and *in vivo* studies on the employment of GNP-bound CpG-ODN as an adjuvant in OVA-targeted cancer immunotherapy, initial trials on the isRNA-mediated immunostimulation clearly demonstrated that GNPs can be of benefit in facilitating to address also the TLR-7 in antitumoral settings. Here, isRNA superiorly entered the target lysosome when transport was GNP-mediated e.g. in contrast to DOTAP-mediated transport. GNPs effectively protected the isRNA from degradation upon RNAse challenge. Immunostimulation was successful as revealed by activation of relevant DC markers such as CD69 and most important, survival of pre-immunized and OVA-expressing tumor challenged mice was significantly prolonged. Ongoing studies indicate that this promising strategy is working in a therapeutic model setting, too. Thus, GNP-based isRNA formulations could be capable to cure existing tumors.

3.2 Immunomodulative effectiveness of GNP-bound CpG-ODN in a preclinical canine study

The impressive benefit of CpG A-class delivery by GNPs to PBMCs in terms of antiallergic IL-10 release was revealed in a canine *in vitro* study. This laid the foundation for further, now starting, *in vivo* studies to elucidate the possibility of a therapeutic option against common canine atopic dermatitis by modulative CpG-based immunotherapy.

3.3 Immunomodulative therapy of RAO horses – preliminary clinical trial

Finally, a novel approach in equine RAO therapy was established, constituting the first-time ever immunotherapeutic clinical study associated with a colloidal carrier system. First, an appropriate combination of nebulizer and spacer to nebulize CpG-GNP formulations was developed. Then, a suitable CpG sequence to stimulate equine BAL cells was identified. However, this chosen CpG 2216 sequence was the prototype of CpG A-class and other sequences might even more potently initiate desired cytokine production. For instance, the potent A-class sequence used for the canine study would be an interesting approach because a CpG with a fully phosphothioated backbone was used. In addition to the originally intended higher backbone stability and resistance against nucleases of

the fully phosphothioated backbone CpG, an eased fashion of particle surface loading could have contributed to an enhanced effect. The fully phosphothioated CpG variant may lead to a lower extend to self-aggregation and auto-particle forming as CpG A-class with chimeric backbones tended to do. Consequently, individual ODNs may remain through increased inter-ODN electrostatic repulsion on the one hand and higher electrostatic attraction to cationized GNPs on the other hand.

On cytokine detection level, it was remarkably possible to distinguish RAO-affected from healthy horses *in vitro*. Most notably, regulatory cytokine IL-10 expression was significantly triggered *in vivo* by five consecutive inhalations in RAO-affected horses. The entirety of clinical parameters assessed after nanoparticle treatment indicated a partial remission of the allergic condition. In particular, breathing rates were lowered to physiologic level, blood oxygen partial pressure was significantly elevated, the pathogenic TBS score values were moderately reduced and the RAO-determinant content of neutrophile granulocytes within the TBS was more than halved on average. Therefore, this preliminary clinical study showed for the first time safety and curative effectiveness of colloidal nanocarrier-mediated immunotherapy in food-producing animals.

3.4 Outlook on further planned clinical studies on RAO

To elucidate its full potential, the therapy's effectiveness has to be validated in further steps. Therefore, higher patient numbers and patients affected with severe RAO will be employed in projected follow-up studies in cooperation with a large pharmaceutical company providing that the constant supply of high-quality GNPs can be maintained in the medium term. Of essential importance will be additional controls to include both placebo and soluble (non GNP-bound) CpG in RAO-affected horses. Moreover, as the present preliminary clinical study just illustrated the effect of a five-fold inhalation protocol over a relatively short period of time (less than a month), evaluation of both immunologic and curative long-term effects and the establishment of a dose-response-curve will be crucial steps towards a possible future drug career.

4. Outlook on the perspective of nanoparticles in nanomedicine

Translating laboratory innovation into clinical products with commercial success is challenging which applies especially to nanoparticle-based Nanomedicine. The Food and Drug Administration (FDA) addressed this issue by releasing the "Critical Path Opportunities List and Report". Comparably, the European Medicines Agency (EMEA) set up a regulatory agenda for Nanomedicine. Essentially, the FDA identified seven main challenges for nanomedicine to achieve market registration approval that must be scientifically overcome. Such challenges range from biodistribution knowledge mentioned in chapter III.4 gained by robust and reliable imaging techniques and insight into the detailed mass transport across compartmental boundaries in the body, new mathematical computer models to predict risk benefit and risk parameters of nanoparticles to finally establish an obligate standard and reference material system to which one can refer in nanomaterial research. The latter is promoted by the National Cancer Institute's Nanotechnology Characterization laboratory.

Future perspectives concerning the clinical use of nanoparticles include both the possibility to detect and treat diseases at earlier stages than available today.

Moreover, nanoparticles could function as a platform for the detection of biomarkers including proteins, nucleic acids or metal ions and therefore be valuable in early stage diagnosis.

Today, nanoparticle-enabled drug delivery stands at a decisive crossroad whether to proceed into the direction of highly complex systems towards "nanorobots" or to turn into a "keep it simple" strategy. At least mid-term orientated, the latter appears to be more reasonable at least for two basic fundamentals: regulatory issues and price. Clearly, the more complex the nanoparticulate device is, the more potential risks does it bear. This covers the manufacturing process, where an incredibly high monitoring effort for specification compliance must be accounted for and finally stretches to the animal or human patient. *In vivo*, a multitude of components might possess their own unique degradation and metabolism pathways. In the end, the two most crucial factors are safety and reproducibility. Resulting costs will be high and only reimbursed by public health authorities and insurances if convincing therapeutic benefits are guaranteed in the increasingly competitive pharmaceutical market. Nevertheless, nanoparticle-based

nanomedicine holds a great promise to contribute to improved health care, more efficient health economics and personalized medicine.

VI References

Abbas, A.K., Lichtman, A.H., and Pillai, S. "Cellular and Molecular Immunology." 6th Edition, Section IV: *Cytokines*, Elsevier Saunders, 267-301. 2010.

Ablasser, A., Poeck, H., Anz, D., Berger, M., Schlee, M., Kim, S., Bourquin, C., Goutagny, N., Jiang, Z., Fitzgerald, K. A., Rothenfusser, S., Endres, S., Hartmann, G., and Hornung, V. Selection of Molecular Structure and Delivery of RNA Oligonucleotides to Activate TLR7 versus TLR8 and to Induce High Amounts of IL-12p70 in Primary Human Monocytes. J.Immunol. 182[11], 6824-6833. 2009.

Aboudan, M., Waldrep, C., and Dhand, R. Comparison of vibrating aperture plate nebulizer with standards jet nebulizer using aqueous and liposomal albuterol formulations. 169[A]. Am. J. Resp. Crit. Care Med. 2004

Ainsworth, D. M. "Just how important is IL 17 in horses wit hRAO." *World Equine Airways symposium*, C. Tessier, and V. Gerber, eds., Pabst Science Publishers, Bern, 100-102. 2009.

Ainsworth, D. M., Grunig, G., Matychak, M. B., Young, J., Wagner, B., Erb, H. N., and Antczak, D. F. Recurrent airway obstruction (RAO) in horses is characterized by IFN-gamma and IL-8 production in bronchoalveolar lavage cells. Vet.Immunol.Immunopathol. 96[1-2], 83-91. 2003.

Akdis, M., Verhagen, J., Taylor, A., Karamloo, F., Karagiannidis, C., Crameri, R., Thunberg, S., Deniz, G., Valenta, R., Fiebig, H., Kegel, C., Disch, R., Schmidt-Weber, C. B., Blaser, K., and Akdis, C. A. Immune responses in healthy and allergic individuals are characterized by a fine balance between allergen-specific T regulatory 1 and T helper 2 cells. J.Exp.Med. 199[11], 1567-1575. 2004.

Alignani, D., Maletto, B., Liscovsky, M., Ropolo, A., Moron, G., and Pistoresi-Palencia, M. C. Orally administered OVA/CpG-ODN induces specific mucosal and systemic immune response in young and aged mice. J.Leukocyte Biol. 77[6], 898-905. 2005.

Allen, T. M., and Cullis, P. R. Drug Delivery Systems: Entering the Mainstream. Science 303[5665], 1818-1822. 2004.

Altieri, D. C. Blocking survivin to kill cancer cells. Methods in Molecular Biology 223[Tumor Suppressor Genes, Volume 2], 533-542. 2003.

Amidi, M., Romeijn, S. G., Borchard, G., Junginger, H. E., Hennink, W. E., and Jiskoot, W. Preparation and characterization of protein-loaded N-trimethyl chitosan nanoparticles as nasal delivery system. J.Controlled Release 111[1-2], 107-116. 2006.

Angel, J. B., Cooper, C. L., Clinch, J., Young, C. D., Chenier, A., Parato, K. G., Lautru, M., Davis, H., and Cameron, D. W. CpG increases vaccine antigen-specific cell-mediated immunity when administered with hepatitis B vaccine in HIV infection. J Immune Based Ther Vaccines 6, 4. 2008.

Anz, D., Koelzer, V. H., Moder, S., Thaler, R., Schwerd, T., Lahl, K., Sparwasser, T., Besch, R., Poeck, H., Hornung, V., Hartmann, G., Rothenfusser, S., Bourquin, C., and Endres, S. Immunostimulatory RNA Blocks Suppression by Regulatory T Cells. J.Immunol. 184[2], 939-946. 2010.

Archakov, A. I., and Ivanov, Y. Analytical nanobiotechnology for medicine diagnostics. Molecular BioSystems 3[5], 336-342. 2007.

Babel, W. "Gelatine - Ein vielseitiges Biopolymer." *Chemie in unserer Zeit*, 30(2), 1-11. 1996.

Balthasar, S., Michaelis, K., Dinauer, N., von Briesen, H., Kreuter, J., and Langer, K. Preparation and characterization of antibody modified gelatin nanoparticles as drug carrier system for uptake in lymphocytes. Biomaterials 26[15], 2723-2732. 2005.

Bandol, Y. Research highlights. Nat. Rev. Iummunol. 10, 380. 2010.

Barbu, E., Molnar, E., Tsibouklis, J., and Gorecki, D. C. The potential for nanoparticle-based drug delivery to the brain: overcoming the blood-brain barrier. Expert Opin.Drug Delivery 6[6], 553-565. 2009.

Barnhart, J., Levene, H., Villapando, E., Maniquis, J., Fernandez, J., Rice, S., Jablonski, E., Gjoen, T., and Tolleshaug, H. Characteristics of Albunex: air-filled albumin microspheres for echocardiography contrast enhancement. Invest Radiol 25 Suppl 1, S162-S164. 1990.

Beck-Broichsitter, M., Gauss, J., Gessler, T., Seeger, W., Kissel, T., and Schmehl, T. Pulmonary Targeting with Biodegradable Salbutamol-Loaded Nanoparticles. J.Aerosol Med.Pulm.Drug Delivery 23[1], 47-57. 2010.

Beck-Broichsitter, M., Gauss, J., Packhaeuser, C. B., Lahnstein, K., Schmehl, T., Seeger, W., Kissel, T., and Gessler, T. Pulmonary drug delivery with aerosolizable nanoparticles in an ex vivo lung model. Int.J.Pharm. 367[1-2], 169-178. 2009.

Bernkop-Schnuerch, A., Heinrich, A., and Greimel, A. Development of a novel method for the preparation of submicron particles based on thiolated chitosan. Eur.J.Pharm.Biopharm. 63[2], 166-172. 2006.

Bernstein, I. L. Bronchoalveolar lavage in asthma--"something old, something new . . .". J Allergy Clin Immunol 74[1], 22-25. 1984.

Bhavsar, M. D., and Amiji, M. M. Oral IL-10 gene delivery in a microsphere-based formulation for local transfection and therapeutic efficacy in inflammatory bowel disease. Gene Ther 15[17], 1200-1209. 2008.

Bhavsar, M. D., and Amiji, M. M. Gastrointestinal distribution and in vivo gene transfection studies with nanoparticles-in-microsphere oral system (NiMOS). J.Controlled Release 119[3], 339-348. 2007.

Bivas-Benita, M., Laloup, M., Versteyhe, S., Dewit, J., De Braekeleer, J., Jongert, E., and Borchard, G. Generation of Toxoplasma gondii GRA1 protein and DNA vaccine loaded chitosan particles: preparation, characterization, and preliminary in vivo studies. International Journal of Pharmaceutics 266[1-2], 17-27. 2003.

Bohle, B. CpG Motifs as Possible Adjuvants for the Treatment of Allergic Diseases. Int.Arch.Allergy Immunol. 129[3], 198-203. 2002.

Borch, R. F., Bernstein, M. D., and Durst, H. D. Cyanohydridoborate anion as a selective reducing agent. J.Amer.Chem.Soc. 93[12], 2897-2904. 1971.

Bourquin, C., Schmidt, L., Lanz, A.L., Storch, B., Wurzernberger, C., Anz, D., Berger, M., Poeck, H., Hartmann, G., Hornung, V., and Endres, S. Immunostimulatory RNA oligonucleotides induce an effective antitumoral NK cell response through TLR7 Journal of Immunology. 183, 6078-6086. 2009.

Bourquin, C., Anz, D., Zwiorek, K., Lanz, A. L., Fuchs, S., Weigel, S., Wurzenberger, C., von der Borch, P., Golic, M., Moder, S., Winter, G., Coester, C., and Endres, S. Targeting CpG Oligonucleotides to the Lymph Node by Nanoparticles Elicits Efficient Antitumoral Immunity. Journal of Immunology 181[5], 2990-2998. 2008.

Bourquin, C., Schmidt, L., Hornung, V., Wurzenberger, C., Anz, D., Sandholzer, N., Schreiber, S., Voelkl, A., Hartmann, G., and Endres, S. Immunostimulatory RNA oligonucleotides trigger an antigen-specific cytotoxic T-cell and IgG2a response. Blood 109[7], 2953-2960. 2007.

Bourquin, C., Schreiber, S., Beck, S., Hartmann, G., and Endres, S. Immunotherapy with dendritic cells and CpG oligonucleotides can be combined with chemotherapy without loss of efficacy in a mouse model of colon cancer. Int J Cancer 118[11], 2790-2795. 2006.

Bouxsein, N. F., McAllister, C. S., Ewert, K. K., Samuel, C. E., and Safinya, C. R. Structure and Gene Silencing Activities of Monovalent and Pentavalent Cationic Lipid Vectors Complexed with siRNA. Biochemistry 46[16], 4785-4792. 2007.

Brannon-Peppas, L., Ghosn, B., Roy, K., and Cornetta, K. Encapsulation of Nucleic Acids and Opportunities for Cancer Treatment. Pharmaceutical Research 24[4], 618-627. 2007.

Braun-Fähränder, C. "Role of environment in asthma, endotoxin and other factors." *Wolrd Equine Airway Symposium*, C. Tessier, and V. Gerber, eds., Pabst Science Publishers, 44-46. 2009.

Brazolot Millan, C. L., Weeratna, R., Krieg, A. M., Siegrist, C. A., and Davis, H. L. CpG DNA can induce strong Th1 humoral and cell-mediated immune responses against hepatitis B surface antigen in young mice. Proc Natl Acad Sci U S A 95[26], 15553-15558. 1998.

Brigger, I., Dubernet, C., and Couvreur, P. Nanoparticles in cancer therapy and diagnosis. Advanced Drug Delivery Reviews 54[5], 631-651. 2002.

Brinckmann, J., Notbohm, H., Mueller, P. K., and Editors. "Collagen: Primer in Structure, Processing and Assembly". 2005.

Brindle, K. New approaches for imaging tumor responses to treatment. Nat.Rev.Cancer 8[2], 94-107. 2008.

Broomfield, S. A., van der Most, R. G., Prosser, A. C., Mahendran, S., Tovey, M. G., Smyth, M. J., Robinson, B. W. S., and Currie, A. J. Locally Administered TLR7 Agonists Drive Systemic Antitumor Immune Responses That Are Enhanced by Anti-CD40 Immunotherapy. J.Immunol. 182[9], 5217-5224. 2009.

Brown, A. R., and George, D. W. Tetrafluoroethane (HFC 134A) propellant-driven aerosols of proteins. Pharm.Res. 14[11], 1542-1547. 1997.

Brown, S. D., Nativo, P., Smith, J. A., Stirling, D., Edwards, P. R., Venugopal, B., Flint, D. J., Plumb, J. A., Graham, D., and Wheate, N. J. Gold Nanoparticles for the Improved Anticancer Drug Delivery of the Active Component of Oxaliplatin. J.Am.Chem.Soc. 132[13], 4678-4684. 2010.

Buckin, V. A., Kankiya, B., I, and Kazaryan, R. L. Hydration of nucleosides in dilute aqueous solutions. Ultrasonic velocity and density measurements. Biophys Chem 34[3], 211-223. 1989.

Buckin, V., O'Driscoll, B., Smyth, C., Alting, A. C., and Visschers, R. W. Ultrasonic spectroscopy for material analysis. Recent advances. Spectroscopy Europe 15[1], 20,22-20,25. 2003.

Butz, N., Porte, C., Courrier, H., Krafft, M. P., and Vandamme, T. Reverse water-in-fluorocarbon emulsions for use in pressurized metered-dose inhalers containing hydrofluoroalkane propellants. Int.J.Pharm. 238[1-2], 257-269. 2002.

Cacciuttolo, M. A., and Arunakumari, A. Scale-up considerations for biotechnology-derived products. Drugs Pharm.Sci. 157[Pharmaceutical Process Scale-Up (2nd Edition)], 129-160. 2006.

Castanotto, D., and Rossi, J. J. The promises and pitfalls of RNA-interference-based therapeutics. Nature (London, U.K.) 457[7228], 426-433. 2009.

Cetin, M., Aktas, Y., Vural, I., Capan, Y., Dogan, L. A., Duman, M., and Dalkara, T. Preparation and In Vitro Evaluation of bFGF-Loaded Chitosan Nanoparticles. Drug Delivery 14[8], 525-529. 2007.

Chadwick, S., Kriegel, C., and Amiji, M. Nanotechnology solutions for mucosal immunization. Adv.Drug Delivery Rev. 62[4-5], 394-407. 2010.

Chalikian, T. V., Plum, G. E., Sarvazyan, A. P., and Breslaver, K. J. Influence of Drug Binding on DNA Hydration: Acoustic and Densimetric Characterizations of Netropsin Binding to the Poly(dAdT).Poly(dAdT) and Poly(dA).Poly(dT) Duplexes and the Poly(dT).Poly(dA).Poly(dT) Triplex at 25 DegC. Biochemistry 33[29], 8629-8640. 1994.

Chavany, C., Trung, L. D., Couvreur, P., Puisieux, F., and Helene, C. Poly(alkyl cyanoacrylate) nanoparticles as polymeric carriers for antisense oligonucleotides. Pharmaceutical Research 9[4], 441-449. 1992.

Chawla, J. S., and Amiji, M. M. Biodegradable poly(.vepsiln.-caprolactone) nanoparticles for tumor-targeted delivery of tamoxifen. Int.J.Pharm. 249[1-2], 127-138. 2002.

Chen, C. Q., Lin, W., Coombes, A. G., Davis, S. S., and Illum, L. Preparation of human serum albumin microspheres by a novel acetone-heat denaturation method. J Microencapsul 11[4], 395-407. 1994.

Cheon, J. W., Choi, J.-S., Yoo, J., Park, J. C., and Chang, Y. Nanoparticles as dual-modality PET/MRI contrast agents. (Industry-Academic Cooperation Foundation, Yonsei University S. Korea and Kyungpook National University Industry-Academic Cooperation Foundation). 2009-KR2441[2009136764], 56pp. 20091112. WO. 8-5-2009.

Childs, C. E. (1975). "Determination of polyoxyethylen glycol in gamma-globulin solutions." *Microchem, J,* 20, 190-192.

Cho, Y. W., Park, J. H., Park, J. S., and Park, K. Pegylation: camouflage of proteins, cells, and nanoparticles against recognition by the body's defense mechanism. Handb.Pharm.Biotechnol. 443-461. 2007.

Cho, Y. W., Park, S. A., Han, T. H., Son, D. H., Park, J. S., Oh, S. J., Moon, D. H., Cho, K. J., Ahn, C. H., Byun, Y., Kim, I. S., Kwon, I. C., and Kim, S. Y. In vivo tumor targeting and radionuclide imaging with self-assembled nanoparticles: Mechanisms, key factors, and their implications. Biomaterials 28[6], 1236-1247. 2006.

Christiansen, C., Vebner, A. J., Muan, B., Vik, H., Haider, T., Nicolaysen, H., and Skotland, T. Lack of an immune response to Albunex, a new ultrasound contrast agent based on air-filled albumin microspheres. Int.Arch.Allergy Immunol. 104[4], 372-378. 1994.

Coester, C. J., Langer, K., Von Briesen, H., and Kreuter, J. Gelatin nanoparticles by two step desolvation-a new preparation method, surface modifications and cell uptake. Journal of Microencapsulation 17[2], 187-193. 2000.

Coester, C., Nayyar, P., and Samuel, J. In vitro uptake of gelatin nanoparticles by murine dendritic cells and their intracellular localisation. European Journal of Pharmaceutics and Biopharmaceutics 62[3], 306-314. 2006.

Coley, W. B. The treatment of malignant tumors by repeated inoculations of erysipelas. With a report of ten original cases. 1893. Clin Orthop Relat Res [262], 3-11. 1893.

Cordeau, M. E., Joubert, P., Dewachi, O., Hamid, Q., and Lavoie, J. P. IL-4, IL-5 and IFN-gamma mRNA expression in pulmonary lymphocytes in equine heaves. Vet.Immunol.Immunopathol. 97[1-2], 87-96. 2004.

Couvreur, P., Kante, B., Roland, M., and Speiser, P. Adsorption of antineoplastic drugs to poly(alkyl cyanoacrylate) nanoparticles and their release in calf serum. J.Pharm.Sci. 68[12], 1521-1524. 1979.

Creticos, P. S., Schroeder, J. T., Hamilton, R. G., Balcer-Whaley, S. L., Khattignavong, A. P., Lindblad, R., Li, H., Coffman, R., Seyfert, V., Eiden, J. J., and Broide, D. Immunotherapy with a ragweed-Toll-like receptor 9 agonist vaccine for allergic rhinitis. New England Journal of Medicine 355[14], 1445-1455. 2006.

Dailey, L. A., Schmehl, T., Gessler, T., Wittmar, M., Grimminger, F., Seeger, W., and Kissel, T. Nebulization of biodegradable nanoparticles: impact of nebulizer technology and nanoparticle characteristics on aerosol features. J.Controlled Release 86[1], 131-144. 2003.

Debbage, P. Targeted drugs and nanomedicine: present and future. Curr.Pharm.Des. 15[2], 153-172. 2009.

DeBoer, D. J., and Marsella, R. The ACVD task force on canine atopic dermatitis (XII): the relationship of cutaneous infections to the pathogenesis and clinical course of canine atopic dermatitis. Vet Immunol Immunopathol 81[3-4], 239-249. 2001.

Debrue, M., Hamilton, E., Joubert, P., Lajoie-Kadoch, S., and Lavoie, J. P. Chronic exacerbation of equine heaves is associated with an increased expression of interleukin-17 mRNA in bronchoalveolar lavage cells. Vet.Immunol.Immunopathol. 105[1-2], 25-31. 2005.

Decuzzi, P., and Ferrari, M. The role of specific and non-specific interactions in receptor-mediated endocytosis of nanoparticles. Biomaterials 28[18], 2915-2922. 2007.

DeFrancesco, L. Dynavax trial halted. Nat.Biotechnol. 26[5], 484. 2008.

Diebold, S. S., Kaisho, T., Hemmi, H., Akira, S., and Reis e Sousa, C. Innate Antiviral Responses by Means of TLR7-Mediated Recognition of Single-Stranded RNA. Science (Washington, DC, United States) 303[5663], 1529-1532. 2004.

Diepold, R., Kreuter, J., Guggenbuhl, P., and Robinson, J. R. Distribution of poly-hexyl-2-cyano-[3-14C]acrylate nanoparticles in healthy and chronically inflamed rabbit eyes. Int.J.Pharm. 54[2], 149-153. 1989.

Dinauer, N., Balthasar, S., Weber, C., Kreuter, J., Langer, K., and von Briesen, H. Selective targeting of antibody-conjugated nanoparticles to leukemic cells and primary T-lymphocytes. Biomaterials 26[29], 5898-5906. 2005.

Dow, S. W. Liposome-nucleic acid immunotherapeutics. Expert Opin.Drug Delivery 5[1], 11-24. 2008.

Duclairoir, C., Orecchioni, A. M., Depraetere, P., Osterstock, F., and Nakache, E. Evaluation of gliadins nanoparticles as drug delivery systems: a study of three different drugs. Int.J.Pharm. 253[1-2], 133-144. 2003.

Duncan, R. Polymer therapeutics into the 21st century. ACS Symposium Series 752[Controlled Drug Delivery], 350-363. 2000.

Duncan, R. Polymer conjugates for drug targeting. From inspired to inspiration! Journal of Drug Targeting 14[6], 333-335. 2006.

Duncan, R., Ringsdorf, H., and Satchi-Fainaro, R. Polymer therapeutics-polymers as drugs, drug and protein conjugates and gene delivery systems: past, present and future opportunities. Journal of Drug Targeting 14[6], 337-341. 2006.

Eggers, F. Ultrasonic velocity and attenuation measurements in liquids with resonators, extending the MHz frequency range. Acustica 76[5], 231-240. 1992.

Eisenbarth, S. C., Colegio, O. R., O'Connor, W., Sutterwala, F. S., and Flavell, R. A. Crucial role for the Nalp3 inflammasome in the immunostimulatory properties of aluminum adjuvants. Nature (London, U.K.) 453[7198], 1122-1126. 2008.

Elhissi, A. M. A., and Taylor, K. M. G. Delivery of liposomes generated from proliposomes using air-jet, ultrasonic, and vibrating-mesh nebulisers. J.Drug Delivery Sci.Technol. 15[4], 261-265. 2005.

Elhissi, A. M. A., Karnam, K. K., nesh-Azari, M. R., Gill, H. S., and Taylor, K. M. G. Formulations generated from ethanol-based proliposomes for delivery via medical nebulizers. J.Pharm.Pharmacol. 58[7], 887-894. 2006.

Fan, Y. F., Wang, Y. N., Fan, Y. G., and Ma, J. B. Preparation of insulin nanoparticles and their encapsulation with biodegradable polyelectrolytes via the layer-by-layer adsorption. Int.J.Pharm. 324[2], 158-167. 2006.

Ferrari, M. Cancer nanotechnology: opportunities and challenges. Nat.Rev.Cancer 5[3], 161-171. 2005.

Ferrari, M. Nanogeometry: beyond drug delivery. Nat Nanotechnol 3[3], 131-132. 2008.

Fey, K. "Nichtinfektiöse Krankheiten der tiefen Atemwege und der Lunge." *Handbuch der Pferdepraxis*, O. Dietz, and B. Huskamp, eds., Enke Verlag, 326-336. 2006.

Finlay, W. H., Roa, W., and Loebenberg, R. Formulation of powder containing nanoparticles for aerosol delivery to the lungs. Can.Patent 2003-624475[2005019270], 12. 20050127. US. 23-7-2003.

Fonseca, D. E., and Kline, J. N. Use of CpG oligonucleotides in treatment of asthma and allergic disease. Adv.Drug Delivery Rev. 61[3], 256-262. 2009.

Franc, B. L., Acton, P. D., Mari, C., and Hasegawa, B. H. Small-animal SPECT and SPECT/CT: important tools for preclinical investigation. J Nucl Med 49[10], 1651-1663. 2008.

Fraunhofer, W., Winter, G., and Coester, C. Asymmetrical Flow Field-Flow Fractionation and Multiangle Light Scattering for Analysis of Gelatin Nanoparticle Drug Carrier Systems. Analytical Chemistry 76[7], 1909-1920. 2004.

Frenkel, V., and Li, K. C. P. Potential role of pulsed-high intensity focused ultrasound in gene therapy. Future Oncol. 2[1], 111-119. 2006.

Friess, W. Collagen. Biomaterial for drug delivery. European Journal of Pharmaceutics and Biopharmaceutics 45[2], 113-136. 1998.

Fuchs, S. "Gelatin Nanoparticles as a Modern Platform for Drug Delivery". Dissertation, Ludwig Maximilans University Munich. 2010

Fuchs, S., Hertel, T. C., Winter, G., Pietzsch, M., and Coester, C. "Transglutaminase, a new approach in gelatin nanoparticle crosslinking". In revision, J Microencap. 2010.

Fuchs, S., Zwiorek, K., Wester, H. J., Winter, G., and Coester, C. "In vivo tracking of Ga-68 labeled gelatin nanoparticles by positron emisson tomography". Proceeding at AAPS Annual Meeting and exposition, Atlanta, 2008

Fuchs, S., Winter, G., and Coester, C. Ultrasonic resonator technology as a new quality control method evaluating gelatin nanoparticles. J.Microencapsulation 27[3], 242-252. 2010.

Fuertges, F., and Abuchowski, A. The clinical efficacy of polyethylene glycol-modified proteins. Journal of Controlled Release 11[1-3], 139-148. 1990.

Fujita, Y., Mie, M., and Kobatake, E. Construction of nanoscale protein particle using temperature-sensitive elastin-like peptide and polyaspartic acid chain. Biomaterials 30[20], 3450-3457. 2009.

Funck, T., De Maeyer, L., Chalikian, T. V., Belonenko, V. N., and Sarvazyan, A. P. A novel approach to the thermodynamic properties of fluid systems using acoustical measurements. Calorimetrie et Analyse Thermique 24, 139-142. 1993.

Gaur, U., Sahoo, S. K., De, T. K., Ghosh, P. C., Maitra, A., and Ghosh, P. K. Biodistribution of fluoresceinated dextran using novel nanoparticles evading reticuloendothelial system. Int.J.Pharm. 202[1-2], 1-10. 2000.

Gekko, K. Hydration of biopolymers. Kobunshi 51[7], 496-499. 2002.

Gekko, K. and Noguchi, H. Compressibility of globular proteins in water at 25 DegC. J.Phys.Chem. 83[21], 2706-2714. 1979.

Geng, Y., Dalhaimer, P., Cai, S., Tsai, R., Tewari, M., Minko, T., and Discher, D. E. Shape effects of filaments versus spherical particles in flow and drug delivery. Nat.Nanotechnol. 2[4], 249-255. 2007.

Gerber, V., Straub, R., Marti, E., Hauptman, J., Herholz, C., King, M., Imhof, A., Tahon, L., and Robinson, N. E. Endoscopic scoring of mucus quantity and quality: observer and horse variance and relationship to inflammation, mucus viscoelasticity and volume. Equine Vet J 36[7], 576-582. 2004.

Gharwan, H., Wightman, L., Kircheis, R., Wagner, E., and Zatloukal, K. Nonviral gene transfer into fetal mouse livers (a comparison between the cationic polymer PEI and naked DNA). Gene Ther. 10[9], 810-817. 2003.

Ghazanfari, T., Elhissi, A. M. A., Ding, Z., and Taylor, K. M. G. The influence of fluid physicochemical properties on vibrating-mesh nebulization. Int.J.Pharm. 339[1-2], 103-111. 2007.

Giljohann, D. A., Seferos, D. S., Patel, P. C., Millstone, J. E., Rosi, N. L., and Mirkin, C. A. Oligonucleotide Loading Determines Cellular Uptake of DNA-Modified Gold Nanoparticles. Nano Letters 7[12], 3818-3821. 2007.

Giroux, H. J., Houde, J., and Britten, M. Preparation of nanoparticles from denatured whey protein by pH-cycling treatment. Food Hydrocolloids 24[4], 341-346. 2010.

Gradishar, W. J., Tjulandin, S., Davidson, N., Shaw, H., Desai, N., Bhar, P., Hawkins, M., and O'Shaughnessy, J. Phase III trial of nanoparticle albumin-bound paclitaxel compared with polyethylated castor oil-based paclitaxel in women with breast cancer. J.Clin.Oncol. 23[31], 7794-7803. 2005.

Grafe, K. A., and Hoffmann, H. Development and validation of an indirect enzyme-linked immunosorbent assay (ELISA) for the nonsteroidal anti-inflammatory drug S-ibuprofen. Pharmazie 55[4], 286-292. 2000.

Gref, R., Luck, M., Quellec, P., Marchand, M., Dellacherie, E., Harnisch, S., Blunk, T., and Muller, R. H. 'Stealth' corona-core nanoparticles surface modified by polyethylene glycol (PEG): influences of the corona (PEG chain length and surface density) and of the core composition on phagocytic uptake and plasma protein adsorption. Colloids Surf., B 18[3,4], 301-313. 2000.

Grenha, A., Seijo, B., and Remunan-Lopez, C. Microencapsulated chitosan nanoparticles for lung protein delivery. Eur.J.Pharm.Sci. 25[4-5], 427-437. 2005.

Gu, W., Xu, Z., Gao, Y., Chen, L., and Li, Y. Transferrin-mediated PEGylated nanoparticles for delivery of DNA/PLL. Nanotechnology 17[16], 4148-4155. 2006.

Hadinoto, K., Zhu, K., and Tan, R. B. H. Drug release study of large hollow nanoparticulate aggregates carrier particles for pulmonary delivery. Int.J.Pharm. 341[1-2], 195-206. 2007.

Halliwell, R. E., McGorum, B. C., Irving, P., and Dixon, P. M. Local and systemic antibody production in horses affected with chronic obstructive pulmonary disease. Vet Immunol Immunopathol 38[3-4], 201-215. 1993.

Hargreaves, R. J. The role of molecular imaging in drug discovery and development. Clin Pharmacol Ther 83[2], 349-353. 2008.

Haroon, A., Waldrep, J. C., and Dhand, R.. Proc. Am. Thorac. Soc. 2[A808]. 2005

Harries, M., Ellis, P., and Harper, P. Nanoparticle albumin-bound paclitaxel for metastatic breast cancer. J.Clin.Oncol. 23[31], 7768-7771. 2005.

Harris, T. J., Green, J. J., Fung, P. W., Langer, R., Anderson, D. G., and Bhatia, S. N. Tissue-specific gene delivery via nanoparticle coating. Biomaterials 31[5], 998-1006. 2010.

Hartl, D., Koller, B., Mehlhorn, A. T., Reinhardt, D., Nicolai, T., Schendel, D. J., Griese, M., and Krauss-Etschmann, S. Quantitative and functional impairment of pulmonary CD4+CD25hi regulatory T cells in pediatric asthma. J.Allergy Clin.Immunol. 119[5], 1258-1266. 2007.

Hartmann, G., and Krieg, A. M. Mechanism and function of a newly identified CpG DNA motif in human primary B cells. J.Immunol. 164[2], 944-952. 2000.

Hashimoto, M., Asahina, Y., Sano, J., Kano, R., Moritomo, T., and Hasegawa, A. Cloning of canine Toll-like receptor 9 and its expression in dog tissues. Vet.Immunol.Immunopathol. 106[1-2], 159-163. 2005.

Heil, F., Hemmi, H., Hochrein, H., Ampenberger, F., Kirschning, C., Akira, S., Lipford, G., Wagner, H., and Bauer, S. Species-Specific Recognition of Single-Stranded RNA via Toll-like Receptor 7 and 8. Science (Washington, DC, U.S.) 303[5663], 1526-1529. 2004.

Hemmi, H., Takeuchi, O., Kawai, T., Kaisho, T., Sato, S., Sanjo, H., Matsumoto, M., Hoshino, K., Wagner, H., Takeda, K., and Akira, S. A Toll-like receptor recognizes bacterial DNA. Nature (London) 408[6813], 740-745. 2000.

Hillaireau, H., and Couvreur, P. Nanocarriers' entry into the cell: Relevance to drug delivery. Cell.Mol.Life Sci. 66[17], 2873-2896. 2009.

Hobohm, U., Stanford, J. L., and Grange, J. M. Pathogen-associated molecular pattern in cancer immunotherapy. Crit.Rev.Immunol. 28[2], 95-107. 2008.

Hoffman, A. M. Bronchoalveolar lavage: sampling technique and guidelines for cytologic preparation and interpretation. Vet Clin North Am Equine Pract 24[2], 423-35, vii. 2008.

Hoffmann, F., Sass, G., Zillies, J., Zahler, S., Tiegs, G., Hartkorn, A., Fuchs, S., Wagner, J., Winter, G., Coester, C., Gerbes, A. L., and Vollmar, A. M. A novel technique for selective NF-kappaB inhibition in Kupffer cells: contrary effects in fulminant hepatitis and ischaemia-reperfusion. Gut 58[12], 1670-1678. 2009.

Hoffmann, F. Decoy gelatin nanoparticles as a novel tool to elucidate the role of NF-kB in Kupffer cells on hepatic ischemia/reperfusion injury. Dissertation, Ludwig Maximilans University Munich. 2006.

Hornung, V., Ellegast, J., Kim, S., Brzozka, K., Jung, A., Kato, H., Poeck, H., Akira, S., Conzelmann, K. K., Schlee, M., Endres, S., and Hartmann, G. 5'-Triphosphate RNA Is the Ligand for RIG-I. Science (Washington, DC, United States) 314[5801], 994-997. 2006.

Hornung, V., Guenthner-Biller, M., Bourquin, C., Ablasser, A., Schlee, M., Uematsu, S., Noronha, A., Manoharan, M., Akira, S., de Fougerolles, A., Endres, S., and Hartmann, G. Sequence-specific potent induction of IFN-alpha by short interfering RNA in plasmacytoid dendritic cells through TLR7. Nat.Med.(N.Y., NY, U.S.) 11[3], 263-270. 2004.

Hornung, V., Rothenfusser, S., Britsch, S., Krug, A., Jahrsdorfer, B., Giese, T., Endres, S., and Hartmann, G. Quantitative expression of Toll-like receptor 1-10 mRNA in cellular subsets of human peripheral blood mononuclear cells and sensitivity to CpG oligodeoxynucleotides. J.Immunol. 168[9], 4531-4537. 2002.

Horohov, D. W., Beadle, R. E., Mouch, S., and Pourciau, S. S. Temporal regulation of cytokine mRNA expression in equine recurrent airway obstruction. Vet.Immunol.Immunopathol. 108[1-2], 237-245. 2005.

Horohov, D. W., Mills, W. R., and Gluck, M. "Specific and innate immunity in the lungs as it relates to equine RAO." *World Equine Airways Symposium*, C. Tessier, and V. Gerber, eds., Pabst Science Publishers, Bern, Switzerland, 106-108. 2009.

House, A. K., Binns, M. M., Gregory, S. P., and Catchpole, B. Analysis of NOD1, NOD2, TLR1, TLR2, TLR4, TLR5, TLR6 and TLR9 genes in anal furunculosis of German shepherd dogs. Tissue Antigens 73[3], 250-254. 2009.

Huang, R., Yang, W., Jiang, C., and Pei, Y. Gene delivery into brain capillary endothelial cells using antp-modified DNA-loaded nanoparticles. Chemical & Pharmaceutical Bulletin 54[9], 1254-1258. 2006.

Hurst, S. J., Lytton-Jean, A. K. R., and Mirkin, C. A. Maximizing DNA loading on a range of gold nanoparticle sizes. Abstracts of Papers, 233rd ACS National Meeting, Chicago, IL, United States, March 25-29, 2007.

Im Hof, M., Williamson, L., Summerfield, A., Balmer, V., Dutoit, V., Kandimalla, E. R., Yu, D., Zurbriggen, A., Doherr, M. G., Peel, J., and Roosje, P. J. Effect of synthetic agonists of toll-like receptor 9 on canine lymphocyte proliferation and cytokine production in vitro. Vet.Immunol.Immunopathol. 124[1-2], 120-131. 2008.

Iwakura, Y., and Ishigame, H. The IL-23/IL-17 axis in inflammation. J.Clin.Invest. 116[5], 1218-1222. 2006.

Janes, K. A., Fresneau, M. P., Marazuela, A., Fabra, A., and Alonso, M. J. Chitosan nanoparticles as delivery systems for doxorubicin. Journal of Controlled Release 73[2-3], 255-267. 2001.

Jang, J. S., Kim, S. Y., Lee, S. B., Kim, K. O., Han, J. S., and Lee, Y. M. Poly(ethylene glycol)/poly(e-caprolactone) diblock copolymeric nanoparticles for non-viral gene delivery: The role of charge group and molecular weight in particle formation, cytotoxicity and transfection. Journal of Controlled Release 113[2], 173-182. 2006.

Janke, M., Poth, J., Wimmenauer, V., Giese, T., Coch, C., Barchet, W., Schlee, M., and Hartmann, G. Selective and direct activation of human neutrophils but not eosinophils by Toll-like receptor 8. J Allergy Clin Immunol 123[5], 1026-1033. 2009.

Jarnicki, A. G., Conroy, H., Brereton, C., Donnelly, G., Toomey, D., Walsh, K., Sweeney, C., Leavy, O., Fletcher, J., Lavelle, E. C., Dunne, P., and Mills, K. H. G. Attenuating Regulatory T Cell Induction by TLR Agonists through Inhibition of p38 MAPK Signaling in Dendritic Cells Enhances Their Efficacy as Vaccine Adjuvants and Cancer Immunotherapeutics. J.Immunol. 180[6], 3797-3806. 2008.

Jevsevar, S., Kunstelj, M., and Porekar, V. G. PEGylation of therapeutic proteins. Biotechnol.J. 5[1], 113-128. 2010.

Jiang, W., Kim, B. Y. S., Rutka, J. T., and Chan, W. C. W. Nanoparticle-mediated cellular response is size-dependent. Nat.Nanotechnol. 3[3], 145-150. 2008.

Jones, O. G., Decker, E. A., and McClements, D. J. Comparison of protein-polysaccharide nanoparticle fabrication methods: Impact of biopolymer complexation before or after particle formation. J.Colloid Interface Sci. 344[1], 21-29. 2010.

Joshi, M. D., and Mueller, R. H. Lipid nanoparticles for parenteral delivery of actives. Eur.J.Pharm.Biopharm. 71[2], 161-172. 2009.

Kanzler, H., Barrat, F. J., Hessel, E. M., and Coffman, R. L. Therapeutic targeting of innate immunity with Toll-like receptor agonists and antagonists. Nat.Med.(N.Y., NY, U.S.) 13[5], 552-559. 2007.

Kaul, G., and Amiji, M. Biodistribution and Targeting Potential of Poly(ethylene glycol)-modified Gelatin Nanoparticles in Subcutaneous Murine Tumor Model. Journal of Drug Targeting 12[9-10], 585-591. 2004.

Kaul, G., and Amiji, M. Cellular interactions and in vitro DNA transfection studies with poly(ethylene glycol)-modified gelatin nanoparticles. Journal of Pharmaceutical Sciences 94[1], 184-198. 2005.

Kawai, K., Suzuki, S., Tabata, Y., Ikada, Y., and Nishimura, Y. Accelerated tissue regeneration through incorporation of basic fibroblast growth factor-impregnated gelatin microspheres into artificial dermis. Biomaterials 21[5], 489-499. 2000.

Kawashima, Y., Yamamoto, H., Takeuchi, H., Fujioka, S., and Hino, T. Pulmonary delivery of insulin with nebulized dl-lactide/glycolide copolymer (PLGA) nanospheres to prolong hypoglycemic effect. J.Cont Rel 62[1-2], 279-287. 1999.

Keller, M. Innovations and perspectives of metered dose inhalers in pulmonary drug delivery. Int.J.Pharm. 186[1], 81-90. 1999.

Keppel, K. E., Campbell, K. L., Zuckermann, F. A., Greeley, E. A., Schaeffer, D. J., and Husmann, R. J. Quantitation of canine regulatory T cell populations, serum interleukin-10 and allergen-specific IgE concentrations in healthy control dogs and canine atopic dermatitis patients receiving allergen-specific immunotherapy. Vet.Immunol.Immunopathol. 123[3-4], 337-344. 2008.

Kim, C. K., Kim, S. W., Park, C. S., Kim, B. I., Kang, H., and Koh, Y. Y. Bronchoalveolar lavage cytokine profiles in acute asthma and acute bronchiolitis. J.Allergy Clin.Immunol. 112[1], 64-71. 2003.

Kissel, T., and Roser, M. Influence of chemical surface-modifications on the phagocytic properties of albumin nanoparticles. Proc.Program Int.Symp.Controlled Release Bioact.Mater., 18th , 275-276. 1991.

Kline, J. N. Immunotherapy of asthma using CpG oligodeoxynucleotides. Immunol.Res. 39[1-3], 279-286. 2007.

Ko, S., and Gunasekaran, S. Preparation of sub-100-nm beta -lactoglobulin nanoparticles. J.Microencapsulation 23[8], 887-898. 2006.

Koh, C. G., Zhang, X., Liu, S., Golan, S., Yu, B., Yang, X., Guan, J., Jin, Y., Talmon, Y., Muthusamy, N., Chan, K. K., Byrd, J. C., Lee, R. J., Marcucci, G., and Lee, L. J. Delivery of antisense oligodeoxyribonucleotide lipopolyplex nanoparticles assembled by microfluidic hydrodynamic focusing. J.Controlled Release 141[1], 62-69. 2010.

Kommareddy, S., and Amiji, M. Biodistribution and pharmacokinetic analysis of long-circulating thiolated gelatin nanoparticles following systemic administration in breast cancer-bearing mice. J.Pharm.Sci. 96[2], 397-407. 2006.

Kreuter, J. Evaluation of nanoparticles as drug-delivery systems. III: materials, stability, toxicity, possibilities of targeting, and use. Pharm Acta Helv 58[9-10], 242-250. 1983.

Krieg, A. M. Applications of CpG motifs from bacterial DNA in cancer immunotherapy. Cancer Immune Therapy , 268-286. 2002.

Krieg, A. M. CpG motifs in bacterial DNA and their immune effects. Annu.Rev.Immunol. 20, 709-760. 2002.

Krieg, A. M. Therapeutic potential of Toll-like receptor 9 activation. Nat.Rev.Drug Discovery 5[6], 471-484. 2006.

Krieg, A. M. Development of TLR9 agonists for cancer therapy. J.Clin.Invest. 117[5], 1184-1194. 2007.

Krieg, A. M., Yi, A. K., Matson, S., Waldschmidt, T. J., Bishop, G. A., Teasdale, R., Koretzky, G. A., and Klinman, D. M. CpG motifs in bacterial DNA trigger direct B-cell activation. Nature (London) 374[6522], 546-549. 1995.

Kuijpers, A. J., Engbers, G. H., Krijgsveld, J., Zaat, S. A., Dankert, J., and Feijen, J. Cross-linking and characterisation of gelatin matrices for biomedical applications. Journal of biomaterials science.Polymer edition 11[3], 225-243. 2000.

Kundu, J., Chung, Y., Kim, Y. H., Tae, G., and Kundu, S. C. Silk fibroin nanoparticles for cellular uptake and control release. Int J Pharm 388[1-2], 242-250. 2010.

Kunz, W. Specific ion effects in colloidal and biological systems. Curr.Opin.Colloid Interface Sci. 15[1-2], 34-39. 2010.

Kunzle, F., Gerber, V., Van der Haegen, A., Wampfler, B., Straub, R., and Marti, E. IgE-bearing cells in bronchoalveolar lavage fluid and allergen-specific IgE levels in sera from RAO-affected horses. J.Vet.Med., A 54[1], 40-47. 2007.

Kurata, K., Iwata, A., Masuda, K., Sakaguchi, M., Ohno, K., and Tsujimoto, H. Identification of CpG oligodeoxynucleotide sequences that induce IFN-gamma production in canine peripheral blood mononuclear cells. Vet.Immunol.Immunopathol. 102[4], 441-450. 2004.

Lammel, A. S., Hu, X., Park, S. H., Kaplan, D. L., and Scheibel, T. R. Controlling silk fibroin particle features for drug delivery. Biomaterials 31[16], 4583-4591. 2010.

Langer, K., Balthasar, S., Vogel, V., Dinauer, N., Von Briesen, H., and Schubert, D. Optimization of the preparation process for human serum albumin (HSA) nanoparticles. Int.J.Pharm. 257[1-2], 169-180. 2003.

Lavoie, J. P., Maghni, K., Desnoyers, M., Taha, R., Martin, J. G., and Hamid, Q. A. Neutrophilic airway inflammation in horses with heaves is characterized by a Th2-type cytokine profile. Am J Respir Crit Care Med 164[8 Pt 1], 1410-1413. 2001.

Lee, J., Lee, J., Hwang, H., Jung, E., Huh, S., Hyun, J., and Park, D. Promotion of stem cell proliferation by vegetable peptone. Cell Proliferation 42[5], 595-601. 2009.

Lehr, C. M. Nanomedicines for the improved delivery of drugs across biological barriers. Drug Delivery Technology 7[5], 34,36-34,39. 2007.

Lemaitre, B., Nicolas, E., Michaut, L., Reichhart, J. M., and Hoffmann, J. A. The dorsoventral regulatory gene cassette spatzle/Toll/cactus controls the potent antifungal response in Drosophila adults. Cell 86[6], 973-983. 1996.

Lentz, Y. K., Anchordoquy, T. J., and Lengsfeld, C. S. Rationale for the Selection of an Aerosol Delivery System for Gene Delivery. J.Aerosol Med. 19[3], 372-384. 2006.

Lewkowicz, P., Lewkowicz, N., Sasiak, A., and Tchorzewski, H. Lipopolysaccharide-Activated CD4+CD25+ T Regulatory Cells Inhibit Neutrophil Function and Promote Their Apoptosis and Death. J.Immunol. 177[10], 7155-7163. 2006.

Lin, W., Coombes, A. G. A., Garnett, M. C., Davies, M. C., Schacht, E., Davis, S. S., and Illum, L. Preparation of sterically stabilized human serum albumin nanospheres using a novel dextranox-MPEG crosslinking agent. Pharm.Res. 11[11], 1588-1592. 1994.

Liu, J., Gong, T., Fu, H., Wang, C., Wang, X., Chen, Q., Zhang, Q., He, Q., and Zhang, Z. Solid lipid nanoparticles for pulmonary delivery of insulin. Int.J.Pharm. 356[1-2], 333-344. 2008.

Liu, W., Dreher, M. R., Furgeson, D. Y., Peixoto, K. V., Yuan, H., Zalutsky, M. R., and Chilkoti, A. Tumor accumulation, degradation and pharmacokinetics of elastin-like polypeptides in nude mice. J.Controlled Release 116[2], 170-178. 2006.

Lloyd, C. M., and Hawrylowicz, C. M. Regulatory T cells in asthma. Immunity 31[3], 438-449. 2009.

MacDonald, C. A., Sboros, V., Gomatam, J., Pye, S. D., Moran, C. M., and McDicken, W. N. A numerical investigation of the resonance of gas-filled microbubbles: resonance dependence on acoustic pressure amplitude. Ultrasonics 43[2], 113-122. 2004.

Maham, A., Tang, Z., Wu, H., Wang, J., and Lin, Y. Protein-Based Nanomedicine Platforms for Drug Delivery. Small 5[15], 1706-1721. 2009.

Maitra, A. Calcium phosphate nanoparticles: second-generation nonviral vectors in gene therapy. Expert Rev.Mol.Diagn. 5[6], 893-905. 2005.

Mann, M. J., and Dzau, V. J. Therapeutic applications of transcription factor decoy oligonucleotides. Journal of Clinical Investigation 106[9], 1071-1075. 2000.

March, J. Advanced Organic Chemistry: Reactions, Mechanisms, and Structure, Fourth Edition. 1495. 1992.

Marsella, R., and Girolomoni, G. Canine Models of Atopic Dermatitis: A Useful Tool with Untapped Potential. J.Invest.Dermatol. 129[10], 2351-2357. 2009.

Marti, E. "Role of IgE and perspectives on clinical allergy testing." *Wolrd Equine Airway Symposium*, C. Tessier, and V. Gerber, eds., Pabst Science Publishers, Bern, 109-111. 2009.

Marty, J. J., Oppenheim, R. C., and Speiser, P. Nanoparticles--a new colloidal drug delivery system. Pharm Acta Helv 53[1], 17-23. 1978.

Matsumura, Y., and Maeda, H. A new concept for macromolecular therapeutics in cancer chemotherapy: mechanism of tumoritropic accumulation of proteins and the antitumor agent smancs. Cancer Research 46[12, Pt. 1], 6387-6392. 1986.

Mayer, G., Vogel, V., Weyermann, J., Lochmann, D., van den Broek, J. A., Tziatzios, C., Haase, W., Wouters, D., Schubert, U. S., Zimmer, A., Kreuter, J., and Schubert, D. Oligonucleotide-protamine-albumin nanoparticles: Protamine sulfate causes drastic size reduction. J.Controlled Release 106[1-2], 181-187. 2005.

Meyer, M., Zintchenko, A., Ogris, M., and Wagner, E. A dimethylmaleic acid - melittin-polylysine conjugate with reduced toxicity, pH-triggered endosomolytic activity and enhanced gene transfer potential. J.Gene Med. 9[9], 797-805. 2007.

Michaelis, K., Hoffmann, M. M., Dreis, S., Herbert, E., Alyautdin, R. N., Michaelis, M., Kreuter, J., and Langer, K. Covalent linkage of apolipoprotein E to albumin nanoparticles strongly enhances drug transport into the brain. J.Pharmacol.Exp.Ther. 317[3], 1246-1253. 2006.

Millerick-May, M.. "Quantification and control of environmental contaminations in stables." *World Equine Airway Symposium*, C. Tessier, and V. Gerber, eds., Pabst Science Publishers, Bern, Switzerland, 192-194. 2009.

Minchin, R. Sizing up targets with nanoparticles. Nat.Nanotechnol. 3[1], 12-13. 2008.

Mintzer, M. A., and Simanek, E. E. Nonviral Vectors for Gene Delivery. Chem.Rev.(Washington, DC, U.S.) 109[2], 259-302. 2009.

Mishra, V., Mahor, S., Rawat, A., Gupta, P. N., Dubey, P., Khatri, K., and Vyas, S. P. Targeted brain delivery of AZT via transferrin anchored pegylated albumin nanoparticles. J.Drug Targeting 14[1], 45-53. 2006.

Moreno-Aspitia, A., and Perez, E. A. Nanoparticle albumin-bound paclitaxel (ABI-007): A newer taxane alternative in breast cancer. Future Oncol. 1[6], 755-762. 2005.

Mori, Y., Nakamura, S., Kishimoto, S., Kawakami, M., Suzuki, S., Matsui, T., and Ishihara, M. Preparation and characterization of low-molecular-weight heparin/protamine nanoparticles (LMW-H/P NPs) as FGF-2 carrier. Int.J.Nanomed. 5, 147-155. 2010.

Morishita, R., Tomita, N., Kaneda, Y., and Ogihara, T. Molecular therapy to inhibit NFkB activation by transcription factor decoy oligonucleotides. Current Opinion in Pharmacology 4[2], 139-146. 2004.

Mutwiri, G., Pontarollo, R., Babiuk, S., Griebel, P., van Drunen Littel-van den Hurk, Mena, A., Tsang, C., Alcon, V., Nichani, A., Ioannou, X., Gomis, S., Townsend, H., Hecker, R., Potter, A., and Babiuk, L. A. Biological activity of immunostimulatory CpG DNA motifs in domestic animals. Vet.Immunol.Immunopathol. 91[2], 89-103. 2003.

Negredo, C., Monks, E., and Sweeney, T. A novel real-time ultrasonic method for prion protein detection using plasminogen as a capture molecule. BMC Biotechnol 7, 43. 2007.

Numata, K., Subramanian, B., Currie, H. A., and Kaplan, D. L. Bioengineered silk protein-based gene delivery systems. Biomaterials 30[29], 5775-5784. 2009.

Nyambura, B. K., Kellaway, I. W., and Taylor, K. M. G. The processing of nanoparticles containing protein for suspension in hydrofluoroalkane propellants. Int.J.Pharm. 372[1-2], 140-146. 2009.

Ofokansi, K. C., Fricker, G.,Coester, C. Matrix-loaded biodegradable gelatin nanoparticles as new approach to improve drug loading and delivery. European Journal of Pharmaceutics and Biopharmaceutics in press. In press. 2010.

Olivry, T., and Sousa, C. A. The ACVD task force on canine atopic dermatitis (XIX): general principles of therapy. Vet Immunol Immunopathol 81[3-4], 311-316. 2001.

Olivry, T., Foster, A. P., Mueller, R. S., McEwan, N. A., Chesney, C., and Williams, H. C. Interventions for atopic dermatitis in dogs: a systematic review of randomized controlled trials. Vet Dermatol 21[1], 4-22. 2010.

Oppenheim, R. C. Solid colloidal drug delivery systems: nanoparticles. Int.J.Pharm. 8[3], 217-234. 1981.

Ozpolat, B., Sood, A. K., and Lopez-Berestein, G. Nanomedicine based approaches for the delivery of siRNA in cancer. J.Intern.Med. 267[1], 44-53. 2009.

Park, J., Fong, P. M., Lu, J., Russell, K. S., Booth, C. J., Saltzman, W. M., and Fahmy, T. M. PEGylated PLGA nanoparticles for the improved delivery of doxorubicin. Nanomedicine (N.Y., NY, U.S.) 5[4], 410-418. 2009.

Pasare, C., and Medzhitov, R. Toll-like receptors: balancing host resistance with immune tolerance. Curr.Opin.Immunol. 15[6], 677-682. 2003.

Patil, S. D., Rhodes, D. G., and Burgess, D. J. DNA-based therapeutics and DNA delivery systems: A comprehensive review. AAPS J. 7[1], E61-E77. 2005.

Pauwels, E. K. J., and Erba, P. Towards the use of nanoparticles in cancer therapy and imaging. Drug news & perspectives 20[4], 213-220. 2007.

Peer, D., Karp, J., Hong, S., and Langer, R. (2007). "Nanocarriers as an emerging platform for cancer therapy." *Nature Nanotechnology*, 2, 751-760.

Perez, C., Sanchez, A., Putnam, D., Ting, D., Langer, R., and Alonso, M. J. Poly(lactic acid)-poly(ethylene glycol) nanoparticles as new carriers for the delivery of plasmid DNA. Journal of Controlled Release 75[1-2], 211-224. 2001.

Petri, B., Bootz, A., Khalansky, A., Hekmatara, T., Mueller, R., Uhl, R., Kreuter, J., and Gelperina, S. Chemotherapy of brain tumour using doxorubicin bound to surfactant-coated poly(butyl cyanoacrylate) nanoparticles: Revisiting the role of surfactants. Journal of Controlled Release 117[1], 51-58. 2007.

Pishvaei, M., Cassagnau, P., and McKenna, T. F. Modelling of the rheological properties of bimodal emulsions. Macromol.Symp. 243[Polymer Reaction Engineering VI], 63-71. 2006.

Poeck, H., Besch, R., Maihoefer, C., Renn, M., Tormo, D., Morskaya, S. S., Kirschnek, S., Gaffal, E., Landsberg, J., Hellmuth, J., Schmidt, A., Anz, D., Bscheider, M., Schwerd, T., Berking, C., Bourquin, C., Kalinke, U., Kremmer, E., Kato, H., Akira, S., Meyers, R., Haecker, G., Neuenhahn, M., Busch, D., Ruland, J., Rothenfusser, S., Prinz, M., Hornung, V., Endres, S., Tueting, T., and Hartmann, G. 5'-triphosphate-siRNA: turning gene silencing and Rig-I activation against melanoma. Nat.Med.(N.Y., NY, U.S.) 14[11], 1256-1263. 2008.

Poeck, H., Wagner, M., Battiany, J., Rothenfusser, S., Wellisch, D., Hornung, V., Jahrsdorfer, B., Giese, T., Endres, S., and Hartmann, G. Plasmacytoid dendritic cells, antigen, and CpG-C license human B cells for plasma cell differentiation and immunoglobulin production in the absence of T-cell help. Blood 103[8], 3058-3064. 2004.

Postema, M., and Schmitz, G. Ultrasonic bubbles in medicine: Influence of the shell. Ultrason.Sonochem. 14[4], 438-444. 2007.

Purewal, T. S. Alternative propellants for metered dose inhalers. Aerosol Spray Rep. 37[11/12], 20-25. 1998.

Rankin, R., Pontarollo, R., Ioannou, X., Krieg, A. M., Hecker, R., Babiuk, L. A., and Van Drunen Littel-Van Den Hurk, S. CpG motif identification for veterinary and laboratory species demonstrates that sequence recognition is highly conserved. Antisense Nucleic Acid Drug Dev. 11[5], 333-340. 2001.

Reinero, C. R., Cohn, L. A., Delgado, C., Spinka, C. M., Schooley, E. K., and DeClue, A. E. Adjuvanted rush immunotherapy using CpG oligodeoxynucleotides in experimental feline allergic asthma. Vet.Immunol.Immunopathol. 121[3-4], 241-250. 2008.

Reischl, D., and Zimmer, A. Drug delivery of siRNA therapeutics: potentials and limits of nanosystems. Nanomedicine (N.Y., NY, U.S.) 5[1], 8-20. 2009.

Riemann, B., Schafers, K. P., Schober, O., and Schafers, M. Small animal PET in preclinical studies: opportunities and challenges. Q J Nucl Med Mol Imaging 52[3], 215-221. 2008.

Roberts, W. G., and Palade, G. E. Neovasculature induced by vascular endothelial growth factor is fenestrated. Cancer Res. 57[4], 765-772. 1997.

Robinson, N. E. (2001). "Recurrent airway obstruction (Heaves)." *Equine Respiratory Diseases*, P. Lekeux, ed., International Veterinary Information Service, Ithaca, New York.

Romberg, B., Hennink, W. E., and Storm, G. Sheddable Coatings for Long-Circulating Nanoparticles. Pharm.Res. 25[1], 55-71. 2008.

Roy, I., Ohulchanskyy, T. Y., Bharali, D. J., Pudavar, H. E., Mistretta, R. A., Kaur, N., and Prasad, P. N. Optical tracking of organically modified silica nanoparticles as DNA carriers: A nonviral, nanomedicine approach for gene delivery. Proceedings of the National Academy of Sciences of the United States of America 102[2], 279-284. 2005.

Rytting, E., Nguyen, J., Wang, X., and Kissel, T. Biodegradable polymeric nanocarriers for pulmonary drug delivery. Expert Opin.Drug Delivery 5[6], 629-639. 2008.

Sarvazyan, A. P. Ultrasonic velocimetry of biological compounds. Annual Review of Biophysics and Biophysical Chemistry 20, 321-342. 1991.

Sato, H., and Ueberreiter, K. Surface tension of aqueous gelatin solution. Polym.Prepr., Am.Chem.Soc., Div.Polym.Chem. 20[1], 907-908. 1979.

Schaefer, J., and Stejskal, E. O. "Carbon-13 Nuclear Magnetic Resonance of Polymers Spinning at the Magic Angle." *Journal of the American Chemical Society*, 98, 1031. 1976.

Schmallenbach, K. H., Rahman, I., Sasse, H. H. L., Dixon, P. M., Halliwell, R. E. W., McGorum, B. C., Crameri, R., and Miller, H. R. P. Studies on pulmonary and systemic Aspergillus fumigatus-specific IgE and IgG antibodies in horses affected with COPD. Vet.Immunol.Immunopathol. 66[3-4], 245-256. 1998.

Schmidt, C. Clinical setbacks for toll-like receptor 9 agonists in cancer. Nat.Biotechnol. 25[8], 825-826. 2007.

Schnabl, B., Bettenay, S., V, Dow, K., and Mueller, R. S. Results of allergen-specific immunotherapy in 117 dogs with atopic dermatitis. Vet Rec 158[3], 81-85. 2006.

Schneberger, D., Caldwell, S., Suri, S. S., and Singh, B. Expression of Toll-like receptor 9 in horse lungs. Anat.Rec. 292[7], 1068-1077. 2009.

Schnell, A., Goretzki, L., and Weinhold, W. Oberflächenstrukturen von Bodenbelägen. Fb 1090. 2007. Dortmund, Schriftenreihe der Bundesanstalt für Arbeitsschutz und Arbeitsmedizin.

Schnockel, U., Reuter, S., Stegger, L., Schlatter, E., Schafers, K. P., Hermann, S., Schober, O., Gabriels, G., and Schafers, M. Dynamic 18F-fluoride small animal PET to noninvasively assess renal function in rats. Eur J Nucl Med Mol Imaging 35[12], 2267-2274. 2008.

Schultes, S. "Nanoparticles for RNA Interference - Novel Preclinical Formulations for siRNA Mediated Gene Therapy." Dissertation, Ludwig Maximilians University, Munich. 2009.

Senti, G., Johansen, P., Haug, S., Bull, C., Gottschaller, C., Muller, P., Pfister, T., Maurer, P., Bachmann, M. F., Graf, N., and Kunding, T. M. Use of A-type CpG oligodeoxynucleotides as an adjuvant in allergen-specific immunotherapy in humans: a phase I/IIa clinical trial. Clin.Exp.Allergy 39[4], 562-570. 2009.

Shah, R. B., Zidan, A. S., Funck, T., Tawakkul, M. A., Nguyenpho, A., and Khan, M. A. Quality by design: characterization of self-nano-emulsified drug delivery systems (SNEDDs) using ultrasonic resonator technology. Int J Pharm 341[1-2], 189-194. 2007.

Sham, J. O. H., Zhang, Y., Finlay, W. H., Roa, W. H., and Lobenberg, R. Formulation and characterization of spray-dried powders containing nanoparticles for aerosol delivery to the lung. Int.J.Pharm. 269[2], 457-467. 2004.

Sharma, R., and Sharma, C. L. Macromolecular drugs: novel strategy in target specific drug delivery. J.Clin.Diagn.Res. 2[4], 1020-1023. 2008.

Sharp, F. A., Ruane, D., Claass, B., Creagh, E., Harris, J., Malyala, P., Singh, M., O'Hagan, D. T., Petrilli, V., Tschopp, J., O'Neill, L. A. J., and Lavelle, E. C. Uptake of particulate vaccine adjuvants by dendritic cells activates the NALP3 inflammasome. Proc.Natl.Acad.Sci.U.S.A. 106[3], 870-875. 2009.

Shida, M., Kadoya, M., Park, S. J., Nishifuji, K., Momoi, Y., and Iwasaki, T. Allergen-specific immunotherapy induces Th1 shift in dogs with atopic dermatitis. Vet.Immunol.Immunopathol. 102[1-2], 19-31. 2004.

Simons, F. E., Shikishima, Y., Van Nest, G., Eiden, J. J., and HayGlass, K. T. Selective immune redirection in humans with ragweed allergy by injecting Amb a 1 linked to immunostimulatory DNA. J.Allergy Clin.Immunol. 113[6], 1144-1151. 2004.

Smith, C. A., de la Fuente, J., Pelaz, B., Furlani, E. P., Mullin, M., and Berry, C. C. The effect of static magnetic fields and tat peptides on cellular and nuclear uptake of magnetic nanoparticles. Biomaterials 31[15], 4392-4400. 2010.

Sokolova, V., Kovtun, A., Prymak, O., Meyer-Zaika, W., Kubareva, E. A., Romanova, E. A., Oretskaya, T. S., Heumann, R., and Epple, M. Functionalization of calcium phosphate nanoparticles by oligonucleotides and their application for gene silencing. Journal of Materials Chemistry 17[8], 721-727. 2007.

Solaro, R., Chiellini, F., and Battisti, A. Targeted delivery of protein drugs by nanocarriers. Materials 3, 1928-1980. 2010.

Speiser, D. E., Lienard, D., Rufer, N., Rubio-Godoy, V., Rimoldi, D., Lejeune, F., Krieg, A. M., Cerottini, J. C., and Romero, P. Rapid and strong human CD8+ T cell responses to vaccination with peptide, IFA, and CpG oligodeoxynucleotide 7909. J.Clin.Invest. 115[3], 739-746. 2005.

Stehle, M. "Wirkung essentieller Fettsäuren auf die Proliferation von peripheren mononukleären Zellen und Expression von Zytokinen bei Hunden mit atopischer Dermatitis." Dissertation, Ludwig Maximilan University Munich. 2008.

Sun, G., Xu, J., Hagooly, A., Rossin, R., Li, Z., Moore, D. A., Hawker, C. J., Welch, M. J., and Wooley, K. L. Strategies for optimized radiolabeling of nanoparticles for in vivo PET imaging. Adv.Mater.(Weinheim, Ger.) 19[20], 3157-3162. 2007.

Sun, X., Duan, Y. R., He, Q., Lu, J., and Zhang, Z. R. PELGE nanoparticles as new carriers for the delivery of plasmid DNA. Chemical & Pharmaceutical Bulletin 53[6], 599-603. 2005.

Sung, J. C., Pulliam, B. L., and Edwards, D. A. Nanoparticles for drug delivery to the lungs. Trends Biotechnol. 25[12], 563-570. 2007.

Sussman, E. M., Clarke, M. B., Jr., and Shastri, V. P. Single-Step Process to Produce Surface-Functionalized Polymeric Nanoparticles. Langmuir 23[24], 12275-12279. 2007.

Swartz, M. A. The physiology of the lymphatic system. Adv.Drug Delivery Rev. 50[1-2], 3-20. 2001.

Tabata, Y., and Ikada, Y. Protein release from gelatin matrixes. Advanced Drug Delivery Reviews 31[3], 287-301. 1998.

Taylor, A., Verhagen, J., Blaser, K., Akdis, M., and Akdis, C. A. Mechanisms of immune suppression by interleukin-10 and transforming growth factor-beta : the role of T regulatory cells. Immunology 117[4], 433-442. 2006.

Thotathil, Z., and Jameson, M. B. Early experience with novel immunomodulators for cancer treatment. Expert Opin.Invest.Drugs 16[9], 1391-1403. 2007.

Thurn, K. T., Brown, E. M. B., Wu, A., Vogt, S., Lai, B., Maser, J., Paunesku, T., and Woloschak, G. E. Nanoparticles for applications in cellular imaging. Nanoscale Res.Lett. 2[9], 430-441. 2007.

Tikhonov, D. A., Kiselyov, O. E., Sarvazyan, A. P., and Sarkisov, G. N. Ultrasonic approach to obtaining partial thermodynamic characteristics of solutions. Ultrasonics 33[4], 301-310. 1995.

Tinkov, S., Winter, G., Coester, C., and Bekeredjian, R. New doxorubicin-loaded phospholipid microbubbles for targeted tumor therapy: Part I - Formulation development and in-vitro characterization. J.Controlled Release 143[1], 143-150. 2010.

Tokunaga, T., Yamamoto, H., Shimada, S., Abe, H., Fukuda, T., Fujisawa, Y., Furutani, Y., Yano, O., and Kataoka, T. Antitumor activity of deoxyribonucleic acid fraction from Mycobacterium bovis BCG. I. Isolation, physicochemical characterization, and antitumor activity. JNCI, J.Natl.Cancer Inst. 72[4], 955-962. 1984.

Torchilin, V. P. Recent advances with liposomes as pharmaceutical carriers. Nature Reviews Drug Discovery 4[2], 145-160. 2005.

Torchilin, V. P. Targeted pharmaceutical nanocarriers for cancer therapy and imaging. AAPS Journal 9[2], E128-E147. 2007.

Tseng, C. L., Su, W. Y., Yen, K. C., Yang, K. C., and Lin, F. H. The use of biotinylated-EGF-modified gelatin nanoparticle carrier to enhance cisplatin accumulation in cancerous lungs via inhalation. Biomaterials 30[20], 3476-3485. 2009.

Tseng, C. L., Wang, T. W., Dong, G. C., Wu, S. Y.-H., Young, T. H., Shieh, M. J., Lou, P. J., and Lin, F. H. Development of gelatin nanoparticles with biotinylated EGF conjugation for lung cancer targeting. Biomaterials 28[27], 3996-4005. 2007.

Tsung, K., and Norton, J. A. Lessons from Coley's Toxin. Surg Oncol 15[1], 25-28. 2006.

Umetsu, D. T., and DeKruyff, R. H. The regulation of allergy and asthma. Immunol.Rev. 212, 238-255. 2006.

Vafaei, S., Purkayastha, A., Jain, A., Ramanath, G., and Borca-Tasciuc, T. The effect of nanoparticles on the liquid-gas surface tension of Bi2Te3 nanofluids. Nanotechnology 20[18], 185702-1-185702/6. 2009.

Van Scott, M. R., Justice, J. P., Bradfield, J. F., Enright, E., Sigounas, A., and Sur, S. IL-10 reduces Th2 cytokine production and eosinophilia but augments airway reactivity in allergic mice. Am.J.Physiol. 278[4, Pt. 1], L667-L674. 2000.

Vaughn, J. M., McConville, J. T., Burgess, D., Peters, J. I., Johnston, K. P., Talbert, R. L., and Williams, R. O. I. Single dose and multiple dose studies of itraconazole nanoparticles. Eur.J.Pharm.Biopharm. 63[2], 95-102. 2006.

Vignali, D. A. A., Collison, L. W., and Workman, C. J. How regulatory T cells work. Nat.Rev.Immunol. 8[7], 523-532. 2008.

von Garnier, C., and Nicod, L. P. Immunology taught by lung dendritic cells. Swiss Med.Wkly. 139[12/13], 186-192. 2009.

Vonarbourg, A., Passirani, C., Saulnier, P., and Benoit, J. P. Parameters influencing the stealthiness of colloidal drug delivery systems. Biomaterials 27[24], 4356-4373. 2006.

Waldrep, J. C., and Dhand, R. Advanced nebulizer designs employing vibrating mesh/aperture plate technologies for aerosol generation. Curr.Drug Delivery 5[2], 114-119. 2008.

Wang, G., and Uludag, H. Recent developments in nanoparticle-based drug delivery and targeting systems with emphasis on protein-based nanoparticles. Expert Opin.Drug Delivery 5[5], 499-515. 2008.

Ward, A. C., Courts, A., and Editors. Food Science and Technology. The Science and Technology of Gelatin. 564. 1977.

Warheit, D. B. Long-term Inhalation Toxicity Studies with Multiwalled Carbon Nanotubes: Closing the Gaps or Initiating the Debate? Toxicol.Sci. 112[2], 273-275. 2009.

Weber, C., Coester, C., Kreuter, J., and Langer, K. Desolvation process and surface characterization of protein nanoparticles. International Journal of Pharmaceutics 194[1], 91-102. 2000.

Weibel, E. R., and Gomez, D. M. Architecture of the human lung. Use of quantitative methods establishes fundamental relations between size and number of lung structures. Science 137, 577-585. 1962.

Weissleder, R., and Pittet, M. J. Imaging in the era of molecular oncology. Nature (London, U.K.) 452[7187], 580-589. 2008.

Wernette, C. M., Smith, B. F., Barksdale, Z. L., Hecker, R., and Baker, H. J. CpG oligodeoxynucleotides stimulate canine and feline immune cell proliferation. Vet.Immunol.Immunopathol. 84[3-4], 223-236. 2002.

Whitehead, K. A., Langer, R., and Anderson, D. G. Knocking down barriers: Advances in siRNA delivery. [Erratum to document cited in CA150:230130]. Nat.Rev.Drug Discovery 8[6], 516. 2009.

Wilson, K. D., de Jong, S. D., and Tam, Y. K. Lipid-based delivery of CpG oligonucleotides enhances immunotherapeutic efficacy. Adv.Drug Delivery Rev. 61[3], 233-242. 2009.

Won, Y. W., and Kim, Y. H. Preparation and cytotoxicity comparison of type A gelatin nanoparticles with recombinant human gelatin nanoparticles. Macromol.Res. 17[7], 464-468. 2009.

Wurzenberger, C., Koelzer, V. H., Schreiber, S., Anz, D., Vollmar, A. M., Schnurr, M., Endres, S., and Bourquin, C. Short-term activation induces multifunctional dendritic cells that generate potent antitumor T-cell responses in vivo. Cancer Immunol.Immunother. 58[6], 901-913. 2009.

Xiao, K., Luo, J., Fowler, W. L., Li, Y., Lee, J. S., Xing, L., Cheng, R. H., Wang, L., and Lam, K. S. A self-assembling nanoparticle for paclitaxel delivery in ovarian cancer. Biomaterials 30[30], 6006-6016. 2009.

Yamamoto, M., Ikada, Y., and Tabata, Y. Controlled release of growth factors based on biodegradation of gelatin hydrogel. Journal of biomaterials science.Polymer edition 12[1], 77-88. 2001.

Yan, H. B., Zhang, Y. Q., Ma, Y. L., and Zhou, L. X. Biosynthesis of insulin-silk fibroin nanoparticles conjugates and in vitro evaluation of a drug delivery system. J.Nanopart.Res. 11[8], 1937-1946. 2009.

Yang, S., Yuan, W., and Jin, T. Formulating protein therapeutics into particulate forms. Expert Opin.Drug Delivery 6[10], 1123-1133. 2009.

Yasuda, K., Yu, P., Kirschning, C. J., Schlatter, B., Schmitz, F., Heit, A., Bauer, S., Hochrein, H., and Wagner, H. Endosomal translocation of vertebrate DNA activates dendritic cells via TLR9-dependent and -independent pathways. J Immunol 174[10], 6129-6136. 2005.

Young, S., Wong, M., Tabata, Y., and Mikos, A. G. Gelatin as a delivery vehicle for the controlled release of bioactive molecules. Journal of Controlled Release 109[1-3], 256-274. 2005.

Zensi, A., Begley, D., Pontikis, C., Legros, C., Mihoreanu, L., Wagner, S., Buechel, C., von Briesen, H., and Kreuter, J. Albumin nanoparticles targeted with Apo E enter the CNS by transcytosis and are delivered to neurons. J.Controlled Release 137[1], 78-86. 2009.

Zhang, Y. Q., Shen, W. D., Xiang, R. L., Zhuge, L. J., Gao, W. J., and Wang, W. B. Formation of silk fibroin nanoparticles in water-miscible organic solvent and their characterization. J.Nanopart.Res. 9[5], 885-900. 2007.

Zhao, Y., Yang, J., Gao, Y. d., and Guo, W. Th17 Immunity in Patients with Allergic Asthma. Int.Arch.Allergy Immunol. 151[4], 297-307. 2010.

Zillies, J. Gelatin Nanoparticles for Targeted Oligonucleotide Delivery to Kupffer Cells - Analytics, Formulation Development, Practical Application. Dissertation, Ludwig Maximilians University, Munich. 2007.

Zillies, J., and Coester, C. Evaluating gelatin based nanoparticles as a carrier system for double stranded oligonucleotides. Journal of Pharmacy & Pharmaceutical Sciences 7[4], 17-21. 2004.

Zillies, J. C., Zwiorek, K., Hoffmann, F., Vollmar, A., Anchordoquy, T. J., Winter, G., and Coester, C. Formulation development of freeze-dried oligonucleotide-loaded gelatin nanoparticles. Eur J Pharm Biopharm 70[2], 514-521. 2008.

Zillies, J. C., Zwiorek, K., Winter, G., and Coester, C. Method for quantifying the PEGylation of gelatin nanoparticle drug carrier systems using asymmetrical flow field-flow fractionation and refractive index detection. Anal.Chem.(Washington, DC, U.S.) 79[12], 4574-4580. 2007.

Zintchenko, A., Philipp, A., Dehshahri, A., and Wagner, E. Simple modifications of branched PEI lead to highly efficient siRNA carriers with low toxicity. Bioconjugate Chem. 19[7], 1448-1455. 2008.

Zwiorek, K. "Gelatin Nanoparticles as Delivery System for Nucleotide-Based Drugs." Dissertation, Ludwig Maximilians University, Munich. 2006

Zwiorek, K., Bourquin, C., Battiany, J., Winter, G., Endres, S., Hartmann, G., and Coester, C. Delivery by Cationic Gelatin Nanoparticles Strongly Increases the Immunostimulatory Effects of CpG Oligonucleotides. Pharm.Res. 25[3], 551-562. 2008.

Zwiorek, K., Kloeckner, J., Wagner, E., and Coester, C. Gelatin nanoparticles as a new and simple gene delivery system. Journal of Pharmacy & Pharmaceutical Sciences 7[4], 22-28. 2004.

VII Appendix

This thesis is associated with the following publications:

Original Research and Review Articles

Published

Fuchs, S. and Coester, C.
Protein based nanoparticles as drug delivery system: chances, risks, perspectives. Journal of Drug Delivery Science and Technology, 20(5), 331-342. 2010.

Fuchs, S., Kutscher, M., Hertel, T., Winter, G., Pietzsch, M., Coester, C.,
Transglutaminase: new insights into gelatin nanoparticle cross-linking
Journal of Microencapsulation, 27(8), 747-754. 2010.

Fuchs, S., Winter, G., Coester, C.
Ultrasonic resonator technology as a new quality control method evaluating gelatin nanoparticles. Journal of Microencapsulation, 27(3), 242-252. 2010.

Wurzenberger, C., Bourquin, C., Heidegger, S., Fuchs, S., Anz, D., Weigel, S., Sandholzer, N., Winter, G., Coester, C., Endres, S.,
Delivery of immunostimulatory RNA oligonucleotides by gelatin-based nanoparticles triggers an efficient antitumoral response. J Immunotherapy, 33(9), 935-944. 2010

Hoffmann, F., Sass, G., Zillies, J., Zahler, S., Tiegs, G., Hartkorn, A., Fuchs, S., Wagner, J., Winter, G., Coester, C., Gerbes, A. L., Vollmar, A. M.,
A novel technique for selective NF-.kappa.B inhibition in Kupffer cells: contrary effects in fulminant hepatitis and ischaemia-reperfusion. Gut, 58(12), 1670-1678. 2009.

Bourquin, C., Anz, D., Zwiorek, K., Lanz, A., Fuchs, S., Weigel, S., Wurzenberger, C., Borch, P., Golic, M., Moder, S., Winter, G., Coester, C., Endres, S.
Targeting CpG oligonucleotides to the lymph node by nanoparticles elicits efficient antitumoral immunity. Journal of Immunology, 181(5), 2990-2998. 2008

In revision

Klier, J., May, A., Fuchs, S., Schillinger, U., Plank, C., Winter, G., Gehlen, H., Coester, C.,
Immunostimulation of bronchoalveolar lavage cells from recurrent airway obstruction-affected horses by different CpG-classes bound to gelatin nanoparticles. J. Vet. Immunol. and Immunopathol. 2010.

In preparation

Fuchs, S., Klier, J., May, A., Winter, G., Coester, C., Gehlen, H.,
Towards an Inhalative *in vivo* Application of Immunomodulating Gelatin Nanoparticles in RAO Horses – Related Preformulation Studies. 2010.

Fuchs, S., Klier, J., May, A., Schillinger, U., Plank, C., Winter, G., Coester, C., Gehlen, H.,
A nebulized gelatin nanoparticle-based CpG formulation is effective in immunotherapy of allergic horses. 2010.

Rostaher, A., Fuchs, S., Weber, K., Winter, G., Coester, C., Mueller, R.,
In vitro effects of CpG oligodeoxynucleotides delivered by gelatin nanoparticles on canine peripheral blood mononuclear cells of atopic and healthy dogs.

Patent applications

Gehlen, H., Coester, C., Fuchs, S., Klier, J., Winter, G.,
An immunomodulating gelatin nanoparticle oligodeoxynucleotide formulation for inhalation therapy of equine recurrent airway obstruction
Filing No. EP10002266. 2010

Renner, W., Bachmann, M., Cielens, I., Coester, C., Dietmeier, K., Fuchs, S., Manolova, V., Maurer, P., Pumpens, P., Renhofa, R., Tissot, A., Zou, Y.,
RNA bacteriophage or virus-like particles comprising immunostimulatory nucleic acids for treatment of hypersensitivity and IgE-mediated allergy, PCT Int. Appl., WO 2006-EP69734 20061214. 2007

Oral Presentation

Fuchs, S., Wurzenberger, C., Bourquin, C., Winter, G., Coester, C.,
Gelatin Nanoparticles are Suitable Carriers for Immunostimulatory RNA Oligonucleotides to Trigger Efficient Antitumoral Immune Responses. 2nd PharmSciFair, Nice, France, June 9th-12th 2009

Proceedings and Abstracts contributed to international conferences

Fuchs, S., Klier, J., May, A., Winter, G., Gehlen, H., Coester, C.,
Towards an Inhalative *in vivo* Application of Immunomodulating GelatinNanoparticles in RAO Horses – Related Preformulation Studies. 7th World Meeting on Pharmaceutics, Biopharmaceutics and Pharmaceutical Technology, Malta, March 8th - 11th, 2010.

Fuchs, S., Kutscher, M., Hertel, T., Winter, G., Pietzsch, M., Coester, C.,
Transglutaminase, a New Approach in Gelatin Nanoparticles Cross-Linking. 7th World Meeting on Pharmaceutics, Biopharmaceutics and Pharmaceutical Technology, Malta, March, 8th-11th, 2010.

Fuchs, S., Winter, G., Coester, C.,
Gelatin Nanoparticles as a Promising and Comprehensively Characterized Delivery Platform for Oligonucleotides in Antitumoral and Antihypersensitivity Immunotherapy. Science to Market Conference - EAPB, Hannover, Germany, October 6th-7th, 2009.

Fuchs, S., Auernheimer, J., Zwiorek, K., Wester, H.J., Winter, G., Coester, C.,
In Vivo Tracking Of Ga-68 Labeled Gelatin Nanoparticles By Positron Emission Tomography. AAPS Annual Meeting and Exposition, Atlanta, GA, November 16th-20th, 2008.

Fuchs,S., Parlitz, R., Gau, D., Winter, G., Coester, C.,
Towards Better Quality Control of Nanoparticulate Delivery Preparations by Ultrasonic Resonator Technology. 6th World Meeting on Pharmaceutics, Biopharmaceutics and Pharmaceutical Technology, Barcelona, Spain, April, 6th-10th, 2008.

Fuchs S, Parlitz R, Winter G, Coester C
Determination of Low to High Gelatin Nanoparticle Concentrations and Oligonucleotide Loading by Ultrasonic Resonator Technology. Pharmaceutical Sciences World Congress, Amsterdam, The Netherlands, 22nd-25th April 2007.

Curriculum Vitae

Sebastian Fuchs

Personal data

Date of birth	July 10th, 1980
Place of birth	Heinsberg
Nationality	German
Martial status	unmarried

Work experience and academic training

Since 06/2010	Trainee Patent Attorney, Vereenigde Octrooibureaux N.V. Munich, Germany and The Hague, Netherlands
Since 04/2009	Pharmacist (retail), Unterschleissheim, Germany
07/2006 – 04/2010	PhD studies at the Department of Pharmacy Pharmaceutical Technology and Biopharmaceutics Ludwig-Maximilian University Munich, Germany Supervisor: Prof. Dr. Gerhard Winter
02/2009 – 04/2009	Research stay at the School of Pharmacy University of Colorado at Denver, CO, USA Supervisor: Prof. Dr. Thomas J Anchordoquy

Education

11/2005 – 05/2006	Practical education in pharmacy, diploma thesis at Department of Pharmaceutical Research, Hoffmann La Roche AG, Basel, Switzerland
05/2005 – 10/2005	Practical education in pharmacy (retail), Kreuz-Apotheke, Heinsberg, Germany
04/2001 – 04/2005	Study of pharmacy, Eberhard-Karl University, Tübingen, Germany
07/2000 – 04/2001	Military Service at the German Air force NATO E3A Component, Geilenkirchen, Germany
09/1991- 06/2000	High School, Kreisgymnasium Heinsberg, Germany, Graduation with “Abitur”